Universitat Autònoma de Barcelona

THE USE OF SPECTROSCOPIC AND DIFFRACTOMETRIC TECHNIQUES IN THE STUDY OF BONES AND ITS IMPLICATIONS IN ANTHROPOLOGY, FORENSIC SCIENCES AND PALEONTHOLOGY

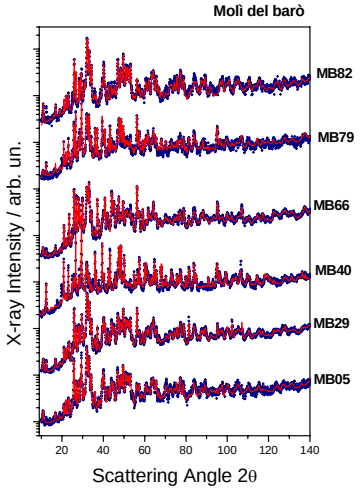

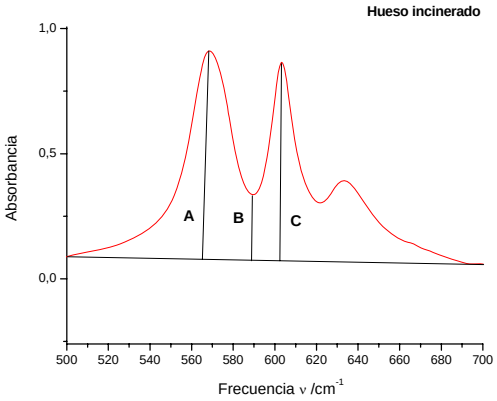

Giampaolo Piga
Doctoral Thesis
2012

UNITAT D'ANTROPOLOGIA BIOLOGICA

DEPARTMENT DE BIOLOGIA ANIMAL, BIOLOGIA VEGETAL I ECOLOGIA

Doctorat en Biodiversitat

The use of spectroscopy and diffraction techniques in the study of bones and implications in Anthropology, Palaeontology and Forensic Sciences

Tesi Doctoral

Giampaolo Piga

2012

Director:

Prof. Assumpció Malgosa

Codirector:

Prof. Stefano Enzo

Abstract

In the development of the current thesis we have addressed two different although very related topics: analyzing and differentiating the microstructural changes in the bones due to the heat treatment and/or to diagenesis and fossilization processes.

During the study of several human skeletal samples, we have observed that some bones show modifications in colour, texture and morphology that could be interpreted as alterations due to heat exposure. However, colours may also be due to bone interaction with environmental materials. After burial, bone may be altered and may change colour as a result of soil composition, sediment pH, temperature or moisture, and the changes may occur in the bone tissue as ionic substitution

Thus, we need techniques that permit us to distinguish between diagenesis and thermal treatment and, if possible, that differentiate the various partial thermal exposures. However, as human skeletal materials showing this kind of treatment are unique, these techniques should be as non-destructive as possible.

To address this type of analysis we used different physico-chemical and spectroscopic techniques (XRD, FT-IR) that have produced important results, which can be applied in various forensic, archaeological and paleontological contexts.

In relation to the analysis of burned bones, we can conclude that the analysis of different contexts with burned bones permit us to affirm that the physico-chemical techniques described here (XRD, FT–IR) can be used as a more accurate determinant of crystallite change during heating, thus providing an additional means of determining the effects of heat treatment on biogenic hydroxylapatite or tracing burning practices in the forensic and archaeological records.

Therefore, the combined used of XRD, FT–IR and SAXS techniques is a powerful tool to assess whether the bones have subjected to fire and, with fairly good reliability, to which temperature. The application of these techniques to archaeological context is useful to verify if a bone has been burned or not, find explanations to some specific funerary rites, get a reasonably precise temperature range across the entire body, temperature homogeneity throughout the skeleton and its duration.

In spite of the powerful us of these techniques, it is not easily possible to distinguish animal and human bones on the basis of powder diffraction patterns. A large number of variables have to be taken into proper account. Therefore, any claims to be able to distinguish animal and human bones should be treated with caution

In relation to the analysis of fossil bones, we can conclude that the combined investigations and analyses by FT–IR, XRD and XRF techniques supplied detailed and to a certain extent satisfactory accounts of the post-mortem integral changes to which the fossil bones have been subjected during geological times. The crystallization induced by just the time is overlapped by other factors depending on the geological formation that may inhibit or enhance the process. The extreme variability of francolite average crystallite size values suggests that correlation between crystallisation indices and bone age has to be regarded with obvious caution.

Resum

En el desenvolupament de la present tesi s'han tractat dos temes diferents encara que molt relacionats: l'anàlisi i diferenciació dels canvis microestructurals en els ossos a causa del tractament tèrmic i /o dels processos de diagènesi i fossilització.

Durant l'estudi de diferents mostres d'esquelets humans, s'ha observat que alguns ossos mostren modificacions en el color, la textura i morfologia que es podrien interpretar com alteracions per exposició al calor. No obstant això, el color també pot ser degut a la interacció entre l'os i els diversos materials ambientals. Després d'enterrament, l'os pot estar alterat i pot canviar de color com a conseqüència de la composició del sòl, el pH del sediment, la temperatura o la humitat, i els canvis poden ocórrer tant en el teixit ossi com en la substitució iònica.

Per tant, es necessiten tècniques que ens permetin distingir entre la diagènesi i el tractament tèrmic i, si és possible, que diferenciïn les diverses exposicions tèrmiques parcials. No obstant això, atès que els materials esquelètics humans que mostren aquest tipus de tractament són únics, aquestes tècniques han de ser el menys destructives possibles. Per fer front a aquest tipus d'anàlisi es van utilitzar diferents tècniques

fisicoquímiques i espectroscòpiques (XRD, FT-IR) que han produït resultats importants, que es poden aplicar en diferents contexts forenses, arqueològics i paleontològics.

En relació amb l'anàlisi d'ossos cremats, l'anàlisi dels diferents contexts amb ossos cremats ens permeten afirmar que les tècniques fisicoquímiques descrites aquí (XRD, FT-IR) es poden utilitzar per a determinar de manera molt precisa els canvis dels cristalls durant l'escalfament, proporcionant així un mitjà addicional de determinar els efectes del tractament tèrmic sobre la hidroxiapatita biogènica i detectar pràctiques de cremació en els registres forenses i arqueològiques.

Així doncs la combinació de tècniques de XRD, FT-IR i SAXS constitueix una poderosa eina per avaluar si els ossos s'han sotmès al foc i, amb una fiabilitat bastant bona, a quina temperatura. L'aplicació d'aquestes tècniques al context arqueològic és útil per verificar si un os s'ha cremat o no, trobar explicacions a alguns ritus funeraris específics, obtenir un rang de temperatura raonablement precisa, determinar l'homogeneïtat de la temperatura en tot l'esquelet i la seva durada.

Tot i el seu innegable poder en l'estudi dels canvis dels cristalls d'hidroxiapatita, no és possible distingir fàcilment els ossos animals i humans sobre la base dels patrons de difracció ja que s'han de tenir en compte un gran nombre de variables. Per tant, la possibilitat aquesta l'ús d'aquestes tècniques per distingir ossos d'animals i humans s'ha de tractar amb precaució

En relació amb l'anàlisi d'ossos fòssils, es pot concloure que les investigacions conjuntes i les anàlisis amb FT-IR, XRD i XRF proporcionen informació dels canvis post mortem als que els ossos fòssils han estat sotmesos durant els temps geològics. Cal tenir en compte que la cristal·lització deguda al temps transcorregut es solapa amb altres factors que depenen de la formació geològica i que poden inhibir o potenciar el procés. La variabilitat extrema dels valors mitjans dels cristalls de francolita suggereix que la correlació entre els índexs de cristal·lització i l'edat òssia s'ha de considerar amb precaució òbvia.

Resumen

En el desarrollo de la presente tesis se han tratado dos temas diferentes aunque muy relacionados: el análisis y diferenciación de los cambios microestructurales en los huesos debido al tratamiento térmico y / o los procesos de diagénesis y fosilización.

Durante el estudio de diferentes muestras de esqueletos humanos, se ha observado que algunos huesos muestran modificaciones en el color, la textura y morfología que podrían ser interpretados como alteraciones por exposición al calor. Sin embargo, el color también puede ser debido a la interacción entre el hueso y los materiales ambientales. Después de enterramiento, el hueso puede estar alterado y puede cambiar de color como consecuencia de la composición del suelo, el pH del sedimento, la temperatura o la humedad, y los cambios pueden ocurrir tanto en el tejido óseo como en la sustitución iónica.

Por lo tanto, se necesitan técnicas que nos permitan distinguir entre la diagénesis y el tratamiento térmico y, si es posible, que diferencien las diversas exposiciones térmicas parciales. Sin embargo, como los materiales esqueléticos humanos que muestran este tipo de tratamiento son únicos, estas técnicas deben ser lo menos destructivas posible. Para hacer frente a este tipo de análisis se utilizaron diferentes técnicas fisicoquímicas y espectroscópicas (XRD, FT-IR) que han producido resultados importantes, que se pueden aplicar en diferentes contextos forenses, arqueológicos y paleontológicos.

En relación con el análisis de huesos quemados, se puede concluir que el análisis de los diferentes contextos con huesos quemados nos permiten afirmar que las técnicas fisicoquímicas descritas aquí (XRD, FT-IR) se pueden utilizar para determinar de manera muy precisa el cambio de cristales durante el calentamiento, proporcionando así un medio adicional de determinar los efectos del tratamiento térmico sobre hidroxiapatita biogénica y detectar prácticas de cremación en los registros forenses y arqueológicas.

Así pues la combinación de técnicas de XRD, FT-IR y SAXS constituye una poderosa herramienta para evaluar si los huesos se han sometido al fuego y, con una fiabilidad bastante buena, a qué temperatura. La aplicación de estas técnicas al contexto arqueológico es útil para verificar si un hueso se ha quemado o no, encontrar explicaciones a algunos ritos funerarios específicos, obtener un rango de temperatura razonablemente precisa, determinar la homogeneidad de la temperatura en todo el esqueleto y su duración.

A pesar de su innegable poder en el estudio de los cambios de los cristales de hidroxiapatita, no es posible distinguir fácilmente los huesos animales y humanos sobre la base de los patrones de difracción ya que se deben tener en cuenta un gran número de

variables. Por lo tanto, la posibilidad esta el uso de estas técnicas para distinguir huesos de animales y humanos debe ser tratado con precaución.

En relación con el análisis de huesos fósiles, se puede concluir que las investigaciones conjuntas y los análisis con FT-IR, XRD y XRF proporcionan información de los cambios post mortem a las que los huesos fósiles han sido sometidos durante los tiempos geológicos. Hay que tener en cuenta que la cristalización debida al tiempo transcurrido se solapa con otros factores que dependen de la formación geológica y que pueden inhibir o potenciar el proceso. La variabilidad extrema valores medios de los cristales de francolita sugiere que la correlación entre los índices de cristalización y la edad ósea debe considerarse con una precaución obvia.

Table

1: INTRODUCTION

1.1: Chemical bone structure

Bone mineral is a significant biomaterial with a range of uses across a number of disciplines such as: Biomedicine, Archaeology, Forensic Sciences, Anthropology and Paleontology.

Bone has a hierarchical structure composed of different structural units at different size scales (Weiner and Traub, 1992). These units work in concert to perform different functions and especially to impart good mechanical properties to the bone (Rho et al., 1998; Weiner and Wagner, 1998; Currey, 2002).

The material is constituted by both organic (largely collagen, ~30 wt%) and inorganic (largely calcium phosphate) components. Macroscopically a typical bone is comprised of several different layers (the periosteum, cortical bone, and endosteum) and different bone types (compact and cancellous). Microscopically, the mineral phase, which accounts for 60-70 weight % (Wang et al., 2010) can be referred to as an impure, nonstoichiometric and poorly crystalline form of hydroxylapatite (HA), with a basic nanosized apatite structure of $\mathbf{Ca_{10}(PO_4)6(OH)_2}$ embedded in an organic matrix (Weiner and Price, 1986; Wagner and Weiner, 1992; Weiner and Traub, 1992; D'Elia et al., 2007; Etok et al., 2007; Mkukuma et al., 2004; Wang et al., 2010).

However, whereas hydroxylapatite as has a Ca:P ratio of 5:3 (1.67), bone mineral itself has Ca:P ratios ranging from 1.37–1.87. This is because the composition of bone mineral is much more complex and contains additional ions such as strontium, magnesium, zinc and sodium substituting for calcium, and carbonate groups substituting for phosphate PO_4^{3-} groups.

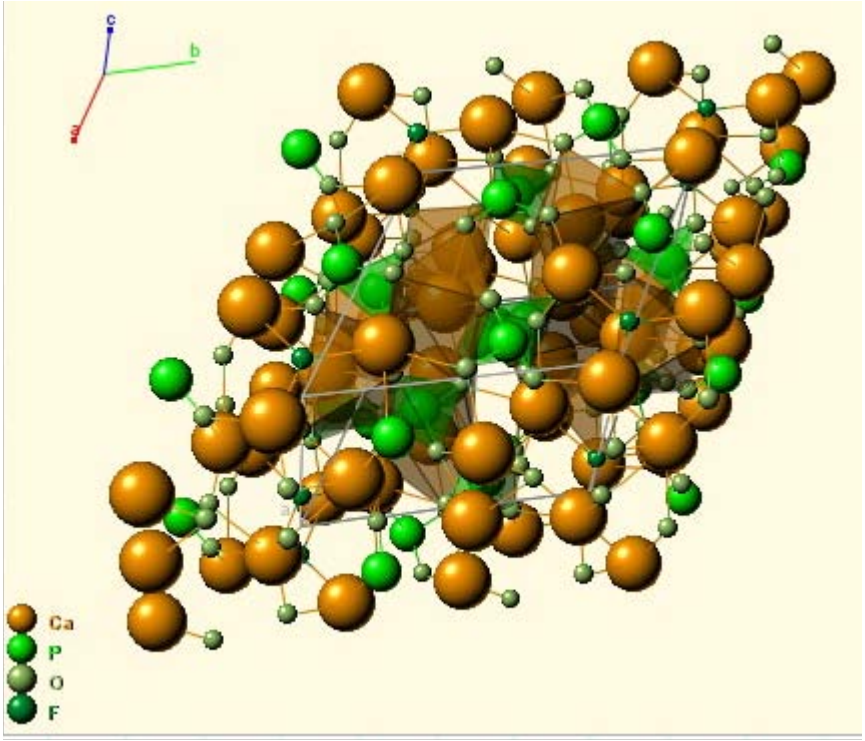

Fig.1: Structure of the hydroxylapatite mineral (Representation obtained from: http://www.minsocam.org/).

Figure 1 shows the arrangement of 4 molecules of hydroxylapatite **$Ca_5(PO_4)_3(OH)$** that build the unit cell in a crystal. This means that the natural bioapatite crystal may be envisaged as an ordered arrangement of such unit cell repeated periodically along the three orthogonal spatial directions. Biological apatites of bones are made by tiny microcrystals of apatite that have been shown to be of needle-like shape having characteristic size length of the order from 50-60 Å to 150–180 Å (1 Å = 10^{-8} cm).

A number of different factors can alter this mineral composition. One of the more significant changes to the microstructure of bone (i.e. to its spatial extension) occurs when this material is heated. Heated bone is one of the most challenging osteological materials to study, since the process of heating produces a range of complicated changes within the material already complex by itself.

Changes involving the structure and chemical composition of bones may also occur during the fossilization process.

The full description of those two processes will be presented separately.

1.2: Burned bones

The study of burned human remains is of considerable importance in Archaeology, Forensic Science, Forensic Anthropology and crime scene investigation. The ability to identify burning and burned bone in the forensic and archaeological records has long been an important and contentious issue.

The presence of burnt bones in an archaeological site may be the result of different anthropogenic behaviors. Their study provides information in broader areas such as the use of space in prehistoric settlements (Bellomo, 1993), combustion technology (Laloy, 1981; Théry Parissot, 1998; Costamagno et al., 1999), burial practices (Susini 1988; Piga et al., 2010a; 2010b), taphonomy and knowledge of the environment (Person et al., 1995, Shahack-Gross et al., 1997, Bennett, 1999).

Thermal treatment is, of course, related to multiple variables associated with anthropological research; in other words, incineration of the body as a means of disposing of the dead (López et al., 1976; Carpenter et al., 2003), the incineration of dry human bones found during an inhumation, or the roasting of body parts in the course of a ritual or an act of cannibalism. The previously described alterations are related to structural changes in the bone, associated with changes of texture and bone colour (Pijoan et al., 2004).

Several techniques to determine burning or heating regimen used in archaeology have been derived, with varying levels of success (Perinet, 1964; Shipman et al., 1984; Parker, 1985; Chandler, 1987; Brain and Sillen, 1988; Nicholson, 1993; Stiner et al., 1995). Determination of the temperature and duration of burning, as well as the background noise of potential diagenetic effects (Bennett, 1999) would shed light on the origin of early use of fire and cooking practices, cremation as a burial rite, and other archaeological and paleoanthropological contexts (Enzo et al., 2007; Piga et al., 2008a; 2010a; 2010b)

More precisely know the temperatures at which a bone was subjected is an index to better understand the modifications suffered by bone structures due to combustion (March, 1996), to promote the differentiation between natural and anthropogenic phenomena and to better interpret the techniques used by the people who use fire for symbolic or funerary reasons.

For example it appears particularly interesting to be able to assess the temperature reached by the pyres used by civilizations within their funerary practices and to estimate a possible time scale for the fire treatment of bodies (Piga et al., 2012). This also represents useful information concerning the fire and materials technology used in the past. In addition to this, an investigation of fire temperatures seems advisable in order to confirm or reject the possibility of occasional non-ritualistic fires in civilizations where the use of funerary rites has never been verified in depth (Piga et al, 2008a).

Further, the effects of burning on bone specimens and the determination of the techniques used are crucial in the resolution of forensic cases where cremation or other fire damage to remains is present (Owsley, 1993; Murray and Rose, 1993; Holden et al., 1995; Kennedy, 1996; Cattaneo et al., 1999).

An understanding of the changes that the body has undergone as a result of burning can provide significant information regarding the context and conditions of the burning event itself. Such crime scene information can include the temperature of the fire, the position of the body in respect to fire and the eventual presence of accelerants. Unfortunately, the act of burning also causes a number of substantial changes within the skeleton, which in turn can affect attempts to provide an identification of the deceased. Research has shown that both morphological and metric methods of anthropological assessment are affected (Thompson, 2002; 2004), in addition to methods of dating (Olsen et al., 2008), DNA extraction and stable isotopic analysis (an analytical techniques of increasing importance in the forensic field) (Munro et al., 2007; Ubelaker, 2008).

Traditionally, a macroscopic inspection of the remains has been used to suggest whether the bones have been subjected to fire (Holck, 1986; Eckert et al., 1988; Etxeberria, 1994), and beyond this, associations have been made between bone colour and fracturing with fire temperature and presence of soft tissues (McKinley, 2000; Mayne Correia, 1997; Fairgrieve, 2008; Schmidt and Symes, 2008). Shipman et al. (1984) devised five distinct groups based on the heating stages of bone tissue and the resulting colours at different temperatures ranging from pale yellow through brown, black, bluish grey, light grey and white.

Nonetheless, it has been noted by a number of authors that colour is a poor criterion in judging the degree of incineration and the examination of colour alone cannot determine the attained temperature of a cremation pyre as heat varied throughout the structure (Herrmann, 1977; Thompson, 2004). Furthermore the colour of bone may have changed after deposition in the ground (Taylor et al., 1995). In fact, many infiltrations are possible into the ground. An example would be the dark brown bones, whose colour is due to manganese in the soil in which they were buried (Greenlee and Dunnell, 1992; Shahack-Gross et al. 1997), but also the presence of iron, calcium carbonate can color a bone. Brain and Sillen (1988) have used the carbon/nitrogen ratio by examining a series of modern bones whose combustion temperature is known and archaeological bones in which the surface is obscured by the $CaCO_2$ and from MnO_2. Comparing the results, they were able to differentiate the coloration due to heat and the coloring due to the presence of manganese.

Stiner et al. (1995) investigated the relationship between four factors: the visible changes of the color, changes in organic and mineral matter, alterations of the mechanical properties of bone and the soil effects of on the buried bones. Shipman et al. (1984) also studied four types of changes that occur during the combustion of the bones: the change of color, the microscopic morphology, crystal structure and the reduction of dimensions of the bones.

Nicholson (1993) applied the method of Shipman et al. (1984) on a series of bones of mammals and non-mammals and compared the results obtained on archaeological bones. Nicholson (1996; 1998) also studied experimentally the diagenesis of unburned bone and of cooked or boiled bone. Person et al. (1996) conducted an experiment of burnt bones, although in a different perspective, which concerns the diagenesis of bone rather than combustion.

Bonucci and Graziani (1975) examined the effects of physical variables that could be related to the color of fossil and sub-fossil bones (IV^{th}–V^{th} century B.C). They defined the temperature at which a bone has been exposed between of 200 and 650° C (± 50° C).

On the other hand, fragmentation, scratches and cracks are often due to thermal treatments, but may also result from taphonomic processes. According Shipman et al.

(1984), 645°C is the temperature, above which a bone becomes calcined, loses its coherent structure and increases the hydroxylapatite crystals size.

However, between the various experimental studies, the conditions are not similar. For the experiments are often used bones of mammals belonging to common species (goat, sheep or cow). This is the case of Shipman et al. (1984), Brain and Sillen (1988) and Shahack–Gross et al. (1997); Stiner et al. (1995) and Nicholson (1993) instead of using organic bones addressed the study of several species of recent mammals and non-mammalian bones (birds and fish). After being burned at the same temperature, they concluded that the same thermal alteration process take place on bone structure.

In addition there are significant variations between the color of bones of different species burned at the same temperatures. Susini (1988) studied the thermal behavior of the cortical bone of human adults calcined up to 1400°C. In this work, the temperature and the duration of combustion varies greatly and thus can give different results.

Furthermore, it has also been shown both experimentally and statistically that the most important changes in bone that can predict burning contexts involve changes within the skeletal microstructure (Thompson, 2005). At this microscopic scale, there are two key features influenced by heating that are worth exploring: changes to the elemental composition and changes to the crystalline structure of the bone. Although changes to the elemental composition of bone have been successfully used to examine heat-induced change (e.g.: Bergslien et al., 2008; Schurr and Hayes, 2008), more information is known generally about the structure of bone than the elemental composition, and therefore it makes most sense to focus efforts here at this current time. In addition, understanding and manipulating heat–induced changes to the crystalline structure of bone is important for a number of reasons: clinically to ensure that biomaterials to be placed within the body have a similar crystalline structure to natural bone (Nakano et al., 2002; Wang et al., 2010), and to understand the nature of pathologies and diseases (Mkukuma et al., 2004).

Within the material sciences, crystallinity is related to solubility (Nakano et al., 2002). Heating the biomaterial is one way to influence the degree of bone mineral crystallinity. More generally an understanding of the influence of heating on

crystallinity can be important for understanding diet, hunting practices and funerary custom within archaeological contexts (Schiegl et al., 2003; Piga et al., 2010a; Piga et al., 2010b; Squires et al., 2011; Thompson et al., 2011) or for determining whether criminal activity has occurred and to aid in the identification process in forensic scenarios (Thompson 2004; 2005). Note that other techniques such as mechanical grinding can also be used to influence bone mineral crystallinity (Nakano et al., 2002; Surovell and Stiner, 2001).

In recent decades, research and experience of cases have greatly increased the ability to recognize and interpret the burnt bones. The ability to distinguish between burned human remains and other materials, and the determination of the combustion temperature, time duration and intensity distribution throughout the body after focusing on microscopic changes in the bone may be important in various situations such as accidents, suicides/homicides and studying the crime scene. Thus, new experimental methods are needed to clarify the variety of factors that lead to varying levels of thermal effects.

In addition to traditional research methods, the application of chemical and physical techniques such as X-ray diffraction (XRD) and Fourier transform infrared spectroscopy (FT-IR) is increasingly accepted in forensic contexts. X-ray diffraction and FT-IR analysis have several significant advantages which are complementary for our full understanding of the firing process whether in anthropological and forensic contexts.

1.3: Fossil bones

Hard tissues such as bones and teeth are often the only direct fossil remains of animals and humans and hence represent valuable archives for palaeoecology and palaeoenvironment.

If the bones are not subjected to microbial or biotic erosion or the processes are affected by drastic physical or chemical changes, fossilization may occur soon after burial (Trueman and Martill, 2002; Pfretzschner, 2004; Farlow and Argast, 2006). Some processes may occur to preserve rather than degrading fossils, particularly the

incorporation of new ions into the crystal structure and/or recrystallisation of skeletal apatite (Elorza et a., 1999; Hedges, 2002; Trueman and Tuross, 2002; Wings, 2004; Farlow and Argast, 2006). These processes are mainly controlled by abiotic, physical and chemical environmental soil conditions, particularly groundwater chemistry around the buried bone material (Trueman et al., 2004; Wings, 2004; Tütken et al., 2008).

The bone and tooth microstructure is often well-preserved down to the μm-scale in fossil specimens recording growth marks and other histological features that are often used for life history reconstructions of extinct animals or humans (e.g., Erickson, 2005; Smith, 2008).

The chemical composition of both the mineral phase bioapatite and the protein phase, predominantly collagen, yields important information about the palaeobiology and palaeoecology of fossil vertebrates (Overviews in: Kohn and Cerling, 2002; Hedges et al., 2006; Koch, 2007; LeeThorp, 2008). Especially tooth enamel is least affected by diagenetic alteration and able to preserve original element and isotope compositions over geological time scales of millions of years (e.g., Sponheimer and Lee-Thorp, 2006; Fricke et al., 2008; Heuser et al., 2011).

However, chemical *in vivo* signals are often altered during the fossilisation process of bones and teeth.

These chemical, mineralogical and histological changes during diagenesis themselves are a valuable source of information in their own right. They enable us to characterize the post mortem history, diagenetic milieu, taphonomic processes and the timing of fossilization (Berna et al., 2004; Pfretzschner, 2004; Trueman et al., 2006; Kohn, 2008; Tütken et al., 2008; Turner-Walker and Jans, 2008; Herwartz et al., 2011). Understanding, characterising and quantifying diagenetic processes in fossil skeletal remains are important to decipher to which degree the original chemical information stored in the bioapatite has been altered or retained. To characterize and quantify diagenetic processes and their influence on the structural and chemical integrity of fossil bones and teeth different chemical (IRMS, ICPMS), mineralogical (XRD, XRF), optical (light microscopy, CL, TEM), and spectroscopic (Raman, FT-IR) techniques can be applied.

Diagenesis of bones and teeth is however always a complex process that is very site specific, not linearly related with burial time and controlled by different external

factors such as microbial attack, temperature, humidity, hydrology, pH, redox conditions of the burial environment but also the skeletal tissue itself (e.g., Hedges and Millard, 1995; Hedges et al., 1995; Hedges, 2002; Pfretzschner, 2004; Berna et al., 2004).

Diagenetic alteration of bone starts immediately post-mortem (e.g., Bell et al., 1996) and significant alteration occurs even before burial (e.g., Trueman et al., 2004; Fernández-Jalvo et al., 2010).

The degradation of the collagen by microbial attack and/or hydrolysis (Collins et al., 2002) is one of the early and most fundamental alteration steps during bone diagenesis. The collagen molecules themselves, however, are fairly robust until a critical point in fibril denaturation due to hydrogen bond breaks is reached (Koon, 2006; Koon et al., 2010).

Collagen loss causes an exposure of the thermodynamically instable, nm-sized bioapatite crystals with a large and reactive surface area, leading to dissolution and/or recrystallisation and hence increasing apatite crystal size (e.g., Person et al., 1995; Berna et al., 2004; Trueman et al., 2004). During these fossilization processes an intense chemical and isotope exchange of the bone with the environment is possible either by adsorption of ions, diffusion, ion exchange in the apatite lattice or precipitation of secondary minerals in pore space (e.g., Nelson et al., 1986; Trueman and Tuross, 2002; Lee-Thorp, 2002; Kohn 2008).

Microbial attack by bacteria and fungi occurs rapidly post-mortem and is commonly observed in archaeological bone, resulting in characteristic tunnelling and destruction of the bone microstructure causing collagen loss and a spatial redistribution of bone material (Hedges et al., 1995; Bell et al., 1996; Jans et al., 2004; Turner-Walker and Jans, 2008; Jans, 2008).

In contrast, most palaeontological bones older than Middle Pleistocene do not show microbial alteration (Hedges, 2002; Trueman et al., 2002) and often a have perfectly preserved bone microstructure making them valuable archives for palaeohistology (Erickson, 2005). This highlights the importance of the early bone diagenesis (~10^3-10^4 years) for the fate of fossil bones of which many, especially those weakened by microbial attack, were dissolved and do not survive into the fossil record if stability conditions (appropriate soil pH) are not met in the burial environment (Berna

et al., 2004). Those fossil bones surviving in the burial environment were stabilized and in the long term lithified by the diagenetic processes.

Bone apatite crystallite size already begin to increase a few years post-mortem (Trueman et al., 2004), further increases when the collagen is lost, creating pore space for apatite crystal growth and may last up to ~5 Ma until Pliocene times (Piga et al., 2009a).

In the hypothesis that the post-mortem and burial changes (diagenesis) are associated to crystallinity of apatite from XRD analysis, it was suggested to relate this index to the age. This correlation was found by Bartsiokas and Middleton (1992) after examining 15 bony specimens, two of which were rejected from the analysis because of their "state of histological conservation". In the hypothesis of a first-order kinetics process, the relationship was expressed by a linear regression between the crystallinity index (CI) and logarithm of age.

Soon after, Person et al. (1995, 1996) defined a slightly different CI after considering a larger number of specimens of various provenance and age. They did not observe any significant correlation between the increase in the CI and the age of the sample, even in bones from the same locality. More recently (Farlow and Argast, 2006) it was reported further data consistent with the results of Person et al. (1995, 1996) in showing no relationship between bone crystallinity and age. However, for late Pleistocene and younger specimens, their data were consistent with the observations of Bartsiokas and Middleton (1992) and Sillen and Parkington (1996) for mammalian bone.

The apatite crystal size in ancient fossil bones is quite variable and some dinosaur specimens can even retain some crystallites similar in size to modern bone (Dumont et al., 2011). However, most fossil bones have larger average apatite crystallite sizes than modern bones but the crystal size in fossil bones remains in the few 100 nm-range (Piga et al., 2009a).

Thus fossilization processes of the phosphatic bone tissue predominantly take place at the sub-μm scale, explaining why the bone microstructure with histological features in the μm-range is usually so well preserved. On the other hand, the bone macro porosity such as blood vessel canals or bone cell voids as well as diagenetic cracks are often filled with secondary mineral infillings such as pyrite, calcite, quartz,

manganese- or iron(hydr)oxides and others. These minerals form at different stages either early or late during diagenesis and allow inferring the physicochemical milieu prevailing within the bone and in its burial environment during their formation and thus to trace taphonomic conditions (Barker et al., 1996; Hubert et al., 1996; Pfretzschner, 2000, 2001a,b, 2004).

1.4: Physico-chemical techniques applied for bone microstructure analysis

1.4.1: X-ray diffraction (XRD)

Powder X-Ray Diffraction (XRD) is actually one of the most widely used techniques to characterize the state of condensed, inorganic, organic materials, and sometimes biological molecules. It is a useful tool in different fields such as: solid state Chemistry, Pharmaceuticals, Natural Sciences, Metallurgy, Archaeometry, Archeology, Physical Anthropology and Forensic Sciences. In all these areas most of the crystallized matter that we can investigate are in fact in polycrystalline state; each crystal is the size of a few microns or even just a few nanometers.

The major breakthrough of the powder diffraction as a quantitative tool in material sciences happen in 1969 with the introduction of the so called Rietveld method (Rietveld, 1969) or whole pattern fitting profile refinement, a technique for crystal structure refinement which, for the first time, made use of the entire powder pattern instead of analyzing individual non-overlapped Bragg reflections. This method permitted an extension of the diffraction technique on polycrystalline compounds, from structural refinement to quantitative and structural and microstructural characterization.

In the Rietveld's approach the experimental powder diffraction data are utilized without extraction of the individual integrated intensities, and all structural, microstructural and instrumental parameters are optimized by a least-squared refinements method until to carry out the best fit between the experimental data and calculated pattern.

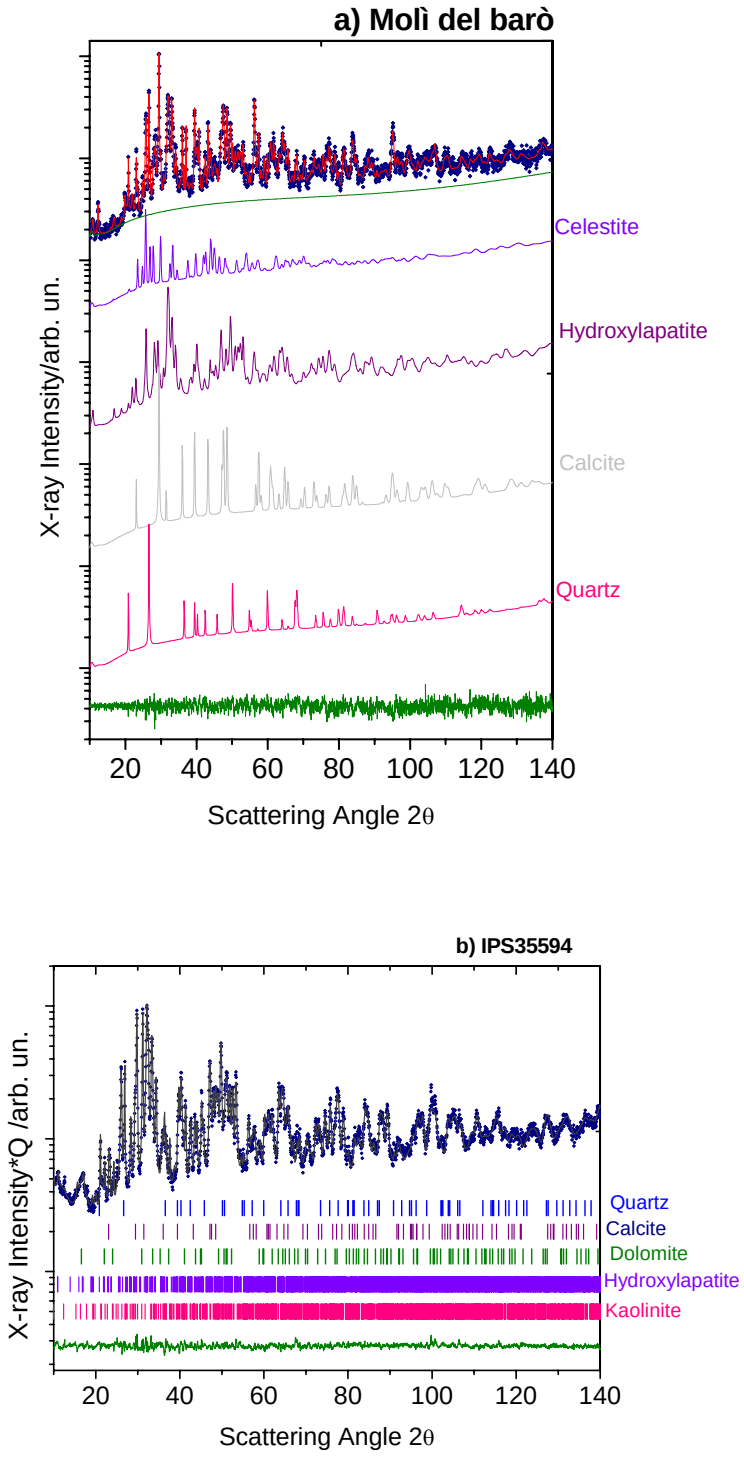

Figure 2: Two examples of fossil bones multiphase patterns a) the XRD pattern (data points) and Rietveld fit (full line) of *Molì del Baró* (Isona i Conca Dellà, Lleida, Spain) dinosaur specimen shows a rather complex phase constitution of four phases, with the notable presence of the celestite structure $SrSO_4$. b) the XRD pattern of *IPS 35594 Seimuromorpha* specimen (Middle Triassic, 245 Ma) also highlights a complex five phase constitution.

Full profile refinement is computationally intense and requires a reasonable starting structural model and a good set of experimental data for the analysis success.

An important application of the Rietveld's method in powder material field is on multiphase samples (see figure2a and 2b).

The knowledge of the spatial arrangement of atoms and molecule inside the unit cell and the fraction composition of different phases present in the polycrystalline compound under investigation, are complemented with the possibility to determine the microstructural information, such us dimension, orientation of crystallites and lattice disorder. The knowledge of these details can allow to determine or to hypothesize possible properties of such analysed materialWith all this in mind, it has been argued that a better and more reliable means of addressing the microstructural study of burned and fossil bones is the X-ray diffraction (XRD) approach, possibly combined with other types of physico-chemical and spectroscopic approaches (Shipman et al, 1984; Newesely, 1988; Stiner et al., 1995; Ravaglioli et al., 1996; Rogers and Daniels, 2002), with a particular view to the hydroxylapatite mineral phase, which is the main inorganic component of bones.

The hydroxylapatite phase is made of tiny micro- (or nano-) crystals with average size dimension around ca. 17 nm, that are subjected to growth changes when stimulated by the temperature of fire. Broadly speaking, higher temperatures result in larger average sizes of hydroxylapatite nano-crystals, more ordered crystal structures and sharper XRD peak profiles. These heat-induced crystal changes are akin to those resulting from standard bone diagenesis, and therefore we acknowledge that in the absence of important thermal effects, bone material decomposing for millions of years may undergo to a similar crystal growth mechanism, which can be suitably detected and accurately measured with help of the XRD patterns (Bartsiokas and Middleton, 1992; Person et al., 1995; Farlow and Argast, 2006).

In 1926, De Jong (*In* Susini, 1988) connects the small crystals with diffuse diffraction lines and noted that the cremated bones patterns have finest lines. According to Payne (1937), refinement of lines observed is due to a mechanism of recrystallization of the bones. In the same way, Baud et al. (1954) reported that this refinement was due to the increase in crystal size.

The XRD technique was first applied to archaeological subjects in 1964 (Perinet, 1964) to study burnt bones at different temperatures. Perinet (1964) found no changes in the mineral before 550°C. According to him, an abrupt change occurs when tricalcium phosphate is converted into a little crystalline hydroxylapatite between 550 and 600°C. At 700° C, crystallization improves revealing refinement of the diffraction peaks. Finally, at high temperature, there would be no change in the diagrams. In addition Perinet (1964) observed that at 600°C the hydroxylapatite mineral is very little crystalline and only at 650°C improves his crystalline state. From 700°C, the crystalline phase is stable. On the basis of this work, there is no difference between bones and the bones as they are burned at least 600°C.

Later Bonucci and Graziani (1975) demonstrated that high temperatures of fire treatment induce a growth of the average crystallite size of hydroxylapatite, which can be appreciated relatively well from the line broadening/sharpening analysis of diffraction peaks. Since then, XRD has become a standard tool in anthropological work, although its adoption in forensic anthropology has been slow.

However, subsequently Bartsiokas and Middleton (1992), with the aim of characterizing and dating recent and fossil animal and human bones, suggested measuring a so-called crystallization index from their diffraction patterns, which can be mainly ascribed to the presence of natural apatite phase. The crystallization index, which is strictly related to the peak sharpening effects, was actually defined as the intensity ratio of (300)/(202) line profiles of hexagonal apatite, which normally occur as shoulder of the most intense (211) line in the 2θ angular range from 31° to 35° when using CuKα radiation (Person et al., 1995; 1996). A linear correlation between crystallinity index and bone age was reported over a period length of more than 10^6 years. It should also be noted that another crystallinity index was almost concomitantly defined by Person et al. (1995) using more peaks belonging to the same angular range.

It is clear that the two above mentioned lines of work may be conflicting especially if the bones were subjected simultaneously to both physical effects of burning and blackening across very long periods of time. This is further complicated but the fact that there have been very few studies exploiting this technique in the twenty years since it is first serious adoption.

Studies by Newesely (1988), Holden et al. (1995), Stiner et al. (1995), and Rogers and Daniels (2002) have superficially investigated this source of information, but lack the cohesive nature necessary to allow one to overcome this sort of conflicts.

However, in a sufficiently short period of time it seems that the two effects can be assumed well distinct. As a matter of fact, the time period investigated by Bartsiokas and Middleton (1992) requires some millions of years to observe significant changes in the crystallization index, which is a quantity determined with a small percentage error. This means that the crystallinity index may be regarded virtually unchanged in a period in the order of ten thousand years, that is, in a period that comprise archaeological and forensic times.

In the first critical study of its kind, Shipman et al. (1984) investigated the microscopic morphology of various osteological materials and used X-ray diffraction in order to assess whether specimens of unknown taphonomic history were burnt and the maximum temperature reached by those specimens. Like the previously cited studies, these investigations were based on the fact that heating of bone causes a sharpening of diffraction patterns, attributed to increased crystallite size and decreased lattice strain (i.e. increased organisation of the crystal structure) of osteological phases. Holden et al. (1995), Rogers and Daniels (2002) and other recent works (Thompson, 2005; Kalsbeek and Richter, 2006) have also recorded key crystalline changes within the temperature range of 700-1100° C. The potential for XRD to associate crystal change to burning context is therefore not in doubt. The heat-induced (H-I) changes in bone have been categorised by Mayne Correia (1997) and modified by Thompson (2004). All heat-induced changes (colour change, weight loss, fracture formation, changes in strength, recrystallisation, porosity change, dimensional change) can be placed within one of the four stages of H-I degradation (Dehydration, Decomposition, Inversion, Fusion). These four stages in themselves do not explain all of the fundamental causal changes occurring within hard tissues, and to date are entirely theoretical (Thompson, 2004).

In Physical Anthropology perspective, the temperature range 700–1100°C is significant because it is during this transition that the size of the bone alters to a statistically significant degree (Shipman et al, 1984; Thompson, 2005). This in turn will not only impact on microstructural studies of bone, but also on macroscopic analysis with a view to determining a biological profile (sex determination, age-at-death

estimation etc) of the burned individual. The accuracy of such biological or osteological profiles is dependent on the use of unmodified bone. This is true for both metric and morphological anthropological techniques. Therefore it is essential that we understand the osseous changes during this temperature range so that it is possible to create either new techniques devised specifically for burned bone or new methods of statistically correcting the output of current anthropological techniques when used on burned bone (Thompson, 2005).

Furthermore, a more solid appreciation of these changes will allow archaeologists to differentiate burned bone from non-burned bone using XRD as has been attempted so infrequently (Stiner et al, 1995).

In order to further extend the validity of XRD methodologies that appear in the literature, Piga et al. (2008b; 2009b) did a calibration for bones and teeth as a function of a range of temperatures of burning (200°C–1000°C), while simultaneously noting the effect of duration of burning (0, 18, 36 and 60 min). This would enable a more general account of a real firing process. In fact, with this approach it will be possible to make an accurate estimation of both temperature and likely time duration of the firing process involved. In particular, Piga et al. (2008b; 2009b) analysed the behaviour of the bone sample for some intermediate temperatures (650, 750, 775, 825, 850°C) to closely investigate and describe the two-stage growth regime of hydroxylapatite previously observed around 700°C (Enzo et al, 2007). This is not possible with current macroscopic approaches.

The kinetics of crystallite growth is followed in relation to the temperature and time duration in order to quickly and reliably evaluates the various aspects involved in the cremation process. In fact, with this approach it will be possible to make an accurate estimation of both temperature and likely time duration of the cremation rite.

1.4.2: Fourier Trasform Infra-Red Spectroscopy (FT-IR)

The Crystallinity Index (CI), or Splitting Factor (SF) is a measure of the crystallinity, or microscopic structural order, of osseous material. It is an arithmetic determination based on spectral data, and can be applied to both bone and teeth, although judging by

comments made by the few studies that have used it on teeth (Piga et al., 2009b) it is unlikely that the two apatite structures can be directly compared. This structural order is reflected by the splitting of the phosphate absorption peaks as seen in these spectra (Brock et al., 2010; Lebon et al., 2010). In fresh, unaltered bone, the crystal structure is poorly ordered, contains small crystals and as a consequence has a greater strain; unaltered bone therefore has a low CI value. Altered bone, whether that is due to age-related diagenesis or heat-induced transformation, has an increasingly ordered crystal structure with larger crystals and less strain, which therefore results in a measurably higher CI value. Naturally, the reality is more complicated. There is some debate as to whether CI values increase due to an increase in crystal size or a removal of more soluble, less ordered crystals (Wright and Schwarcz, 1996). Rogers and Daniels (2002) argue that their X-ray Diffraction data support the increase in crystal size, but they also add the caveat that the change could be due to the redistribution of existing crystals. Hiller et al. (2003) concur with the increase in crystal size as recorded by small-angle X-ray scattering (SAXS) but note that crystal shape and thickness also change with burning. Person et al. (1996) argue for the importance of the organic phase in protecting the inorganic phase from change and therefore has an influence on CI although this will only occur up until the point that the organic phase is lost. Trueman et al. (2008) and Lebon et al. (2010) concur, but explain this more specifically by arguing for the significance of the organic phase in reducing bone porosity and therefore crystal surface area exposure to the environment.

CI can be measured with both X-ray Diffraction (XRD) and Fourier Transform Infrared Spectroscopy (FT–IR). Although both methods have been used in the literature (e.g: Piga et al., 2010a) the Crystallinity Index values created using XRD cannot be directly compared to those created using FT–IR (Chakraborty et al., 2006; Rogers and Daniels, 2002; Thompson et al., 2009), although attempts at calibration have been made (e.g. Munro et al., 2007; Pucéat et al., 2004). This is because the XRD method utilises a volume averaging approach while the FT–IR method uses an area average approach (Rogers and Daniels, 2002). Both methodologies are complementary, but FT–IR does allow for the examination of CO_3^{2-} content and fluorine substitution, for the detection of trace components within the analysed material, has the potential for being portable into the field, can be cheaper to use and has been shown to be more accurate at lower

burning temperatures (Munro et al., 2007; Weiner et al., 1993; Wright and Schwarcz, 1996). However FT-IR approach is not free of criticisms; in this sense Pucéat et al. (2004) stated that it is overly sensitive to CI changes at low crystallinities and that carbonate content has more influence on FT–IR results than XRD. In addition, Rogers et al. (2010) argue that it does not provide necessary information on crystal shape and orientation.

The earliest examples of CI were provided by Shemesh (1990) and Weiner and Bar-Yosef (1990) and can be calculated using FT–IR by adopting the following equation:

$$\mathbf{CI = A_{565} + A_{605} / A_{595}}$$

the heights of the absorptions at about 605 and 565 cm^{-1} were added and then divided by the height of the minimum between them, where A_x is the absorbance at given frequency x (see Fig. 3a).

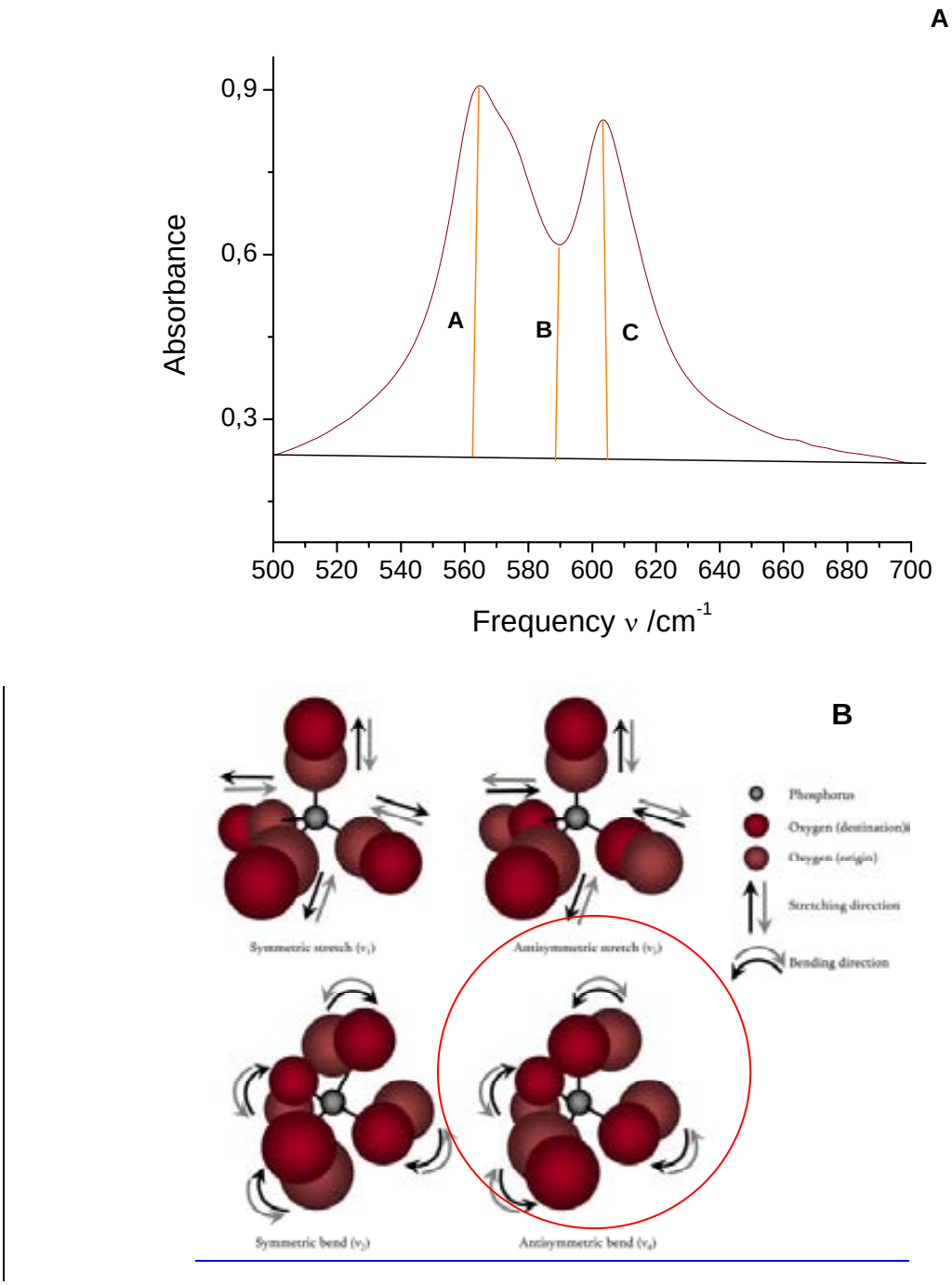

Figure 3: a) a FT–IR spectra of unburned bone, shown in the range of 500-700 cm^{-1}, corresponding to the phosphate group PO_4^{3-}characteristic of the hydroxylapatite. The dimensions factor CI are calculated numerically in this group of peaks. b) The asymmetric bending to which the two most intense lines are referred have a physical counterpart evidenced by the circle in the left hand side scheme of motions available for the phosphate group

Both A_{565} and A_{605} correspond to the two anti-symmetric bending vibration bands of phosphate (ν_4 PO_4) (Lebon et al., 2010) (see Fig. 3b). It is assumed that the value of the CI is related to crystal size or structural order.

As crystal size increases, A_{565} and A_{605} both also increase whilst A_{595} decreases. This has the effect of CI increase. This CI determination has been followed with remarkable consistency by those who have attempted to apply this methodology in bioarchaeological contexts. Unfortunately for osteoarchaeologists, the changes to crystallinity resulting from burning mirror those caused through natural ageing, and unpicking these two signals from CI values is problematic.

Bartsiokas and Middleton (1992) argue that such time-based changes take tens of millennia. The reality is far from clear, although Rogers et al. (2010) have noted differences in crystal shape and orientation as a result of the two forms of change. Nonetheless it has been successfully, if not widely, adopted by the archaeological community.

Another index useful to make the difference is the Carbonate/Phosphate ratio. The Carbonate (CO_3) gives absorption peaks at 710, 874 and 1415 cm^{-1} whereas PO_4 gives absorption peaks at 565, 605 and 1035 cm^{-1}. The carbonate absorption peak at 710 cm^{-1} is characteristic of $CaCO_3$ and can therefore be used to detect absorbed $CaCO_3$ contaminants.

As the absorption peak height at 1415 cm^{-1} and 1035 cm^{-1} is proportional to the content of carbonate and phosphate, the Carbonate/Phosphate ratio is given by the equation below:

$$\mathbf{C/P = A_{1415} / A_{1035}}$$

where Ax is the absorbance at given wavelength x. (Shemesh, 1990; Wright and Schwarcz,1996; Koon et al., 2003; Olsen et al., 2008; Thompson et al., 2009, 2011; Piga et al.,2010a).

Note that some publications use a slightly different definition for this ratio (Pucéat et al., 2004). Since these peaks correlate to the amount of carbonate and phosphate, this ratio allows one to comment upon changes to the carbonate content bone following burning (Thompson et al., 2009). Combination of both CI and CP has been

used to successfully show differences in cremation and funerary practices (Squires et al., 2011).

1.4.3: Applications of the FT-IR Cristallinity index in Bioarchaeology and Anthropology

Generally, when the CI has been applied to bioarchaeological contexts it has been from one of three main perspectives.

First, it has been used to distinguish bone samples from one contextual sequence from another one. The underlying principle is that bone from context A will have undergone different diagenetic changes than bone from context B.

Generally these contexts differ as a result of chronological age. Work using real samples has shown that actually, there is a great deal of variation in the CI values of specimens within the Holocene period alone (Sillen and Morris, 1996). In terms of relating CI to the age of a sample, there seems to be many complicating factors which influence the rate of CI increase. These are highly related to the specific burial environment, and include both hydrology and geology (Piga et al., 2009a; Sillen and Morris, 1996).

Furthermore it is worth noting that burial environments do not remain static over time (Zapata et al., 2006). Cave environments in particular are noted as being particularly problematic in terms of diagenetic pathways (Sillen and Morris, 1996). Regardless of the specific deposition environment, separating samples into different age periods will always be more accurate with samples that are spatially located closer to each other (Sillen and Morris, 1996). Nevertheless, the difference between younger and considerably older samples is great enough to allow separation of samples into different contexts. Sillen and Morris (1996) demonstrated this by placing bone samples from unknown contexts into one of two specific sequences (modern or Middle Stone Age) at Border Cave, South Africa.

More recently Stiner et al. (2001) utilised CI to examine stratigraphic layers from Hayonim Cave in Israel. Examination of apatite crystallinity using FT–IR has also been used to distinguish between natural and synthetic calcium hydroxylapatite

(Chakraborty et al., 2006). It has also been noted that natural, geological apatite, as opposed to bioapatite has an inherently more ordered crystalline structure (Bergslien et al., 2008) and the two are therefore distinguishable. Whilst there seems to be great potential in relating crystallinity or crystal size to age (Bartsiokas and Middleton, 1992; Piga et al., 2009a) or depositional sequence, it is tempered by the fact that some studies have found little or no correlation between CI and the age of a bone sample (Person et al., 1996; Schwarz et al., 2009; Shemesh, 1990).

Second, CI has been used as a proxy for preservation, or rather as a means of determining the degree of degradation of an osseous sample. This is used prior to more expensive and complicated analyses, such as DNA extraction. Generally within Bioarchaeology, "no simple, or single, method has yet been proposed that is a reliable measure of bone integrity, i.e. one that is capable of predicting whether any biological information is retained" (Trueman et al., 2008; 160). As such, there is great interest in the CI since it may have the potential to be this method.

States of preservation have been correlated to CI on a number of occasions (Bartsiokas and Middleton, 1992; Sillen and Morris, 1996; Wright and Schwarcz, 1996). Other more recent studies have found no relationship between crystallinity or degree of preservation and quality of biomolecules contained within the bone (Brock et al., 2010; Lebon et al., 2010; Misner et al., 2009; Pucéat et al., 2004; Schwarz et al., 2009; Trueman et al., 2008). This may be due to the continued change in crystallinity after the loss of the organic material, thus negating the relationship between the two (Brock et al., 2010; Trueman et al., 2008).

Third, the CI has been used within the burned bone powders as a means of commenting on the severity of burning experienced. This can begin, as with Shahack-Gross et al. (1997) and Piga et al. (2008b), with simply determining if burning took place on dark coloured bones; but this can be extremely difficult with low intensity heating events (Koon et al., 2003). Oftentimes CI is applied with the aim of predicting the temperature of burning event. This is of value in itself, but it has also been argued that changes at microscopical level of bone need to be understood fully if we want to be able to reconstruct the pre-burning conditions and dimensions of bones, and therefore create corrections for our osteological profiling techniques (Thompson, 2004, 2005). Different works have consistently shown that the relationship between crystallinity and

temperature of burning is non-linear (Enzo et al., 2007; Person et al., 1996; Piga et al., 2008b; Surovell and Stiner, 2001; Thompson et al., 2009). This may be the result of the protection of the crystal structure by the organic phase as suggested by Person et al. (1996) with a subsequent increase in CI change after the organic phase is lost resulting in the non-linear relationship. Indeed Munro et al. (2007) noted that even a loss of 25% of the organic content does not seem to affect the CI values. Unfortunately the sample sizes of these studies are often small, which results in the burning temperature prediction equations being of use only on samples from the same context. Even then, some blind studies are quite inaccurate (see Thompson et al., 2009). A significantly larger collection of data will help to resolve this problem, and may result in more universal formulae.

2: AIMS OF THE THESIS

The main aim of this thesis is to found some objective methods to evaluate the most extreme states of alteration of bone due to cremation and fossilization processes.

The investigators were already aware of the dramatic changes occurring in the bone structure since the last three decades. Archaeological, Anthropological, Paleontological and Forensic issues required specific studies to solve some puzzling questions arising either from examination of archaeological and crime scene and specific digging contexts. In these sense, applications of physico-chemical techniques seems to be very useful, especially X-Ray Diffraction (XRD) and Fourier Transform Infrared Spectroscopy (FT–IR).

To reach these objectives, we have considered various sub-objectives at least in two different situations in the following:

2.1: Burned bones:

a) evaluating the applications of physico-chemical techniques in Forensic Sciences.
b) evaluating the possibility of a multi-technique approach by XRD, SAXS and FT–IR for the analysis of burned archaeological bones.
c) applying physical-chemical analysis to different archaeological contexts in order to verify if a bone has been burned or not; finding explanations to some specific funerary rites, getting a reasonably precise temperature range and its duration across the entire body; checking temperature homogeneity throughout the skeleton.
d) assessing whether the lattice parameters of bioapatite obtained by XRD data are helpful when trying to distinguish human bones from animal bones.

2.2: Fossil bones:

a) applying the physical-chemical analysis to evaluate the diagenesis of fossil bones.
b) evaluating the use of average crystallite size as dating method.

3: METHODS

3.1. Diffraction data collection and analysis

Exactly 0.5 grams of each bone was ground in an agate jar for one-minute using a SPEX mixer-mill model 8000. Our sample holder for XRD analysis has a circular cavity of 25 mm in diameter and 3 mm in depth, and can hold 420 mg of pressed powder bone.

Given the high number of specimens to be examined, the XRD patterns were recorded overnight using Bruker D8 (see figure 4), Philips PW-1050 and Siemens D-500 diffractometers in the Bragg–Brentano geometry with CuKα radiation (λ = 1.54178 Å).

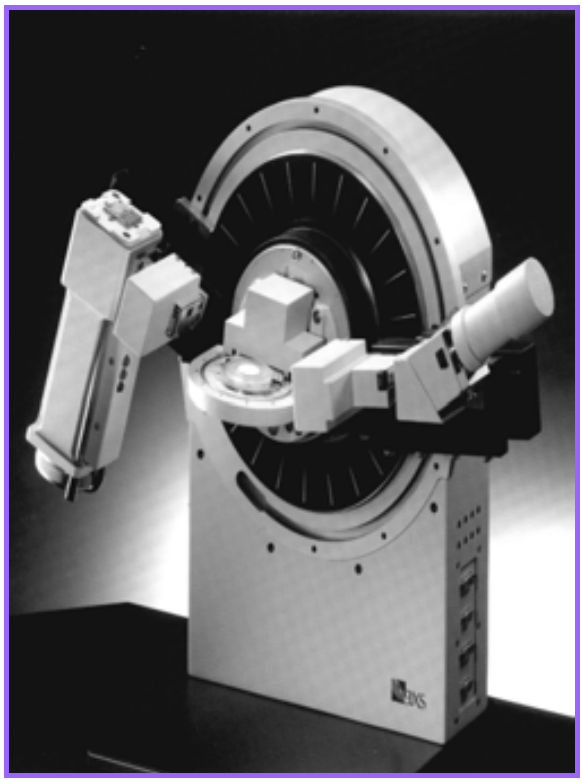

Figure 4: Bruker D8 diffractometer

The instruments were employed in the Bragg-Brentano geometry using fixed wavelength CuKα radiation and a graphite monochromator in the diffracted beam. The patterns were collected with a scintillation detector in the 2θ angular range from 9 to 140°, with a step-size of 0.05°; the counts at each data point being accumulated for 40s

in order to ensure accurate statistics for the intensity data and to reduce the uncertainty associated with the determination of lattice parameters.

The X-ray generator worked at a power of 40 kV and 40 mA and the resolution of the instruments (0.5° divergent and 0.1 mm antiscatter slits) was determined using α-SiO_2 and α-Al_2O_3 standards which were free from the effect of reduced crystallite size and lattice defects (Enzo et al., 1988).

The precision and accuracy of lattice parameters depends largely upon the number of peaks assessed and the relative location in the 2θ scale with respect to the whole angular range investigated (Masciocchi and Artioli, 1996; Petersen, 2005). Note that the use of position sensitive detectors for faster data collection may speed-up the data collection, the configuration used here (with a monochromator in the diffracted beam) has the advantage of controlling the background due to specific fluorescence effects. This will increase the time taken for data collection, and we are aware that the laboratory high-resolution conditions may be overtaken by accessing synchrotron radiation facilities for powder XRD.

Starting with some basic information on the sample (e.g., the alleged constituent elements, the space group of phases) it is possible to obtain qualitative information (type of phase, crystal habit and quantity -by weight or volume fraction of the phases present- unit cell size, crystallite size, microstran).

The phase content, the lattice parameters of the elementary cell, the degree of occupancy of atomic sites, the size of the coherent diffracting domains and the degree of deformation of the crystallites can be refined using the Rietveld approach with some precision that depends significantly on the experimental quality of the pattern,

Practically, each crystalline phase leads to a characteristic diffractogram that corresponds to a fingerprint of the substance. The presence of several phases obviously complicates the spectra interpretation.

However, it is commercially available a series of programs of automatic recognition of phases sufficiently reliable that makes use of the archive of the diffractograms of all substances hitherto qualified with the diffraction. Unfortunately it can happen that the spectra of diffraction can not be always collected with the necessary signal to noise ratio because of the lesser amount of available substance. In addition, not all spectra catalogued in the database have been resolved correctly.

Under these conditions, the automatic assignment of phases is unlikely to be successful, providing results that may be unreasonable. Obviously, this method of recognition is valid when our patterns refer to phases that had been previously resolved with adequate accuracy.

The Rietveld method (Rietveld, 1967; Young, 1993) is based on an iterative best-fit strategy of experimental data. We have made use of the MAUD programme (for: *Material Analysis Using Diffraction*) which simulates the pattern by incorporating the instrument function and convolving the crystallographic model based on the knowledge of chemical composition and space group with selected texture and microstructure models (Lutterotti and Bortolotti, 2003).

The programme MAUD permits a selection of variables for the least squares minimization such as lattice parameters of the unit cell, atomic positions, temperature factors, occupancy of the sites, an/isotropic size and strain broadening.

Concerning the structure of bones, it is known that they are made mainly by the bioapatite phase, in particular circumstances accompanied by other secondary phases like calcite or others. There is a debate in the literature whether the monoclinic $P2_1/b$ rather than hexagonal $P6_3/m$ choice of the space group is more suitable to describe the bioapatite structure of bone. Extensive comparisons of the use of these two representations for the symmetry properties were missing in the literature. In particular it was not assessed whether such choice may have direct consequences for determining the values of the lattice parameters. The success of the procedure is generally evaluated throughout a combination of integrated agreement factors (R_{wp} is the most considered) and distribution of residuals (Young, 1993).

3.2: FT–IR analysis

Infrared spectroscopy is an extremely reliable and well recognized fingerprinting method. Many substances can be characterized, identified and also quantified. One of the strengths of IR spectroscopy is its ability as an analytical technique to obtain spectra from a very wide range of solids, liquids and gases.

A few milligrams of each sample were ground with an agate mortar and pestle to obtain a grain size smaller than 5 μm. 7-mm Pellets were prepared by mixing 2.5 ± 0.1 mg of bone powder with ca. 300 mg of KBr. This mixture was compressed at 11 ton/cm^{-2} for 1.5 min following the protocol described by Fröhlich (1989). Infrared spectra were collected using a Bruker Vertex 70V spectrometer (see figure 5) by accumulation of 128 scans with a resolution of 2 cm^{-1}.

Figure 5: Bruker Vertex 70V spectrometer.

The mineral composition was monitored using carbonate and phosphate vibration bands. Relative carbonate content was estimated from the ratio between the absorbance of the ν_3CO_3 band at 1415 cm^{-1} and the ν_3PO_4 band around 1045 cm^{-1} (Wright and Schwarcz, 1996). The splitting factor (SF) was measured from the two anti-symmetric bending vibration bands of phosphate (ν_4PO_4) at 565 and 605 cm^{-1} following the method of Weiner and Bar-Yosef (1990) between 495 and 750 cm^{-1}.

The peaks were processed using standard non-linear least squares fitting procedures incorporated in the Origin® software assuming for the transmitted line shape a symmetric Pearson VII type function and a polynomial background of order 1 or 2.

3.3: XRF analysis

XRF measurements have been carried out using portable equipment composed of an X-ray tube (molybdenum anode, Oxford Instruments) working at 25 kV and 0.1 mA. For the analysis we pressed ~ 200 mg of powdered bone tissue to form a pellet

with a diameter of 10 mm and a thickness of 1 mm. An aluminium collimator 1 cm long and with an internal hole of 1 mm in diameter permits irradiation of an area of the object of about 0.2 cm^2 to be analysed, at a distance tube window-sample of about 2 cm. A Si-PIN detector from AMPTEK was employed with a thickness of about 300 μm and characterized by an energy resolution of about 200 eV at 5.9 keV. 30 minutes was dedicated for each sample pattern without use of any standard.

4: RESULTS

Chapter 4.1: Aplicaciones de técnicas químicas-físicas en Antropología Forense

Authors: **Giampaolo Piga, Assumpcio Malgosa.**

Cuadernos de Medicina Forense 18 (1), 9–17.

In recent decades, research and experience of cases have greatly increased the ability to recognize and interpret the burnt bones. The ability to distinguish between burned human remains and other materials, and the determination of the combustion temperature, time duration and intensity distribution throughout the body after focusing on microscopic changes in the bone may be important in various situations such as accidents, suicides/homicides and studying the crime scene. Thus, new experimental methods are needed to clarify the variety of factors that lead to varying levels of thermal effects.

In addition to traditional research methods, the application of chemical and physical techniques such as X-ray diffraction (XRD) and Fourier transform infrared spectroscopy (FT–IR) is increasingly accepted in forensic contexts. X-ray diffraction and FT–IR analysis have several significant advantages which are complementary for our full understanding of the firing process whether in anthropological, forensic or palaeontological contexts.

Contribución especial

Aplicaciones de técnicas físico-químicas en Antropología Forense

The application of physico-chemical techniques to Forensic Anthropology

G. Piga[1,2]
A. Malgosa[1]

[1]GROB (Grup de Recerca en OsteoBiografia). Unitat d'Antropologia Biològica, Departament de Biologia Animal, Biologia Vegetal i Ecologia, Universitat Autònoma de Barcelona, España.
[2]Dipartimento di Chimica e Farmacia, Università di Sassari. Italia.

Correspondencia:
Dra. Assumpció Malgosa.
E-mail: assumpcio.malgosa@uab.cat.

Resumen

Los efectos del calor extremo sobre los restos óseos es un tema de gran interés para el mundo forense. La literatura en rápido crecimiento en esta área de las ciencias forenses incluye investigaciones experimentales que analizan la dinámica del impacto térmico sobre la estructura del esqueleto y su morfología. Además de los métodos tradicionales de investigación, la aplicación de técnicas químico-físicas como la difracción de rayos X (DRX) y la espectroscopia de infrarrojos por transformada de Fourier (FT-IR) es cada vez más aceptada en distintos contextos forenses. Los campos de aplicación se refieren principalemente a la capacidad para distinguir entre restos humanos quemados y otros materiales, la determinación de la temperatura, el tiempo de combustión y su intensidad en todo el cuerpo, en diversas situaciones como accidentes, suicidios/homicidios y el estudio de la escena del crimen.

Palabras clave: Huesos quemados. DRX. FT-IR. Índice de cristalinidad. Temperatura.

Abstract

The effects of extreme heat on the skeletal remains are a subject of great interest to the forensic world. The rapidly growing literature in this area of forensic science includes experimental investigations that analyze dynamics of thermal impact on the skeletal structure and morphology.

In addition to traditional research methods, the application of chemical and physical techniques such as X-ray diffraction (XRD) and, Fourier transform infrared spectroscopy (FT-IR) is increasingly accepted in forensic contexts. The ability to distinguish between burned human remains and other materials, and the determination of the temperature, the combustion time and intensity throughout the body may be important in various situations such as accidents, suicides / homicides and studying the crime scene.

Key words: Burned bones. XDR. FT-IR. Cristallinity index. Temperature.

Introducción

El estudio de los restos humanos quemados es de gran importancia en la arqueología, las ciencias forenses, la antropología forense y la investigación de la escena del crimen. En el campo de las ciencias forenses, existen una gran variedad de situaciones que pueden conllevar la cremación de restos óseos, incluyendo los accidentes de aviación, los bombardeos, las explosiones y terremotos. También los homicidios, suicidios y muertes accidentales pueden implicar el uso de fuego con resultados variables sobre los restos humanos.

El fuego es un método común para tratar de ocultar la evidencia de la actividad criminal infligida sobre víctimas humanas. El fuego puede ser utilizado por el autor para: 1) destruir totalmente el cuerpo, 2) destruir las características que permiten la identificación de víctimas (rasgos faciales, huellas dactilares), o 3) destruir pruebas relacionadas con las circunstancias que rodean la muerte[1]. El deterioro o la desaparición de los tejidos blandos por el fuego dificulta notablemente o impide totalmente el análisis por otros especialistas (como los médicos forenses) y, por tanto, el análisis de los restos humanos quemados es una tarea comúnmente atribuida a los antropólogos forenses.

Fecha de recepción: 17.MAR.2012
Fecha de aceptación: 23.MAR.2012

Por otro lado, también las muestras arqueológicas pueden presentar evidencias de incineración y su análisis proporciona datos relevantes para reconstruir el ritual funerario y por tanto para entender cuestiones trascendentales de las poblaciones del pasado[2,3].

Así pues, la comprensión de los cambios que el cuerpo ha sufrido como consecuencia de su exposición al fuego puede proporcionar información importante sobre el contexto y las condiciones del evento de cremación. Dicha información puede incluir la escena del crimen, la temperatura del fuego, y la presencia de acelerantes. En este sentido, se dispone de información sobre la temperatura que alcanzan algunos combustibles al arder al aire libre: por ejemplo, la grasa animal a 800-900ºC, el queroseno a 990ºC, la gasolina a 1.026ºC, la madera a 1.027ºC y el metanol a 1.200ºC[4].

Puesto que la cremación puede conducir a la fragmentación extrema del hueso, se requiere una especial atención durante el análisis de la escena. Los escenarios de incendios mortales suelen ser mucho más complejos, no sólo porque el cuerpo y los elementos de identificación son drásticamente modificados por el fuego, sino porque todo el entorno, todo el contexto, también se modifica en la misma manera, resultando en una coloración homogénea y en la mezcla de todos los materiales.

Idealmente, los antropólogos forenses deberían participar en la recuperación, ya que están capacitados para reconocer los restos humanos fragmentados. Aún así, puede ser un reto, incluso para antropólogos entrenados, el distinguir pequeños fragmentos de huesos quemados y dientes a partir de fragmentos carbonizados de materiales de construcción y otros.

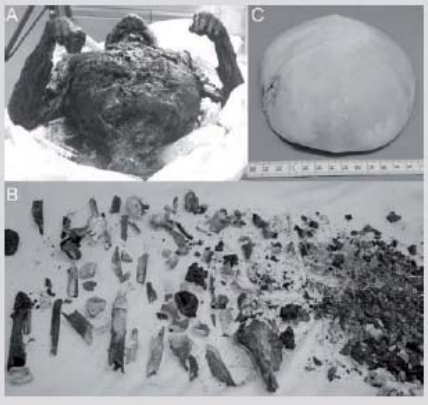

Figura 1.
Cadáver que fue sometido a incineración afectando de forma parcial el cuerpo (1a). La parte inferior fue reducida a cenizas (1b), mientras que la calota craneal permaneció intacta (1c) (fotos por cortesía del Dr. Ignasi Galtès).

Por otro lado, la capacidad de discriminar entre restos humanos quemados (cenizas) y polvo de otros materiales de apariencia similar puede ser de gran importancia en una variedad de situaciones. El incidente de Tri-State en Noble (Georgia, Estados Unidos)[5] es el ejemplo más conocido. A principios de 2002, se descubrió que en lugar de realizar las incineraciones contratadas, el propietario de Tri-State enterraba los cuerpos alrededor de su propiedad, sin ningún tipo de ceremonia. Con el tiempo se recuperaron más de 330 cuerpos, mientras que las urnas que habían recibido muchas familias a menudo contenían polvo de cemento, sílice, piedra y otros materiales. La confusión fue enorme ya que la mayoría de los cuerpos recibidos antes de cierta fecha fueron realmente incinerados, y más tarde, algunos cuerpos podrían haber sido enviados a otras instalaciones para una incineración apropiada. Cientos de familias no estaban seguros del contenido de las urnas en su poder. Así pues, incluso las cremaciones comerciales presentan problemas para el médico forense y las disputas sobre las cremaciones comerciales pueden desembocar en un litigio civil que puede implicar el análisis forense de los materiales recuperados.

El análisis de los restos resultantes de la cremación comercial incluye también la evaluación del número mínimo de individuos y de las posibles mezclas, así como la identificación. Frecuentemente la recuperación y el análisis de inclusiones, tales como placas metálicas de identificación, restauraciones dentales y los materiales quirúrgicos facilitan las identificaciones.

Por desgracia, el acto de quemar aunque no llegue a la incineración total provoca una serie de cambios sustanciales en el cuerpo y en el esqueleto, que a su vez puede afectar los intentos de proporcionar la identificación de los fallecidos. La investigación ha demostrado que tanto los métodos morfológicos y métricos de evaluación antropológica como los métodos de datación, elementos traza[6] y análisis de isótopos estables, se ven afectados.

Tradicionalmente se ha utilizado la inspección visual de los restos para discriminar si los huesos han sido sometidos al fuego, y más allá de esto, asociaciones entre el color del hueso y el tipo de fractura con la temperatura del fuego, o con la presencia o ausencia de tejidos blandos en el momento de la exposición[7,8].

Sin embargo, estas asociaciones son complejas, no totalmente biunívocas, y los vínculos espurios. Por ejemplo, en algunos casos de homicidio en los que el fuego fue usado para encubrir las pruebas, los cuerpos fueron sometidos a diversos grados de combustión (Figura 1a y 1b); la observación del color de

las diversas partes del esqueleto como única referencia, podría haber proporcionado una información inexacta o incompleta en la que incluso se puede excluir la presencia de fuego en alguna parte del esqueleto (Figura 1c).

También se ha demostrado experimental y estadísticamente que los cambios más importantes en el hueso que pueden predecir el contexto de una cremación implican cambios en la microestructura ósea[9]. Por ello, se ha argumentado que la mejor forma, y la más confiable, para abordar los problemas relacionados con la exposición al fuego es la utilización de métodos físico-químicos, posiblemente en combinación con otros tipos de métodos microscópicos, dedicando una atención especial a la fase mineral de la hidroxiapatita (HA), que es el principal componente inorgánico del esqueleto.

Las técnicas de difracción de rayos X (XRD) y la espectroscopia de infrarrojos (FT-IR) se pueden utilizar para distinguir los materiales óseos de otros tipos de materiales cuando el contexto forense no está claro, y para evaluar la estructura cristalina del hueso quemado, lo que, a su vez, se puede relacionar con la temperatura y la intensidad de la cremación.

Métodos químicos-físicos para el análisis de cremaciones

La medida del índice de cristalinidad (IC) se ha utilizado para estudiar los cambios en la microestructura del hueso. El IC es una medida del orden existente dentro del cristal, de la deformación y la organización en el hueso. Cuando el hueso es fresco, la estructura química es poco cristalina[10,11], en parte como resultado de la sustitución de carbonatos por fosfatos causando un desorden del cristal[12].

La cristalinidad no es uniforme en todo el esqueleto, y varía entre los diferentes tejidos mineralizados del cuerpo humano[13]. También se ha demostrado que la edad afecta la cristalinidad, ya que a menor edad el hueso es menos cristalino que un hueso maduro[10].

Como resultado de la acción del calor sobre el hueso y su posterior cremación, la estructura cristalina de hueso se vuelve más ordenada y se caracteriza por cristales más grandes, con lo que aumenta el valor del IC. Por ello, el IC ha sido utilizado para estudiar el mineral óseo calentado en un gran número de contextos; diversos ejemplos incluyen el uso del índice de cristalinidad para determinar si el hueso fue quemado o no[14] y para observar la existencia de diferencias en las prácticas funerarias[3,15].

El cálculo del IC se puede realizar tanto mediante la difracción de rayos X (DRX), como con la espectroscopía infrarroja con transformada de Fourier (FTIR), aunque los cálculos específicos y los valores serán diferentes entre ambos.

Difracción de rayos X (DRX)

La espectrometría de Difracción de rayos X (DRX) es una de las herramientas analíticas más potentes para la identificación de sustancias cristalinas desconocidas. Tiene varias ventajas sobre otras técnicas analíticas para la identificación de los restos cremados ya que no es destructiva, requiere cantidades relativamente pequeñas de material (aproximadamente 0,5 gr), no se ve afectado por las variaciones elementales presentes en la bioapatita, y se puede utilizar para el cálculo semi-cuantitativo de los componentes de una mezcla, determinando así el nivel relativo de contaminación de una muestra.

El método se basa en el hecho de que todos los cristales están compuestos por planos regulares y repetitivos de átomos que forman un retículo. Cuando los rayos X coherentes se dirigen a un cristal, los rayos-X interactúan con cada átomo en el cristal, excitando los electrones y haciéndolos vibrar con la frecuencia de la radiación incidente. Los electrones se convierten en fuentes secundarias de rayos X, re-irradiando esta energía en todas las direcciones en la misma longitud de onda del haz incidente, un fenómeno conocido como dispersión coherente. Estos rayos X difractados se pueden comparar con las ondas que viajan en todas direcciones y forman patrones de interferencia muy similares a las interferencias que se forman cuando se dejan caer dos piedras en el agua. Esta interferencia puede ser constructiva, formando olas mayores, o destructiva, anulando totalmente las olas. El patrón de interferencia creado depende de la distancia entre las capas atómicas, la composición química, y el ángulo en que los rayos X difractan lejos de los átomos, por lo que indirectamente revela la estructura de los cristales.

En el espectrómetro de difracción de rayos X, el tubo de rayos X y el detector se hacen girar alrededor de la muestra. El espectro de difracción creado por interferencia constructiva es registrado por el detector del haz. La relación entre el ángulo en el que se producen los picos de difracción y la distancia entre los átomos de una red cristalina (distancia interplanar d) se expresa por la ley de Bragg: $\mathbf{n\lambda = 2d \sin\theta}$.

Por razones históricas, los difractogramas se expresan en grados dos theta (2θ). Los espectros de difracción se recogen en el rango angular de 9° a 140° en 2θ y

se analizan con un software llamado MAUD (*Material Analysis Using Diffraction*)[16], que permite corregir los datos para la función instrumental y evaluar cuantitativamente las fases mineralógicas presentes en los huesos junto con los parámetros reticulares y microestructurales. Se requieren de 12 a 24 horas para recoger un espectro.

Puesto que cada sustancia tiene una estructura cristalina única (fase cristalográfica), los ángulos de interferencia constructiva forman un patrón único. Al comparar las posiciones e intensidades de los picos de difracción con una biblioteca de materiales cristalinos conocidos, se puede identificar la composición de las muestras de la fase desconocida, como si fuera la huella digital de la substancia. Esto es cierto también para una mezcla de sustancias. En la práctica, la mezcla de 5-6 fases cristalográficas se pueden resolver con un grado de confianza aceptable.

En 1975 se demostró que las altas temperaturas que se consiguen con el tratamiento con fuego inducen un aumento de las dimensiones medias de los microcristales de la apatita, que se puede medir a partir del alargamiento/restricción de los picos de difracción[17].

A fin de afrontar la problemática relativa al estudio de restos humanos arqueológicos quemados o presuntamente quemados, en nuestro laboratorio efectuamos la calibración de una muestra de hueso que se utilizó como referencia. Para ello se simuló la exposición al fuego real en función de distintas temperaturas de tratamiento controlado (200-1100° C), tomando en consideración la dependencia del tiempo (0, 18 y 60 minutos)[14].

En particular se analizó el comportamiento del hueso de referencia a determinadas temperaturas intermedias (650, 750, 775, 825, 850 °C) a fin de monitorizar y explicar el doble régimen de crecimiento en los cristales de la hidroxiapatita en el que se aprecia un aumento súbito entorno a los 700°C, acercándose luego a un valor constante más alto, siguiendo un comportamiento sigmoidal con un tipo de función logística[14]. Este intervalo de temperatura es importante porque durante esta transición el tamaño de los cristales de los huesos se altera a un grado estadísticamente significativo[9,18].

Asimismo, se puede cuantificar la cinética del crecimiento de los cristales en relación a la temperatura y al tiempo de tratamiento, para disponer de un punto inmediato de referencia en la aplicación de la calibración de los restos presuntamente quemados. De esta forma, se puede no sólo determinar con más exactitud la temperatura alcanzada por los restos, sino que también es posible hacer una aproximación al tiempo de cremación.

Estos datos tienen sus limitaciones ya que debe tenerse en cuenta que se ha trabajado sobre hueso seco. A pesar de ello, Bohnert y colaboradores[19] han observado que para la total incineración de un cuerpo a través de la cremación se precisan cerca de dos horas a una temperatura de 800 °C, mientras que para la destrucción de las partes blandas son necesarios al menos 50 minutos. Así pues los tiempos de estudio programados en nuestro laboratorio son coherentes con una cremación real.

La Figura 2 muestra el espectro de difracción del hueso humano no quemado usado como referencia. Los puntos se refieren a los datos experimentales, mientras la línea continua es la aproximación (fit) conseguida con el método de Rietveld después del ajuste iterativo de los parámetros estructurales y microestructurales. Los picos de difracción de la hidroxiapatita resultan extremadamente alargados debido a la naturaleza nanocristalina del material óseo que comporta dimensiones medias de los cristales extremamente reducidas y una elevada concentración de desorden reticular. Después de haber tenido en cuenta los efectos instrumentales, el método de Rietveld es capaz de distinguir y separar el alargamiento de los picos de difracción en términos de dimensiones medias de los cristales y de densidad del desorden reticular, expresadas en Angstroms (1 Å = 10^{-8} cm). En particular, la dimensión media de los cristales resulta ser de 170 (±5) Å.

Así pues estos valores pueden ser considerados representativos de un hueso no quemado.

Las temperaturas de 200 hasta a 600 °C (0 minutos) muestran procesos de crecimiento de los cristales muy débiles. El calentamiento isocrono de la muestra (velocidad 20 °C/min) seguida de un calentamiento isotermo a las temperaturas establecidas (18, 36 e 60 minutos) parece tener efectos limitantes sobre el crecimiento de los cristales debido a una relativa estabilidad del sistema. Contrariamente, es evidente un efecto de crecimiento rápido de los cristales a temperaturas superiores a 700 °C (60 min), ulteriormente distinguible en el intervalo de temperatura entre 750° y 850 °C, y observable en todos los tiempos en los que se ha actuado (0, 18, 36 y 60 min).

En lo concerniente a los huesos tratados a temperaturas mayores de 850 °C y que han permanecido largamente en el horno, las dimensiones de los cristales son superiores a 1.500 Å aunque la determinación de su valor medio es bastante difícil ya que se sitúa en el límite instrumental de la técnica.

Para temperaturas superiores a 1.000 °C, las dimensiones medias de los cristales parecen aproximarse a los valores máximos asintóticos siguiendo un proceso de crecimiento de tipo sigmoidal (Tabla 1)[14].

Temperatura / °C	0 Minutos	18 Minutos	36 Minutos	60 Minutos
No quemado	170			
200	175	175	175	175
300	180	184	186	188
400	195	203	204	205
500	202	202	205	210
600	204	226	230	256
650	213	240	250	258
700	229	294	463	486
750	268	611	712	800
775	350	836	880	920
800	432	1030	1160	1200
825	732	1120	1140	1254
850	923	1380	1450	1500
900	1.351	>1.500 (1616)	>1.500 (1680)	>1.500 (2621)
1000	>1.500 (1569)	>1.500 (2195)	>1.500 (2600)	>1.500 (2950)

Tabla 1.
Tamaño medio de cristales de la fase mineral hidroxiapatita (1 Å = 10-8 cm) (de Piga et al, 2009).

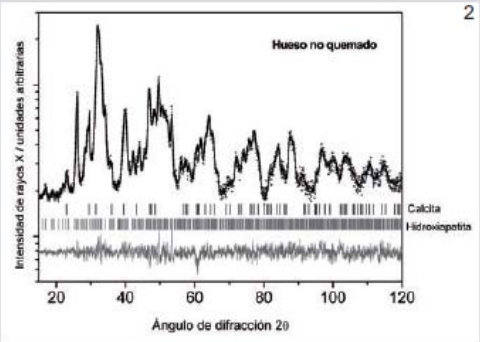

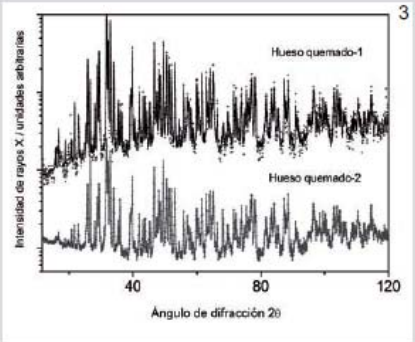

Figura 2.
Patrón de DRX de hueso humano no tratado usado como patrón de referencia. La línea con puntos muestra los datos experimentales, la línea continua es el ajuste de Rietveld en base a la estructura de la hydroxiapatita y la calcita. La línea inferior se refiere a los valores residuales; es decir la diferencia entre la raiz cuadrada de las intensidades calculadas y obtenidas, la cual es indicativa de la bondad de los resultados.

Figura 3.
Difractogramas de dos huesos tratados a elevadas temperaturas (1.000°C), en los que es evidente una considerable agudización y estrechamiento de los picos de rayos X.

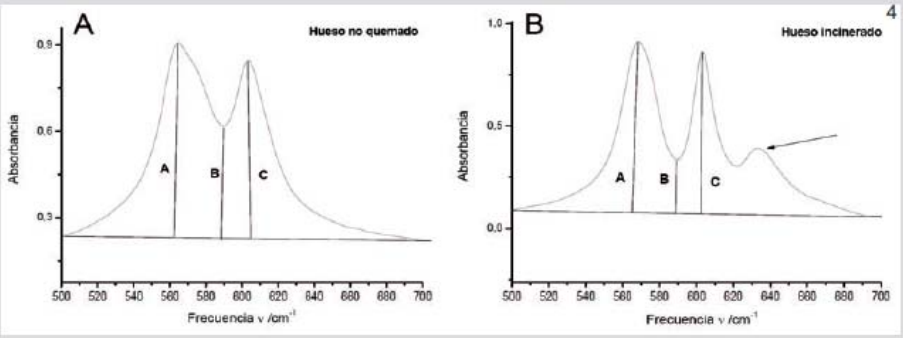

Figura 4a.
Espectro de FT-IR de un hueso no quemado, mostrado en la gama de 500-700 cm⁻¹, correspondiente al grupo PO_4^{3-} característico de la hidroxiapatita. El factor de dimensiones SF se calcula numéricamente en este grupo de picos.

Figura 4b.
Espectro de la banda de los fosfatos de un hueso quemado. La anchura de las dos bandas en 565 y 605 cm⁻¹ disminuye a medida que aumenta la temperatura, con la aparición simultánea de un tercer pico a aproximadamente 630 cm⁻¹.

En las dos muestras incineradas mostradas en la Figura 3 se puede observar la notable reducción de los picos de difracción, debido al notable crecimiento de los microcristales y a la reducción del desorden reticular inducido por el considerable tratamiento térmico (1000 °C) al que fueron sometidos.

FTIR

Para apoyar e integrar los resultados obtenidos también se ha utilizado la técnica de espectroscopia de Infrarrojos por transformada de Fourier (FT-IR), un diagnóstico ampliamente utilizado en la química-física que permite reconocer la presencia de grupos o especies moleculares característicos de las muestras sometidas a examen.

Contrariamente a la difracción de rayos X, esta medida tiene la ventaja de usar cantidades de muestra del orden de unos pocos miligramos (aproximadamente 0,003 gr) y requerir tiempos de adquisición del espectro muy cortos (aproximadamente 50 segundos). El espectro característico de los grupos moleculares está determinado por las frecuencias de absorción específicas de los movimientos de rotación, flexión o "estiramiento" (que consiste en la contracción y expansión de las distancias entre los átomos).

Con respecto al material óseo humano y animal, por lo general se analizan las características del banda de fosfatos (PO_4^{3-}), detectables en la gama de frecuencias entre 500 cm^{-1} y 700 cm^{-1}.

Como puede verse en la Figura 4a, la banda de fosfatos en el material óseo no quemado está compuesto de al menos dos componentes, que son lo suficientemente grandes, pero que disminuyen a medida que aumenta la temperatura, con la consiguiente aparición de otro pico a aproximadamente 630 cm^{-1} (Figura 4b). El estrechamiento de estos dos componentes se puede medir numéricamente con una buena precisión utilizando un índice de cristalinidad llamado *Splitting factor* SF ("factor de división").

El índice de cristalinidad SF se calcula por (A + C) / B), donde A, B y C representan la distancia a la línea de base. Así pues, en la línea de base del espectro, se suman las alturas de las absorciones en aproximadamente 605 y 565 cm^{-1} y se divide por la altura mínima entre ellos (en 595 cm^{-1}).

Esta fórmula fue propuesta por primera vez por Shemesh[20] y Weiner y Bar-Yosef[21] y ha sido habitualmente utilizado desde entonces.

Las longitudes de onda en 565 cm^{-1} y 605 cm^{-1} corresponden a las bandas de vibración de flexión de fosfatos y se incrementan con el aumento de la cristalinidad. La longitud de onda en 595cm^{-1} disminuye provocando así un aumento global en el valor de SF. Nótese que aunque el aumento de temperatura provoca un aumento de el SF, la relación no es lineal sino que sigmoidal[22].

Las bandas con mayor frecuencia indican la presencia de grupos carbonatos (CO_3^{2-}) que proporcionan informaciones adicionales útiles de características químico-físicas sobre el hueso.

Una estimación del contenido de carbonato viene dada por la relación de la absorción del pico a 1428 cm^{-1} (CO_3^{2-}) y del pico a 1042 cm^{-1} (PO_4^{3-}); se indica como C/P. El valor de este índice disminuye cuando aumenta la temperatura.

El uso combinado de ambas técnicas (DRX y FITR) constituye una poderosa herramienta para evaluar si los huesos se han sometido al fuego y a qué temperatura, con una gran fiabilidad[22].

Aplicaciones

Existen casos en los que un tratamiento térmico no es particularmente evidente, lo que comportaría quizás una línea errónea en la investigación de los hechos. Para ilustrar estos casos utilizamos el caso arqueológico de la necrópolis fenicia y púnica de Monte Sirai (Carbonia, Cerdeña-Italia)[22] en la que la cremación se utilizó como rito funerario durante la época fenicia, mientras que la época púnica se caracteriza por la inhumación de los cadáveres.

Sin embargo, algunos esqueletos de época púnica mostraron algunas trazas oscuras sobre los huesos aunque el conjunto esquelético se presentaba completo y en posición anatómica (Figura 5). Los antecedentes de cremación en la población fenicia nos indujeron a realizar un análisis físico-químico sobre los restos.

Mientras el espectro DRX relativo al esqueleto de la Tumba 252 (Figura 6) muestra inequívocamente las características de una incineración -rito en uso por parte de la población fenicia hasta el siglo VI a.C., los datos relativos a los individuos de la tumba 8, 12 e 255 muestran también una exposición al fuego, aunque de menor intensidad. Este hecho está en principio en desacuerdo con lo que se podría esperar en el caso de tumbas púnicas, época posterior a la fenicia y cuyo rito generalizado es la inhumación. Los resultados obtenidos con ambas técnicas se muestran en la Tabla 2.

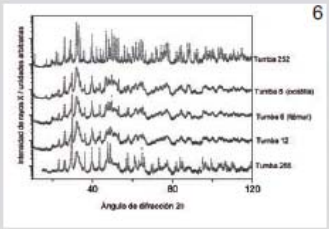

Figura 5.
Restos esquelético de la tumba nº 8 de época púnica del yacimiento sardo de Monte Sirai.

Figura 6.
Patrones de los espectros de DRX de 5 muestras procedentes del yacimiento sardo de Monte Sirai.

Figura 7.
Reconstrucción en el laboratorio del esqueleto procedente de la tumba 252 conservado de manera excepcional.

Muestra	Tamaño medio de los cristales / Å	Temperatura DRX / °C	Splitting Factor (SF)	Temperatura / °C FT-IR
Tumba 252	>1500 (2297)	1000	6,18	>900
Tumba 8-1	251	≅650	4.20	695
Tumba 8-2	248	≅650	4.45	715
Tumba 12	220	600<T< 700	3.59	610
Tumba 255	205	400	3.27	520

Tabla 2.
Tamaño de los microcristales de hidroxiapatita, SF y estimaciones de las temperaturas calculadas mediante las dos técnicas de espectrometría. Ambas técnicas ofrecen resultados concordantes.

Parte del cuerpo	Tamaño medio de los cristales/(Å)	Temperatura/DRX (Piga et al, 2009)/°C	Splitting Factor (SF)-FTIR	Temperatura/FTIR (Piga et al, 2010)/°C
Cráneo	>1500 (1520)	900<T<1000	7,32	1000
Mandíbula	>1500 (2297)	1000	6,18	> 900
Mandíbula(azul)	230	700	4,32	700<T<800
Costilla	>1500 (2306)	1000	6,93	1000
Costilla (azul)	224	700	4,30	700<T<800
Vértebra 1	>1500 (2200)	1000	6,66	Circa 900
Vértebra 2	>1500 (1940)	1000	6,52	800<T<900
Vértebra 3	>1500 (1900)	1000	7,21	1000
Vértebra 4	>1500 (2248)	1000	8,08	1000
Vértebra 5	>1500 (2303)	1000	6,91	1000
Cúbito derecho	>1500 (2079)	1000	7,08	1000
Cúbito izquierdo	>1500 (1724)	1000	6,67	900
Fémur derecho	>1500 (2316)	1000	6,86	900
Fémur izquierdo	>1500 (1480)	900<T<1000	5,58	800<T<900
Tibia izquierda	>1500 (1364)	900	6,08	> 800
Tibia derecha	>1500 (1412)	900	6,68	900

Tabla 3.
Tamaño de los microcristales de hidroxiapatita, Splitting Factor y la estimación de las temperaturas calculadas con las dos técnicas de espectrometría. Ambas técnicas ofrecen resultados concordantes.

La Tabla 2 muestra en detalle los resultados obtenidos mediante las técnicas de difracción de rayos X / FT-IR, que muestran un acuerdo sustancial entre ellos. Las diferencias que no superan los 120° C no son tan importantes como afectar a la validez de las dos técnicas, teniendo en cuenta las diferencias en la base químico-física de las teorías elaboradas.

Del análisis de estos resultados, se puede evidenciar la posibilidad de que los ritos funerarios púnicos de inhumación del Monte Sirai fueran precedidos de una combustión parcial de los cuerpos que pretendería quizás eliminar de forma rápida las partes blandas. Con toda probabilidad el fuego se interrumpiría después de pocos minutos (18 minutos, máximo 36) y los cuerpos (normalmente 2 por tumba) aún íntegros eran depositados en posición primaria uno encima del otro. También podría interpretarse como una combustión superficial mediante la quema de materiales vegetales sobre el mismo cuerpo, lo cual estaría en consonancia con la posición primaria de los cuerpos y la mayor temperatura alcanzada en la parte superior del hueso.

Sin embargo, el ritual en cuestión supone no pocos problemas puesto que, a pesar de que los cuerpos se encontraron en posición primaria, la fosa que los contenía, practicada en el tufo volcánico, no conservaba la más mínima traza de combustión. Merece la pena destacar que en el mismo yacimiento se identificó la zona dedicada al "ustrinum" o zona dedicada a la cremación de los cuerpos, pero es preciso añadir que a menudo en el interior de la misma sepultura se han encontrado dos cuerpos superpuestos, ambos en idéntico estado de semicombustión. Así pues, en el caso de Monte Sirai parece que se trata de un ritual nuevo, cuya práctica fue limitada en el tiempo y practicada quizás sólo alrededor del año 500 a.C. En la literatura antropológica no se han encontrado ejemplos similares en las necrópolis del mundo fenicio ni púnico[22]. Del mismo modo, la aplicación de estos mismos métodos a casos como el del cráneo mostrado en la Figura 1, indicaría sin lugar a dudas su exposición al fuego, a pesar de su apariencia no alterada.

Otra aplicación importante se refiere a la tumba de incineración 252. El descubrimiento excepcional de casi todas las partes del esqueleto nos ha permitido de realizar un análisis detallado para analizar la homogeneidad de la temperatura y la intensidad del fuego en diversas partes representante de todo el cuerpo.

Este tipo de análisis no es habitual pues es prácticamente imposible en tales contextos recuperar restos "in situ" de todo el esqueleto. Dado el excepcional estado de conservación de los diversos fragmentos (Figura 7), fue posible evaluar la eventual uniformidad de la temperatura en muestras representativas de todo el cuerpo.

La Tabla 3 muestra en detalle los resultados obtenidos mediante las técnicas de DRX/FT-IR. Los datos obtenidos con las dos técnicas son prácticamente concordantes, salvo en unos pocos casos (vértebras 1 y 2, cúbito izquierdo y ambos fémures) en los que las temperaturas obtenidas con el análisis de difracción de rayos X son ligeramente más elevados. Estas diferencias no exceden los 100°C y no son significativas.

Los cambios de coloración y textura de los huesos así como los análisis de DRX/FT-IR sugieren una cremación a elevada temperatura, aproximadamente a 1000 ºC, aunque algunos fragmentos de coloración azulada sufrieron una temperatura menor entre 700 y 800 ºC.

De ambos tipos de análisis sobresale además el hecho que el calor debió afectar de forma bastante homogénea a lo largo del esqueleto, con lo que la pira debió ser alimentada en su conjunto, sin que existiera un centro principal.

Conclusiones

En las últimas décadas, la investigación y la experiencia de casos han aumentado en gran medida la capacidad de reconocer e interpretar los restos óseos quemados. Sin embargo, son necesarios nuevos métodos experimentales para aclarar la variedad de factores que conducen la gran cantidad de efectos térmicos.

La difracción de rayos X y análisis de FT-IR tienen varias ventajas significativas para la identificación de una cremación y para la estimación de la temperatura y la duración de un evento de cremación forense, centrándose en los cambios microscópicos en el hueso.

Los importantes avances en hardware han mejorado mucho la velocidad y la accesibilidad de DRX. Sin duda, estas técnicas de análisis tendrán un papel cada vez más importante en el campo de la ciencia forense en el futuro.

Agradecimientos

Los autores quieren agradecer al Prof. Stefano Enzo, Dr. Michele Guirguis (Universidad de Sassari, Italia), Dr. Massimo Piccinini (Porto Conte Ricerche, Alghero, Italia) y Dr. Ignasi Galtès su ayuda. Este trabajo ha sido posible gracias al proyecto "Giovani Ricercatori"

de la Regione Autonoma della Sardegna, titulado: *Studio archeometrico, antropologico e paleogenetico del materiale archeologico appartenente al sito fenicio-punico di Monte Sirai (Carbonia)*, y a los proyectos del MEC, CGL2008-800800/BOS y PR2009-0128.

Bibliografía

1. Symes SA, Rainwater CW, Chapman EN, Gipson DR, Piper AL. Patterned Thermal Destruction of Human Remains in a Forensic Setting. In: CW Schmidt, S.A. Symes (eds): The Analysis of Burned Human Remains. London: Academic Press, 2008;15-54.
2. Trancho GJ. Análisis antropológico de las necrópolis de cremación. Rev. Esp. Antr. Fis. 2010;31: 205-32.
3. Piga G, Hernández-Gasch JH, Malgosa A, Ganadu ML, Enzo S. Cremation practices coexisting at the "S'Illot des Porros" Necropolis during the Second Iron Age in the Balearic Islands (Spain). Homo 2010;61:440-52.
4. Dehaan JD. Kirk's Fire Investigation. 5th ed. Brady Publishing. New Jersey: Upper Saddle River, 2002.
5. Markiewicz D.A: Few takers for fake cremains; GBI seeks 'closure' in crematory scandal; families conflicted, The Atlanta Journal-Constitution Metro News, August 10 2005, 1B pp.
6. Subira M.E., Malgosa A: The Effect of Cremation on the Study of Trace Elements. Int. J. Osteoarchaeol. 1993;3:115-8.
7. Etxeberria F. Aspectos macroscópicos del hueso sometido al fuego. Revisión de las cremaciones descritas en el País Vasco desde la Arqueología. Munibe 1994;46:111-6.
8. Guillon F. Brules frais ou brules secs?. Anthropologie Physique et Archéologie. París: Ed. C.N.R.S. 1987, 191-3.
9. Thompson TJU. Heat-induced dimensional changes in bone and their consequences for forensic anthropology. J. Forensic Sci. 2005;50(5):1008-15.
10. Paschalis EP, Betts F, DiCarlo E, Mendelsohn R, Boskey AL. FTIR Microspectroscopic analysis of normal human cortical and trabecular bone. Calcif. Tissue Int. 1997;61:480-6.
11. Thompson TJU, Islam M, Piduru K, Marcel A. An investigation into the internal and external variables acting on crystallinity index using Fourier Transform Infrared Spectroscopy on unaltered and burned bone. Palaeogeogr. Palaeoclimateol, Palaeoecol. 2011; 299: 168–174.
12. Wang XY, Zuo Y, Huang D, Hou X-D, Li YB: Comparative study of inorganic composition and crystallographic properties of cortical and cancellous bone. Biomed. Environ. Sci. 2010;23:473-480.
13. Nakano T, Tokumura A, Umakoshi Y. Variation in crystallinity of hydroxyapatite and the related calcium phosphates by mechanical grinding and subsequent heat treatment. Metall. Mater. Trans. 2002;A33:521–5.
14. Piga G, Thompson TJU, Malgosa A, Enzo S. The potential of X-Ray Diffraction (XRD) in the analysis of burned remains from forensic contexts. J. Forensic Sci. 2009;54(3):534-539.
15. Squires KE, Thompson TJU, Islam M, Chamberlain A. The application of histomorphometry and Fourier Transform Infrared Spectroscopy to the analysis of early Anglo-Saxon burned bone. J. Archaeol. Sci. 2011;38:2399-409.
16. Lutterotti L, Bortolotti M: Object oriented programming and fast computation techniques in MAUD, a program for powder diffraction analysis written in java. IUCr: Compcomm Newsletter 2003;1:43–50.
17. Bonucci E, Graziani G: Comparative thermogravimetric X-ray diffraction and electron microscope investigations of burnt bones from recent, ancient and prehistoric age. Atti della accademia Nazionale dei Lincei, Rendiconti, classe di scienze fisiche, matematiche e naturali 1975;59:517–32.
18. Shipman P, Foster G, Schoeninger M: Burnt bones and teeth: an experimental study of color, morphology, crystal structure and shrinkage. J. Archaeol. Sci. 1984;11:307-25.
19. Bohnert M, Rost T, Pollak S. The degree of destruction of human bodies in relation to the duration of the fire. Forensic Sci. Int. 1998;95:11-21.
20. Shemesh A. Crystallinity and diagenesis of sedimentary apatites. Geochim. Cosmochim. Acta 1990;54:2433-8.
21. Weiner S, Bar-Yosef O. States of preservation of bones from prehistoric sites in the Near East: a survey. J. Archaeol. Sci. 1990;17:187-96.
22. Piga G, Guirguis M, Bartoloni P, Malgosa A, Enzo S. A funerary rite study of the Phoenician-Punic Necropolis of Mount Sirai (Sardinia, Italy). Int. J. Osteoarchaeol. 2010;20:144-57.

Chapter 4.2: A multi-technique approach by XRD, FT-IR and SAXS for the analysis of burned archaeological bones

Authors: **Giampaolo Piga, Assumpcio Malgosa, Stefano Enzo.**

"Stones, Bones and Thoughts - festschrift in honor of Milton Núñez". Book edited by Sirpa Niinimäki, Anna-Kaisa Salmi, Jari-Matti Kuusela and Jari Okkonen. Milton Núñez's festschrift committee Publisher

A more nuanced understanding of how the analysis of heat-induced change in bone can provide valuable information about pyre technology and the funerary process is given by a multi techniques approach of physico-chemical and spectroscopic methods, that would allow a greater insight of the cremation process and its effects on human bones as has been demonstrated by studies on skeletal material from various archaeological periods and from forensic contexts.

X–ray diffraction employed to illustrate that heating causes an increase in the crystal size of hydroxylapatite in cremated bone (Rogers and Daniels, 2002; Hiller et al., 2003; Piga et al., 2008, 2009). Small angle X-ray scattering (SAXS) determines the crystal size, shape, and orientation within bone, independent of crystal lattice perfection at different temperatures (Hiller et al., 2003) and Fourier Transform Infrared Spectroscopy (FT–IR) employed to examine changes to the Crystallinity index or Splitting Factor (SF); carbonate to phosphate ratio (C/P) and carbonate to carbonate ratio (C/C) (Shahack-Gross et al., 1997; Stiner et al., 2001; Surovell and Stiner 2001; Chakraborty et al. 2006; Nagy et al. 2008; Thompson et al. 2009; Thompson et al., 2010).

Five archeological burned bones with different intensities of burning, belonging to the necropolis of *S'Illot des Porros* (Majorca, Spain), were investigated in order to evaluate the thermal treatment which samples underwent. Mineralogical nature and extension of crystalline domains were evaluated by applying the Rietveld method to the X–ray diffraction patterns.

To evaluate the temperature to which the bones were subjected, a method has been applied to the XRD data, based on our calibration of the heat treatment as a function of temperature and time by following the average cristallite size evolution of hydroxylapatite biomineral phase (Piga et al., 2008b; 2009b).

Fourier transform infrared (FT–IR) spectra are dominated by the typical hydroxylapatite bands apart from weak components typical of carbonates. Our data confirm findings about the thermal treatment samples undergo, in fact, the shoulder at ca. 630 cm^{-1} for the less "crystalline" specimens is replaced by a further peak in the specimens which appeared to have been treated at higher temperature.

Small Angle X–ray Scattering (SAXS) data analysis supplies a further point of view of the same process allowing to obtaining some information on the morphologies of samples. Crystal shape evolves as a function of the physical-chemical modification, diagenesis or thermal treatments that bones have undergone. Particles turn out to be composed at a nanoscopic level by small inhomogeneities defined with sharp interface that agglomerate to form bigger clusters of fractal geometry. The fractal index of the powdered system decreases on increasing the temperature of thermal treatment. The XRD/SAXS data of small particle size are in a very good agreement.

Thus, the combined used of those techniques is a powerful tool to assess whether the bones have subjected to fire and, with fairly good reliability, to which temperature.

The applications of these methods to archaeological or forensic scenarios can contribute to archaeologists and forensic doctors' understanding of the efficiency of these techniques, especially with regards to archaeological and modern material from unknown contexts.

A multi-technique approach by XRD, FT-IR and SAXS for the analysis of burned archaeological bones

Giampaolo Piga[1], Assumpció Malgosa[1] & Stefano Enzo[2]

[1]Departament de Biologia Animal, de Biologia Vegetal i d'Ecologia, Universitat Autonoma de Barcelona, Spain

[2] Dipartimento di Chimica e Farmacia, Universitá di Sassari, Italy

Abstract

Archaeological bones with alterations due to thermal exposure were found in the necropolis of S'Illot des Porros, one of the most important prehistoric funerary sites of the Balearic Islands (Spain). The bones were investigated by a combination of X-ray diffraction (XRD), Fourier transform infrared (FT-IR) and small angle X-ray scattering (SAXS) tecniques. They provided useful information on their physical and chemical state such as the deterioration degree of the bone structure that was parameterised through indices such as crystallinity, average crystallite size, splitting factor and fractal dimension. As some of the reported modifications could be attributed to diagenesis, a discussion is presented in terms of bone crystallinity and ionic exchange processes. Furthermore, the different average crystallite size of bone specimens was ascribed to the different fire treatment. Indeed, thermal treatment alters the structure and morphology of bone at a very fine level (microscopic and nanometric), while morphology follows the structural modifications. We concluded that the studied human bones were thermally treated at different temperatures on account of the fire rituals after death.

Introduction

There is at present a growing interest in the application of forensic science to clarify, for example, pending questions in civil or criminal court cases after burning or to study human remains for purposes of identification after cremation (Eckert *et al.* 1988; Thompson 2005; Harbeck *et al.* 2011) as well as in archaeology (Piga *et al.* 2008a; 2010a) to account for the funerary habits and customs of ancient civilisations. Therefore, the retrieval of detailed information pertaining to the individual or population such as those collected from non-cremated bones utilising the methodological approaches available from diffraction and spectroscopy is highly appreciated not only for forensic scientists, but also for anthropologists, palaeontologists and archaeologists focusing on fossil or historical human remains (Stathopoulou *et al.* 2008; Piga *et al.* 2009a; 2011).

The effects of heating and burning on bone mineral have previously been studied using techniques such as X-ray diffraction (XRD) with the aim of discerning a characteristic signature of crystal change. The powder diffraction diagrams were found to sharpen as a function of thermal treatment, on account of effect due to simultaneous average crystallite size growth and

lattice strain decrease. These data were discussed coherently for the first time by Perinet (1964) and Bonucci & Graziani (1975), and accompanied by an electron microscopy investigation of the bone materials with the aim of assessing directly the growth process induced by heating. Early XRD studies on burned remains were further addressed by Shipman *et al.* (1984) using a crystallinity index (CI) inversely related to the broadening of the peaks of hexagonal hydroxylapatite. Because of the anisotropic broadening of hydroxylapatite peaks, Person *et al.* (1995; 1996) suggested a more objective definition of the crystallinity index by examining the envelope of peaks in the 2θ range from 30 to 39° using the CuKa radiation. Rogers and Daniels (2002) made an effort to give a comprehensive view of the whole diffraction pattern by reporting the broadening of some dozens of peaks as a function of their angular position. It should be noted that a parallel line of research was developed by FT-IR spectroscopy, where the hydroxylapatite phosphate bands ν_4 in the range 500-700 cm^{-1} were examined in terms of a splitting factor similar to the crystallinity index (Weiner & Bar-Yosef 1990; Stiner *et al.* 1995).

An alternative method of studying the archeological bones was recently suggested by using the small angle X-ray scattering technique (SAXS) (Hiller *et al.* 2003; Hiller & Wess 2006).

Since X-rays are primarily scattered by electrons, X-ray small angle scattering is observed, when electron density inhomogeneities exist in the sample. Considering that any scattering process is accompanied by a reciprocity law, which gives an inverse relationship between particle size and scattering angle, particle dimension from ten to several hundred Å (1 Å = 10^{-10} m) are enormously large compared to the wavelengths of X-ray used, (CuKa line 1.54 Å) this makes the angular range of observable scattering correspondingly small. The scattering of various particles can be treated at various extents and specific information on the size, shape, polydispersion, spatial arrangement and interaction among particles have been obtained since 1938, when Guinier postulated the scattering form spherical isolated particles (Guiner & Fournet 1955). Notwithstanding, SAXS has been applied only in a few cases to artefacts of interest in the field of cultural heritage for specific purposes. The use of SAXS has recently found a new application in the study of mineral change in archaeological bones (Hiller & Wess 2006; Hiller *et al.* 2004; Pijoan *et al.* 2007). This method allows for the accurate determination of crystal size, shape and orientation within the bone (Child 1995; Wachtel & Weiner 1994). It was shown that SAXS provides information regarding particle morphology and is complementary to other techniques employed in archaeological contexts (Camacho *et al.* 1999). In addition, it was recently used to characterise diagenetic change in bone and other materials of archaeological interest (Wess *et al.* 2001; 2002). The measurement of subtle changes to crystallite thickness or shape could provide a window to the events leading to mineral alteration in archaeological bone, including diagenetic processes as well as human interventions such as burning (Piga *et al.* 2009a).

Experimental data obtained from the analysis of some archaeological bones will be discussed and analysed to obtain an evaluation of the thermal treatments applied to the samples. Sizes evaluated from the SAXS data are compared with the size of crystalline domains obtained by applying the Rietveld method to the XRD patterns. Analogies and differences will be discussed. Finally we will describe how our results confirm previous FT-IR spectra analysis findings.

Experimental

Materials

The fragments of bones were found during the excavations in the Funerary chambers of S'Illot des Porros necropolis, one of the most important prehistoric funerary sites of the Balearic Islands (Spain), which was in use from the 6th and 5th century BCE until the 1st century CE. The archaeological site is located in a funerary area which contains two cemeteries and one sanctuary and is constituted by three funerary chambers named A, B and C, respectively (Piga *et al.* 2010a).

The analysed bones were extracted from a collection attributed to at least 67 burned individuals (Table 1) and are representative of cremations at different temperatures in the three funerary chambers. Six fragments of 0.5 g were prepared for physical analyses by hand grinding with an agate mortar and pestle until reduced to a sufficiently fine powder.

Methods

The X-ray diffraction (XRD) patterns were recorded using Bruker D8 and Siemens D- 500 diffractometers in the Bragg-Brentano geometry with Cu Ka radiation (λ=1.54178 Å). The goniometer was equipped with a graphite monochromator in the diffracted beam and the patterns were collected with 0.05 of step size. The X-ray generator worked at a power of 40 kV and 30 mA and the resolution of the instrument (divergent and antiscatter slits of 0.5°) was determined using a-SiO_2 and a-Al_2O_3 standards free from the effect of reduced crystallite size and lattice defects (Enzo *et al.*, 1988). The powder patterns were analysed according to the Rietveld method (Young 1993), using the programme MAUD (Lutterotti & Bortolotti 2003).

These experiments and analyses are supposed to be reliable for a precise description of the growth phenomena (i.e., degree of organisation), which are induced in the hydroxyapatite (HA) micro- (or nano-) crystals as a function of fire temperature. As a matter of fact, the procedure is not limited to the analysis of a few selected peaks but evaluates the pattern with the maximum collectable evidence. As for apatite evidenced in our XRD patterns, following Elliott *et al.* (1973) we have adopted a monoclinic description of the unit cell (Space Group P21/c, 4 molecular units) rather than the usual hexagonal cell of S. G. P63/m with two molecules of

Table 1. list of the six burnt remains analyzed, belonging to S'Illot des Porros necropolis, with anthropological information (age, sex, part of the body taken for the spectroscopic analysis).

Sample code	Age	Sex	Part of the body analyzed
IPC764-2	Adult	♂	Cranium
IPA9	15 years old	-	Cranium
IPC764	Adult	♂	Femur
IPC64B	Juvenile	-	Cranium
IPA11	Adult	♂	Cranium
IPB14-62	Adult	♂	Cranium

hydroxyapatite. As a matter of fact, the lattice parameter of the monoclinic phase aM coincides with that of the hexagonal phase a_H, but b_M is ca $2 \times a_H$, $c_M = c_H$ and $\beta_M \approx 120°$.

The Rietveld method is an efficient approach that evaluates quantitatively the amount, structure and microstructure parameters of mineralogical phases while taking into account the instrumental parameters. While the average crystallite size parameter does not depend on the order of reflections, the lattice strain does.

The programme MAUD calculates numerically the convolution equations in order to correctly distinguish and evaluate both crystallite size and strain terms in the experimental peak broadening. Also, one important advantage of the Rietveld method is that no standard is required for quantitative evaluation of phases, thus minimizing the work on sample preparation.

It was necessary to make reference to a calibration that was worked out with a sample of human bone subjected to selected temperatures of cremation to evaluate the temperature to which the bones were presumably subjected. Our previous applications of the XRD technique to human bones were based on a calibration of the thermal treatment as a function of temperature and time by following the average grain size of hydroxyapatite (HA) biomineral phase. We have assessed with our method that the average grain size in untreated human bones is ca 170 Å and remains approximately constant until 500–600°C. The average crystallite size then quickly increases around 700°C, subsequently leveling off at a new value according to a sigmoidal behavior typical of a logistic function (Piga *et al.* 2008b; 2009b).

It is possible to estimate with good reliability the temperature, to which the bones were subjected during the burning process by following the quantitative interpretation of XRD data in terms of the growth mechanism of HA microcrystals induced by thermal treatment. In turn, this permits us to ascertain the fire technology in use and, with specific concern to the site here investigated, it supplies valuable information on the possible coexistence of inhumation and cremation practices.

A simultaneous investigation was carried out by FT-IR spectroscopy, whose absorption bands are related to the bond strength of carbonate and phosphate groups of HA. The bands that are considered are generally constituted by overlapped lines whose width decreases as a function of treatment temperature according to an empirical crystallisation index also called splitting factor (SF) (Weiner & Bar-Yosef 1990).

FT-IR spectra were collected with a Bruker Vertex 70V spectrometer in terms of absorbance vs wavenumber n in the range 400-4500 cm^{-1}. About 3 mg bone were hand-grinded and mixed with potassium bromide (KBr) in the weight ratio 1:100 respectively, to make pellets suitable for beam irradiation.

In particular, the cluster of bands of HA in the range 50.000–70.000 m^{-1} was analysed because it is generally recognized as the most reliable zone in which to define the splitting factor SF as a function of temperature treatment. SF is defined from the sum of band intensities of the two peaks divided by the intensity of the valley between them (Weiner & Bar-Yosef 1990). The peaks were processed using standard non-linear least squares fitting procedures incorporated in the Origin® software assuming for the transmitted line shape a symmetric Pearson VII type function and a polynomial background of order 1.

Small angle X-ray scattering measurements were carried out with a Bruker AXS Nanostar-U instrument having a Cu rotating anode working at 40 kV and 18 mA. The X-ray

beam is monochromatized at a wavelength λ_{Cu}=1.54178 Å using two cross-coupled Göbel and is collimated using a series of three pinholes with diameters of 500, 150, and 500 μm. The detector is an Hi-Star Bruker. A two-dimensional Multiwire Proportional Counter (MWPC) sensitive to the energy of X-ray was used. The hand-ground bone powders were placed inside lime-glass capillary. Samples were directly mounted on the sample stage to avoid additional scattering from the holder. Data were collected at room temperature for 1000 s and 24 cm from the sample. The measurements were carried out in two different portions of each sample to check the homogeneity.

Results and discussion

The XRD diagrams of the six examined specimens are reported in Figure 1 and show a remarkable change of their crystallinity property. The crystallinity referred to here should not be confused with the analogous term used in polymer science for partially amorphous systems, where it is referred to as ratio between the amount of crystalline components in an otherwise amorphous matrix.

Except for the IPC764 specimen, the phase analysis by the Rietveld method of the XRD patterns suggests that the specimens are almost single phase hydroxylapatite, apart from a minor contamination of calcite that seems likely of endogenous origin, although this is difficult to demonstrate in archaeological material aged more than two thousand years ago (see data reported in Table 2).

It can be seen that the bottom pattern (data points) consists of broad peaks described satisfactorily with the monoclinic structure of hydroxylapatite on account of a limited extension of the crystallites and a fairly large degree of lattice strain. It should be maintained that in the isotropic model here used the peak broadening due to crystallite reduction is independent from the order of reflection, while the component due to strain increases proportional to the reciprocal lattice variable. Actually, it is known that the assumption of isotropic size and strain may be questionable dealing with osteo-materials. In particular the (002) peak at d = 3.44 (2θ = 25.85°) appears sharper than the others, which confirms the existence of texture along this direction (Zizak *et al.* 2000). Nevertheless, the average crystallite size obtained by XRD using the isotropic model is reported in Table 2. It can be regarded as a first approximation for a

Table 2. Phase, average crystallite size, splitting factor and estimated temperature of the hydroxylapatite mineral phase.

Sample code	Phases	Average cristallize Size /(Å)	estimated T with XRD / °C	Splitting Factor (SF)	estimated T with FT-IR / °C
IPC764-2	Apatite 97 % Calcite 3 %	2008 ±200	1000	6.15 ± 0.05	> 900
IPA9	Apatite 97 % Calcite 3 %	957 ±100	800-900	6.0± 0.05	>800
IPC764	Apatite 89 % Calcite 11 %	321 ±20	700-775	5.70± 0.05	>800
IPC64B	Apatite 96 % Calcite 4 %	248 ± 10	650-700	3.86± 0.05	600<T<700
IPAI1	Apatite 99% Calcite 1 %	213 ±10	650	3.63± 0.05	≈ 600
IPB14-62	Apatite 97.5 % Calcite 2.5 %	196 ±10	0-400	2.95± 0.05	Not burned

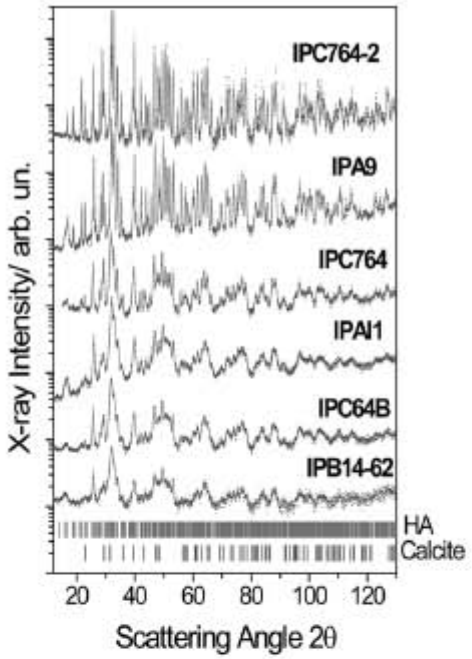

Figure 1. the XRD patterns of cremated bones from S'Illot des Porros necropolis; it is evident that IP-B14-62, IPC64B and IPAI1 samples display a large peak broadening with respect to the remaining specimens on account of a weak thermal treatment received. With the Rietveld method the goodness of the fit between calculated and experimental pattern is measured in terms of numerical agreement factors so this approach appears the most complete for evaluating simultaneously experimental data quality (i.e. signal-to-noise-ratio) and/or credibility of model assumptions.

volume weighted average size of crystallites, regardless their shape and texture.

As shown in Figure 1, the peak broadening decreases going from bottom to top, which is indicative of the thermal treatment to which the bones were subjected. On the basis of a previous calibration (Piga *et al.* 2008b), it was shown that similar "crystallinity" changes can be related to a temperature treatment to which presumably the bodies were subjected. The "equivalent temperature range" of treatment is also reported in Table 2. It is known that also taphonomy and diagenesis may affect the microstructure of bones, but it was assessed that this effect is relatively reduced in a palaeontological collection of human and animal bones (Piga *et al.* 2009a) if compared with effects due to cremation or incineration practices.

FT-IR spectroscopic data are presented in Figure 2a and b for the same collection of specimens in the wave-number n range from 400 to 2000 cm^{-1}. It is possible to recognise three main groups of band in the range 500-700 cm^{-1}, 1000-1200 cm^{-1} and 1400-1600 cm^{-1}, which are generally assigned to the energy mode ν_4 of phosphate groups, ν_3 of phosphate groups and to the ν_3 of carbonate groups respectively.

These carbonates bands assessed by spectroscopy may refer either to CO_3^{2-} groups from calcite or to CO_3^{2-} groups that are substituting for phosphate groups in the structure of hydroxylapatite.

The possibility that these carbonate groups are referred to a $[Ca_5(PO_4)_3]_2(CO_3)$ structure was also considered in the literature (Elliott *et al.* 2002). In Figure 2b, the ν_4 band of the phosphate groups is subjected to a sharpening similar to the diffraction patterns. It is customary to represent the sharpening of the ν_4 envelope (Weiner & Bar-Yosef 1990; Stiner *et al.* 1995), using the splitting factor SF, reported in Table 2. Futhermore, the shoulder at ca. 630 cm^{-1} for the less "crystalline" specimens is replaced by a further peak in the specimens which appeared to have been treated at higher temperature according to the XRD investigation.

The graphs in Figure 2 are a magnification of FT-IR spectra in the range 500-700 cm^{-1} and highlight the band structure of ν_4 phosphate groups from the point of view of the splitting factor SF.

In our previous calibration of FT-IR spectra, it was established that the appearance of the shoulder at ca 634 cm^{-1} indicates fire temperature between ca 700 and 800°C and persists until 1000 °C (Piga *et al.* 2010b).

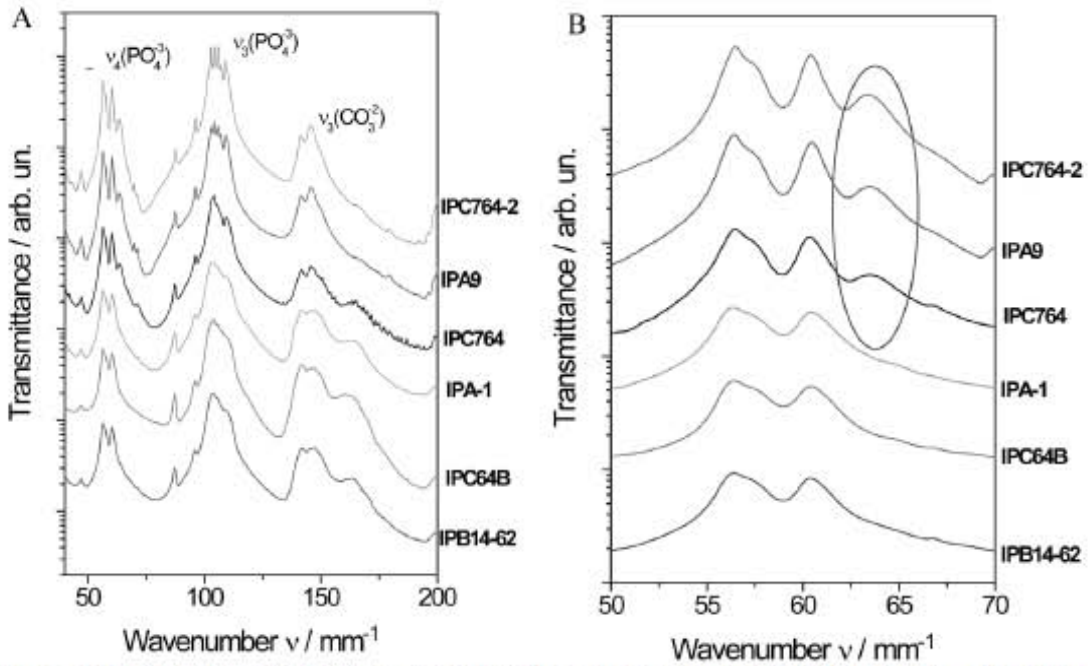

Figure 2: a) the FT-IR spectra where the graphs of the same specimens are reported in the wave-number range from 400 to 2000 cm^{-1}. It is possible to recognize three main groups of band in the range 500-700 cm^{-1}, 1000-1200 cm^{-1} and 1400-1600 cm^{-1}, which are generally assigned to the energy mode 4 of phosphate groups, 3 of phosphate groups and to the 3 of carbonate groups respectively. The spectra are ordered on increasing SF factor

b) the FT-IR transmittance peaks of the phosphate group where the SF is evaluated. Note the appearance of a shoulder at 634 cm-1 for temperatures above 700 °C ,in the IPC764, IPA9 and IPC764-2 specimens, as indicated by arrow.

Table 2 shows in detail the results obtained through the techniques XRD/FT-IR. Estimates temperatures obtained with the two techniques, according to our previous calibrations (Piga *et al.* 2008b; 2009 b) are almost concordant, except in a few cases (IPC764 and IPAI1 specimens). These differences do not exceed 100° C and are not significant. Thus, the combined use of both techniques is a powerful tool to assess whether the bones have subjected to fire and, with fairly good reliability, to which temperature (Piga *et al.* 2010b).

Data of the SAXS isotropic bidimensional patterns were converted in the scattering curve intensity versus the scattering vector Q ($Q = 4\ \pi\sin\theta/\lambda$, where 2θ is the scattering angle and λ is the wavelength of the X-ray beam) by integration in annular rings.

The obtained intensities for the same collection of samples, after correction for the sample transmission and for the contribution of the empty capillar, are shown as a function of the scattering vector Q in Figure 3.

The intensity monotonically decreases for all samples, but the decay law looks different from one sample to another. The absence of a linear region in Figure 3b indicates that the Guinier approximation (Guiner & Fournet 1955) does not hold, probably as a consequence of a high polidispersity in size, thus preventing the evaluation of the particle size.

According to Wess *et al.* (2001) in Figure 3c the experimental data are, thus, reported on a $Q^2I(Q)$ vs. Q in order to evaluate the crystal thickness parameter, T, and to obtain indication on the shape of the mineral crystallites. Data indicate that samples have undergone different

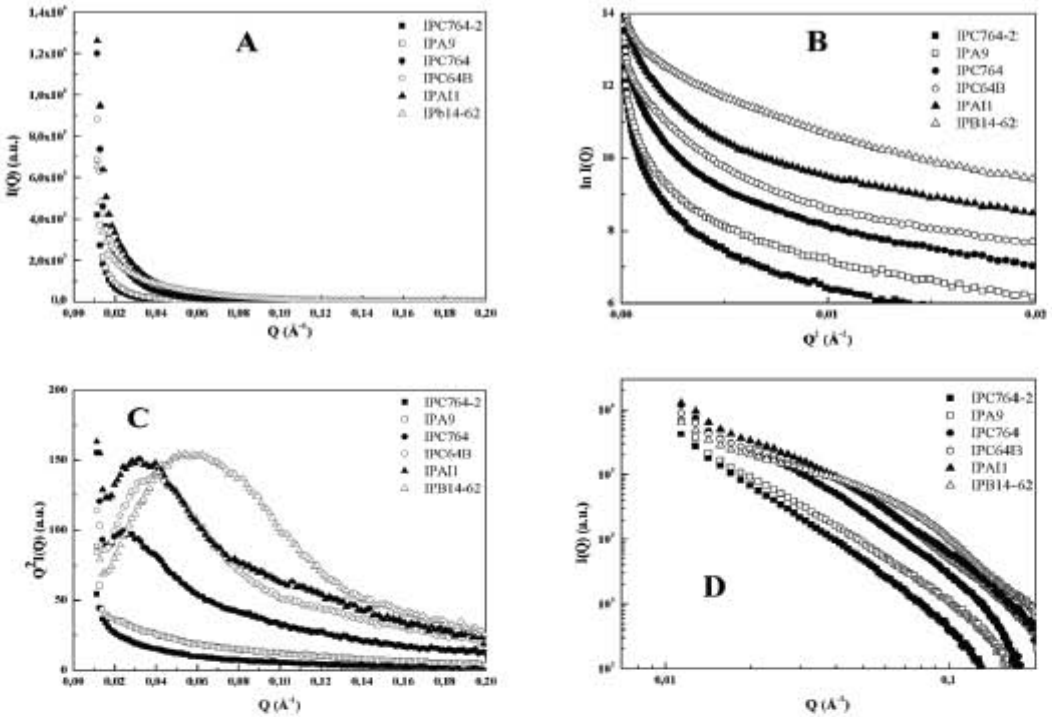

Figure 3. SAXS intensities vs. scattering vector Q for the bones samples. A) I(Q) vs Q. B) Log I(Q) vs. Q2 (Guinier plot). C) Q2I(Q) vs. Q (Kratky plot). D) LogI vs Log Q. For clarity reasons data related to samples IAI1 and IPB14-62 on graphs B and C were multiplied by factors 2 and 4, respectively.

processes on the basis of the discussion reported in Camacho *et al.* (1999). In particular, the behavior at very low Q observed for sample IPC764-2 suggests that it is constituted by large and highly polidisperse crystallites, indicating that this bone has undergone a diagenetic remodeling. The observed behavior for sample IPA9 indicates that this bone has still undergone a little diagenetic alteration and the shape of the curve is typical of plate-like crystals as usually observed for human bones. In contrast, the scattering profiles obtained for samples IPC764, IPC64B, IPAI1 and IPB14-62 are typical of needle-like apatite crystals, thus pointing to some thermal treatment rather than to diagenesis (Pijoan *et al.* 2007). Moreover, the observed intensity increase and the displacement of the maximum toward higher Q values could be consistent with some variation in sizes probably related to treatments at higher temperature or longer times.

Table 3. Results of the linear fits of Log[I(Q) - C] vs. Log Q for the two linear regions. Subscript 1 refers to the low-Q region, 2 to the high-Q region.

Sample	T (nm)	$Log(2\pi \Delta\rho^2 S)_1$	$-P_1$	$Log(2\pi \Delta\rho^2 S)_2$	$-P_2$	$Bi/B_{IPB14-62}$	$r_{cristallite\ size}$
IPC764-2	2.6	0.03(2)	2.83(1)	-1.13(6)	3.86(7)	15.5	10.9
IPA9	2.4	0.45(2)	2.68(2)	-0.89(6)	4.01(7)	8.9	5.2
IPC764	2.1	1.50(6)	2.30(6)	-0.38(3)	3.94(4)	2.75	1.74
IPC64B	1.6	2.17(7)	1.97(5)	-0.13(4)	3.94(4)	1.55	1.35
IPAI1	1.9	2.31(5)	1.90(4)	-0.09(3)	3.99(4)	1.41	1.16
IPB14-62	1.7	2.91(5)	1.44(3)	0.06(4)	3.96(4)	1	1

The obtained values are reported in Table 3. In all cases they are lower than the values obtained for fresh human bones (Fratzl *et al.* 1996). In addition, values obtained for samples IPC764, IPC64B, IPAI1 and IPB14-62 are smaller than those obtained for samples IPC764-2 and IPA9.

It is surprising the apparent correlation with the shape of crystallites although it could not be explained in terms of thermal treatments unless an anisotropic growth occurs.

A new approach has been used to shed light on this aspect and to attempt to estimate the total sizes of the crystallites. The Log I vs Log Q pattern in Figure 3d demonstrates the differences on the decay law. The bi-logarithm plots display the presence of two linear regions for all samples that could be ascribed to the contemporary presence of small primary particles that agglomerate to form clusters (Beaucage 1995). The analysis of the two linear regions draws some information on the kind of interface according to the equation:

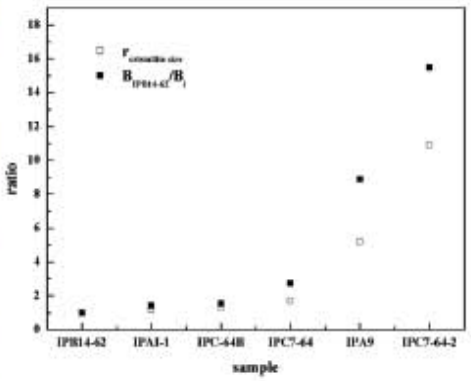

Figure 4. Comparison between relative sizes of IPB14-62 sample (calculated as described) and those obtained from the XRD data analysis.

$$\text{Log } [I(Q) - C] = \text{Log}(2\pi\Delta\rho^2 S) + P \text{ Log } Q$$

Where Dr is the difference in scattering length density between particles and medium, S is the total surface area, P is the exponent of Q related to the kind of interface and C is a constant term, that derives from incoherent scattering and from instrumental noise. Values of Log ($2\pi \Delta\rho^2$ S) and P, derived from the best fits in the two regions, are collected in Table 3, where the ratio between crystalline size obtained by XRD analysis are also reported.

The two sets of data are compared in Figure 4, where each sample is arbitrarily reported on the x-axis. Data of small particle size are in a very good agreement. The increasing difference between the two sets of results at higher particle size could be due to a greater uncertainty in the crystalline size on becoming the XRD peak narrower. Of course another source of uncertainty may be ascribed to the relatively low resolution Q_{min} of the Small Angle Scattering peak In fact, Q_{min} of our apparatus corresponds ca to 800 Å, suggesting that larger particle size are the effect of extrapolation procedures, deserving some degree of arbitrariness.

Conclusions

Samples of archaeological bones were investigated in order to obtain an evaluation of the thermal treatment applied to the samples. Sizes and mineralogical nature of crystalline domains were evaluated by applying the Rietveld method to the XRD patterns. The analysis was conducted on mostly single phase hydroxylapatite specimens, but a minor contamination of calcite probably of endogenous origin has been evidenced in some samples.

To evaluate the temperature to which the bones were subjected, a method based on a calibration of the heat treatment as a function of temperature and time by following the average

grain size of hydroxyapatite (HA) biomineral phase has been applied to the XRD data.

FT-IR spectra are dominated by the typical hydroxylapatite bands apart from weak components typical of carbonates. Data confirm findings about the thermal treatment samples undergo, in fact, the shoulder at ca. 630 cm^{-1} for the less "crystalline" specimens is replaced by a further peak in the specimens which appeared to have been treated at higher temperature.

SAXS data analysis further confirms the above findings. In addition, it allows obtaining some information on the morphologies of samples. Crystal shape evolves as a function of the physical-chemical modification, diagenesis or thermal treatments, that bones have undergone. Crystals result composed at a nanoscopic level by small particles characterised by a sharp interface that agglomerate to form bigger clusters of fractal geometry. The fractal nature reduces on increasing the temperature of thermal treatment.

Acknowledgements

The authors thank Dr. Massimo Piccinini (Porto Conte Ricerche, Alghero-Sassari) for FT-IR spectrometer data collection, Prof. Eugenio Caponetti, Dr. Delia Chillura Martino and Dr. Maria Luisa Saladino (Università degli Studi di Palermo) for SAXS measurements. SAXS experimental data were provided by Centro Grandi Apparecchiature—UniNetLab—Universita` di Palermo.

This work was partially supported by a project of Ministerio de Ciencia y Tecnología de España, CGL2008-00800.

Bibliography

Beaucage, G. 1995. Approximations Leading to a Unified Exponential/Power-Law Approach to Small-Angle Scattering. *Journal of Applied Crystallography* 28, 717–728.

Bonucci, E. & Graziani, G. 1975. Comparative thermogravimetric X-ray diffraction and electron microscope investigations of burnt bones from recent, ancient and prehistoric age. *Atti della accademia Nazionale dei Lincei, Rendiconti, classe di scienze fisiche, matematiche e naturali* LIX, 517–532.

Camacho, N.P., Rinnerthaler, S., Paschalis, E.P., Mendelsohn R., Boskey, A.L. & Fratzl, P. 1999. Complementary information on bone ultrastructure from scanning small angle X-ray scattering and Fourier-transform infrared microspectroscopy. *Bone* 25 (3), 287–293.

Child, A.M. 1995. Towards an understanding of microbial decomposition of archaeological bone in the burial environment. *Journal of Archaeological Science* 22, 165–174.

Eckert, W.G, James, S. & Katchis, S. 1988. Investigation of cremations and severely burned bodies. *American Journal of Forensic Medicine and Pathology* 9, 188–200.

Elliott, J.C., Mackie, P.E. & Young, R.A. 1973. Monoclinic hydroxyapatite. *Science* 180, *1055*–1057.

Elliott, J.C., Wilson, R.M. & Dowker, S.E.P. 2002. Apatite structures. *Advances in X-ray Analysis* 45, 172–181.

Enzo, S., Fagherazzi, G., Benedetti, A. & Polizzi, S. 1988. A profile-fitting procedure for analysis of broadened X-ray diffraction peaks. I Methodology. *Journal of Applied Crystallography* 21: 536–542.

Fratzl, P., Schreiber, S. & Klaushofer K. 1996. Bone mineralization as studied by small-angle x-ray scattering. *Connective Tissue Research* 34 (4), 247–254.

Guinier, A. & Fournet, G. 1955. Small-Angle Scattering of X-rays. Wiley & Sons, New York.

Harbeck, M., Schleuder, R., Schneider, J., Wiechmann, I., Schmahl, W.W. & Grupe, G. 2011. Research potential and limitations of trace analyses of cremated remains. *Forensic Science International* 204, 191–200.

Hiller, J., Thompson, T.J.U., Evison, M.P., Chamberlain, A.T. & Wess, T.J. 2003. Bone mineral change during experimental heating: An X-ray scattering investigation. *Biomaterials* 24, 5091–5097.

Hiller, J.C. & Wess T.J. 2006. The use of small-angle X-ray scattering to study archaeological and experimentally altered bone. *Journal of Archaeological Science* 33, 560–572.

Hiller, J.C., Collins M.J., Chamberlain A.T. & Wess, T.J. 2004. Small angle X-ray scattering: a high throughput method for investigating archaeological bone preservation. *Journal of Archaeological Science* 31, 1349–1359.

Lutterotti, L. & Bortolotti, M. 2003. Object oriented programming and fast computation techniques in MAUD, a program for powder diffraction analysis written in java. *IUCr: Compcomm Newsletter* 1, 43–50.

Perinet, G. 1964 Determination par diffraction X de la temperature de cuisson d'un ossement calcinè. Application au materiel prehistorique. *Comptes Rendus d'Acudemie des Sciences, Paris (Series D)* 258, 4115–4116.

Person, A., Bocherens, H., Saliege, J.F., Paris, F., Zeitoun, V. & Gerard, M. 1995. Early diagenetic evolution of bone phosphate: an X-ray diffractometry analysis. *Journal of Archaeological Science* **22**, 211–221.

Person, A., Bocherens, H., Mariotti, A. & Renard, M. 1996. Diagenetic evolution and experimental heating of bone phosphate. *Palaeogeography, Palaeoclimatology, Palaeoecology* 126, 135–149.

Piga, G., Malgosa, A., Mazzarello, V., Bandiera, P., Melis, P. & Enzo, S. 2008a. Anthropological and physico-chemical investigation on the burnt remains of Tomb IX in the "Sa Figu" hypogeal necropolis (Sassari-italy)-Early Bronze Age. *International Journal of Osteoarcheology* 18, 167–177.

Piga, G., Malgosa, A., Thompson, T.J.U. & Enzo, S. 2008b. A new calibration of the XRD technique for the study of archaeological burnt remains. *Journal of Archaeological Science* 35, 2171–2178.

Piga, G., Santos-Cubedo, A., Moya Solà, S., Brunetti, A., Malgosa, A. & Enzo, S. 2009a. An X-Ray Diffraction (XRD) and X-Ray Fluorescence (XRF) investigation in human and animal fossil bones from Holocene to Middle Triassic. *Journal of Archaeological Science* 36, 1857–1868.

Piga, G., Thompson, T.J.U., Malgosa, A. & Enzo, S. 2009b. The potential of X-Ray Diffraction (XRD) in the analysis of burned remains from forensic contexts. *Journal of Forensic Sciences* 54 (3), 534–539.

Piga, G., Hernández-Gasch J.H., Malgosa, A., Ganadu, M.L. & Enzo, S. 2010a. Cremation practices coexisting at the *S'Illot des Porros* Necropolis during the Second Iron Age in the Balearic Islands (Spain). *Homo* 61, 440–452.

Piga, G., Guirguis, M., Bartoloni, P., Malgosa, A. & Enzo, S. 2010b. A funerary rite study in the Phoenician-Punic Necropolis of Mount Sirai (Carbonia-Sardinia-Italy), *International Journal of Osteoarcheology* 20, 144–157.

Piga, G., Santos-Cubedo, A., Brunetti, A., Piccinini, M., Napolitano, E., Malgosa, A. & Enzo, S. 2011. A multi-technique approach by XRD, XRF, FT-IR to characterize the diagenesis of dinosaur bones from Spain. *Palaeogeography, Palaeoclimatology, Palaeoecology* 310, 92–107.

Pijoan, C.MA. Mansilla J., Leboreiro, I. Lara, V.H. & Bosch, P. 2007. Thermal alterations in archaeological bones. *Archaeometry* 49(3), 713–727.

Rogers, K.D. & Daniels, P. 2002. An X-ray diffraction study of the effects of heat treatment on bone mineral microstructure. *Biomaterials* 23 (12), 2577–2585.

Shipman, P., Foster, G. & Schoeninger, M. 1984. Burnt bones and teeth: an experimental study of color, morphology, crystal structure and shrinkage. *Journal of Archaeological Science 11, 307*–325.

Stathopoulou, E.T., Psycharis, V. & Chryssikos, G.D. 2008. Bone diagenesis: new data from Infrared spectroscopy and X-Ray Diffraction. *Palaeogeography, Palaeoclimatology, Palaeoecology* 266, 168–174.

Stiner, M.C., Kuhn, S.L., Weiner, S. & Bar-Yosef, O. 1995. Differential burning, recrystallization, and fragmentation of archaeological bone. *Journal of Archaeological Science* 22, 223–237.

Thompson, T.J.U. 2005. Heat-induced dimensional changes in bone and their consequences for forensic anthropology. *Journal of Forensic Sciences* 50(5), 1008–1015.

Wachtel, E. & Weiner, S. 1994. Small-angle X-ray scattering study of dispersed crystals from bone and tendon. *Journal of Bone and Mineral Research* 9 (10), 1651–1655.

Weiner, S. & Bar-Yosef, O. 1990. States of preservation of bones from prehistoric sites in the Near East: a survey. *Journal of Archaeological Science* 17, 187–196.

Wess, T., Alberts I., Hiller J., Drakopoulos, M., Chamberlain, A.T. & Collins, M. 2002. Microfocus small angle X-ray scattering reveals features in archaeological bone samples; detection of changes in bone mineral habit and Size. *Calcified Tissue International* 70 (2), 103–110.

Wess, T.J. Drakopoulos M., Snigirev A., Wouters J., Paris O., Fratzl P., Collins M., Hiller J. & Nielsen K. 2001. The use of Small-Angle X-Ray Diffraction studies for the analysis of structural features in archaeological aamples. *Archaeometry* 43 (1), 117–129.

Young, R.A. (ed.) 1993. The Rietveld Method. University Press, Oxford.

Zizak, O., Paris, P., Roschger, S., Bernstorff, H., Amenitsch, K., Klaushofer, P. & Fratzl, P. 2000. Investigation of bone and cartilage by synchrotron scanning-SAXS and -WAXD with micrometer spatial resolution. *Journal of Applied Crystallography* 33, 820–823.

Chapter 4.3: Cremation practices coexisting at the *S'Illot des Porros* Necropolis during the Second Iron Age in the Balearic Islands (Spain)

Authors: **Giampaolo Piga, Jordi Hernández-Gasch, Assumpciò Malgosa, Maria Luisa Ganadu, Stefano Enzo.**

Homo 61, 440–452. (http://dx.doi.org/10.1016/j.jchb.2010.09.003).

The combined use of macroscopic examination, XRD and FT–IR analysis is rarely incorporated in studies examining various aspects of the burning process, such as duration and temperature of the funerary pyre or the temperature uniformity throughout the skeleton, and it could provide a great amount of informations. For this reason the context of the necropolis of *S'Illot des Porros* (Maiorca, Spain) is particularly interesting.

The necropolis of *S'Illot des Porros* is one of the most important prehistory funerary sites of the Balearic Islands and certainly the better documented in terms of anthropological studies. The archaeological site presented three sepulchral areas called "chambers A, B and C" excavated in the rock-bed. In all three chambers have been found inhumations and remains of burnt bones at various levels of burning. The cremated bones were attributed at least to 67 individuals (out of a whole of 285).

The aim of our paper is to assess whether the funerary chambers in *S'Illot des Porros* were specifically devoted to inhumation, rather than cremation or uncompleted body combustion due to purification activities and to determine for the first time in the Balearic prehistory when the funerary practices involving fire were introduced in relation to specific events.

The availability of bone samples of a relative accuracy in terms of dating allows to place quite precisely in time the period when these practices took over and, thus, to attempt an historical explanation. So far evidences of cremations in the Balearic Islands have been underlined without undergoing any further research, even less around their social meaning.

In order to achieve these goals we investigate the structure and microstructure properties of all the cremated remains from the site using X–ray diffraction (XRD) partially supported by Fourier Transform Infrared (FT–IR) spectroscopy which have

been demonstrated able to discriminate the degree of fire treatment to which the bones were possibly subjected.

The combined use of these techniques pointed out to the simultaneous use of inhumation and cremation funerary rites at various levels of burning, probably due to existing social differences.

HOMO - Journal of Comparative Human Biology 61 (2010) 440–452

Contents lists available at ScienceDirect

HOMO - Journal of Comparative Human Biology

journal homepage: www.elsevier.de/jchb

Cremation practices coexisting at the S'Illot des Porros Necropolis during the Second Iron Age in the Balearic Islands (Spain)

Giampaolo Piga[a,c], Jordi Hernández-Gasch[b], Assumpciò Malgosa[a,*], Maria Luisa Ganadu[c], Stefano Enzo[c]

[a] *Grup de Recerca en Osteobiografia (GROB), Unitat d'Antropologia Biologica, Departament de Biologia Animal, Biologia Vegetal i Ecologia, Universitat Autonoma de Barcelona, Edifici C, 08193 Bellaterra - Barcelona, Spain*

[b] *Grup de Recerca d'Arqueologia Social Mediterrània, Departament de Prehistòria, Universitat Autònoma de Barcelona, 08193 Bellaterra - Barcelona, Spain*

[c] *Dipartimento di Chimica, Università di Sassari, via Vienna n. 2, I-07100 Sassari, Italy*

ARTICLE INFO

Article history:
Received 25 November 2009
Accepted 25 September 2010

ABSTRACT

The necropolis of S'Illot des Porros, one of the most important prehistoric funerary sites of the Balearic Islands (Spain), was in use from the VIth and Vth century BCE until the Ist century CE. Located in a funerary area which contains two cementeries and one sanctuary, this site is constituted by three funerary chambers named A, B and C, respectively. Investigations on all the human burnt bone remains of the chambers, carried out mainly by the X-ray diffraction and supplemented in some cases by Fourier Transform Infrared spectroscopy pointed to the simultaneous use of inhumation and cremation funerary rites, probably due to existing social differences.

In particular, it was argued that the chambers were differentiated, i.e., B was dedicated to inhumations and A to cremations, the cremations found in chamber B very likely being a result of a cleaning-purification of the burial area. Moreover, chamber C, which is the most ancient (IVth century BCE) and with the largest number of inhumed remains, contains the smallest number of remains that were exposed to fire and just in one case it seems possible to attribute a genuine high-temperature cremation.

* Corresponding author. Tel.: +34 935811317; fax: +34 935811321.
E-mail address: assumpcio.malgosa@uab.es (A. Malgosa).

0018-442X/$ – see front matter © 2010 Elsevier GmbH. All rights reserved.
doi:10.1016/j.jchb.2010.09.003

1. Introduction

The necropolis of S'Illot des Porros is one of the most important prehistoric funerary sites of the Balearic Islands (Western Mediterranean Spain) and certainly among the best documented in terms of anthropological studies. S'Illot des Porros is located in a rocky little island of approximately 3040 m^2, which is only 1.5 m above the sea level (Fig. 1a and b). The archaeological site occupied 450 m^2, prior to the destruction in 2001, and consisted of three sepulchral areas called "chambers A, B and C" excavated in the rock-bed. They were partially built by cyclopean walls defining an apsidal plan and accompanied by a nearby burial area of small tombs and pits.

The site was first explored at the end of the 1950s, but it was mainly excavated during the 1960s. The excavations were resumed and finalised at the end of the 1990s (Hernández et al., 1998; Tarradell, 1964).

The cemetery belongs to the final period of the Balearic Islands' prehistory, the so-called Balearic culture, which occurred during the Second Iron Age (VIth–IInd c. BCE).

The first use of the island is traced back to the period called the Middle Navetiform Period (ca 1400–1200 BCE) and it appears to have continued until the Late Navetiform Period (ca 1200–1050 BCE) then to the Proto-Talayotic Period (ca 1050–850 BCE).

It has been suggested, that the S'Illot des Porros area in the earliest times was used for trade exchange as a store and shipping centre (Salvà and Javaloyas, in press) but not for funerary purposes. The necropolis was only established around the VIth–Vth century BCE and lasted until the beginning of the Flavian Period of the Early Roman Empire (70 CE).

It was in the IVth century BCE that the C chamber was established and very likely the stones from previous constructions were used as building material for this funerary chamber.

Until this period the only burial rite was inhumation, with bodies deposited in foetal position, although in the upper layers some burnt bones were found and initially attributed to cremation practices (Hernández et al., 1998; Tarradell, 1964). This attribution is supported by the archaeological context and radiocarbon dating (Van Strydonck et al., 2002), despite the uncertainty of the calibrated date.

Chambers A and B were likely built after chamber C was filled up, that is around the IIIrd century BCE. Following the sequence of construction, chamber B appears to be later than A, since it leans on it and remains located between A and C chambers (Fig. 2).

For chamber B a radiocarbon date is available with a calibration from the IVth to the IInd century BCE. The archaeological materials excavated from the lower levels of the sepulchral chambers allow for better evaluation of this chronology, indicating that it is likely that they began to be used in the second half of the IInd century BCE. This is the period when the practice of cremation clearly emerges amongst a burial tradition that still exists, as shown by the discovery of inhumations in foetal position at the bottom of chamber B (Hernández et al., 1998).

Concerning the inner sedimentation, the documentation of early excavations shows the existence of two distinct layers for chamber A. In the lower level, about 0.5 m in depth, is preserved clear evidence

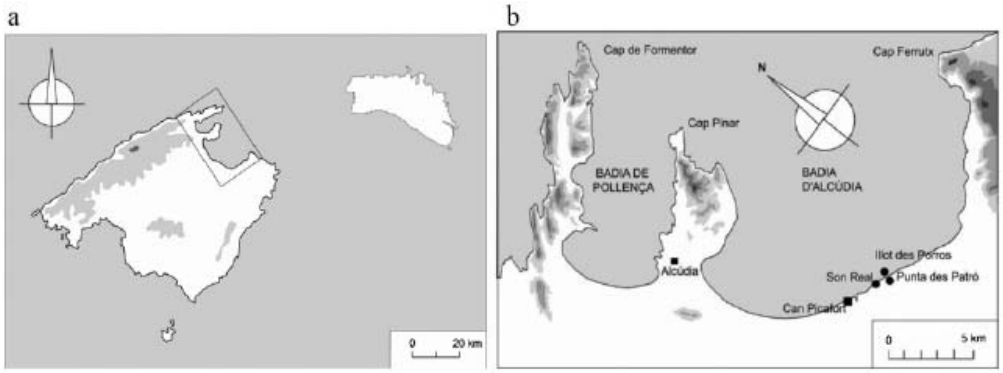

Fig. 1. (a) Map of the Balearic Islands: Mallorca to the South-west and Minorca to North-east. (b) Map of the North-east bay in Mallorca, with location of the Son Real funerary area.

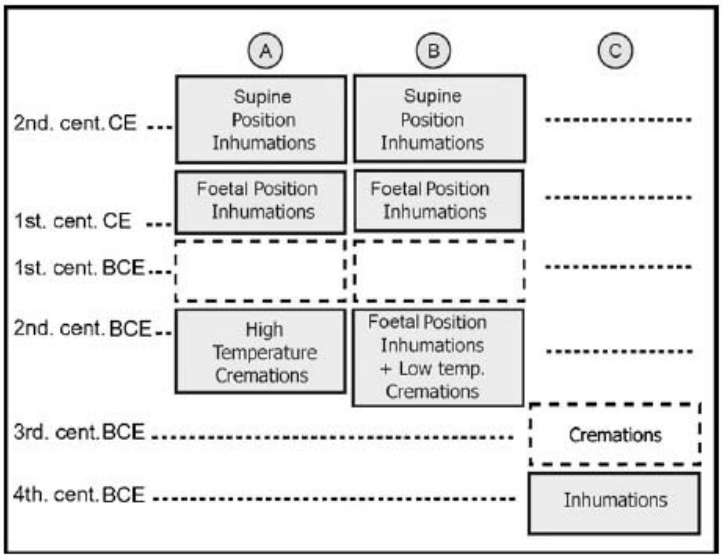

Fig. 2. Pattern of burial rites' evolution in the three chambers of S'Illot des Porros necropolis.

of fire such as ashes and cremated remains reduced to a small size, with an absence of long bones and complete cranial bones (Fig. 3).

Presence of irregularly distributed lime was also observed on top of some cremation zones. It can be surmised that the cremated remains were kept separated by small amounts of lime mixed with soil and sand (Hernández et al., 1998; Fig. 4).

With regard to chamber B, the lower level (about 0.4–0.8 m in depth) appeared to be constituted similar to chamber A, mostly by cremated remains, though it may be suspected that the "intensity" of the cremation was lower. The remains appeared blackened due to fire, but the absence of the typical signs of high-temperature cremation must be noted, i.e., grey or white spots, transverse fractures and bone size reduction (Fig. 5).

By the time chambers A and B were in use, the southwestern portion of the site was also destined to be a necropolis with a collection of individual oval-plan pits covered by stones. In such cases the rite was always inhumation with bodies in a tightly flexed lateral position and without funerary items.

Finally, when the chamber was totally covered with sediment and the original access closed, new walls were erected above the ground level with an approximately rectangular shape. The late inhumations are associated with this space.

Fig. 3. Two incinerated cranial fragments relevant to one individual from chamber A; note the fractures typical of cremation carried out on fresh bone.

Fig. 4. Two fragments of long bones with lime aggregates.

Particularly, the lower level showed bodies in foetal position which were dated to around the half of the Ist century CE while the upper level showed bodies in a supine position without further material to provide a date (Hernández et al., 1998).

The anthropological material of S'Illot des Porros was recovered in several excavation campaigns between 1959 and 1969 (Hernández-Gasch, 1998; Hernández et al., 1998; Tarradell, 1964; Tarradell and Woods, 1959). The study of human remains has been undertaken since the eighties. These studies took into consideration various anthropological issues concerning type, morphology and pathology in relation to the sexual dimorphism, diet and infant growth (Alesán et al., 1999; Carrasco and Malgosa, 1990; Castellana and Malgosa, 1991; Castellana et al., 1991; Malgosa, 1985, 1992; Malgosa and Campillo, 1991; Pérez, 1990; Rissech and Malgosa, 1997; Subirà and Malgosa, 1992; Subirà et al., 1992).

The aim of this contribution is to assess whether the funerary chambers in S'Illot des Porros were specifically devoted to inhumation, rather than cremation or incomplete body combustion due to purification activities.

So far, evidence of cremations in the Balearic Islands has been presented without undergoing any further research, particularly of their social meaning. The availability of bone samples of a relative accuracy in terms of dating, allows us to place quite precisely in time, the period when these practices took over and, thus, to attempt an historical explanation.

Fig. 5. Drilled cranium of the individual IPB6[1] completely stained by fire. Note the absence of transverse fractures.

In general, we will try to determine when the funerary practices involving fire were introduced for the first time in the Balearic prehistory, in relation to specific events.

In order to achieve these goals, we investigated the structure and microstructure properties of cremated remains from the site using the X-ray diffraction (XRD) and Fourier Transform Infrared (FT-IR) techniques. These techniques, under specific assumptions, have been demonstrated to be able to discriminate the degree of fire treatment to which the bones were possibly subjected (Enzo et al., 2007; Piga et al., 2008a, 2010; Shipman et al., 1984; Surovell and Stiner, 2001; Thompson et al., 2009).

2. Materials and methods

The cremated bones were attributed to at least 67 individuals (out of a total of 285). Fragments of 0.5 g of bone from each cremated individual were prepared for XRD analysis by hand grinding with an agate mortar and pestle until reduced to a sufficiently fine powder.

The X-ray diffraction patterns were recorded using Bruker D8, Philips PW-1050 and Siemens D-500 diffractometers in the Bragg–Brentano geometry with CuKα radiation (λ = 1.54178 Å). The goniometer was equipped with a graphite monochromator in the diffracted beam. In analogy with the work by Michel et al. (1995), we have recently suggested the collection of X-ray patterns in an extended angular range employing long periods of acquisition (Piga et al., 2009a,b, 2010). Our patterns were collected with 0.05° of step size in the angular range 10–140° in 2θ, with a counting time of 40 s per point.

The X-ray generator worked at a power of 40 kV and 30 mA and the resolution of the instruments (divergent and antiscatter slits of 0.5°) was determined using α-SiO_2 and α-Al_2O_3 standards free from the effect of reduced crystallite size and lattice defects.

The powder patterns were analysed according to the Rietveld (1967) method, using the programme MAUD (Lutterotti et al., 1998).

These experiments and analyses are supposed to be more reliable for a precise description of the growth phenomena (i.e., degree of organization), which are induced in the hydroxyapatite (HA) micro- (or nano-) crystals as a function of fire temperature. As a matter of fact, the procedure is not limited to the analysis of a few selected peaks but evaluates the pattern with the maximum collectable evidence. As for apatite evidenced in our XRD patterns, following Elliott et al. (1973) we have adopted a monoclinic description of the unit cell (Space Group P21/c, 4 molecular units) rather than the usual hexagonal cell of S. G. P63/m with two molecules of hydroxyapatite.

As a matter of fact, the lattice parameter of the monoclinic phase a_M coincides with that of the hexagonal phase a_H, but b_M is ca $2 \times a_H$, $c_M = c_H$ and $\beta_M \approx 120°$.

The Rietveld method is an efficient approach that evaluates quantitatively the amount, structure and microstructure parameters of mineralogical phases while also taking into account the instrumental parameters. While the average crystallite size parameter does not depend on the order of reflections, the lattice strain does.

The programme MAUD calculates numerically the convolution equations in order to correctly distinguish and evaluate both crystallite size and strain terms in the experimental peak broadening. Also, one important advantage of the Rietveld method is that no standard is required for quantitative evaluation of phases, thus minimizing the work on sample preparation.

To evaluate the temperature to which the bones were presumably subjected, it is necessary to make reference to a calibration that was worked out with a sample of human bone subjected to selected temperatures of cremation (Piga et al., 2008b, 2009a).

Our previous applications of the XRD technique to human bones were based on a calibration of the heat treatment as a function of temperature and time by following the average grain size of hydroxyapatite (HA) biomineral phase. We have assessed with our method that the average grain size in untreated human bones is ca 170 Å (1 Å = 10^{-10} m) and remains approximately constant until 500–600 °C. The average crystallite size then quickly increases around 700 °C, subsequently levelling off at a new value according to a sigmoidal behaviour typical of a logistic function (Piga et al., 2008b, 2009a).

Thus, following the quantitative interpretation of XRD data in terms of the growth mechanism of HA microcrystals induced by thermal treatment, it is possible to estimate with good reliability the temperature, to which the bones were subjected during the burning process.

In turn, this permits us to ascertain the fire technology in use and, with specific concern to the site here investigated, it supplies valuable information on the possible coexistence of inhumation and cremation practices.

A concomitant investigation was carried out by FT-IR spectroscopy, whose absorption bands are related to the bond strength of carbonate and phosphate groups of HA. The bands that are considered, are generally constituted by overlapped lines whose width decreases as a function of treatment temperature according to an empirical crystallisation index also called splitting factor (SF) (Weiner and Bar-Yosef, 1990).

The hand-ground bone powders were mixed with potassium bromide (KBr) in the weight ratio 1:100 respectively, to make pellets suitable for FT-IR spectra that were collected with a JASCO FT 480 spectrometer in terms of absorbance vs. wavenumber ν in the range 40,000–450,000 m^{-1}. In particular, the cluster of bands of HA in the range 50,000–70,000 m^{-1} was analysed because it is generally recognised as the most reliable zone in which to define the splitting factor SF as a function of temperature treatment. SF is defined from the sum of band intensities of the two peaks divided by the intensity of the valley between them (Weiner and Bar-Yosef, 1990).

The peaks were processed using standard non-linear least squares fitting procedures incorporated in the Origin® software assuming for the transmitted line shape a symmetric Pearson VII type function and a polynomial background of order 1.

3. Results

Data from all the burnt bones examined and belonging to the chamber's necropolis are collected in Table 1. For the sake of simplicity we will discuss mainly the XRD data in terms of average crystallite size given in Ångstrom (Å) units and corresponding temperature of fire associated with it, according to our previous calibrations (Piga et al., 2008b, 2009a).

The graphs of Figs. 6 and 7a and b are referred to XRD patterns and FT-IR spectra of six representative specimens belonging to all the necropolis chambers, in order to appropriately compare both of the techniques employed (Fig. 8).

Firstly, the XRD patterns reveal that the examined samples are almost totally single phase, i.e., in all cases they are dominated by the HA fingerprint (Fig. 6).

The presence of carbonate units CO_3^{2-}, that may substitute for phosphate groups PO_4^{3-} in the apatite structure, may separate from the bone during the deposition time and may amount to not more than 7–8 wt% according to Wopenka and Pasteris (2005) if they are of endogenous origin. Only a minor quantity of calcite ($CaCO_3$) (less than 5 wt%) is found in the specimen IPC764, which seems compatible with an endogenous origin, even if we cannot totally reject the presence of calcite due to lime in the nearby environment.

From XRD a large peak broadening from bottom-to-top, in the patterns of specimens IPB14-62, IPC64B and IPA-1 respectively, is also evident.

For the other specimens, an increase in sharp peaks is also visible, which is generally ascribed to growth processes of the apatite phase when subjected to high-temperature fire, such as that created during a cremation process. Thus, it can be surmised that some of the bones were subjected to cremation practices at high temperature, while others were subjected to a low temperature treatment.

Similar deductions are supported also by the FT-IR spectra of Fig. 7a, where the graphs of the same specimens are reported in the wave-number ν range from 40,000 to 200,000 m^{-1}. It is possible to recognise three main groups of bands in the range 50,000–70,000 m^{-1}, 100,000–120,000 m^{-1} and 140,000–160,000 m^{-1}, which are generally assigned to the energy mode ν_4 of phosphate groups, ν_3 of phosphate groups and to the ν_3 of carbonate groups respectively (Lafon et al., 2008).

The graphs in Fig. 7b are a magnification of FT-IR spectra in the range 50,000–70,000 m^{-1} and highlight the band structure of ν_4 phosphate groups from the point of view of the splitting factor SF. In our previous calibration of FT-IR spectra it was established that the appearance of the shoulder at ca 63,400 m^{-1} indicates fire temperature between ca 700 and 800 °C and persists until 1000 °C (Piga et al., 2010).

It can be quickly observed that the sharper peaks of XRD structure factor and the sharper of ν_4 splitting factor in FT-IR spectra are in overall agreement. Thus, the combined use of both techniques is

Table 1
List of 67 burnt remains from the S'Illot des Porros necropolis, with anthropological information, part of the body analysed, the average domain size of HA crystallites and corresponding temperatures to which the bones were likely subjected according to our calibration (Piga et al., 2008b, 2009a).

Sample code	Age	Sex	Chamber	Part of the body analysed	Average crystallite size (Å)	Temperature (°C)
IPA-62 cr.2	4–5 years old	–	A	Cranium	1115	825
IPA-2	14–15 years old	–	A	Cranium	974	850–900
IPA-2(2)	14–15 years old	–	A	Cranium	920	775
IPA-9	14–15 years old	–	A	Cranium	957	850–900
IPA-7	Adult	♂	A	Cranium	260	650
IPA-8	3–7 years old	–	A	Cranium	2108	1000
IPA-8(2)	14–17 years old	–	A	Cranium	2236	1000
IPAI-1(1961)	Adult	♂	A	Cranium	213	650
IPAI-4	Adult	♂	A	Cranium	185	300
IPAI-7a	Adult	♂	A	Cranium	205	400
IPAI-2	Adult	♀	A	Cranium	223	600
IPAI-3	Adult	♀	A	Cranium	221	650
IPA-6	Middle aged	Undetermined	A	Cranium	2138	1000
IPA-10	Undetermined	Undetermined	A	Cranium	2784	1000
IPA-2 (1961)	Adult	♀	A	Cranium	1829	1000
IPA-11	Middle aged	♀	A	Cranium	1850	1000
IPA13	Adult	♂	A	Cranium	199	400–500
IPAI-5 (1961)	Adult	Undetermined	A	Cranium	190	300
IPB3′	Infantile	Undetermined	B	Cranium	2158	1000
IPB13	Middle aged	♂	B	Vertebra	195	400
IPB13 (1961)-2	Middle aged	♂	B	Mandible	193	400
IPB-21	4–5 years old	–	B	Cranium	194	400
IPB-28	<19–20 years old	–	B	Temporal bone	182	300
IPB-9[12]	Middle aged	♂	B	Cranium	195	400
IPB-14 (1961)	Adult	♂	B	Cranium	196	400
IPB-6 (1961)	Senile	♂	B	Cranium	175	200
IPB-22″	Senile	♂	B	Cranium	180	300
IPB-6[1]	Middle aged	♂	B	Cranium	196	400
IPB-8″ (1962)	Middle aged	♂	B	Mandible	203	400
IPB-9 (1961)	Middle aged	♂	B	Cranium	186	300
IPB-7 (1962)	Adult	♀	B	Cranium	183	300
IPB-9″	Adult	♀	B	Cranium	176	200
IPB-ni (1962)	40–50 years old	♀	B	Mandible	185	300
IPB-20	Senile (60 years old)	♂	B	Cranium	190	300
IPB-23 (1961)	Adult	♀	B	Cranium	192	300
IPC7 (1964)	Adult	♂	C	Femur	321	750-775
IPC7 (1964)-2	Adult	♂	C	Cranium	2008	1000
IPC-8	9–10 years old	–	C	Cranium	252	650
IPC-64B	Juvenile	–	C	Cranium	248	650
IPC-35 (1964)	Adult	♀	C	Cranium	193	400
IPC-4	Undetermined	Undetermined	C	Cranium	195	400
IP-27d	11 years old	–	Undetermined	Femur	1340	900
IPH-4-1	Juvenile	–	Burial H	Cranium	184	300
IPN-3	Juvenile (17–18)	♀	Undetermined	Mandible	197	400
IPN-8	Adult	♂	Undetermined	Cranium	195	400
IPN-37	Adult	♂	Undetermined	Cranium	182	300
IPN-32	Adult	♂	Undetermined	Mandible	186	300
IPN-33	Adult	♂	Undetermined	Cranium	181	300
IPN-41	Middle aged	♂	Undetermined	Cranium	198	400
IPN-42	Middle aged	♂	Undetermined	Cranium	181	300
IPN-43	Juvenile-adult	♀	Undetermined	Cranium	183	300
IPN-45	Middle aged	♂	Undetermined	Cranium	184	300
IPN-48	Adult	♂	Undetermined	Cranium	190	300
IPN-50	Middle aged	♂	Undetermined	Cranium	191	300
IPN-24	Middle aged	♀	Undetermined	Cranium	185	300

Table 1 (*Continued*)

Sample code	Age	Sex	Chamber	Part of the body analysed	Average crystallite size (Å)	Temperature (°C)
IPN-34	Adult	♀	Undetermined	Cranium	190	300
IPN-46	Adult	♀	Undetermined	Cranium	198	400
IPN-38	Middle aged	Undetermined	Undetermined	Cranium	186	300
IPN-39	Adult	Undetermined	Undetermined	Cranium	194	400
IPN-40	Adult	Undetermined	Undetermined	Cranium	192	300
IPN-10	Adult	Undetermined	Undetermined	Cranium	240	650
IPN-11	Adult	Undetermined	Undetermined	Cranium	197	400
IPN-35	Adult	Undetermined	Undetermined	Cranium	180	300
IPN-44	Adult	Undetermined	Undetermined	Cranium	190	300
IPN-47	Adult	Undetermined	Undetermined	Cranium	190	300
IPN-20	Adult	♀	Undetermined	Cranium	185	300
IPN-25	30–40 years old	Undetermined	Undetermined	Femur	1340	900

a powerful tool to assess whether the bones have been subjected to fire and, with fairly good reliability, to which temperature (Piga et al., 2010). In the present context we have restricted our analysis of "crystallinity" making reference only to the values of the average crystallite size from XRD for which the data inspection was complete.

Concerning chamber A, the large values of the average crystallite size for 10 out of 18 specimens examined seem sufficient to conclude that they were preferentially subjected to a cremation pro-

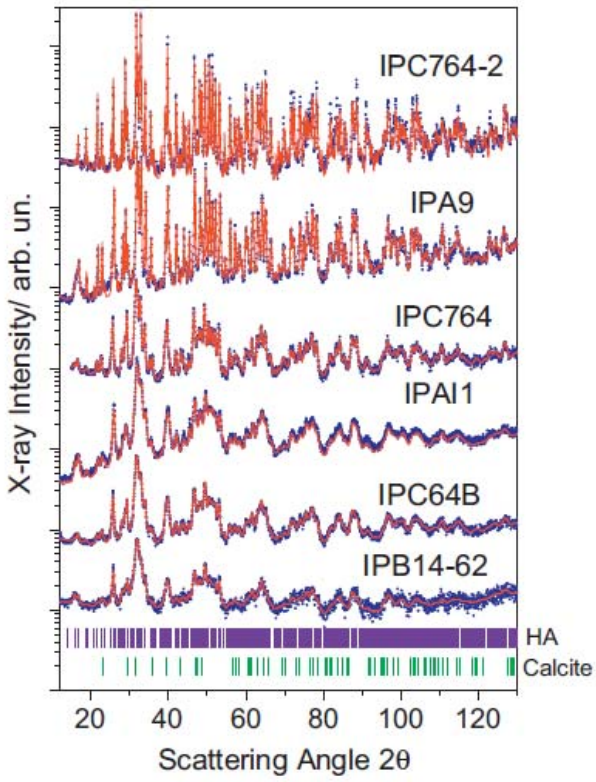

Fig. 6. XRD patterns of cremated bones from the S'Illot des Porros necropolis; IP-B14-62, IPC64B and IPAI1 samples display a large peak broadening with respect to the remaining specimens on account of a weak thermal treatment received. With the Rietveld method the goodness of the fit between calculated and experimental patterns is measured in terms of numerical agreement factors so, this approach appears the most complete for evaluating simultaneously experimental data quality (i.e. signal-to-noise ratio) and/or credibility of model assumptions.

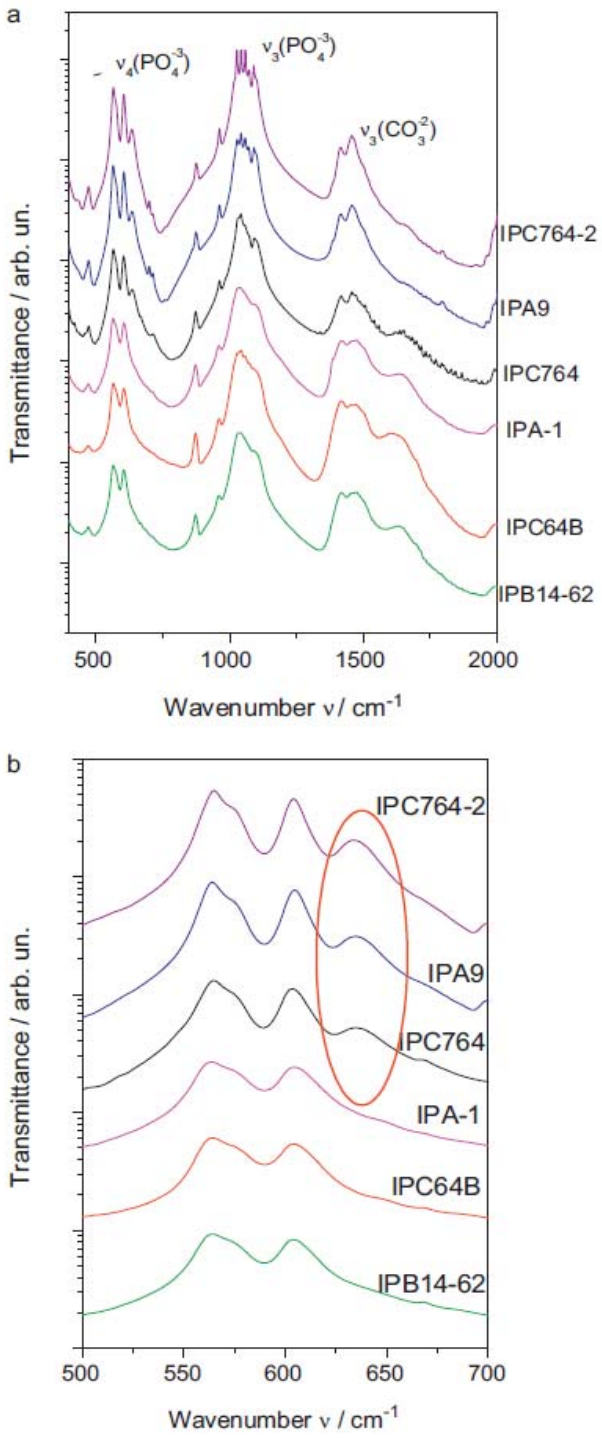

Fig. 7. (a) FT-IR spectra where graphs of the same specimens are reported in the wave-number ν range from 40,000 to 200,000 m^{-1}. It is possible to recognise three main groups of bands in the range 50,000–70,000 m^{-1}, 100,000–120,000 m^{-1} and 140,000–160,000 m^{-1}, which are generally assigned to the energy mode ν_4 of phosphate groups, ν_3 of phosphate groups and to the ν_3 of carbonate groups respectively. The spectra are ordered on increasing SF factor. (b) FT-IR transmittance peaks of the phosphate group where the SF is evaluated. Note the appearance of a shoulder at 63,400 m^{-1} for temperatures above 700 °C, in the IPC764, IPA9 and IPC764-2 specimens, as indicated by the circle.

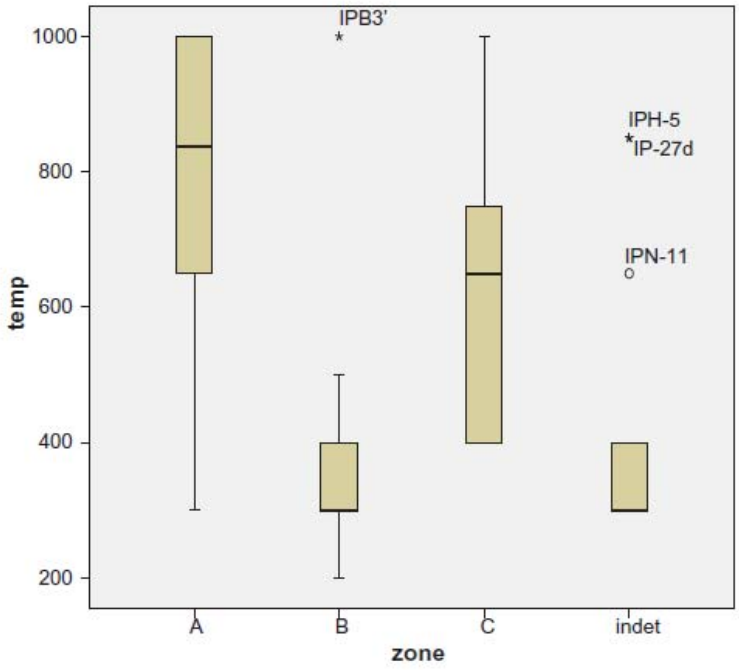

Fig. 8. Plot showing a range of temperatures vs. each necropolis chamber mainly estimated after the analysis of XRD data. The estimated thermal treatment of bones without information on their original provenance is also reported.

cess, as it is also reflected in the corresponding temperatures which were estimated according to our calibration; four bone specimens (IPAI-4, IPAI-7a, IPA13 and IPAI5-1961) appeared to be treated in a temperature range from 600 to 650 °C, which might be ascribed to an incomplete cremation. This can be attributed to an insufficient amount of combustive material used in the pyre or to any other accidental interruption of the ignition process.

There are at least two possibilities to consider: either the bodies were first stripped of flesh and later cremated (that is what is meant by secondary cremation) or, a fire was used after the burials in order to clean the chamber of decomposed remains.

Data relevant to the individuals retrieved from chamber B reveal a different situation with respect to the one that emerged from chamber A. In fact, only the specimen IPB3[1] appeared to be cremated at high temperature, while the remaining specimens where subjected to a mild heat-treatment as it is testified by the low crystallite size of HA nanocrystals. From these data the temperature of heat treatment should be in the range 200–400 °C, which confirms the morphological visual observations carried out on the remains of chamber B. The bones appeared stained but without any morphological feature typical of a high-temperature cremation.

We can rationalise this situation by admitting occurrence of one or several "cleaning" or "purification" fires that affected the previously inhumed bodies. From this, it can be surmised that chamber B was used for remains cremated at high temperature only in exceptional cases, such as that represented by IPB3[1].

In chamber C, the number of available individuals is reduced compared with the previous two chambers. In any case, we observe a variable situation, from a case typical of a high-temperature cremation for sample IPC7 (1964)-2, to three cases of intermediate and incompleted combustion to finally, two specimens that were apparently treated at moderate temperatures (<400 °C).

Concerning the specimens for which information related to the funerary chamber of provenance was lost, we may conjecture that the majority very likely belong to chamber B, except for the specimen (IP-27d), that turned out to be cremated at high temperature, which is characteristic for chamber A.

Finally, the specimen IPN-11 (treated at 650 °C) may have been allocated either to A or to C chamber, if the trends pointed out before, for the use of each chamber, turn out to be true.

4. Concluding remarks

The C chamber of S'Illot des Porros, the most ancient (IVth century BCE) and with the largest number of inhumed remains, contains the smallest number of remains that were exposed to fire and in just one case it seems possible to attribute a genuine high-temperature cremation. The cremated bones were found in the upper layer of the chamber. Thus, we are dealing with individuals that were deposited there during the last use of the funerary structure, probably at the beginning of the IIIrd century BCE. From this layer onward we do not possess remains with a clear attribution of temperature level and the calibrated radiocarbon dating does not overtake the limit of 210 BCE. Actually, this is the oldest date for Majorcan cremations as some other remains have been dated with lower precision between the IVth and the IInd century BCE (Guerrero et al., 2005).

It was only afterwards, very likely at the end of the IInd century BCE, that chambers A and B began to be used. In addition, the pottery and other materials found belong to the IInd century BCE, going from the second half to the end of the century, which is consistent with the radiocarbon date reported before.

We may argue, that when chamber C was considered obsolete, chambers A and B were established almost simultaneously, although from the stratigraphic point of view the use of chamber B appears to be later to chamber A. Furthermore, chamber A appears to have high-temperature cremations, while the cremations in chamber B appeared to be carried out at lower temperature. Inhumations were also retrieved at the bottom layers. In these chambers, cremations at high and low temperatures appear to belong to the lower layers together with some inhumed bodies; this matches with a cleaning ritual at low temperature, as suggested before.

Therefore, based on the results presented here, we can exclude earlier interpretations that cremation rite was following inhumation with a short period of coexistence (Fig. 2). Thus, the basic distinction between cremations at high and low temperatures allows us to suggest very distinct rites, the first one involving a special treatment of the body during the funeral, and the second likely following a treatment to the chamber rather than to the bodies themselves.

These cleaning operations have been known for the same period in collective inhumation caves in the nearby area of Pollença (Majorca; Encinas, 1970).

Both the Pollença's Bay and the Alcudia's Bay, where S'Illot des Porros and Son Real are located, are the closest areas of Majorca to the near island of Minorca, where cremations have also been reported (Veny, 1982; Gornés et al., 2006). Finally, we have to recall that for earlier times the use of lime upon the inhumed bodies helped to maintain the caves availability for further burials (Waldren, 1982).

Then, it is possible to argue that the two new chambers were differentiated, where B was dedicated to inhumations and A to cremations, the cremations found in B being very likely a result of a cleaning-purification of the burial area.

This latter hypothesis is also supported by the fact that in chamber A the cremations appear to be carried out on fresh bones, as suggested by the bone reduction and transverse fractures. Conversely, in chamber B the fire appeared to be carried out on dry bones since the materials do not show any fracturing lines nor the associated contraction due to evolution of collagen and water. For sure, the fracturing features were influenced by the low temperature of the combustion.

In general terms, these funerary chambers are relevant to the whole context of the Balearic Islands, because most of the indigenous population at this time was buried in natural or artificial caves (Coll, 1989; Micó, 2005). So, a costly though still collective monument appears in S'Illot des Porros, while even in the nearby cemetery of Son Real the tombs built in stone are, in terms of the cost, much poorer than the prior ones in the same necropolis (Hernández-Gasch, 1998). However, the relative absence of wealthy funerary items in the site has to be considered, with respect to the cemeteries in the island of Majorca and, in any case, particular differences in the funerary items between chambers were not observed, implying no evident social differentiation.

Cremation is supposed to be a prestigious and distinct rite associated with the best chamber (likely chamber A). Not only the costs of fuel for cremation are higher compared with a simple inhumation, but also the introduction of a new cultural rite may be associated with social groups, who wanted to show themselves different with respect to the remaining population by adopting distinguishable and costly customs and products of foreign people.

This hypothesis echoes some anthropological data for S'Illot de Porros burials, suggesting that the presence of people taller and slimmer with respect to other communities of the island could be interpreted as elite, though it has to be maintained that these observations refer to an inhumed series (Malgosa, 1992; Rihuete Herrada, 2003).

Finally, if we take for granted the existence of distinct family tradition to account for different burial rites, we could then relate it to some kind of social condition. In this context it is possible that some male individuals (probably adult and young) were in touch with other societies, such as Punic or Italic people, who were using cremation. It is historically possible to relate this population to the mercenaries following Carthage during the Second Punic War (218-201 BCE) and fighting against Rome (Sánchez León, 2003a,b), as most of the cremated remains can be dated to the IInd century BCE. Alternatively, or in addition to it, we need to bear in mind that the Balearic Islands begin to fall into the commercial orbit of Rome in the IInd century (Puig, 2005), as cremation was also a funerary practice related to family tradition in the Italian peninsula.

Acknowledgements

This work was partially support by a project of Ministerio de Ciencia y Tecnología de España, CGL2008-00800. The authors thank Dr. Xavi Jordana for useful discussions.

References

Alesán, A., Malgosa, A., Simó, C., 1999. Looking into the demography of an iron age population from Western Mediterranean. I. Mortality. Am. J. Phys. Anthropol. 110, 285–301.

Carrasco, T., Malgosa, A., 1990. Paleopatología oral y dieta. Interpretación de la patología dental de individuos procedentes de una necrópolis talayótica mallorquina (siglo VI al II aC). Dynamis. Acta Hispanica ad Medicinae Scientiarumque Historiam Illustrandum 10, 17–37.

Castellana, C., Malgosa, A., 1991. Morphology of the facets of the proximal tarsi bones from an ancient population. Int. J. Anthropol. 8, 213–220.

Castellana, C., Malgosa, A., Campillo, D., 1991. Estudio de las artropatías de la necrópolis talayótica de "S'Illot des Porros" (Mallorca). In: Actas del IX Congreso Nacional de Historia de la Medicina, Zaragoza. Universidad de Zaragoza, pp. 1207–1217.

Coll, J., 1989. La evolución del ritual funerario en la cultura talayótica. Universitat de les Illes Balears (microfitxa), Palma.

Elliott, J.C., Mackie, P.E., Young, R.A., 1973. Monoclinic hydroxyapatite. Science 180, 1055–1057.

Encinas, J.A., 1970. Las cuevas de incineración en Pollensa (Mallorca). In: I Congreso Nacional de Espeleología, Barcelona 1970, Ayuntamiento de Barcelona, Barcelona, pp. 137–142.

Enzo, S., Bazzoni, M., Mazzarello, V., Piga, G., Bandiera, P., Melis, P., 2007. A study by thermal treatment and X-ray powder diffraction on burnt fragmented bones from Tombs II, IV and IX belonging to the hypogeic necropolis of "Sa Figu" near Ittiri-SS (Sardinia-Italy). J. Archaeol. Sci. 34, 1731–1737.

Gornés, J.S., Gual, J.M., Gómez, J.L., 2006. Avanç dels contextos arqueològics i de la cronologia absoluta de l'hipogeu XXI de Calascovas. Mayurqa 31. Universitat de les Illes Balears, Palma, pp. 165–181.

Guerrero, V.M., Ensenyat, J.A., Calvo, M., Orvay, J., 2005. El abrigo rocoso de Son Gallard- Son Marroig. Nuevas aportaciones treinta y siete años después. Mayurqa 30, Universitat de les Illes Balears, Palma, pp. 79–140.

Hernández-Gasch, J., 1998. Son Real. Necrópolis talayótica de la edad del hierro. Estudio arqueológico y análisis social. Arqueomediterrània 3 (II), Treballs de l'Àrea d'Arqueologia de la Universitat de Barcelona, Barcelona.

Hernández, J., Sanmartí, J., Malgosa, A., Alesán, A., 1998. La necròpoli talaiòtica de S'Illot des Porros. Pyrenae 28, Barcelona, pp. 69–95.

Lafon, J.P., Champion, E., Bernache-Assollant, D., 2008. Processing of AB-type carbonated hydroxyapatite $Ca_{10-x}(PO_4)_{6-x}(CO_3)_x(OH)_{2-x-2y}(CO3)_y$ ceramics with controlled composition. J. Eur. Ceram. Soc. 28, 139–147.

Lutterotti, L., Ceccato, R., Dal Maschio, R., Pagani, E., 1998. Quantitative analysis of silicate glass in ceramic materials by the Rietveld method. Mater. Sci. Forum 278–281, 87–92.

Malgosa, A., 1985. Estudio de los restos humanos de la necrópolis talayótica de S'Illot des Porros. PhD thesis, Universitat Autònoma de Barcelona.

Malgosa, A., 1992. La població talaiòtica de Mallorca. Institut d'Estudis Catalans, Barcelona.

Malgosa, A., Campillo, D., 1991. Visión general de las patologías halladas en los individuos de la necrópolis talayótica de S'Illot des Porros (Majorca). In: Actas del IX Congreso Nacional de Historia de la Medicina, Zaragoza. Universidad de Zaragoza, pp. 1409–1421.

Michel, V., Ildefonse, Ph., Morin, G., 1995. Chemical and structural changes in *Cervus elaphus* tooth enamels during fossilization (Lazaret cave): a combined IR and XRD Rietveld analysis. Appl. Geochem. 10, 145–159.

Micó, R., 2005. Cronología absoluta y periodización de la prehistoria de las islas baleares. British Archaeological Reports, International Series, 1373, Oxford.

Pérez, V., 1990. Técnica de análisis de los patrones de microdesgaste dentario (m.o.) como indicadores de dieta. Master's dissertation, Universitat Autònoma de Barcelona.

Piga, G., Malgosa, A., Mazzarello, V., Bandiera, P., Melis, P., Enzo, S., 2008a. Anthropological and physico-chemical investigation on the burnt remains of Tomb IX in the "Sa Figu" hypogeal necropolis (Sassari-Italy)—Early Bronze Age. Int. J. Osteoarchaeol. 18, 167–177.

Piga, G., Malgosa, A., Thompson, T.J.U., Enzo, S., 2008b. A new calibration of the XRD technique for the study of archaeological burnt remains. J. Archaeol. Sci. 35, 2171–2178.
Piga, G., Thompson, T.J.U., Malgosa, A., Enzo, S., 2009a. The potential of X-ray diffraction (XRD) in the analysis of burned remains from forensic contexts. J. Forensic. Sci. 54, 534–539.
Piga, G., Santos-Cubedo, A., Moya Solà, S., Brunetti, A., Malgosa, A., Enzo, S., 2009b. An X-ray diffraction (XRD) and X-ray fluorescence (XRF) investigation in human and animal fossil bones from Holocene to Middle Triassic. J. Archaeol. Sci. 36, 1857–1868.
Piga, G., Guirguis, M., Bartoloni, P., Malgosa, A., Enzo, S., 2010. A funerary rite study in the Phoenician-Punic Necropolis of Mount Sirai (Carbonia-Sardinia-Italy). Int. J. Osteoarchaeol. 20, 144–157.
Puig, A., 2005. L'entrada de Mallorca en l'esfera imperialista de la República romana. Una contextualització històrica de l'evidència arqueològica anterior a la conquista romana del 123 aC. In: Sánchez León, M.L., Barceló Crespí, M. (Eds.), XXIII Jornades d'Estudis Històrics Locals, Institut d'Estudis Baleàrics, Palma de Mallorca, pp. 247–259.
Rissech, C., Malgosa, A., 1997. Sex prediction by discriminant function with central portion measures of innominate bones. Homo 48, 22–32.
Rietveld, H.M., 1967. Line profiles of neutron powder-diffraction peaks for structure refinement. Acta Crystallogr. 22, 151–152.
Rihuete Herrada, C., 2003. Bio-arqueología de las prácticas funerarias. Análisis de la comunidad enterrada en el cementerio prehistórico de la Cova des Càrritx (Cuitadella, Menorca), ca. 1450-800 cal ANE, British Archaeological Report, International Series 1161, Oxford.
Salvà, T., Javaloyas, D., (in press). Las islas del fin del mundo? Las comunidades baleáricas y los contactos interculturales durante el Bronce Medio y final (1400-850 A.C.). In: IIe Colloque International Séminaire de Formation 15–18 Septembre 2005. Projet Collectif de Rechercher Mariana et la Vallée du Golo. Université d'Automne de Mariana. Les lingots «peau de bœuf» et la navigation en Méditerranée centrale.
Sánchez León, M.L., 2003a. La ciudad de Mago (Maó, Menorca): continuidades y rupturas. Mayurqa 29, Palma, pp. 97–109.
Sánchez León, M.L., 2003b. Magón y Barca y las Islas Baleares. In: González, A., Vita, J.P., Zamora, J.A. (Eds.), De la Tablilla a la Inteligencia Artificial. Homenaje al Profesor Jesús-Luís Cunchillos en su 65 aniversario, 1, Zaragoza, pp. 389–394.
Shipman, P., Foster, G., Schoeninger, M., 1984. Burnt bones and teeth: an experimental study of color, morphology, crystal structure and shrinkage. J. Archaeol. Sci. 11, 307–325.
Subirà, M.E., Malgosa, A., 1992. Multi-element analysis for dietary reconstruction at a Balearic Iron Age site. Int. J. Osteoarchaeol. 2, 199–204.
Subirà, M.E., Alesan, A., Malgosa, A., 1992. Criba orbitalia y déficit nutricional. Estudio de elementos traza. Munibe 8, 153–158.
Surovell, T.A., Stiner, M.C., 2001. Standardizing infra-red measures of bone mineral crystallinity: an experimental approach. J. Archaeol. Sci. 28, 633–642.
Tarradell, M., 1964. La necrópolis de Son Real y la Illa dels Porros (Mallorca), Excavaciones Arqueológicas en España 24, Madrid, pp. 3–31.
Tarradell, M., Woods, D.E., 1959. The cemetery of Son Real, Mallorca. Archaeology 12, 194–202.
Thompson, T.J.U., Gauthier, M., Islam, M., 2009. The application of a new method of Fourier transform infrared spectroscopy to the analysis of burned bone. J. Archaeol. Sci. 36, 910–914.
Van Strydonck, M., Landrie, M., Boudin, M., Grootes, P.M., Nadeau, M.-J., Aprks, R., Keppens, E., 2002. Radiocarbon dates, XVIII. Royal institute for cultural Heritage, Brussels.
Veny, C., 1982. La necrópolis protohistórica de Cales Coves, Menorca. Biblioteca Prehistórica Hispana XX, Madrid.
Waldren, W.H., 1982. Balearic prehistoric ecology and culture: the excavation and study of certain caves, rock shelters and settlements. British Archaeological Reports, International Series I, 49. Oxford.
Weiner, S., Bar-Yosef, O., 1990. States of preservation of bones from prehistoric sites in the Near East: a survey. J. Archaeol. Sci. 17, 187–196.
Wopenka, B., Pasteris, J.D., 2005. A mineralogical perspective on the apatite in bone. Mater. Sci. Eng. C 25, 131–143.

Chapter 4.4: A unique case of prone position in the primary cremation Tomb 252 of *Monte Sirai* necropolis (Carbonia, Sardinia, Italy).

Authors: **Giampaolo Piga, Assumpciò Malgosa, T.J.U. Thompson, Michele Guirguis, Stefano Enzo.**

International Journal of Osteoarchaeology (DOI: 10.1002/oa.2270).

Another extremely interesting case concerns the Phoenician-Punic Necropolis of *Monte Sirai* (Carbonia, Sardinia, Italy). In this necropolis there is a wide archaeological documentation about different and peculiar funeral rites (Guirguis, 2011). This paper presents the case of Tomb 252 that contained the cremated remains of an individual, probably male. Comparison of the excavation records alongside reconstruction of the bone material itself makes clear that the individual was cremated in a prone position. This is the first case of prone cremation reported in the literature.

The exceptional state of preservation of almost the entire skeleton allows the distribution of temperature on representative parts of the whole body to be assessed, and determination of the possible existence of a central focus.

Macroscopic examination of bones is useful to gain a general idea of temperature, though more advanced techniques, in the form of XRD and FT–IR analysis are required to gain a more precise temperature range across the entire body. The combined use of these methods can contribute to our understanding of cremation temperature, its homogeneity throughout the skeleton and its duration.

Both the X-ray crystallinity and the SF value of the ν_4 phosphate band converge to similar values of temperature, which is further supported by those deducible from C/P of $\nu_3\ CO_3^{2-}$ and $\nu_3\ PO_4^{3-}$

Data obtained with the two techniques are almost concordant, except in a few cases (vertebrae 1 and 2, left ulna and both femurs) where the temperatures obtained with the analysis of X-ray diffraction are a little higher. These differences do not exceed 100°C and are not worthy of further interpretation since they may be thought to coincide within their experimental uncertainty.

International Journal of Osteoarchaeology
Int. J. Osteoarchaeol. (2012)
Published online in Wiley Online Library
(wileyonlinelibrary.com) **DOI**: 10.1002/oa.2270

A Unique Case of Prone Position in the Primary Cremation Tomb 252 of *Monte Sirai* Necropolis (Carbonia, Sardinia, Italy)

G. PIGA,[a,b]* A. MALGOSA,[a] T. J. U. THOMPSON,[c] M. GUIRGUIS[d] AND S. ENZO[b]

[a] *GROB (Grup de Recerca en OsteoBiografia), Unitat d'Antropologia Biologica, Department de Biologia Animal, Biologia Vegetal i Ecologia, Universitat Autonoma de Barcelona, 08193 Barcelona, Spain*
[b] *Dipartimento di Chimica, Università di Sassari, I-07100 Sassari, Italy*
[c] *School of Science & Engineering, Teesside University, Middlesbrough, UK*
[d] *Dipartimento di Storia, Università di Sassari, 07100 Sassari, Italy*

ABSTRACT A series of graves belonging to the Phoenician period were investigated after the campaign excavation of 2007 in the Phoenician-Punic necropolis of *Monte Sirai* (Carbonia, Sardinia, Italy). One tomb in particular (labelled 252) is presented here because of its uniqueness. Tomb 252 contained the cremated remains of an individual, probably male, and comparison of the excavation records alongside reconstruction of the bone material itself makes clear that the individual was cremated in a prone position. It represents the first case of prone cremation reported in the literature.

To investigate whether the temperature of the cremation was homogenous across the entire body, we have conducted a combined physical–chemical analysis using X-ray diffraction spectroscopy and Fourier transform infrared.

Key words: Fourier transform infrared spectroscopy; Phoenician age; primary incineration; prone position; X-ray diffraction

Introduction

Historical background of the site

The site of *Monte Sirai* is located in the South-Western part of Sardinia near the city of Carbonia [Figure 1 (a and b)]. It is thought to have been established by the Phoenicians of Sulky (today known as *S. Antioco*) or by the early settlers living in the anonymous downtown of Portoscuso around 740 BC (Botto, 1994). Soon after its foundation, the site assumed an importance for its strategic position near the coastline and as a gateway to the Campidano plane of the island. Around the year 540 BC, Carthaginians attempted to occupy the island and, after initial defeat, was successful a few years later. The population of *Monte Sirai* was massacred and the city almost completely destroyed. On the basis of funerary evidence, in the form of 13 Punic-type tombs thought to represent family tombs, it is estimated that only a dozen families inhabited the settlement after this event. This situation remained approximately the same until 360 BC, when Carthage decided to strengthen various Sardinian sites, including *Monte Sirai*. After 238 BC, and during the Neo-punic period, the fortress of *Monte Sirai* was completely demolished, and a new city plan that utilised four large building arrays was established. By 110 BC, the site was abandoned and only sporadically inhabited thereafter (Bartoloni, 2000).

This abrupt end, coupled with an absence of imperial Roman occupation (which has disturbed the archaeology of other major Sardinian settlements such as Sulky, Tharros, Cagliari, and Nora) allows the thorough investigation of Phoenician and Punic burial customs.

Evidence for burial customs at Monte Sirai

Excavations at *Monte Sirai* were conducted between 1963 and 1966 AD and then again from 1980 to between 2005 and 2010 AD (Bartoloni, 2000; Guirguis, 2010).

These research excavations identified three distinct burial areas (Figure 2). The first is a broad valley that

* Correpondence to: Giampaolo Piga, GROB (Grup de Recerca en OsteoBiografia), Unitat d'Antropologia Biologica, Department de Biologia Animal, Biologia Vegetal i Ecologia, Universitat Autonoma de Barcelona, Edifici C, 08193 Bellaterra, Barcelona, Spain.
e-mail: kemiomara@yahoo.it

Received 25 November 2011
Revised 27 July 2012
Accepted 14 August 2012

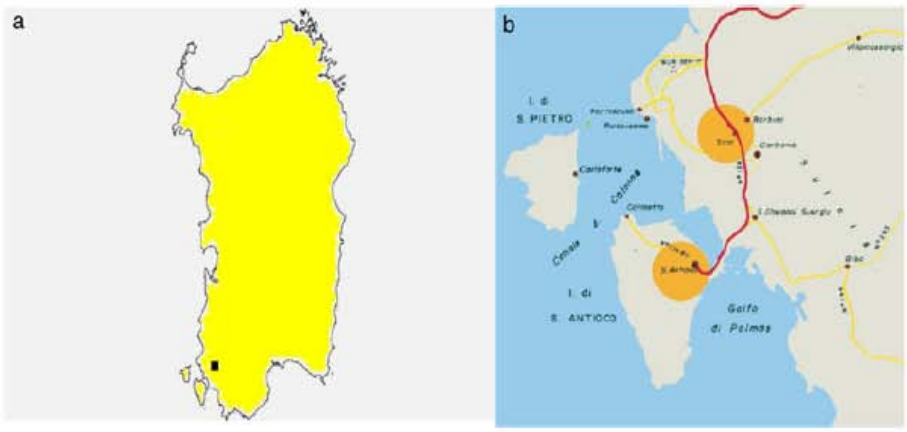

Figure 1. (a) The location of Monte Sirai Necropolis and (b) a magnification of its nearby context in the island of Sardinia (reproduced by kind permission of Prof. Bartoloni). This figure is available in colour online at wileyonlinelibrary.com/journal/oa.

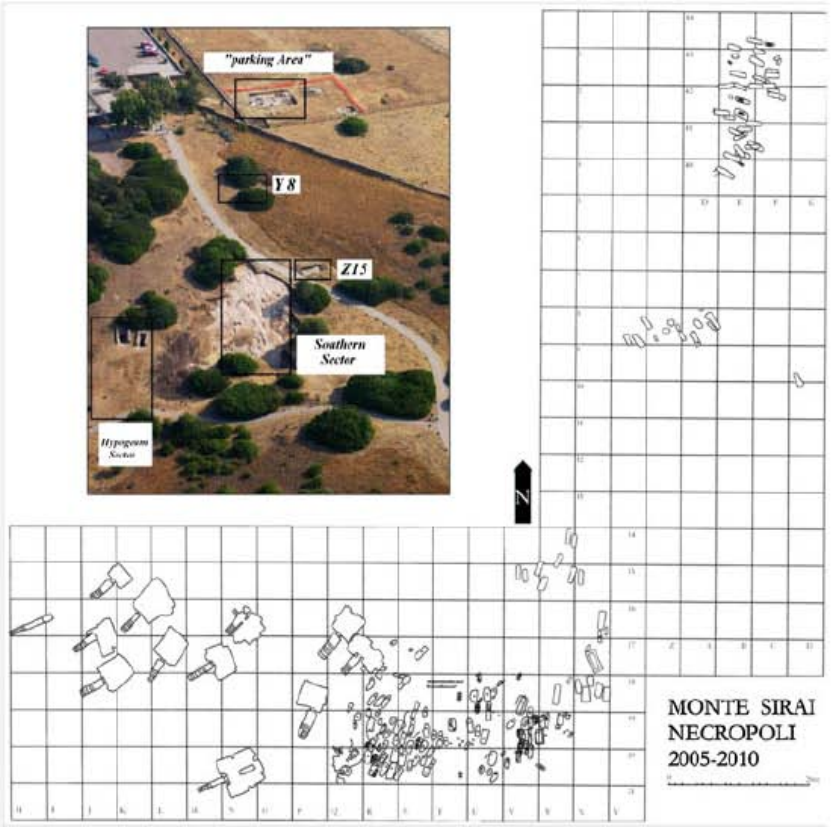

Figure 2. Aerial view and the overall site plan of the different sectors of the Monte Sirai necropolis (elaboration by R. Pla Orquín).This figure is available in colour online at wileyonlinelibrary.com/journal/oa.

opens just east of the Chambers tombs and is of Punic age (Hypogeum sector), with two other distinct areas along the north-east direction. The southern sector has returned the oldest evidence to date (late 6th century BC), whereas the Y8 square directed eastward and northern to the so-called parking area gradually achieved the horizons of late archaic and early Punic age. The primary cremation graves were located mainly in the southern sector of the necropolis (Figure 3), where the natural troughs of tuff are more pronounced. The chronology of these tombs ranges from the late 7th century BC until the second half of the 6th century BC (Guirguis, 2011).

During the most recent campaign, 96 burials were identified and attributed to an extended chronological period between the end of the 7th and the second half of 4th century BC, which allow diachronic changes in funerary rites to be detected.

During the earliest phases of the site, there is some variety in funeral rites. During the Phoenician era (between the late 7th to the end of 6th century BC), body cremation was the predominant rite, but in the Punic age, that is, after the Carthaginian conquest, inhumations began to appear, with the bodies often being placed within hypogeal chamber tombs (Bartoloni, 2000; Guirguis, 2011).

Finally, a recent study by Piga *et al.* (2010a) identified the existence of a rite midway between incineration and inhumation, called semi-combustion, that was associated with the burials dating to the late archaic/early Punic age (from the late 6th and throughout 5th century BC). Evidence for this was recovered from the periphery of this necropolis and appears to be present only at this site (Piga *et al.*, 2010b).

The rite of primary cremation in the necropolis of Monte Sirai

Within the *Monte Sirai* necropolis, Tombs 250 and 252 are typical Phoenician primary cremation burials in a grave, whose ritual performance was described in detail by Bartoloni (2000). The process, as exemplified by Tomb 250, can be summarised as follows: First, an

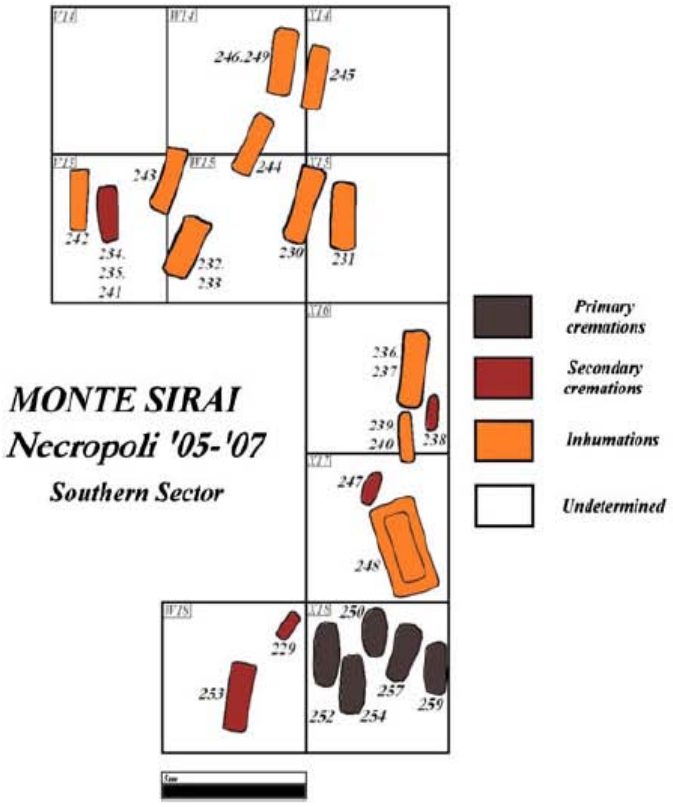

Figure 3. Plan of the southern sector with an indication of the burial rituals identified (reproduced by kind permission of Dr. Guirguis). This figure is available in colour online at wileyonlinelibrary.com/journal/oa.

ellipsoid cavity was dug about 2 m in length and about 40 cm in depth, the gravediggers retaining some tuff for later use.

Analysis of ancient funerary kits, including pitchers thought to contain ointment, suggests that the bodies were cleaned and anointed with special ritual vessels.

After the anointing, the body was equipped with jewels, amulets, and other objects. In addition to personal items, the bodies of women were accompanied by a set of pots. Generally, five vessels, including the ritual vessels, were placed inside with the women, whereas the men had three vessels and children only one.

The body was then wrapped in a shroud and laid on some boards that had served as a deathbed. In the meantime, branches of oleaginous shrubs were collected and placed along the length of the grave. Firewood was stacked above the branches and the body laid on the woodpile, which was then set alight (Figure 4).

The combustion was of relatively short duration, but continued until the bones were calcined and to the point when the wood was charred completely and collapsed into the grave. The remaining flames and hot coals were probably extinguished with water. This is suggested by the excellent state of preservation of charred wood, recovered in large fragments (Guirguis, 2010) (Figure 5).

In the case of Tomb 250, it seems that some large fragments of amphorae walls were deposited, whereas the two jugs used for rituals anointing of the body were placed at the bottom of the grave (Figure 6).

After the deposition, the bones and the charred wood were completely covered and sealed with the tuff previously set aside together with clays. Thus, the grave was covered with a mound formed by stones and earth. Finally, a stone was used to highlight the presence of the tomb.

The main aim of this study is to analyse all the biological elements of this special ritual in Tomb 252, to determine the state and position of the body and

Figure 5. A large trunk of charred wood, residue of the funeral pyre, found in Tomb 250, which overlooks the shallow pit where the bones and funerary kit were deposited after turning off the fire intentionally. This figure is available in colour online at wileyonlinelibrary.com/journal/oa.

the temperature of the pyre. The discovery of almost all parts of the skeleton allows us to undertake a detailed analysis not always possible in such contexts, that is, to analyse the homogeneity of the temperature and intensity of fire in various parts representative of the whole body.

Materials and methods

Both X-ray diffraction (XRD) and Fourier transform infrared (FT-IR) can be used to assess the nature of the crystal

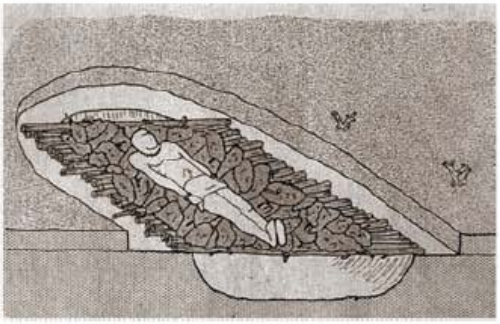

Figure 4. The body was buried along with equipment and personal items on the woodpile and leafy (reproduced by kind permission of Prof. Bartoloni). This figure is available in colour online at wileyonlinelibrary.com/journal/oa.

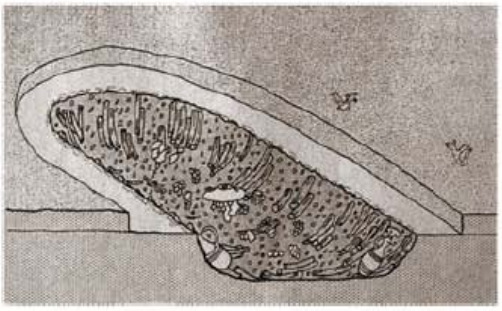

Figure 6. When combustion occurred, the funeral kit consisting of one or more clay pots was laid (reproduced by kind permission of Prof. Bartoloni). This figure is available in colour online at wileyonlinelibrary.com/journal/oa.

structure of burned and cremated bone, and this in turn can be related to the temperature or intensity of burning.

The XRD approach correlates crystal size with temperature (Piga *et al.*, 2008b, 2009), whereas the FT-IR method links the splitting factor (SF) with the same. Both approaches have been used in experimental studies (e.g., Rogers & Daniels, 2002; Thompson *et al.*, 2009, 2011; Piga *et al.*, 2010a; Rogers *et al.*, 2010) and are now being increasing applied to real-world archaeological sites and contexts (e.g., Enzo *et al.*, 2007; Piga *et al.*, 2008a, 2010b; Squires *et al.*, 2011). Their application is becoming increasingly accepted and sophisticated and is allowing better interpretation of ancient funerary practices.

Bone samples

The recovered bones were of different sizes and very fragile. Where possible, the cremated remains were cleaned with water. Unidentifiable fragments were classified simply by type of bone. The partial and total recovered remains were weighed to assess the percentage of recovery of each body area. Standard criteria (Ferembach *et al.*, 1977–1979; Krogman & Iscan, 1986; Ubelaker, 1999; Curtin, 2008) were used for the creation of the osteological profile.

XRD analysis

In an agate jar, we ball-milled 0.5 g of each bone fragment for 1 min using a Spex mixer-Mill from SPEX Industries, Edison, New Jersey (USA). Our sample holder for XRD analysis is a circular cavity of 25 mm in diameter and 0.3 mm in depth. It contains about 420 mg of powder bone.

The XRD patterns were recorded overnight using Siemens D-500 and Bruker D8 from Bruker Scientific Instruments (Bruker AXS Inc., Madison, WI, USA) in the Bragg–Brentano geometry with CuKα radiation ($\lambda = 1.54178$ Å). The X-ray generator worked at a power of 40 kV and 30 mA, and the resolution of the instruments (divergent and antiscatter slits of 0.5°) was determined using α-SiO_2 and α-Al_2O_3 standards free from the effect of reduced crystallite size and lattice defects (Enzo *et al.*, 1988).

The goniometer was equipped with a graphite monochromator in the diffracted beam, and the patterns were collected with 0.05° of step size, which turned out to be adequate for the range of crystallite size in apatite phases here investigated. The powder patterns were collected in the angular range 9–140° in 2θ, with counting time of 40 s per point. Digitised diagrams were analysed according to the Rietveld (1967) method, using the programme MAUD (*Materials Analysis Using Diffraction*) (Lutterotti & Bortolotti, 2003), which is able to incorporate the instrument function determined separately as explained earlier.

FT-IR analysis

FT-IR spectra were collected with a Bruker Vertex 70V from BrukerScientific Instruments (Bruker AXS Inc., Madison, WI, USA) interferometer in terms of absorbance versus wavenumber ν in the range 400–4500 cm^{-1}, with a resolution of 4 cm^{-1}. About 3 mg bone was hand-grinded and mixed with KBr to a weight ratio 1:100, respectively, to make pellets suitable for beam irradiation. Every spectrum was obtained by averaging 250 interferograms.

It should be considered that bands of the infrared spectrum of recent and fossil bones are relevant to obtain molecular information concerning the phosphate/carbonate group ratio. Additional bands may also be evaluated because of minerals other than those related to the apatite-like structure.

Crystallinity index and other ratios

The crystallinity index adopted here is the same as what has been used in the majority of archaeological

Figure 7. Reconstruction in the laboratory of the skeleton from Tomb 252, exceptionally preserved. This figure is available in colour online at wileyonlinelibrary.com/journal/oa.

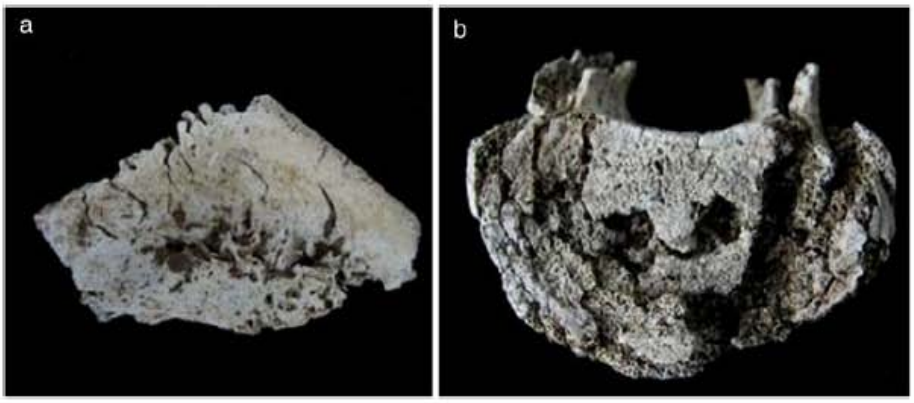

Figure 8. (a) Right orbital roof with the presence of cribra orbitalia. (b) Vertebra with Schmorl's nodes. This figure is available in colour online at wileyonlinelibrary.com/journal/oa.

applications. The absorption bands at 605 and 565 cm^{-1} were used following baseline correction, and the heights of these absorptions peaks were summed and then divided by the height of the minimum between them (Weiner & Bar-Yosef, 1990). The carbonate/phosphate ratio (C/P) was also calculated. Here the absorption peak at 1415 cm^{-1} was divided by the peak at 1035 cm^{-1} as used in Shemesh (1990), Wright and Schwarcz (1996), Koon *et al.* (2003), Olsen *et al.* (2008), Thompson *et al.* (2009, 2011) and Piga *et al.* (2010a). Note that some publications use a slightly different definition for this ratio (Pucéat *et al.*, 2004). As these peaks correlate to the amount of carbonate and phosphate, this ratio allows one to comment upon changes to the carbonate content bone following burning (Thompson *et al.*, 2009). A combination of both CI and C/P has been used to successfully show differences in cremation and funerary practices (Squires *et al.*, 2011).

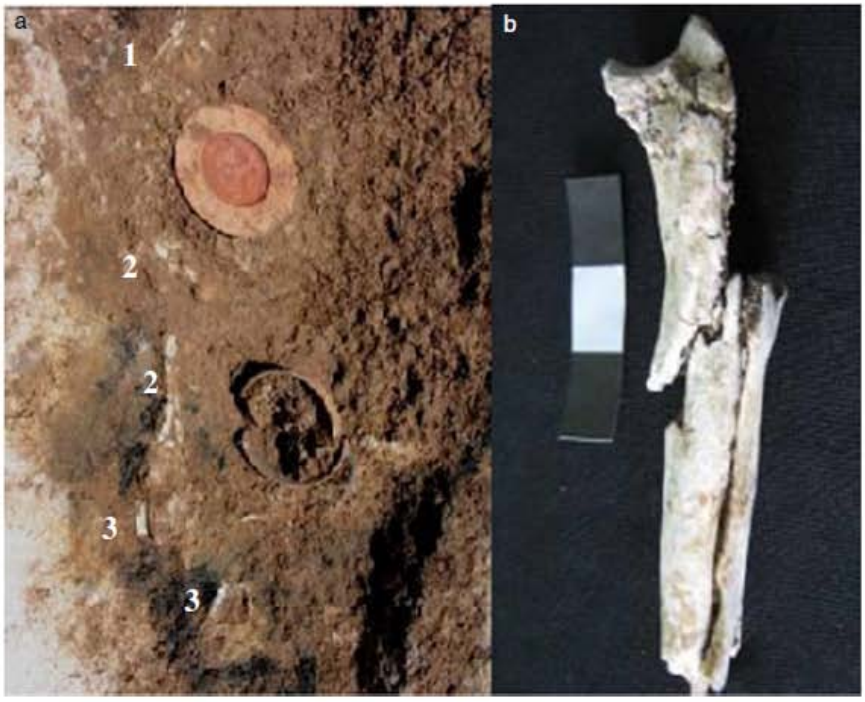

Figure 9. (a) Tomb 252 in which are observed the disposition of various bones compatible with ulna (1), femur (2) and tibia (3). (b) Proximal epiphysis of left ulna reconstructed in the laboratory. This figure is available in colour online at wileyonlinelibrary.com/journal/oa.

Results

Anthropological study of the cremated remains and description of the prone position

The recovered bones generally have a white coloration (there are also fragments of blue colour), transverse fractures and marked warping. The grave contains the remains of at least one cremated individual that is very well preserved for cremated remains (Figure 7), to the extent that pathologies such as Schmorl's nodes (Ustundag, 2009) are still detectable.

The markers to determine the age are limited to the epiphyses and the state of the cranial sutures. Concerning the first, the humeral, femoral and tibial epiphyses show no trace of the epiphysial line. However, the coronal obliteration shows an onset of intracranial suture subtracting exocraneal at fully open and so are the rest of the sutures.

Overall, both markers suggest that this is a fairly young adult: The epiphysis fusion is observed in the range 14–18 years old for women and in 16–19 years old for men (Krenzer, 2006). Unfortunately it is not possible to refine the ageing further.

With regard to biological sex, the orbital rim, the maxilla and mandible, and the epiphyses of the bones of the forearms all show a gracile nature. The pelvis shows a narrow sciatic notch, typical of male individuals, although bone shrinkage and fragmentation of the cortex may have caused some changes. The diameter of the left femoral head (42.20 mm) is intermediate, although the bicondilar width (73.35 mm) falls within the range of a male individual (Krenzer, 2006). Again, shrinkage can have an impact here, but generally, this is to mask men as women (Gonçalves, 2011). No major morphological changes are observed related to arthritic problems or anomalies due to special pathologies, although there is the presence of *cribra orbitalia* (Subirà *et al.*, 1992) in the right orbital roof, and Schmorl's nodules in at least two vertebral bodies are worth of note [Figure 8(a and b)], the former being an affliction of childhood.

Two diaphyseal bone fragments of the upper extremities are observed in the northern part of the grave, namely, the proximal epiphysis and diaphysis of the left ulna [Figure 9(a and b)].

In the centre of the grave, next to a dish, we can clearly see the left proximal femoral epiphysis (Figure 10), as well as a distal femur and proximal tibia that appear to be articulated [Figure 11(a–c)].

Overall, it is possible to reconstruct the original position of the body, oriented north–south (head to toe). Bone fragments corresponding to the left half of the body (ulna, pelvic, femur and tibia) were found in the western half of the tomb retaining some joints and the bones of the right half of the body (the proximal epiphysis of right humerus, the proximal fragment of the right olecranon base of radium, the proximal region of right femur with surgical neck and neck anatomy) on the opposite side, which is an anomaly when one considers the usual cremation of the body in supine position.

Figure 10. Left coxal and left proximal epiphysis of the femur (1–2), distal diaphysis and epiphysis of the left femur (3) and proximal epiphysis of the left tibia (4) in situ. This figure is available in colour online at wileyonlinelibrary.com/journal/oa.

It is highly unlikely that the skeletal elements would have switched sides as a result of the cremation process, and this therefore suggests a deliberate deposition of the body in a prone position. Presence of blackening on the anterior distal left femur from charcoal (Figure 12) further supports this hypothesis. This disposition of the bones, along with the mixture of charcoal and soil, suggests that the cremation was carried out *in situ*. This is indicated also by the smallest bones recovered during excavation, such as Wormian bones and phalanges, whose inventory is not usual when the remains of a cremation are collected for deposition in an urn or in a grave dedicated only to contain the remains from the *ustrinum*.

XRD/FT-IR analysis

The exceptional state of preservation of almost the entire skeleton allows the distribution of temperature

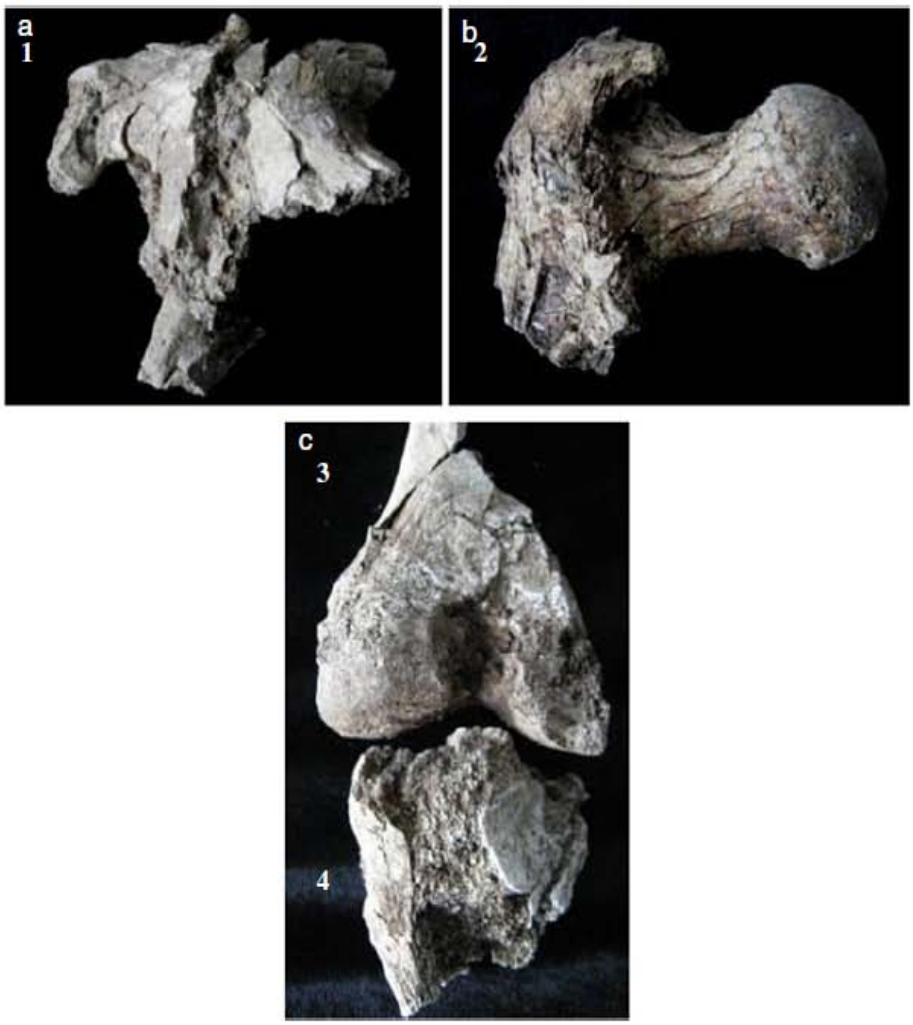

Figure 11. (a) Left coxal (1). (b) Proximal epiphysis of the left femur (2). (c) Diaphysis of distal femur and proximal tibial epiphysis (3, 4) photographed in the laboratory. This figure is available in colour online at wileyonlinelibrary.com/journal/oa.

on representative parts of the whole body to be assessed and to determine the possible existence of a central focus.

Figure 13 shows the experimental XRD patterns (blue dots) of two specimens that show the largest difference in terms of crystallinity found in the course of the present investigation.

The data are depicted in the y-axis according to the experimental intensity times the variable $q = 4(\pi/\lambda)\sin\theta$ (logarithmic scale) in order to emphasise the presence of weak peaks, which are very important in diffraction in order to reveal the fine details of the whole structure inspected.

The full curves are their relevant fit according to the Rietveld method. The featureless curves represent the background line determined by the numerical procedure. As usual, at the bottom of each pattern, we show the band of residuals that supplies a complementary insight of how 'good' is the fit with respect to the experimental data.

Moreover, the two specimens turned out to be made by a single bioapatite phase, and the sequence of bars represents the location of each peak expected on the basis of the monoclinic apatite structure (Elliott *et al.*, 1973). The different degree of crystallinity in the two patterns is related to the different peak sharpening clearly evaluable from the direct comparison of the data. In turn, the degree of sharpening has been used to estimate the temperature to which the bioapatite of bones was treated during the cremation process.

Phoenician Prone Position Cremation

Figure 12. Front of the left femur blackened by contact with charcoal in the soil. This figure is available in colour online at wileyonlinelibrary.com/journal/oa.

Table 1 shows in detail the results obtained through the techniques of XRD/FT-IR, according to the methodology established by Piga *et al.* (2008b, 2009, 2010a) and Thompson *et al.* (2009, 2011) for both techniques and their application on burnt remains (Piga *et al.*, 2010b; Squires *et al.*, 2011).

Both the X-ray crystallinity and the SF value of the ν_4 phosphate band converge to similar values of temperature, which is further supported by those deducible from C/P of ν_3 CO_3^{2-} and ν_3 PO_4^{3-} bands, used in the study of cremated bones. In particular, the C/P values are in the range between 0.04 and 0.10, index of an intense and/or complete cremation (Squires *et al.*, 2011), whereas in only two cases (blue rib and blue mandible), we found a value of 0.15, which confirms, together with the low values of SF and the X-ray crystallinity, a less intense cremation.

As it can be seen from the FT-IR data (Figure 14), the carbonate bands in the range 1400–1500 cm^{-1} can be referred either to the main band of the phosphate group ν_3 in the range 1000–1100 cm^{-1} or to the phosphate ν_4 band in the range 500–700 cm^{-1}. An additional carbonate band occurs at ~870 cm^{-1}. In any case, the figure points out a difference between the two cases examined (the blue rib, bottom curve; and the vertebra 4, top curve) in terms of carbonate group content.

It can be surmised that in the former case, the bone was subjected to a mild thermal treatment (temperature estimated of 700°C) whereas in the latter, all the indices extracted suggest a stronger thermal treatment (equivalent to 1000°C or above).

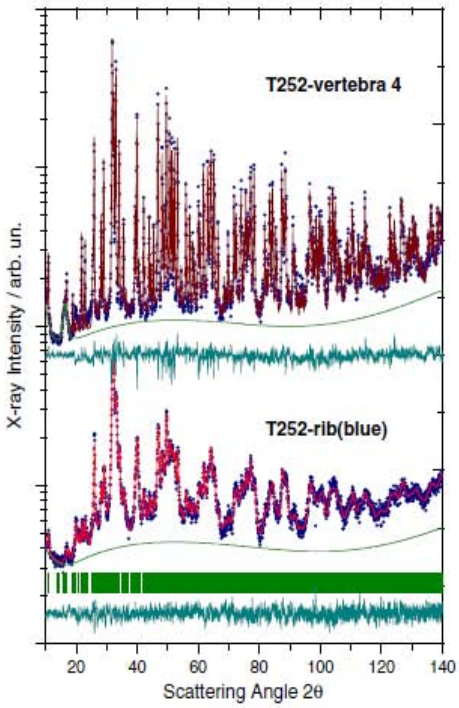

Figure 13. A comparison of the XRD patterns from blue mandible and vertebra 4 showing the different degrees of peak broadening enabling the estimation of a different temperature reached by the bones after the cremation process. See text for details about the curves. This figure is available in colour online at wileyonlinelibrary.com/journal/oa.

Data obtained with the two techniques are almost concordant, except in a few cases (vertebrae 1 and 2, left ulna and both femora) where the temperatures obtained with the analysis of X-ray diffraction are a little higher. These differences do not exceed 100°C and are not worthy of further interpretation as they may be thought to coincide within their experimental uncertainty.

The values of the SF determined by the FT-IR technique in the bone remains are systematically much higher than the values of the laboratory calibration (Piga *et al.*, 2008b, 2009, 2010a; Thompson *et al.*, 2009, 2011). This may be due to at least three reasons:

(a) A 'real' cremation differs from burning in the laboratory for various factors: the presence of viscera and soft tissues (which can act as additional fuel); the physical characteristics of the cadaver, such as its weight (Bohnert *et al.*, 1998; Shannon, 2011); and so on. This means that a real fire can be much more intense and lasting that a heat treatment in a muffle, and that the bones have effectively undergone a heat treatment to temperatures over 1000°C.

Table 1. Average crystallite size of hydroxyapatite, splitting factor, C/P values and estimating the temperatures calculated with both spectrometric techniques according to Piga *et al.* (2008b, 2009, 2010a) and Thompson *et al.* (2009, 2011) (both techniques give concordant results)

Part of the body	Average crystallite size/(Å) (±10%)	Temperature/XRD (Piga *et al.*, 2008b, 2009)/°C	SF- (KBr)FT-IR (±0.05)	SF C/P (±0.05)	Temperature/IR-KBr (Thompson *et al.*, 2009)/°C	Temperature/IR-KBr (Piga *et al.*, 2010a)/°C
Skull	> 1500 (1520)	900 < *T* < 1000	7.32	0.07	>900 (45 min)	1000
Mandible	> 1500 (2297)	1000	6.18	0.07	900 (45 min)	>900
Mandible (blue)	230	≈700	4.32	0.15	600 (45 min) < *T* < 700 (15 min)	700 < *T* < 800
Rib	> 1500 (2306)	1000	6.93	0.06	>900 (45 min)	1000
Rib (blue)	224	700	4.30	0.15	600 (45 min) < *T* < 700 (15 min)	700 < *T* < 800
Vertebra 1	> 1500 (2200)	1000	6.66	0.06	>900 (45 min)	≈900
Vertebra 2	> 1500 (1940)	1000	6.52	0.04	>900 (45 min)	800 < *T* < 900
Vertebra 3	> 1500 (1900)	1000	7.21	0.07	>900 (45 min)	1000
Vertebra 4	> 1500 (2248)	1000	8.08	0.05	>900 (45 min)	1000
Vertebra 5	> 1500 (2303)	1000	6.91	0.07	>900 (45 min)	1000
Right ulna	> 1500 (2079)	1000	7.08	0.07	>900 (45 min)	1000
Left ulna	> 1500 (1724)	1000	6.67	0.10	>900 (45 min)	900
Right femur	> 1500 (2316)	1000	6.86	0.08	>900 (45 min)	900
Left femur	> 1500 (1480)	900 < *T* < 1000	5.58	0.07	900 (45 min)	800 < *T* < 900
Left tibia	> 1500 (1364)	900	6.08	0.09	900 (45 min)	>800
Right tibia	> 1500 (1412)	900	6.68	0.08	>900 (45 min)	900

(b) The bones have been subjected to further processes of 'ageing' as a result of the subsequent burial, which are superimposed on the thermal process and consequently in the values of the crystallinity index.
(c) Differences can also result from the use of different equipment and sample preparation (Piga *et al.*, 2010a; Thompson *et al.*, 2011).

Therefore, we conclude that the skeletal remains of *Monte Sirai* have been treated with fire in a temperature range of 1000°C, across the whole of the body, whereas some specific parts (see the evaluation for the blue mandible and rib in Table 1) may have been subjected to lower temperature values (e.g. 700°C) because of uncompleted combustion processes related to the oxygen available and/or to a dynamics of the fire influenced by the contact of the body with the wood branches.

Discussion and conclusive remarks

The prone position of the burials is generally rare although some graves have been found with this position. Arcini (2009) in her first global study of prone burials suggested that it was a practice used in all societies as disrespect or humiliation to the dead. According to Simmer (1982), the prone position may be related to fear or reverence for the dead. This

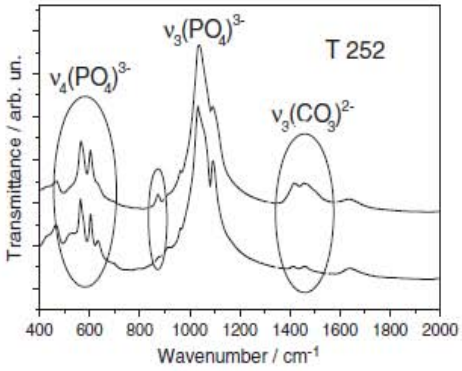

Figure 14. The FT-IR patterns of two cremated specimens: blue rib (upper curve) and the vertebra 4 (bottom curve). The spectra are reported in the wavenumber ν range from 400 to 2000 cm^{-1}. It is possible to recognise three main groups of band in the range 500–700, 1000–1200 and 1400–1600 cm^{-1}, which are generally assigned to the energy mode ν_4 of the phosphate groups, ν_3 of the phosphate groups and ν_3 of the carbonate groups, respectively. The figure points out a sensible difference between the two cases in terms of carbonate group content. Note also the presence of a shoulder at 633 cm^{-1} in the vertebra 4 spectra, which indicates a higher cremation temperature on this specimen.

interpretation can be extended also to a case found in Bologna, Italy (Cornelio Cassai *et al.*, 2008), where the nails of the shoes were found separated from feet and near the skull. The location of the shoes in the tomb and possibility that their feet were bound led to an interpretation that this act was undertaken to prevent the deceased from returning to the living. Brothwell (1981) suggested another explanation for this and other special positions that may be associated with hasty burials or deaths in battles in which the phenomenon of *rigor mortis* prevents any manipulation of the body. Other authors think that the reasons may be ritual, ceremonial or perhaps related to deliberate irreverence, neglect or absence of the person responsible for burial (Mc Whirr *et al.*, 1982). Some burials indicate that the practice is probably linked to different social status and religious beliefs (Murphy, 2008); indeed, it has been highlighted that there is a correlation between individuals buried in prone position and those with marked signs of violence or infectious diseases such as leprosy or tuberculosis (Mc Whirr *et al.*, 1982; Philpott, 1992; Boylston *et al.*, 2000; Polo Cerda & Garcia Prosper, 2002; Murphy, 2008), although we do not see that here.

There are very few cases of prone burials across Spain, France, Germany and Italy, but most relate to the Roman period. For instance, in the region of Veneto (Italy), the practice of prone burial appears to be a tradition of long duration and features the oldest cases in Italy (Zamboni & Zanoni, 2010) (Table 2).

The *Monte Sirai* example presented here represents the first reported case of a prone cremation in Europe. Some cases of prone or anomalous positions associated to the Phoenician age were found in the necropolis of *Khalde* in the south of Beirut (Saïdah, 1966), the

Table 2. Cases of depositions in the prone position in Spain, Italy, France and Germany

Necropolis	Number of cases	Age	References
Yaramila, Tscheremissinott (France)	2	Neolithic	Chambon & Leclerc (2003)
Necropoli Olmo di Nogara (Verona, Italy)	1	Bronze Age	Salzani (2005)
Necropoli Scalvinetto di Legnago (Verona, Italy)	1	Bronze Age	Salzani (1994)
Necropoli di Vallone di Ostiglia (Mantova, Italy)	1	Bronze Age	De Marinis (1987)
Sepolture di Trani (Bari, Italy)	1	Iron Age	Sublimi Saponetti & Scattarella (2003)
Necropoli Franzine Nuove di Villabartolomea (Verona, Italy)	1	13th century BC	Corrain *et al.* (1967)
Necropoli Narde di Fratta Polesine (Rovigo, Italy)	1	12th to 9th century BC	Salzani & Colonna (2005)
Montagnana, Borgo S. Zeno (Padova, Italy)	1	10th century BC	De Min (2005)
Oppeano (Verona, Italy)	3	9th to 5th century BC	Catalano *et al.* (2008)
Necropoli della Colombara di Gazzo Veronese (Verona, Italy)	2	Bronze Age to 6th century BC	Drusini (2001)
Via Tiepolo (Padova, Italy)	2	6th to 4th century BC	Corrain & Capitanio (1968)
Coll del Moro de la Serra d'Almos en Tivisa (Spain)	1	6th century BC	Cela Espin *et al.* (1999)
Necropolis romana de la Calle Quart de Valencia (Valencia, Spain)	11	2nd century BC to 1st century AD	Polo Cerda & Garcia Prosper (2002)
Necropoli Romana Stazione Centrale di Bologna (Italy)	2	1st century AD	Cornelio Cassai *et al.* (2008)
Saint-Paul-Trois-Chateaux (France)	12	1st to 2nd century AD	Bel *et al.* (1992)
Roanne (France)	4	1st to 2nd century AD	Bel *et al.* (1992)
Necropoli di Alba Pompeia (Italy)	2	2nd century AD	Filippi (1997)
Necropoli di Porta Palio (Verona, Italy)	2	1st to 2nd century AD	Cavalieri Manasse & Bolla (1998)
Parque de Miraflores y Centro de Congresos de Córdoba (Córdoba, Spain)	3	1st to 2nd century AD	Casal García *et al.* (2004)
Necropoli Osteria del Curato (Roma, Italy)	1	1st to 3rd century AD	Catalano *et al.* (2005)
Necropoli di Egnazia (Brindisi, Italy)	1	1st to 3rd century AD	Andreassi (1987), Cocchiaro & Andreassi (1988)
Necropoli di Via Cappuccini (Brindisi, Italy)	1	1st to 3rd century AD	Cocchiaro & Andreassi (1988)
Plaça de la Vila de Madrid (Barcelona, Spain)	2	1st to 3rd century AD	Jordana & Malgosa (2007)
Scofa (Aquileia, Italy)	1	2nd to 3rd century AD	Tiussi (1999)
Necropoli Università Cattolica (Milano, Italy)	6	1st to 5th century AD	Sannazaro (2001)
Necropoli S. Pietro in Carpignano (Imperia, Italy)	1	4th century AD	Martino (1998)
Necropoli di Himera (Palermo, Italy)	1	4th to 7th century AD	Vassallo (2005)
Kaiseraugst (Germany)	1	4th to 7th century AD	Martin (1991)
Calles Huertos-Alorco y Plaza Morería de Sagunt (Spain)	1	5th to 6th century AD	Cerdá Polo & Prósper García (2005)
Carretera de Carmona número 6 de Sevilla (Sevilla, Spain)	1	5th to 7th century AD	Carrasco Gomez & Doreste Franco (2005)
Pieve di Pava (Siena, Italy)	1	12th century AD	Mongelli *et al.* (2011)

Phoenician necropolis of *Lagos* (Málaga) (Aubet, 1995) and the necropolis from *Himera*, in the northern-central coast of Sicily (Vassallo, 2005).

The reasons that justify this particular position, perhaps linked to social factors, are difficult to understand because of their specificity. No other apparent case of anomalous deposition was observed in *Monte Sirai* necropolis and no known cases in Sardinia at the moment. However, several graves with skeletons covered with rocks were observed in the *Monte Sirai* necropolis. This was interpreted as a ritualistic gesture intended to contain within the tomb the spirits of the dead (called *Rephaim*) so they could not bother the living (Simmer, 1982; Bartoloni, 2000).

A possible explanation might be related to the winding of the body in a shroud, as described in the rite of primary incineration by Bartoloni (2000) and a subsequent accidental and incorrect positioning on the pyre. This might also be responsible for the observed difference in temperature to which some bones of the body turned out to be subjected to. Of course, another plausible hypothesis may be the intentional prone deposition of the body during the incineration ritual, perhaps to emphasise some diversity of the individual within the community.

It is interesting to note, in all of this discussion, that Tomb 252 is not removed from other supine burials at this site and has therefore not been made peripheral in terms of the actual burial.

Acknowledgements

The authors thank Prof. Piero Bartoloni (Università di Sassari) and Dr Massimo Piccinini (Porto Conte Ricerche, Alghero-Sassari). G. Piga is supported by the project 'Giovani Ricercatori' entitled *Studio archeometrico, antropologico e paleogenetico del materiale archeologico appartenente al sito fenicio-punico di Monte Sirai (Carbonia)*, financed by the Regione Autonoma della Sardegna. Assumpciò Malgosa thanks the Ministry of Education PR2009-0128 for the teaching and research stays at foreign institutions seniors for higher education and research, and the Ministry of Education and Science CGL2008-00800.

References

Andreassi G. 1987. L'attività archeologica in Puglia nel 1986. in: Atti del XXVI Convegno di Studi sulla Magna Grecia, (Taranto-Reggio Calabria 9–14 ottobre 1986), Taranto.

Arcini C. 2009. Buried faced down: Prone burials. *Current Archaeology* **20**(231): 30–35.

Aubet ME. 1995. Nueva necrópolis fenicia de incineración en Lagos (Málaga). *Actes du III^e Congrès International des Études Phéniciennes et Puniques*, Tunis 11–16 novembre 1991, Tunis. 20–40.

Bartoloni P. 2000. La necropoli di Monte Sirai. *Collezione di Studi Fenici* **41**. Roma Eds.

Bel V, Tranoy L, Beraud I, Gebara C. 1992. Les nécropoles à incinérations et à inhumations en Gaule Méridionale. In: VIDAL (M.) dir. Incinérations et inhumations dans l'Occident romain aux trois premiers siècles de notre ère. *Actes du colloque International de Toulouse-Montrégeau (IVème Congrès Archéologique de Gaule Méridionale)*, 7–10 octobre 1987. Toulouse, Association pour la promotion du patrimoine archéologique et historique en Midi-Pyrénées, 9–40.

Bohnert M, Rost T, Pollak S. 1998. The degree of destruction of human bodies in relation to the duration of the fire. *Forensic Science International* **95**: 11–21.

Botto M. 1994. Monte Sirai 1. Analisi del materiale anforico relativo alle campagne di scavo 1990 e 1991. *Rivista di Studi Fenici* **22**: 83–116.

Boylston A, Knüsel CJ, Roberts CA. 2000. Investigation of a Romano-British Rural ritual in Bedford, England. *Journal of Archaeological Science* **27**: 241–254.

Brothwell DR. 1981. *Digging Up Bones. The Excavation, Treatment, and Study of Human Skeletal Remains*. Cornell University Press: Ithaca, N.Y. and London.

Carrasco Gomez I, Doreste Franco D. 2005. Continuidad de un espacio funerario en Sevilla. Excavaciones arqueológicas en el entorno de la Trinidad. *Romula* **4**: 213–244.

Casal García MT, León A, Murillo JF, Sánchez S, García B, Vargas S, Sánchez I, Pizarro G. 2004. Informe-Memoria de la intervención arqueológica de urgencia en el S.G. SS-1 (Parque de Miraflores y Centro de Congresos de Córdoba). Primera Fase. *Anuario Arqueológico de Andalucía 2001*, III-Urgencias, Sevilla, 259–274.

Catalano P, Caprara MC, Di Giannantonio S. 2005. Gli inumati in fossa della necropoli eneolitica di Osteria del Curato-via Cinquefrondi (Roma). Atti della XL Riunione scientifica: strategie di insediamento fra Lazio e Campania in etá preistorica e protostorica: Roma, Napoli, Pompei, 30 novembre–3 dicembre 2005: dedicati ad Amilcare Bietti, Volume 1, 583–587.

Catalano P, Caldarini C, De Angelis F, Pantano W. 2008. La sepoltura di Oppeano (Verona): dati antropologici e paleo patologici. In: Atti del convegno Ricerche storiche e archeologiche dell'Università di Verona, Verona, 23–24 maggio 2008.

Cavalieri Manasse G, Bolla M. 1998. Osservazioni sulle necropoli veronesi. In: Bestattungssitte und kulturelle Identität. Grabanlagen und Grabbeigaben der frühen römischen Kaiserzeit in Italien und den Nordwest-Provinzen. *Xantener Berichte* **7**: 116–139.

Cela Espin X, Noguera Guillen J, Rovira Hortalà MC. 1999. Els materials arqueològics del jaciment ibèric del Coll del Moro de Serra d'Almos (Tivissa, Ribera d'Ebre). Col·lecció del Museu Comarcal Salvador Vilaseca de Reus. *Pyrenae* **30**: 91–121.

Cerdá Polo M, Prósper García E. 2005. Estudio bioantropológico de los restos óseos hallados en el interior de la

cloaca de la vía Romana del "solar de la Morería" de Sagunto. *Arse* **39**: 209–228.

Chambon P, Leclerc J. 2003. Les pratiques funéraires néolithiques avant 3500 av. J.-C. en France et les régions limitrophes. *Société Préhistorique Française Mémoire* **33**. Paris.

Cocchiaro A, Andreassi G. 1988. *La necropoli di via Cappuccini a Brindisi*. Schena Editore: Fasano.

Cornelio Cassai C, Cavallari C, Milella M, Belcastro MG, Mariotti V, Cesari L. 2008. Riti funerari non convenzionali in una necropoli di età imperiale: il caso delle tombe 109, 161 e 244 della Stazione Centrale di Bologna. In: Pagani e Cristiani. Forme ed attestazioni di religiosità del mondo antico in Emilia, volume VII.

Corrain C, Capitanio M. 1968. Uno scheletro umano antico in posizione bocconi rinvenuto in via Tiepolo (Padova), in: Atti dell'XI e XII Riunione Scientifica dell'i.i.p.p., 35–42.

Corrain C, Capitanio M, Fasani L. 1967. Un inumato in posizione bocconi nella necropoli Enea di Franzine Nuove di Villabartolomea (Verona). *Quaderni di Antropologia ed Etnologia* **4**: 145–148.

Curtin AJ. 2008. Putting together the pieces: Reconstructing mortuary practices from commingled ossuary cremains. In *The Analysis of Burned Human Remains*. Elsevier-Academic Press: New York, USA; 201–209.

De Marinis R. 1987. Villaggi e necropoli dell'età del Bronzo nel territorio di Ostiglia Ostiglia Eds.

De Min M. 2005. Il mondo religioso dei Veneti antichi. *La città invisibile. Padova preromana. Trent'anni di scavi e ricerche*. Edizioni Tipoarte: Bologna.

Drusini AG. 2001. Scheda antropologica dell'inumato della tomba 61. *Quaderni di Archeologia del Veneto* **XVII**: 83–84.

Elliott JC, Mackie PE, Young RA. 1973. Monoclinic hydroxyapatite. *Science* **180**: 1055–1057.

Enzo S, Fagherazzi G, Benedetti A, Polizzi S. 1988. A profile-fitting procedure for analysis of broadened X-ray diffraction peaks. I Methodology. *Journal of Applied Crystallography* **21**: 536–542.

Enzo S, Bazzoni M, Mazzarello V, Piga G, Bandiera P, Melis P. 2007. A study by thermal treatment and X-ray powder diffraction on burnt fragmented bones from Tombs II, IV and IX belonging to the hypogeic necropolis of "Sa Figu" near Ittiri-SS (Sardinia-Italy). *Journal of Archaeological Science* **34**: 1731–1737.

Ferembach D, Schwidetzky I, Stloukal M. 1977–1979. Raccomandazioni per la determinazione dell'età e del sesso sullo scheletro. *Rivista di Antropologia* **60**: 5–51.

Filippi F. 1997. Alba Pompeia. Archeologia della città dalla fondazione alla Tarda Antichità. *Quaderni della Soprintendenza Archeologica del Piemonte, Monografie* **6**. Alba.

Gonçalves D. 2011. The reliability of osteometric techniques for the sex determination of burned human skeletal remains. *Homo – Journal of Comparative Human Biology* **62**: 351–358.

Guirguis M. 2010. Necropoli fenicia e punica di Monte Sirai. Indagini archeologiche 2005–2007. *Studi di Storia Antica e di Archeologia* **7**. Ortacesus ed., Cagliari.

Guirguis M. 2011. Gli spazi della morte a Monte Sirai (Carbonia – Sardegna). Rituali e ideologie funerarie nella necropoli fenicia e punica (scavi 2005–2010). *Fasti On Line Documents & Research*, **230**.

Jordana X, Malgosa A. 2007. Enterraments d'época Romana a la Plaça de la Vila de Madrid. Resultats de la recerca antropológica. *Quarbis, Època II* **3**: 64–81.

Koon HEC, Nicholson RA, Collins MJ. 2003. A practical approach to the identification of low temperature heated bone using TEM. *Journal of Archaeological Science* **30**: 1393–1399.

Krenzer U. 2006. Compendio de métodos antropológico forenses para la reconstrucción del perfil osteo-biológico. *Tomo II: Métodos para la determinación del sexo*. CAFCA: Guatemala.

Krogman WM, Iscan MY. 1986. *The Human Skeleton in Forensic Medicine* (2nd edn). Charles C. Thomas, Springfield: Illinois.

Lutterotti L, Bortolotti M. 2003. Object oriented programming and fast computation techniques in Maud, a program for powder diffraction analysis written in java. *IUCr: Compcomm Newsletter* **1**: 43–50.

Martin M. 1991. Zur frühmittelalterliche Gürteltracht der Frau in der Burgundia, Francia und Aquitania, in: L'art des Invasions en Hongrie et en Wallonie. *Actes du colloque de Mariemont, 1979*, Morlanwelz, 31–84 (Monographies du Musée Royal de Mariemont, 6).

Martino GP. 1998. Per una crono-tipologia sepolcrale del ponente ligure. *Rivista di studi liguri* **LIV**: 249–268.

Mc Whirr A, Viner L, Wells C. 1982. Romano-British cementeries at Cirencester. Cirencester Excavations II. Cirencester Excavation Committee.

Mongelli V, Vitiello A, Campana S, Lubritto C, Fornaciari G. 2011. La sepoltura privilegiata e la sepoltura prona della Pieve di Pava: un rituale cristiano di consacrazione e un rituale precristiano. Pagani e Cristiani. Forme di attestazione di religiosità del mondo antico in Emilia. Volume X, 149–157.

Murphy EM. 2008. *Deviant Burial in the Archaeological Record*. Oxbow Books: Oxford, UK.

Olsen J, Heinemeier J, Bennike P, Krause C, Hornstrup KM, Thrane H. 2008. Characterisation and blind testing of radiocarbon dating of cremated bone. *Journal of Archaeological Science* **35**: 791–800.

Philpott R. 1992. Burial practices in Roman Britain. *A survey of grave treatment and furnishing A.D 43–410*. Tempus Reparatum BAR British series 219.

Piga G, Malgosa A, Mazzarello V, Bandiera P, Melis P, Enzo S. 2008a. Anthropological and physico-chemical investigation on the burnt remains of Tomb IX in the "Sa Figu" hypogeal necropolis (Sassari-Italy) – Early Bronze Age. *International Journal of Osteoarcheology* **18**: 167–177.

Piga G, Malgosa A, Thompson TJU, Enzo S. 2008b. A new calibration of the XRD technique for the study of archaeological burnt remains. *Journal of Archaeological Science* **35**: 2171–2178.

Piga G, Thompson TJU, Malgosa A, Enzo S. 2009. The potential of X-ray diffraction (XRD) in the analysis of burned remains from forensic contexts. *Journal of Forensic Sciences* **54**(3): 534–539.

Piga G, Guirguis M, Bartoloni P, Malgosa A, Enzo S. 2010a. A funerary rite study in the Phoenician–Punic Necropolis

of Mount Sirai (Carbonia–Sardinia–Italy). *International Journal of Osteoarcheology* **20**: 144–157.

Piga G, Hernández-Gasch JH, Malgosa A, Ganadu ML, Enzo S. 2010b. Cremation practices coexisting at the "SIllot des Porros" Necropolis during the Second Iron Age in the Balearic Islands (Spain). *Homo* **61**: 440–452.

Polo Cerda M, Garcia Prosper E. 2002. Ritual, violencia y enfermedad. Los enterramientos en decúbito prono de la necrópolis fundacional de Valentia. *Saguntum* **34**: 137–148.

Pucéat E, Reynard B, Lécuyer C. 2004. Can crystallinity be used to determine the degree of chemical alteration of biogenic apatites? *Chemical Geology* **205**: 83–97.

Rietveld HM. 1967. Line profiles of neutron powder-diffraction peaks for structure refinement. *Acta Crystallographica* **22**: 151–152.

Rogers KD, Daniels P. 2002. An X-ray diffraction study of the effects of heat treatment on bone mineral microstructure. *Biomaterials* **23**: 2577–2585.

Rogers KD, Beckett S, Kuhn S, Chamberlain A, Clement J. 2010. Contrasting the crystallinity indicators of heated and diagenetically altered bone mineral. *Palaeogeography, Palaeoclimateology, Palaeoecology* **296**: 125–129.

Saïdah R. 1966. Fouilles de Khaldé. Rapport préliminaire sur la première et deuxième campagnes (1961–1962). *Bullettin du Musée de Beyrouth* **19**, Beyrouth.

Salzani L. 1994. Necropoli dell'età del Bronzo a Scalvinetto di Legnago (VR). Campagne di Scavo 1991 e 1994. *Padusa* **30**: 67–83.

Salzani L. 2005. La necropoli dell'Età del Bronzo all'Olmo di Nogara (Verona). Memorie del Museo Civico di Storia Naturale di Verona, 2ª serie.

Salzani L, Colonna C. 2005. Fratta Polesine. Nuova area sepolcrale alle Narde. *Quaderni di Archeologia del Veneto* **XXI**: 48–49.

Sannazaro M. 2001. La ecropolis tardoantica. Milano Eds.

Shannon EM. 2011. The effects of body mass on cremation weight. *Journal of Forensic Sciences* **56**: 3–9.

Shemesh A. 1990. Crystallinity and diagenesis of sedimentary apatites. *Geochimica et Cosmochimica Acta* **54**: 2433–2438.

Simmer A. 1982. Le prelevement des cranes dans l'est de la France a l'epoque merovingienne. *Archeologie Medievale* **12**: 35–49.

Squires KE, Thompson TJU, Islam M, Chamberlain A. 2011. The application of histomorphometry and Fourier transform infrared spectroscopy to the analysis of early Anglo-Saxon burned bone. *Journal of Archaeological Science* **38**: 2399–2409.

Subirà ME, Alesan A, Malgosa A. 1992. Cribra orbitalia y déficit nutricional. Estudios de elementos traza. *Munibe* **8**: 153–158.

Sublimi Saponetti S, Scattarella V. 2003. Probabili pratiche necrofobi che in tombe della prima età del Ferro (IX–VII sec A.C) a Capo Colonna (Trani, Bari). Atti del XV Congresso di Antropologia (Chieti, 28–30 Settembre 2003). Chieti, 479–488.

Thompson TJU, Gauthier M, Islam M. 2009. The application of a new method of Fourier transform infrared spectroscopy to the analysis of burned bone. *Journal of Archaeological Science* **36**: 910–914.

Thompson TJU, Islam M, Piduru K, Marcel A. 2011. An investigation into the internal and external variables acting on crystallinity index using Fourier transform infrared spectroscopy on unaltered and burned bone. *Palaeogeography, Palaeoclimateology, Palaeoecology* **299**: 168–174.

Tiussi C. 1999. Località Scofa. Necropoli della via Amnia. Scavo 1998. *Aquileia Nostra* **70**: 390–398.

Ubelaker DH. 1999. *Human Skeletal Remains: Excavation, Analysis, Interpretation* (3rd edn). Taraxacum DC: Washington.

Ustundag H. 2009. Schmorl's Nodes in a Post-Medieval Skeletal Sample from Klostermarienberg, Austria. *International Journal of Osteoarchaeology* **19**: 695–710.

Vassallo S. 2005. Himera città greca. Guida alla storia e ai monumenti. Beni Culturali – Palermo, 8. Palermo.

Weiner S, Bar-Yosef O. 1990. States of preservation of bones from prehistoric sites in the Near East: A survey. *Journal of Archaeological Science* **17**: 187–196.

Wright LE, Schwarcz HP. 1996. Infrared and isotopic evidence for diagenesis of bone apatite at Dos Pilas, Guatemala: Palaeodietary implications. *Journal of Archaeological Science* **23**: 933–944.

Zamboni L, Zanoni V. 2010. Giaciture non convenzionali in Italia nord-occidentale durante l'età del Ferro. *Quaderni di archeologia dell'Emilia Romagna* **28**: 147–160.

Chapter 4.5: Is X-Ray Diffraction able to distinguish between animal and human bones?

Authors: **Giampaolo Piga, Giuliana Solinas, T.J.U Thompson, Antonio Brunetti, Assumpcio Malgosa, Stefano Enzo.**

Journal of Archaeological Sciences (http://dx.doi.org/10.1016/j.jas.2012.07.004**)**

The separation of animal from human bone is an important component of any archaeological or forensic osteological and histological analysis (Cattaneo et al., 1999; Cuijpers, 2006; McKinley, 1994; Whyte 2001). It can be important for a range of reasons, from determining the minimum number of individuals present, to understanding funerary behavior, to comprehending human-faunal relations. This is also true of burned skeletal material, but this work is greatly complicated by the range of heat-induced changes that bone undergoes when burned (Thompson, 2005). Thus studies which focus on the separation of different species of bone, especially if fragmented, are extremely valuable. With this in mind, Beckett et al. (2011) reported in a recent paper the possibility of determining the human rather than animal origin of bone from the lattice parameters of the inorganic bioapatite phase from the diffraction patterns of bones subjected to a high temperature heating treatment.

In our work, first we address the problem of whether the monoclinic $P2_1/b$ vs hexagonal $P6_3/m$ space group can make a substantial difference in terms of lattice parameter values for the bioapatite of bones. Then we evaluate the most evident structural changes involved after high-temperature treatment. Finally we discuss the lattice parameter values of 42 (belonging to 25 species) heat-treated animal bones and 53 human bone samples from various Spanish and Italian necropolises.

The bones of were treated in a furnace at 1100°C for 36 minutes and compared to 53 cremated human bones collected from a range of ancient Spanish and Italian necropolises.

Our results clearly show that in terms of lattice parameters the variability of human specimens are completely overlapped by the non-human variability making the use of XRD in order to distinguish animal from human bones questionable values.

ARTICLE IN PRESS

Journal of Archaeological Science xxx (2012) 1–8

Contents lists available at SciVerse ScienceDirect

Journal of Archaeological Science

journal homepage: http://www.elsevier.com/locate/jas

Is X-ray diffraction able to distinguish between animal and human bones?

Giampaolo Piga [a,b,*], Giuliana Solinas [c], T.J.U. Thompson [d], Antonio Brunetti [e], Assumpció Malgosa [a], Stefano Enzo [b]

[a] GROB (Grup de Recerca en OsteoBiografia), Unitat d'Antropologia Biologica, Department de Biologia Animal, Biologia Vegetal i Ecologia, Universitat Autonoma de Barcelona, Edifici C, 08193 Bellaterra, Barcelona, Spain
[b] Dipartimento di Chimica e Farmacia, Università di Sassari, via Vienna 2, I-07100 Sassari, Italy
[c] Department of Biomedical Sciences, Laboratory of Epidemiology and Biostatistics, University of Sassari, via Padre Manzella 4, I-07100 Sassari, Italy
[d] School of Science & Engineering, Teesside University, Borough Road, Middlesbrough TS1 3BA, UK
[e] Struttura Dipartimentale di Matematica e Fisica, Università di Sassari, via Vienna n. 2, I-07100 Sassari, Italy

Keywords:
Powder X-ray diffraction
Heat treatment
Hydroxylapatite
Lattice parameters
Human bones
Animal bones
Human bone identification

A B S T R A C T

The possibility of determining the human or animal origin of bones from the lattice parameters of their inorganic bioapatite phase, when subjected to a high temperature treatment using the powder X-ray diffraction (XRD) technique, has been explored on a wide number of specimens. Forty-two animal bones were treated in a furnace at 1100 °C for 36 min and compared to 53 cremated human bones from a range of ancient necropolises. The X-ray diffraction patterns of bioapatite were simulated using both monoclinic P21/b and hexagonal P63/m structures to verify any occurrence of phase transformation and any difference in the lattice parameters due to the model. It was determined that the differences between the *a*-axis and *c*-axis of the monoclinic and hexagonal lattice were unimportant. Some outlying values were revealed to be caused by the presence of chlorine ions diffused into the apatite structure increasing its average unit cell values. Nevertheless, our results clearly show that in terms of lattice parameters the variability of human specimens are completely overlapped by the non-human variability making the use of XRD in order to distinguish animal from human bones questionable.

1. Introduction

The separation of animal from human bone is an important component of any archaeological or forensic osteological and histological analysis (Cattaneo et al., 1999; Cuijpers, 2006; McKinley, 1994; Whyte, 2001). It can be important for a range of reasons, from determining the minimum number of individuals present, to understanding funerary behavior, to comprehending human–faunal relations. This is also true of burned skeletal material, but this work is greatly complicated by the range of heat-induced changes that bone undergoes when burned (Thompson, 2005). Thus studies which focus on the separation of different species of bone, especially if fragmented, are extremely valuable. With this in mind, Beckett et al. (2011) reported in a recent paper the possibility of determining the human rather than animal origin of bone from the lattice parameters of the inorganic bioapatite phase from the diffraction patterns of bones subjected to a high temperature heating treatment. Actually, the structural properties of a substance are inspected by diffraction in terms of symmetry operations compatible with three-dimensional periodicity of the crystals, i.e., specifying one of the 230 possible space groups (see: International Tables for X-ray Crystallography, 1965–68), complemented with the geometry and dimensions of the unit cell of the lattice (so-called lattice parameters) as well as its atomic content and arrangement. For the case of bioapatite crystals found in bones, a space group $P6_3/m$ is generally attributed with a hexagonal unit cell where two lattice parameters *a*- and *c*-axis respectively, need to be determined. According to Beckett et al. (2011), the plot of *a*- vs *c*-axis data points from human being occurs in a typical and distinct area with respect to animals.

The determination of lattice parameters depends upon the precision of locating the peak profiles in XRD diagrams (Masciocchi and Artioli, 1996), but in bioapatite this is difficult to do. This is because of large peak broadening resulting from the small crystallite size of the phase combined with the high amount of lattice strain (Danilchenko et al., 2002). To alleviate this problem, Beckett et al. (2011) have suggested that lattice parameter determination be performed on highly crystallized single phase materials following

* Corresponding author. GROB (Grup de Recerca en OsteoBiografia). Unitat d'Antropologia Biologica, Department de Biologia Animal, Biologia Vegetal i Ecologia, Universitat Autonoma de Barcelona, Edifici C, 08193 Bellaterra, Barcelona, Spain.
E-mail address: kemiomara@yahoo.it (G. Piga).

0305-4403/$ – see front matter © 2012 Elsevier Ltd. All rights reserved.
http://dx.doi.org/10.1016/j.jas.2012.07.004

Please cite this article in press as: Piga, G., et al., Is X-ray diffraction able to distinguish between animal and human bones?, Journal of Archaeological Science (2012), http://dx.doi.org/10.1016/j.jas.2012.07.004

thermal treatment of the bone. However this in turn creates a potential problem in identifying the most appropriate heating temperature for differentiating faunal from human bone.

Another potential issue with the approach in Beckett et al. (2011) stems from the fact that their analysis is limited to a sample of just 8 human specimens vs 65 non-human samples from 12 different species. This may be due to the difficulties in acquiring modern bone for such research, but nevertheless the large availability of human bones from the archaeological context offers considerable scope for the continued investigation of this area (Piga et al., 2007). Thus we have critically investigated the diffraction patterns of a wide variety of bones originating from various contexts routinely met in the course of our archaeological and anthropological investigations (Piga et al., 2010a, 2010b).

Unfortunately the factors regulating the chemistry of bones are still not completely known. Apatites have the general formula, $Ca_5(PO_4)_3X$ or $Ca_{10}(PO_4)_6X_2$ where X is typically F (fluorapatite), OH (hydroxylapatite), or Cl (chlorapatite) in case of natural minerals (Elliott et al., 2002). Typically the mineral of bone and teeth is an impure form of OHA where the major variations in composition focus on a variable Ca/P mol ratio (1.6–1.7, OHAp is 1.66), and a few percent CO_3^{2-} and water. In fact, the apatite lattice is very tolerant to substitutions, vacancies and solid solutions; for example, X in the general chemical formula above can be replaced by $½CO_3^{2-}$ or $½O^{2-}$; Ca^{2+} by Sr^{2+}, Ba^{2+}, Pb^{2+}, Na^{+} or vacancies; and PO_4^{3-} by HPO_4^{2-}, AsO_4^{3-}, VO_4^{3-}, SiO_4^{4-} or CO_3^{2-}. It is the degree of such substitutions that can affect the average lattice parameter values and introduce some voids or strain (Aellach et al., 2010), and these may also be responsible for the unique mechanical properties of bone. Other factors affecting the lattice parameter are the presence of organic materials of biogenic origin, and extra phases (Elliot, 1994).

Wopenka and Pasteris (2005) have recently discussed the over-simplifications involved when using the hydroxylapatite inorganic phase as a model of bones, especially in view of the types of ionic substitutions that can occur in the apatite lattice which may then change the mineral characteristics of the bone material. Instead, Wopenka and Pasteris (2005) locate natural bioapatite inside a hyper-phase diagram with end-members of apatite minerals such as hydroxylapatite, fluorapatite, A-type carbonated apatite, B-type carbonated fluorapatite (formerly known as francolite), and B-type carbonated hydroxylapatite (formerly known as dahllite).

Of course, *post-mortem* taphonomic and diagenetic changes are expected to add further complexity to the structure and microstructure of bones, not only due to new ionic substitutions but also in terms of new biogenic or authigenic phases that form during the conservation, storage and degradation processes of bone (Shinomiya et al., 1998; Piga et al., 2009a, 2011).

The paper by Beckett et al. (2011) has employed a simplified approach for lattice parameter determination starting from the peak positions which are calculated by the automatic location of the maxima of diffraction patterns (which may not be completely satisfactory). In our work care has been exercised in order to measure the lattice parameters of the bioapatite phase with the best practices ensuring precision and accuracy. The Rietveld method (Rietveld, 1967; Young, 1993) appears to be the most orthodox approach for this purpose (Peterson, 2005) and indeed is now standard practice in materials science (although its use has appeared only sporadically in the archaeological and forensic fields). Another important point concerns the most suitable space group for describing the bioapatite structure when using powder XRD. While the most popular space group to represent the structure of bioapatite is $P6_3/m$, a more suitable alternative appears to be a monoclinic description using the $P2_1/b$ space group. This is due to the fact that OH^- is non-spherical and therefore reduces possible crystalline symmetry (Elliott et al., 1973; Wopenka and Pasteris, 2005). Moreover, we must also bear in mind that it was recently reported that a monoclinic-to-hexagonal order/disorder transformation occurs at 220 °C for synthetic apatite (Yashima et al., 2011).

In this work, first we address the problem of whether the monoclinic $P2_1/b$ vs hexagonal $P6_3/m$ space group can make a substantial difference in terms of lattice parameter values for the bioapatite of bones. We then evaluate the most evident structural changes involved after high-temperature treatment. Finally we discuss the lattice parameter values of heat-treated animal and human bone samples from various Spanish and Italian necropolises.

2. Experimental methodology

2.1. Examined specimens

The forty-two animal bone specimens were kindly made available from: the Institut Català de Paleontologia (Sabadell-Barcelona, Spain), the School of Science & Engineering, Teesside University (UK), and the Department of Animal Biology, University of Sassari (Italy). Our collection consists of 25 species, distributed as it follows: mammoth (3), monkey (3), camel (1), deer (2), rhino (1), horse (2), ox (1), pig (1), ruminant (2), sheep (1), goat (2), rodent (1), lagomorph (2), cat (1), lion (1), dog (1), fox (1), crocodile (1), turtle (2), bird (6), whale (1), dolphin (3), tuna (1), swordfish (1), shark (1). The specimens date from the present time back to 900,000 years ago.

Further, the fifty-three human bones were kindly made available from: the Universitat Autonoma de Barcelona (Spain), and the Department of History, University of Sassari (Italy). These bones originate from: the Necropolis of *Aguilar de Montuenga* (Soria, Spain), the Necropolis of *Son Real* and *S'Illot des Porros* (Mallorca, Spain) (Piga et al., 2010b), the Necropolis of Sebès (Tarragona, Spain) (Belarte and Noguera, 2008), the Necropolis of *Mas d'en Boixos* (Pacs del Penedès, Alt Penedès, Spain) and the Necropolis of *Monte Sirai* (Carbonia, Italy) (Guirguis, 2010). Synthetic powder hydroxylapatite was synthesized by Aldrich Chemistry®.

2.2. Thermal treatment

In the present study we have selected historical human bones burned at temperatures above 1000 °C. This is based on our previous laboratory calibrations (Piga et al., 2008, 2009b). The animal bones were subjected to a heat treatment at 1100 °C for 36 min in a furnace, in order to sharpen the peak profiles to be used for determination of the lattice parameters.

2.3. Diffraction data collection and analysis

Exactly 0.5 g of each bone was ground in an agate jar for 1-min using a SPEX mixer-mill model 8000. Our sample holder for XRD analysis has a circular cavity of 25 mm in diameter and 3 mm in depth, and can hold 420 mg of pressed powder bone.

The Bruker D8 instrument was employed in the Bragg-Brentano geometry using fixed wavelength CuKα radiation and a graphite monochromator in the diffracted beam. The patterns were collected with a scintillation detector in the 2θ angular range from 9 to 140°, with a step-size of 0.05°; the counts at each data point being accumulated for 40 s in order to ensure accurate statistics for the intensity data and to reduce the uncertainty associated with the determination of lattice parameters. The X-ray generator worked at a power of 40 kV and 40 mA and the resolution of the instruments (0.5° divergent and 0.1 mm antiscatter slits) was determined using

Please cite this article in press as: Piga, G., et al., Is X-ray diffraction able to distinguish between animal and human bones?, Journal of Archaeological Science (2012), http://dx.doi.org/10.1016/j.jas.2012.07.004

α-SiO_2 and α-Al_2O_3 standards which were free from the effect of reduced crystallite size and lattice defects (Enzo et al., 1988).

The precision and accuracy of lattice parameters depends largely upon the number of peaks assessed and the relative location in the 2θ scale with respect to the whole angular range investigated (Masciocchi and Artioli, 1996; Peterson, 2005). Note that the use of position sensitive detectors for faster data collection may speed-up the data collection, the configuration used here (with a monochromator in the diffracted beam) has the advantage of controlling the background due to specific fluorescence effects. This will increase the time taken for data collection, and we are aware that the laboratory high-resolution conditions may be overtaken by accessing synchrotron radiation facilities for powder XRD.

The Rietveld method (Rietveld, 1967; Young, 1993) is based on an iterative best-fit strategy of experimental data. We have made use of the MAUD programme (for: *Material Analysis Using Diffraction*) which simulates the pattern by incorporating the instrument function and convolving the crystallographic model based on the knowledge of chemical composition and space group with selected texture and microstructure models (Lutterotti and Bortolotti, 2003). The programme permits a selection of variables for the least squares minimization such as lattice parameters of the unit cell, atomic positions, temperature factors, occupancy of the sites, an/isotropic size and strain broadening. In all patterns we have verified whether the monoclinic $P2_1/b$ rather than hexagonal $P6_3/m$ choice of the space group may have direct consequences for the analyzed values of the lattice parameters. The success of the procedure is generally evaluated throughout a combination of integrated agreement factors (R_{wp} is the most considered) and distribution of residuals (Young, 1993).

2.4. XRF analysis

XRF measurements have been carried out using portable equipment composed of an X-ray tube (molybdenum anode, Oxford Instruments) working at 25 kV and 0.1 mA. For the analysis we pressed ~200 mg of powdered bone tissue to form a pellet with a diameter of 10 mm and a thickness of 1 mm. An aluminum collimator 1 cm long and with an internal hole of 1 mm in diameter permits irradiation of an area of the object of about 0.2 cm^2 to be analyzed, at a distance tube window-sample of about 2 cm. A Si-PIN detector from AMPTEK was employed with a thickness of about 300 μm and characterized by an energy resolution of about 200 eV at 5.9 keV. 30 min was dedicated for each sample pattern without use of any standard.

2.5. Statistical analysis

All statistical analysis was performed using Stata software 9.0. In order to investigate the relationship between *c*-axis and *a*-axis values of the monoclinic (pseudo hexagonal) phase we have used the regression analysis by assuming the *a*-axis as the independent variable. Moreover, the Grubbs test was applied with 95% confidence to detect outliers (Grubbs, 1950).

3. Results and discussion

The diffraction patterns of the bones, prior to any thermal treatment conformed to the general appearance of a succession of peaks, attributable to the apatite lattice. Almost all specimens examined here showed a single-phase character, making the XRD structure analysis relatively simple. The widely broadened succession of profiles (see Fig. 1) is generally interpreted in terms of fineness of the apatite average crystallite size and short range disorder in the lattice. In fact the scatter due to collagen and organic components – if present – is negligible and would not affect our data interpretation.

In unburned bioapatites, the XRD line broadening of the (001) peak narrower than the other profile indices (whether in hexagonal or monoclinic description) may be taken as an indication of the anisotropic shape of the crystallites. This behavior is accounted for by the MAUD program with the Popa model (Popa, 1998). In general the model fit results suggest very small average crystallite size whose shape is elongated along the *c*-axis, as it is displayed in the Fig. 1B.

The longer "characteristic size" varies from 80 to 160 Å in unburned bones, which is in agreement with direct observation by Transmission Electron Microscopy and previous XRD work conducted on human fetal bones (Meneghini et al., 2003). Of course various definitions of the average size length can be envisaged when working with particles with irregular shape (Matyi et al., 1987). Note that the behavior of the bioapatite in terms of smallness of crystallite size and strain is different from synthetic hydroxylapatite, where such small characteristic dimensions cannot be achieved. For example, in Fig. 1C we see that the synthetic OHAp, which is supposed to be very pure from the chemical point of view, displays a single-phase condition with relatively sharp peaks in the as-prepared material.

The lattice parameter values *a*- and *c*-axis respectively in the two unburned specimens are reported in Table 1 and appear significantly different even when using a monoclinic space group. This may be related to the diffuse profiles of the pattern. Some shape anisotropy seems to be confirmed by the Popa model as reported in the Fig. 1D (Popa, 1998).

3.1. Transformation behavior of natural and synthetic apatites thermally treated up to 1100 °C

On sintering the bioapatite with thermal treatment, the degree of anisotropic broadening is partially removed from the patterns due to the coarsening mechanism attributable to the temperature treatment. This must be of the coalescence type (Granqvist and Buhrman, 1977). The diffraction data of ox burned bone (Fig. 2A) show narrow peaks and the quality of the fit appears "satisfactory" on the basis of the percentages from the agreement factors (see the R_{wp} values reported in the Table 1). Some anisotropy is still present since the average crystallite size depicted by the anisotropic model has a "potato"-like shape (as shown in the Fig. 2B). Of course we should keep in mind that for this and many other heat-treated specimens, the average size length is ca 1600 Å, i.e., around values close to the instrument resolution limit, above which no larger average crystallites can be assessed by the applied instrumentation (Piga et al., 2008, 2009b).

In a comparison of the monoclinic vs hexagonal geometry we see in Table 1 that the agreement numerical factors for the monoclinic phase are performing slightly better than the hexagonal description in fitting the same experimental data. This further suggests the opportunity for using the monoclinic structure to describe the bioapatite structure, even for high-temperature specimens. The monoclinic space group appears to produce an average crystallite size value slightly larger than when using the hexagonal description for the unburned bones.

It should be recognized that the monoclinic space group deals not only with four lattice parameters adjustable for the best fit but also with a total of 67 parameters due to the atomic coordinates of 5 Calcium, 3 Phosphorous, 12 Oxygen and one OH^-. This is definitely larger than for the hexagonal phase where the procedure adjusts only two lattice parameters and 12 atomic coordinates (Posner et al., 1958). Moreover, even the modeling of microstructure

Please cite this article in press as: Piga, G., et al., Is X-ray diffraction able to distinguish between animal and human bones?, Journal of Archaeological Science (2012), http://dx.doi.org/10.1016/j.jas.2012.07.004

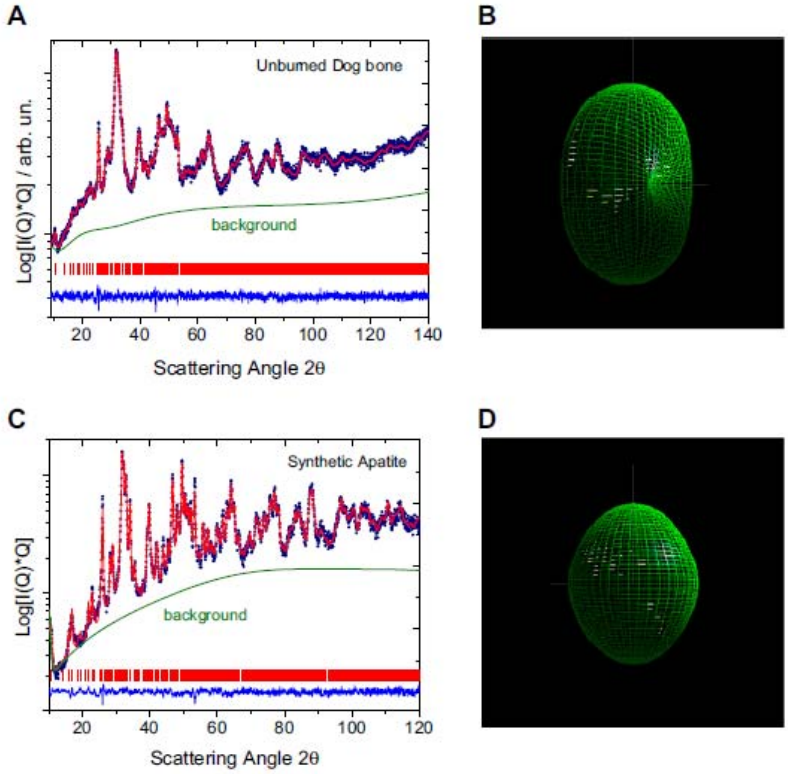

Fig. 1. A) Experimental pattern (data points) and Rietveld fit (full line) of a typical bioapatite from unburned dog bone. The agreement between experiment and model appears satisfactory as it can be concluded from the inspection of residuals (see band at the bottom) and after evaluation of the agreement factor R_{wp}. Nevertheless the procedure has unavoidably an uncertainty associated to the precise location of the peak profiles due to their large broadening. This affects the reliability of the lattice parameter values. B) The figure depicts the average shape of apatite crystallites elongated along the *c*-axis, which is reconstructed from the difference among hkl peak broadening. C) Experimental pattern (data points) and Rietveld fit (full line) of an apatite synthesized in the laboratory according to the equation: $5Ca(OH)_2 + 3H_3PO_4 > Ca_5(PO_4)_3OH + 8H_2O$. The full XRD pattern appears sharper than in the previous case testifying the difficulties in science to mimic a physiological reaction even though the average anisotropic shape (1D) is similar (not the size).

parameters according to Popa (1998) involves a larger number of anisotropic terms in the monoclinic vs hexagonal description. Accounting properly for these detailed parameters may constitute a serious limitation of the monoclinic description in view of the appeal of modeling the whole range of physico-chemical information of the bone with a simpler structure.

One further interpretation related to the chemical composition of bone may be revealed in the single-phase character of the examined samples. We are used to thinking of the inorganic "apatite" component as a single phase after the water and organics are removed, but this may not always be the case once the bone is subjected to a high-temperature treatment. In fact we have verified

Table 1
Comparison of lattice parameter, average crystallite size and agreement factor values for the couple of unburned and heat-treated specimens of dog bone and synthetic apatite, respectively.

Specimen	Hexagonal $P6_3/m$ cell				Monoclinic $P2_1/b$ cell					
	a-axis/Å	*c*-axis/Å	<D>/Å (±10%)	Rwp/%	*a*-axis/Å	*b*-axis/Å	*c*-axis/Å	γ-axis/°	<D>/Å (±10%)	Rwp/%
Synthetic apatite	9.448 (±0.003)	6.880 (±0.001)	286	9.9	9.457 (±0.003)	18.906 (±0.005)	6.884	120.08 (±0.05)	320	7.6
Heat treated synthetic apatite/whitlockite	9.427 (±0.001)	6.8830 (±0.0004)	1070	7.4	9.422 (±0.001)	18.846 (±0.002)	6.882 (±0.0004)	119.93 (±0.05)	1070	6.7
	10.438 (±0.002)	37.438 (±0.005)	1630		10.438 (±0.002)		37.434 (±0.005)		1650	
Unburned Dog bone	9.443 (±0.005)	6.905 (±0.002)	110	5.80	9.432 (±0.005)	18.865 (±0.01)	6.9047 (±0.0005)	119.90 (±0.05)	120	4.2
Burned Dog bone	9.423 (±0.001)	6.8840 (±0.0005)	1430	13.2	9.421 (±0.001)	18.849 (±0.002)	6.8841 (±0.0005)	120.00 (±0.05)	1640	11.2

Please cite this article in press as: Piga, G., et al., Is X-ray diffraction able to distinguish between animal and human bones?, Journal of Archaeological Science (2012), http://dx.doi.org/10.1016/j.jas.2012.07.004

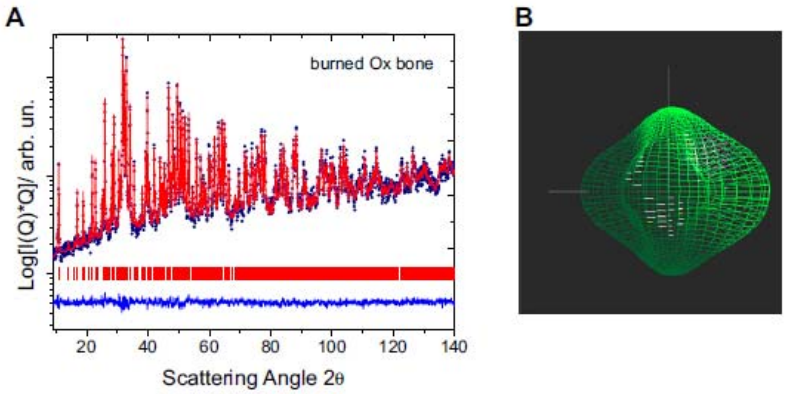

Fig. 2. A) Pattern of a burned ox bone and B) its Rietveld fit using a monoclinic space group for apatite. The approximate, average crystallite shape from Popa model is also reported on account of the observed anisotropic line broadening.

that for biological carbonate apatites treated above 850 °C, the removal of carbonate groups results in the formation of CaO after cooling down to room temperature (RT). When the synthetic powder is subjected to a thermal treatment at 1100 °C for 36 min, not only we notice peak sharpening (useful to determine accurately lattice parameters) but find also a multi-phase condition for the resultant product (see Fig. 3A). This is due to a well-known transformation of a part of OHAp to whitlockite, i.e., to the β-three-calcium-phosphate phase with chemical formula $Ca_3(PO_4)_2$ according to the reaction equation:

$$Ca_{10}(PO_4)_6(OH)_2\,(HT-1100\,^{\circ}C) \rightarrow 3\,\beta-Ca_3(PO_4)_2 + CaO + H_2O$$

Conversely, the bone specimens that have been treated thermally at 1100 °C (in order to make the determination of the lattice parameter values clearer), did not display the important phenomena of phase separation and precipitation apart from two specimens of cormorant (15% and 9% wt of whitlockite, respectively) and a pig bone (see Fig. 3C, bottom pattern). For the pig bone we notice that the unburned bioapatite is less "crystalline" than the synthetic apatite but also that the amount of β-$Ca_3(PO_4)_2$ is definitely lower (23% wt) than in the previous case. In both cases even the average shape of whitlockite was revealed to be isotropic (Fig. 3B and D). Thus we can infer that the mechanical and thermodynamic properties of bone are influenced by the type and nature of atomic substitutions occurring in the apatite lattice. Note that we report the lattice parameters for the apatite phase that have been worked out for human and animal specimens using both the monoclinic $P2_1/b$ and hexagonal $P6_3/m$ unit cells in the Supplementary Tables.

The merit of using the monoclinic cell for describing the apatite structure is that the agreement factors of R_{wp} are systematically lower with respect to the hexagonal description. In general both hexagonal and monoclinic descriptions carried out on the same specimen give reasonably similar lattice parameters values but a higher variability of the results is encountered with the monoclinic case for the untreated specimens. Because the β angle parameter of the monoclinic structure remains close to 120°, the main variability is associated with the *b* lattice parameter (which may deviate significantly from twice the *a* parameter). Whether parameter *b* carries a precise physical meaning or not is difficult to establish in the presence of such very broad peaks. In fact, the standard deviation estimated from the untreated natural bones are relatively large and may be the effect of the large peak broadening, invariably related to a strong parameter correlation due to the mathematical difficulties in fitting the experimental data. In any case the *a-axis* and *c-axis* lattice parameters of the heat treated bones turn out to be the same (within the experimental uncertainty) in both the hexagonal and monoclinic representation.

It may be safe to conclude that, although the monoclinic description of bioapatites found by Elliott et al. (1973) appear to be more suitable for the problem in hand, using the hexagonal approach does not involve significant departures when accounting for the biological lattice of bones.

With these assumptions in mind, plotting animal and human bones lattice parameters in a *a*-axis vs *c*-axis plot as done in Fig. 4 permits verification or rejection of the differences between human bones with respect to non-humans. The ellipses drawn are showing the 95% degree of confidence for each group. The size of the ellipse is strongly influenced by the size of the dataset: the larger the number of data, the tighter the ellipse, even though the spread of data may be large.

From Fig. 4 we can clearly see just one outlier for humans while for non-human the outliers are distributed at shorter and larger values along the *c*-axis. This behavior suggests the presence of at least one more variable affecting the non-humans data. Nevertheless, in Fig. 4 we can see that the distribution of data points for non-human bone overlays the scatter for human bones, contrary to the previous findings (Beckett et al., 2011), therefore suggesting we reject the possibility of using XRD to distinguish human vs animal bones.

The transverse behavior for the ellipse of non-humans can be explained by a physical effect presumably occurring *post-mortem* for some specimens. In particular, the specimens that show shorter *a*-axis values were likely subjected to fluorination reaction, as they refer to paleontological bones (Piga et al., 2009a, 2011).

For the specimens with unusually large *a*-axis lattice parameters, which are exclusively modern bones, we can conjecture that the processing of cleaning the bones involving boiling in salted water has led to partial chlorination with consequent cell expansion mainly in the *a*- (and *b*-) direction. This is confirmed by examining the published lattice parameter values of Chlorapatite (Mackie et al., 1972). Indeed recent work has already demonstrated the effect of chlorine ions on bone when heated in salt water (Trujillo-Mederos et al., 2011) even if no correlation has been established with the lattice parameter values. Note also that the process of boiling the bones in salted water is not a cleaning practice common to archeology and forensics field. Increase of the

Please cite this article in press as: Piga, G., et al., Is X-ray diffraction able to distinguish between animal and human bones?, Journal of Archaeological Science (2012), http://dx.doi.org/10.1016/j.jas.2012.07.004

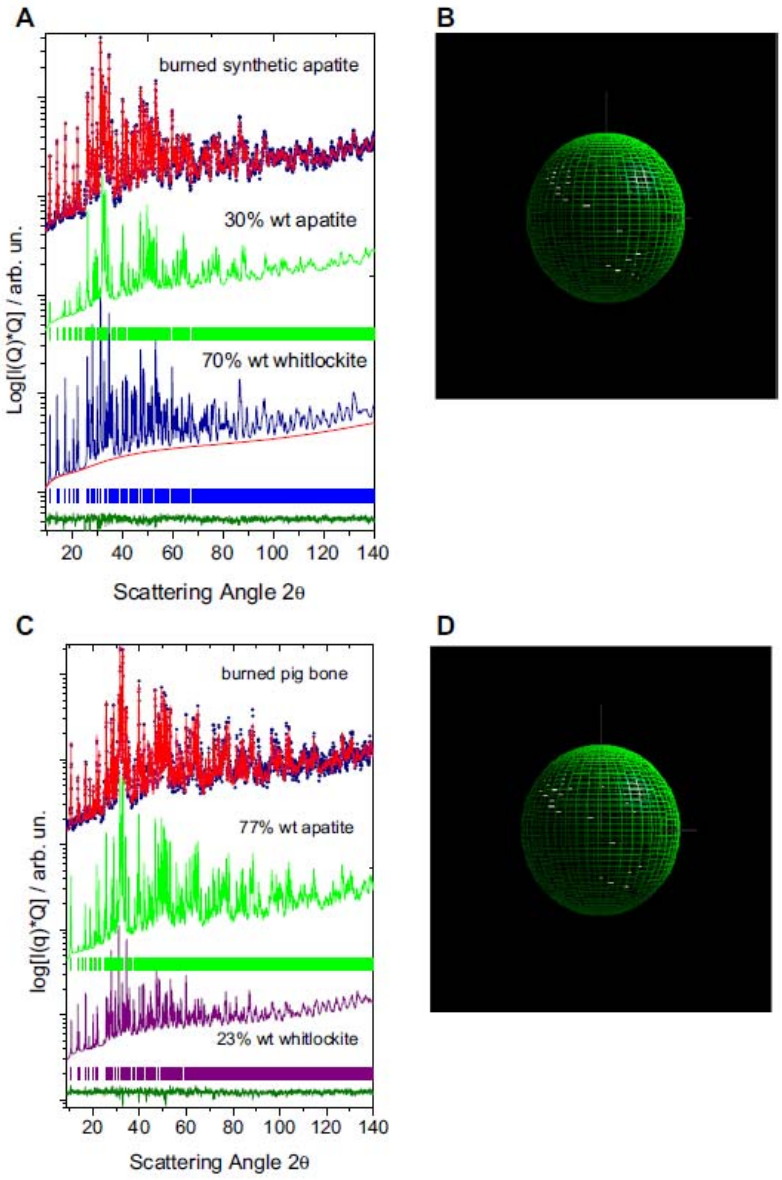

Fig. 3. A) The top of the figure depicts the XRD pattern and its Rietveld fit for the synthetic apatite thermally treated at 1100 °C, which turns out to be a mixture of 70 wt% of whitlockite and only 30% of monoclinic apatite. B) The broadening analysis revealed an isotropic average crystallite size of the apatite component of ca 1000 Å. C) For comparison the bottom pattern refers to the results from the pig bone burned at 1100 °C, one of the rare biological specimens showing a partial transformation to whitlockite. The amount of bioapatite is ca 77 wt% i.e., only 23 wt% belongs to whitlockite on account of a better stability of the biological vs synthetic phase synthesized at RT. D) Note again an isotropic shape of for the average crystallite size of ca 1700 Å for the bioapatite, close to the resolution limit of the instrument. In both cases even the average shape of whitlockite was revealed to be isotropic.

a- and *c*-axis parameter as a function of chlorine concentration were reported recently on synthetic hydroxy-chlorapatites solid solutions by Kannan et al. (2006).

As a matter of fact, the XRF spectra of these specimens in Fig. 5 indeed show the presence of Chlorine, which is readily exchanged in the bone matrix due to the unit cell dimensions of apatite. Of course other anions and cations may be responsible for an observed lattice parameter increase. Moreover, in particular cases the effect of expansion to the cell brought about by the chlorine anions may be compensated by the presence of other small ions. It can be argued that "routine" protocols adopted for cleaning prior to classification of bones may need some further calibration in view of their consequences on bioapatite chemistry and lattice parameter values.

Please cite this article in press as: Piga, G., et al., Is X-ray diffraction able to distinguish between animal and human bones?, Journal of Archaeological Science (2012), http://dx.doi.org/10.1016/j.jas.2012.07.004

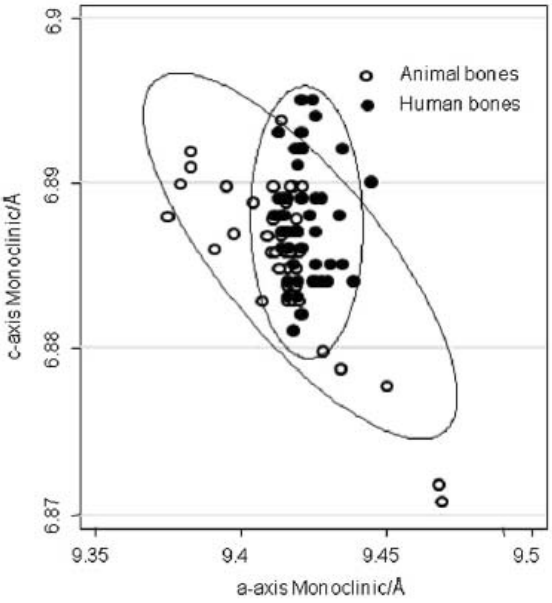

Fig. 4. Plot of *c*- vs *a*-axis for the two groups of bones treated at high-temperature (either in the furnace or after a crematory ritual). Apart from some outliers related to their fossilization processes or to inclusions of chlorine, the two groups of humans and animal bones are overlapped so as to identify a single cluster.

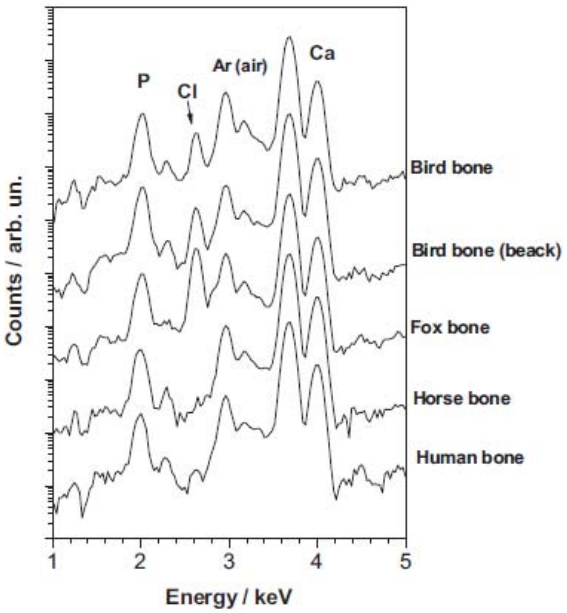

Fig. 5. The XRF spectra of three outlyiers (bird, bird beak and fox bone) compared to the spectrum of human and horse bones that did not show significant departure of its lattice parameters from the calculated average. This suggests that the presence of specific impurities in the bone lattice is relatable to the observed changes in lattice parameters. It is questionable to relate it just to the animal rather then human species.

4. Conclusions

The large availability of burned human bones from some ancient Spanish and Italian necropolises has been exploited in order to assess whether the lattice parameters of bioapatite obtained by XRD are helpful when trying to distinguish human bones from those of animals.

The lattice parameters of bioapatite were measured using the Rietveld method with a relatively high degree of precision on bones subjected to a high-temperature treatment. The bones were heated since this produces a readily observable sharpening of peaks resulting from the growth of the crystallites. While the synthetic apatite was partially transformed to whitlockite after 36 min at 1100 °C, the human bones were unaffected by this transformation. Moreover, this transformation partially occurred in just three of the animal bones studied. It is also useful to note that the *a*-axis and *c*-axis values of bioapatite are not biased by the use of a $P2_1/b$ monoclinic rather than $P6_3/m$ hexagonal unit cell. The different diet of the human species does not appear to affect the chemical composition of bones to the point of inducing systematic differences in the apatite lattice parameters, because of faults, inclusion of extra atoms and/or solid solution formations. However, the apatite unit cell axis can be affected by ion exchange reactions occurring *post-mortem* such fluorination during diagenesis or chlorination during boiling the bones in salted water for cleaning.

On the basis of our experiments involving 42 animal and 53 human bones it is not possible to discriminate human from non-human origin using lattice parameter values and any such claims to be able to do so should be treated with caution.

Our results are perhaps not so surprising, since the biological reactions that lead to the formation of apatite are conducted in a physiological environment that is chemically the same whether dealing with animals or humans.

Acknowledgments

The authors thank Prof. Salvador Moya Solà (Universitat Autonoma de Barcelona; Institut Català de Paleontologia), Angel Galobart, Jordi Galindo Torres, Laura Celià Gelabert (Institut Català de Paleontologia), Prof. Marco Zedda (Dipartimento di Biologia Animale, University of Sassari, Italy), Prof. Piero Bartoloni, Dr. Michele Guirguis, Alessandro Contini (University of Sassari, Italy) and Dr. Massimo Piccinini (Porto Conte Ricerche Science Center, Sassari, Italy); G. Piga is supported by the Regione Autonoma of Sardegna (Italy) within the project "Giovani Ricercatori" entitled: Studio archeometrico, antropologico e paleogenetico del materiale archeologico appartenente al sito fenicio-punico di Monte Sirai (Carbonia).

Appendix A. Supplementary data

Supplementary data related to this article can be found online at http://dx.doi.org/10.1016/j.jas.2012.07.004.

References

Aellach, B., Ezzamarty, A., Leglise, J., Lamonier, C., Lamonier, J.F., 2010. Calcium-deficient and stoichiometric hydroxyapatites promoted by cobalt for the catalytic removal of oxygenated volatile organic compounds. Catalysis Letters 135, 197–206.

Beckett, S., Rogers, K.D., Clement, J.D., 2011. Inter-species variation in bone mineral behavior upon heating. Journal of Forensic Sciences 56, 571–579.

Belarte, M.C., Noguera, J., 2008. El jaciments protohistòrics de Santa Madrona (Ribaroja) i Sebes (Flix), Ribera d'Ebre. Tribuna d'Arqueologia 2007, 127–147.

Cattaneo, C., Di Martino, S., Scali, S., Craig, O.E., Grandi, M., Sokol, R.J., 1999. Determining the human origin of fragments of burnt bone: a comparative study

Please cite this article in press as: Piga, G., et al., Is X-ray diffraction able to distinguish between animal and human bones?, Journal of Archaeological Science (2012), http://dx.doi.org/10.1016/j.jas.2012.07.004

of histological, immunological and DNA techniques. Forensic Science International 102, 181–191.
Cuijpers, A., 2006. Histological identification of bone fragments in archaeology: telling humans apart from horses and cattle. International Journal of Osteoarchaeology 16, 465–480.
Danilchenko, S.N., Kukharenko, O.G., Moseke, C., Protsenko, I.Yu., Sukhodub, L.F., Sulkio-Cleff, B., 2002. Determination of the bone mineral crystallite size and lattice strain from diffraction line broadening. Crystal Research and Technology 37 (11), 1234–1240.
Elliot, J.C., 1994. Structure and Chemistry of the Apatites and Other Calcium Orthophosphates. Elsevier, Amsterdam.
Elliott, J.C., Mackie, P.E., Young, R.A., 1973. Monoclinic hydroxyapatite. Science 180, 1055–1057.
Elliott, J.C., Wilson, R.M., Dowker, S.E.P., 2002. Apatite structures. Advances in X-ray Analysis 45, 172–181.
Enzo, S., Fagherazzi, G., Benedetti, A., Polizzi, S., 1988. A profile-fitting procedure for analysis of broadened X-ray diffraction peaks. I Methodology. Journal of Applied Crystallography 21, 536–542.
Granqvist, C.G., Buhrman, R.A., 1977. Size distributions for supported metal–catalysts – coalescence growth versus Ostwald ripening. Journal of Catalysis 42, 477.
Grubbs, F.E., 1950. Sample criteria for testing outlying observations. Annals of Mathematical Statistics 21, 27–58.
Guirguis, M., 2010. Necropoli fenicia e punica di Monte Sirai. Indagini archeologiche 2005–2007. In: Studi di Storia Antica e di Archeologia, vol. 7. Ortacesus ed., Cagliari.
International Union of Crystallography, 1965-68. International Tables for X-ray Crystallography. The Kynoch Press, Birmingham.
Kannan, S., Rocha, J.H.G., Ferreira, J.M.F., 2006. Synthesis of hydroxy-chlorapatites solid solutions. Materials Letters 60, 864–868.
Lutterotti, L., Bortolotti, M., 2003. Object oriented programming and fast computation techniques in MAUD, a program for powder diffraction analysis written in java. IUCr: Computing Commission Newsletter 1, 43–50.
Mackie, P.E., Elliott, J.C., Young, R.A., 1972. Monoclinic structure of synthetic $Ca_5(PO_4)_3Cl$, chlorapatite. Acta Crystallographica B 28, 1840–1848.
Masciocchi, N., Artioli, G., 1996. Lattice parameters determination from powder diffraction data: results from a Round Robin project. Powder Diffraction 11, 253–258.
Matyi, R.J., Schwartz, L.H., Butt, J.B., 1987. Particle size, particle size distribution, and related measurements of supported metal catalysts. Catalysis Reviews 29 (1), 41–99.
McKinley, J.I., 1994. Bone fragment size in British cremation burials and its implications for pyre technology and ritual. Journal of Archaeological Science 21, 339–342.
Meneghini, C., Dalconi, M.C., Nuzzo, S., Mobilio, S., Wenk, R.H., 2003. Rietveld refinement on X-ray diffraction patterns of bioapatite in human fetal bones. Biophysical Journal 84 (3), 2021–2029.
Peterson, V.K., 2005. Lattice parameter measurement using Le Bail versus structural. Rietveld. refinement: a caution for complex, low symmetry systems. Powder Diffraction 20, 14–17.
Piga, G., Malgosa, A., Mazzarello, V., Bandiera, P., Melis, P., Enzo, S., 2007. Anthropological and physico-chemical investigation on the burnt remains of Tomb IX in the "Sa Figu" hypogeal necropolis (Sassari-italy)-Early Bronze Age. International Journal of Osteoarcheology 18, 167–177.
Piga, G., Malgosa, A., Thompson, T.J.U., Enzo, S., 2008. A new calibration of the XRD technique for the study of archaeological burnt remains. Journal of Archaeological Science 35, 2171–2178.
Piga, G., Santos-Cubedo, A., Moya Solà, S., Brunetti, A., Malgosa, A., Enzo, S., 2009a. An X-ray diffraction (XRD) and X-ray fluorescence (XRF) investigation in human and animal fossil bones from Holocene to Middle Triassic. Journal of Archaeological Science 36, 1857–1868.
Piga, G., Thompson, T.J.U., Malgosa, A., Enzo, S., 2009b. The potential of X-ray diffraction (XRD) in the analysis of burned remains from forensic contexts. Forensic Science International 54 (3), 534–539.
Piga, G., Guirguis, M., Bartoloni, P., Malgosa, A., Enzo, S., 2010a. A funerary rite study in the Phoenician-Punic Necropolis of Mount Sirai (Carbonia-Sardinia-Italy). International Journal of Osteoarchaeology 20, 144–157.
Piga, G., Hernández-Gasch, J.H., Malgosa, A., Ganadu, M.L., Enzo, S., 2010b. Cremation practices coexisting at the S'Illot des Porros Necropolis during the Second Iron Age in the Balearic Islands (Spain). Homo 61, 440–452.
Piga, G., Santos-Cubedo, A., Brunetti, A., Piccinini, M., Napolitano, E., Malgosa, A., Enzo, S., 2011. A multi-technique approach by XRD, XRF, FT-IR to characterize the diagenesis of dinosaur bones from Spain. Palaeogeography, Palaeoclimatology, Palaeoecology 310, 92–107.
Popa, N.C., 1998. The (hkl) Dependence of diffraction-line broadening caused by strain and size for all Laue groups in rietveld refinement. Journal of Applied Crystallography 31, 176–180.
Posner, A.S., Perloff, A., Diorio, A.F., 1958. Refinement of the hydroxyapatite structure. Acta Crystallographica 11, 308–309.
Rietveld, H.M., 1967. Line profiles of neutron powder-diffraction peaks for structure refinement. Acta Crystallographica 22, 151–152.
Shinomiya, T., Shinomiya, K., Orimoto, C., Minami, T., Tohno, Y., Yamada, M., 1998. In- and out-flows of elements in bones embedded in reference soils. Forensic Science International 98, 109–118.
Thompson, T.J.U., 2005. Heat-induced dimensional changes in bone and their consequences for forensic anthropology. Journal of Forensic Science 50 (5), 1008–1015.
Trujillo-Mederos, A., Alemán, I., Botella, M., Bosch, P., 2011. Changes in human bones boiled in seawater. Journal of Archaeological Science 39, 1072–1079.
Whyte, T., 2001. Distinguishing remains of human cremations from burned animal bones. Journal of Field Archaeology 28, 437–448.
Wopenka, B., Pasteris, J.D., 2005. A mineralogical perspective on the apatite in bone. Materials Science and Engineering C 25, 131–143.
Yashima, M., Yonehara, Y., Fujimori, H., 2011. Experimental visualization of chemical bonding and structural disorder in hydroxyapatite through charge and nuclear-density analysis. Journal of Physic Chemistry 115, 25077–25087.
Young, A., 1993. The Rietveld Method. IUCr, Oxford Science Publications.

Please cite this article in press as: Piga, G., et al., Is X-ray diffraction able to distinguish between animal and human bones?, Journal of Archaeological Science (2012), http://dx.doi.org/10.1016/j.jas.2012.07.004

Chapter 4.6: A multi-technique approach by XRD, XRF, FT-IR to characterize the diagenesis of dinosaur bones from Spain

Authors: **Giampaolo Piga, Andrés Santos-Cubedo, Antonio Brunetti, Massimo Piccinini, Assumpciò Malgosa, Emilio Napolitano, Stefano Enzo.**

Palaeogeography, Palaeoclimatology, Palaeoecology 310, 92–107.
(http://dx.doi.org/10.1016/j.palaeo.2011.05.018).

Diagenetic changes are induced in bones over palaeontologist times mainly by complex mineralogical and physico-chemical processes.

The precise understanding of diagenetic and taphonomic processes to which paleontological bones were subjected requires a multidisciplinary approach, taking into account the potentialities and limitations of each analytical technique employed. Particularly, we have used combined X–ray diffraction, X–ray fluorescence and FT–IR analysis to investigate a collection of 60 Spanish dinosaur bone specimens being 150 to 65 Ma to characterize the fossilization in terms of chemical and mineralogical composition, crystallite size, precipitation and infiltration, exchange reactions involving atomic and molecular ion species.

From the crystal lattice parameters of the apatite phase determined by powder XRD, it emerged that these fossil bones invariably underwent a *post-mortem* transformation from bioapatite (hydroxylapatite) to authigenic francolite (fluorapatite) structure.

Concerning the phases constituting the fossil bones, a high variability can be pointed out among the various samples. The diffraction approach assessed in all specimens the presence of fluorapatite at various levels of percentage as the mineral phase constituting the dinosaur bones. Multiple secondary mineral phases, mainly calcite and quartz but also goethite, dolomite and several other minor phases were detected. They occurred as pore space infillings in most dinosaur bones only three out of 60 bones were single phase (fluorapatite) specimens.

The apatite crystal size was variable (from 183 Å to 2100 Å) and varies unpredictably in the analysed specimens, inhibiting a correlation with fossil age. In our previous study (Piga et al., 2009b), we have, however, observed a positive correlation

between average bone apatite crystal size and specimen age in another set of fossils ranging in age from the Middle Triassic (around 245 Ma) to present.

Increasing significantly the sampling of a relatively restricted time range (150 to 65 Ma), no systematic trend of crystal size with age of the specimen or taphonomic setting was found (see figure 11). From the present data it seems that the crystallization induced by just the time is overlapped by other factors depending on the geological Formation that may inhibit (e.g., *4ANA3* sample) or enhance the process.

The infrared spectra of fossil bones show significant changes in the phosphate and carbonate band intensity with respect to a non-fossil bone.

The XRF spectra collected in the energy range from 1.5 to 18 keV supplied analysis profile spectra with the expected presence of Ca and P as major elements. In addition, the presence of carbonate groups substituting for the phosphate group in the hydroxylapatite-like structure was definitely assessed for the single-phase specimens by FT–IR spectroscopy.

In all the fossils examined, varying levels of Fe were detected by XRF that may be present in the goethite phase FeOOH. However, no presence of other Fe-bearing phases such as pyrite, hematite or magnetite was observed. For the specimens that displayed considerable amount of Fe but absence of any Fe-bearing phase in the XRD spectra, the analysis suggested that Fe divalent cations may have substituted for divalent Ca cations in the francolite structure even at a considerable concentration level (up to 12 %) and without significant changes in the unit cell volume. Frequently the major elements Ca and P were also accompanied by varying amounts of transitional elements such as Ti, V, Mn, Cu, As, Rb, Y, Sr and Nb, to list the most frequently encountered.

Palaeogeography, Palaeoclimatology, Palaeoecology 310 (2011) 92–107

Contents lists available at ScienceDirect

Palaeogeography, Palaeoclimatology, Palaeoecology

journal homepage: www.elsevier.com/locate/palaeo

A multi-technique approach by XRD, XRF, FT-IR to characterize the diagenesis of dinosaur bones from Spain

Giampaolo Piga [a,e,*], Andrés Santos-Cubedo [b], Antonio Brunetti [c], Massimo Piccinini [d], Assumpciò Malgosa [a], Emilio Napolitano [e], Stefano Enzo [e]

[a] Unitat de Antropologia Biologica, Departament de Biologia Animal, Biologia Vegetal i Ecologia, Universitat Autonoma de Barcelona, E-08193 Bellaterra, Spain
[b] Institut Català de Paleontologia, C/ Escola Industrial, 23, E-08201 Sabadell, Barcelona, Spain
[c] Struttura Dipartimentale di Matematica e Fisica, Università di Sassari, via Vienna n. 2, I-07100 Sassari, Italy
[d] Porto Conte Ricerche Srl, Loc. Tramariglio , I-07041 Alghero-Sassari, Italy
[e] Dipartimento di Chimica, Università di Sassari, via Vienna 2, I-07100 Sassari, Italy

ARTICLE INFO

Article history:
Received 26 May 2010
Received in revised form 4 May 2011
Accepted 16 May 2011
Available online 20 May 2011

Keywords:
X-ray diffraction
X-ray fluorescence
Fourier Transform Infrared spectroscopy (FT-IR)
Raman spectroscopy
Dinosaur bones
Diagenetic processes

ABSTRACT

A combined investigation by X-ray fluorescence (XRF), Fourier Transform Infrared spectroscopy (FT-IR), Raman spectroscopy and powder X-ray Diffraction (XRD), supplemented with the Rietveld analysis, was conducted on sixty Spanish dinosaur bone specimens from Upper Jurassic/Lower Cretaceous to Upper Cretaceous age to investigate taphonomy and diagenetic processes. The diffraction approach assessed in all specimens the presence of fluorapatite at various levels of percentage as the mineral phase constituting the fossil bone. In addition to fluorapatite, calcite and quartz were also found as main secondary phases in many specimens. The infrared spectra of fossil bones show significant changes in the phosphate and carbonate band intensity with respect to a non-fossil bone. Conversely, the X-ray fluorescence spectra turned out to be mainly dominated by the presence of Ca, obviously accompanied by phosphorus. Simultaneously, other elements accompanying Ca, such as Fe and Sr were found at significant concentration levels.

A considerable amount of Fe and Sr ions were incorporated in the structure of fluorapatite, but when their concentration was found elevated in the fluorescence spectrum, the diffraction data revealed the presence of goethite (FeOOH) and celestite ($SrSO_4$) phases. While the X-ray diffraction phase analysis also revealed the presence of kaolinite, dolomite, barite and gypsum, in some fluorescence spectra further elements like Y, As, Pb, Ti, Mn, Cr, Cu, Zn were present in concentration at trace level. The introduction/substitution of new elements with the infiltration of new phases due to diagenesis is also affecting to various extent the Raman and FT-IR spectra with modification of some bands and/or the appearance of new bands. The average crystallite size of the "apatitic" constituent phase was found to vary from a minimum of ca. 183 Å to an upper level of 2107 Å. No systematic relation between apatite crystallite size and age of the dinosaur bones was found that suggests a high variability of diagenetic processes affecting the growth of bone crystallites even in the same site.

1. Introduction

The study about chemical and mineralogical composition of fossil animal and human bones may be a precious source of information about the past. However, a large fraction of these studies have focused on archaeological samples and biomaterials and only to a little extent on dinosaur fossils (Zocco and Schwartz, 1994; Hubert et al., 1996; Bocherens, 1997; Trueman et al., 2003a, 2003b; Tütken et al., 2004; Fricke et al., 2008; Dumont et al., 2011; Heuser et al., 2011; Pfretzschner and Tütken, 2011; Tütken, 2011;). Changes involving the structure and chemical composition of bones may occur in two different periods, i.e., first during the animal's life, and second during the fossilization process. The time scale of these two stages may be incommensurable and a distinction is made between biostratinomy and fossildiagenesis. During the biostratinomic stage, micro-organisms and other biotic processes can attack the organic and inorganic content of bones, degrading mineral bone phases (e.g. Trueman and Martill, 2002; Jans et al., 2004). In addition, abiotic factors can degrade the bones both before or after burial (e.g. Denys, 2002). If the bones are not subjected to microbial or biotic erosion or the processes are affected by drastic physical or chemical changes, fossilization may occur soon after burial (Trueman and Martill, 2002; Pfretzschner, 2004; Farlow and Argast, 2006).

* Corresponding author at: Unitat de Antropologia Biologica, Departament de Biologia Animal, Biologia Vegetal i Ecologia, Universitat Autonoma de Barcelona, E-08193 Bellaterra, Spain. Tel.: +39 3407840935; fax: +34 935811321.
E-mail addresses: kemiomara@yahoo.it (G. Piga), santos.cubedo@gmail.com (A. Santos-Cubedo), brunetti@uniss.it (A. Brunetti), piccinini@portocontericerche.it (M. Piccinini), napolitano@uniss.it (E. Napolitano), enzo@uniss.it (S. Enzo).

0031-0182/$ – see front matter © 2011 Elsevier B.V. All rights reserved.
doi:10.1016/j.palaeo.2011.05.018

Table 1
List of the Spanish dinosaur bones with classification, geological period and provenance location.

Sample code	Classification	Epoch and geological stage	Formation and basin	Location
Serrat del Corb	Dinosauria (Hadrosauria)	Upper Cretaceous (Maastrichtian)	Tremp Tremp Basin	Isona (Lleida)
Serrat-R2	Dinosauria (Hadrosauria)	Upper Cretaceous (Maastrichtian)	Tremp Tremp Basin	Isona (Lleida)
Molí del Baró	Dinosauria (unclassified)	Upper Cretaceous (Maastrichtian)	Tremp Tremp Basin	Isona (Lleida)
La Penella	Dinosauria (unclassified)	Upper Cretaceous (Maastrichtian)	Tremp Tremp Basin	Peramola (Lleida)
Lo Bas	Dinosauria (unclassified)	Upper Cretaceous (Maastrichtian)	Tremp Tremp Basin	Abella de la Conca (Lleida)
La Llau de Bas	Dinosauria (unclassified)	Upper Cretaceous (Maastrichtian)	Tremp Tremp Basin	Abella de la Conca (Lleida)
Nerets	Dinosauria (unclassified)	Upper Cretaceous (Maastrichtian)	Tremp Tremp Basin	Villamitjana (Lleida)
Pous	Dinosauria (Hadrosauria)	Upper Cretaceous (Maastrichtian)	Tremp Tremp Basin	Basturs (Lleida)
Basturs Poble	Dinosauria (Hadrosauria)	Upper Cretaceous (Maastrichtian)	Tremp Tremp Basin	Basturs (Lleida)
Basturs Poble-07	Dinosauria (Hadrosauria)	Upper Cretaceous (Maastrichtian)	Tremp Tremp Basin	Basturs (Lleida)
Boiga	Dinosauria (unclassified)	Upper Cretaceous (Maastrichtian)	Tremp Tremp Basin	Conques (Lleida)
Peguera 1-Figols	Dinosauria (Hadrosauria)	Upper Cretaceous (Maastrichtian)	Tremp Figols-Vallcebre Basin	Figols (Barcelona)
Psm-Mila	Dinosauria (unclassified)	Upper Jurassic/Lower Cretaceous	Fm. Villar del Arzobispo; Southwestern Iberian Basin	Puebla de San Miguel (Valencia)
Psm-Maite	Dinosauria (unclassified)	Upper Jurassic/Lower Cretaceous	Fm. Villar del Arzobispo; Southwestern Iberian Basin	Puebla de San Miguel (Valencia)
Psm-Andres	Dinosauria (unclassified)	Upper Jurassic/Lower Cretaceous	Fm. Villar del Arzobispo; Southwestern Iberian Basin	Puebla de San Miguel (Valencia)
Psm-Carles	Dinosauria (unclassified)	Upper Jurassic/Lower Cretaceous	Fm. Villar del Arzobispo; Southwestern Iberian Basin	Puebla de San Miguel (Valencia)
CerroTadon	Dinosauria (unclassified)	Upper Jurassic/Lower Cretaceous	Fm. Villar del Arzobispo; Southwestern Iberian Basin	Alpuente (Valencia)
HTCO4-3	Dinosauria (unclassified)	Upper Jurassic/Lower Cretaceous	Fm. Villar del Arzobispo; Southwestern Iberian Basin	Alpuente (Valencia)
Rascaña	Dinosauria (unclassified)	Upper Jurassic/Lower Cretaceous	Fm. Villar del Arzobispo; Southwestern Iberian Basin	Alpuente (Valencia)
Yac-David	Dinosauria (unclassified)	Upper Jurassic/Lower Cretaceous	Fm. Villar del Arzobispo; Southwestern Iberian Basin	Alpuente (Valencia)
Corral de Marin	Dinosauria (unclassified)	Upper Jurassic/Lower Cretaceous	Fm. Villar del Arzobispo; Southwestern Iberian Basin	Alpuente (Valencia)
229	Dinosauria (unclassified)	Upper Jurassic/Lower Cretaceous	Fm. Villar del Arzobispo; Southwestern Iberian Basin	Alpuente (Valencia)
Losilla	Dinosauria (Eusauropoda)	Upper Jurassic/Lower Cretaceous	Fm. Villar del Arzobispo; Southwestern Iberian Basin	Alpuente (Valencia)
Aras de Alpuente	Dinosauria (Eusauropoda)	Upper Jurassic/Lower Cretaceous	Fm. Villar del Arzobispo; Southwestern Iberian Basin	Alpuente (Valencia)
La Ventura	Dinosauria (Eusauropoda)	Upper Jurassic/Lower Cretaceous	Fm. Villar del Arzobispo; Southwestern Iberian Basin	Alpuente (Valencia)
El Collado	Dinosauria (unclassified)	Upper Jurassic/Lower Cretaceous	Fm. Villar del Arzobispo; Southwestern Iberian Basin	La Cuevarruz (Valencia)
El Collado 1	Dinosauria (unclassified)	Upper Jurassic/Lower Cretaceous	Fm. Villar del Arzobispo; Southwestern Iberian Basin	La Cuevarruz (Valencia)
Patiras	Dinosauria (unclassified)	Lower Cretaceous (Aptian)	Arcillas de Morella Maestrat Basin	Todolella (Castellón)
SAV-39	Dinosauria (Eusauropoda)	Lower Cretaceous (Aptian)	Arcillas de Morella Maestrat Basin	Morella (Castellón)
SAV-67	Dinosauria (Eusauropoda)	Lower Cretaceous (Aptian)	Arcillas de Morella Maestrat Basin	Morella (Castellón)
Povet	Dinosauria (Ornithopoda)	Lower Cretaceous (Aptian)	Arcillas de Morella Maestrat Basin	Morella (Castellón)
Camino	Dinosauria (unclassified)	Lower Cretaceous (Aptian)	Arcillas de Morella Maestrat Basin	Morella (Castellón)
EAP 38	Dinosauria (unclassified)	Lower Cretaceous (Aptian)	Arcillas de Morella Maestrat Basin	Morella (Castellón)
EAP 40-39	Dinosauria (unclassified)	Lower Cretaceous (Aptian)	Arcillas de Morella Maestrat Basin	Morella (Castellón)
EAP 43	Dinosauria (unclassified)	Lower Cretaceous (Aptian)	Arcillas de Morella Maestrat Basin	Morella (Castellón)
Comptadors A1	Dinosauria (unclassified)	Lower Cretaceous (Aptian)	Arcillas de Morella Maestrat Basin	Cinctorres (Castellón)
Todolella 1	Dinosauria (unclassified)	Lower Cretaceous (Aptian)	Arcillas de Morella Maestrat Basin	Todolella (Castellón)
Torre Julian	Dinosauria (unclassified)	Lower Cretaceous (Aptian)	Arcillas de Morella Maestrat Basin	Todolella (Castellón)

(continued on next page)

Table 1 (*continued*)

Sample code	Classification	Epoch and geological stage	Formation and basin	Location
A 10	Dinosauria (Theropoda)	Lower Cretaceous (Aptian)	Arcillas de Morella Maestrat Basin	Cinctorres (Castellón)
A 13	Dinosauria (unclassified)	Lower Cretaceous (Aptian)	Arcillas de Morella Maestrat Basin	Cinctorres (Castellón)
2ANA12	Dinosauria (Ornithopoda)	Lower Cretaceous (Aptian)	Arcillas de Morella Maestrat Basin	Cinctorres (Castellón)
2ANA61	Dinosauria (Ornithopoda)	Lower Cretaceous (Aptian)	Arcillas de Morella Maestrat Basin	Cinctorres (Castellón)
2ANA77	Dinosauria (Ornithopoda)	Lower Cretaceous (Aptian)	Arcillas de Morella Maestrat Basin	Cinctorres (Castellón)
3ANA58	Dinosauria (Ornithopoda)	Lower Cretaceous (Aptian)	Arcillas de Morella Maestrat Basin	Cinctorres (Castellón)
4ANA3	Dinosauria (unclassified)	Lower Cretaceous (Aptian)	Arcillas de Morella Maestrat Basin	Cinctorres (Castellón)
4ANA75	Dinosauria (unclassified)	Lower Cretaceous (Aptian)	Arcillas de Morella Maestrat Basin	Cinctorres (Castellón)
Escápula-ANA	Dinosauria (Ornithopoda)	Lower Cretaceous (Aptian)	Arcillas de Morella Maestrat Basin	Cinctorres (Castellón)
Mas Roig	Dinosauria (unclassified)	Lower Cretaceous (Aptian)	Arcillas de Morella Maestrat Basin	Cinctorres (Castellón)
Mas de Rafael-2	Dinosauria (unclassified)	Lower Cretaceous (Aptian)	Arcillas de Morella Maestrat Basin	Todolella (Castellón)
El Maset	Dinosauria (unclassified)	Lower Cretaceous (Barremian)	Cantaperdius Maestrat Basin	Cinctorres (Castellón)
Manzanera	Dinosauria (unclassified)	Lower Cretaceous (Barremian)	Cantaperdius Maestrat Basin	La Mata (Castellón)
CL	Dinosauria (Ornithopoda)	Lower Cretaceous (Barremian)	Cantaperdius Maestrat Basin	Portell (Castellón)
CL 42	Dinosauria (Ornithopoda)	Lower Cretaceous (Barremian)	Cantaperdius Maestrat Basin	Portell (Castellón)
CL 56	Dinosauria (Ornithopoda)	Lower Cretaceous (Barremian)	Cantaperdius Maestrat Basin	Portell (Castellón)
La Cuba	Dinosauria (unclassified)	Lower Cretaceous (Barremian)	Cantaperdius Maestrat Basin	Portell (Castellón)
La Fita	Dinosauria (Ornithopoda)	Lower Cretaceous (Barremian)	Cantaperdius Maestrat Basin	Cinctorres (Castellón)
La Fita balsa	Dinosauria (Ornithopoda)	Lower Cretaceous (Barremian)	Cantaperdius Maestrat Basin	Cinctorres (Castellón)
Qurolles III	Dinosauria (Ornithopoda)	Lower Cretaceous (Barremian)	Cantaperdius Maestrat Basin	Portell (Castellón)
Qurolles M	Dinosauria (Ornithopoda)	Lower Cretaceous (Barremian)	Cantaperdius Maestrat Basin	Portell (Castellón)
MC1-5	Dinosauria (Ornithopoda)	Lower Cretaceous (Barremian)	Cantaperdius Maestrat Basin	Portell (Castellón)

Some processes may occur to preserve rather than degrading fossils, particularly the incorporation of new ions into the crystal structure and/or recrystallisation of skeletal apatite, (Elorza et al., 1999; Hedges, 2002; Trueman and Tuross, 2002; Wings, 2004; Farlow and Argast, 2006). These processes are mainly controlled by abiotic, physical and chemical environmental soil conditions, particularly groundwater chemistry around the buried bone material (Trueman et al., 2004; Wings, 2004; Tütken et al., 2008). The bioapatite of animal and human bones turns out to be very similar at an atomic level and the structure is generally approximated using the stoichiometric mineral hydroxylapatite $Ca_5(PO_4)_3OH$.

Wopenka and Pasteris (2005) have recently discussed the limitations of such an inorganic phase as a model of bones especially in view of several types of ionic substitutions in the apatite lattice that may change the mineral characteristics. Of course, *post-mortem* taphonomic and diagenetic changes are expected to add further complexity to the structure and microstructure of fossil bones, not only due to new ionic substitutions but also in terms of new biogenic or authigenic phases that form in the fossilizing bone. Wopenka and Pasteris (2005) locate the natural bioapatite inside an hyper-phase diagram with end-members of apatite minerals such as hydroxylapatite, fluorapatite, A-type carbonated apatite, B-type carbonated fluorapatite (old mineral name francolite), B-type carbonated hydroxylapatite (old mineral name dahllite). A good knowledge of the chemical and mineralogical composition of fossil bones as the result of a whole host of physical, chemical and biological processes can be obtained directly from fluorescence and powder diffraction of X-rays (Bradley et al., 2007). For the study of molecular features in bones, the above techniques have been recently supplemented by Infrared and Raman spectroscopy (e.g. Pucéat et al., 2004; Thomas et al., this issue). It should be considered that the fluorescence technique gives direct information on the elemental composition that can be usefully compared with the quantitative phase evaluation from X-ray diffraction and with information about the molecular groups as derived from Raman and Infrared spectroscopy. The recent numerical development of powder X-ray Diffraction technique according to the Rietveld method has supplied a new approach to reveal the structure details of natural apatites, as we have recently verified in archaeological and geological contexts (Piga et al., 2009).

Chipera and Bish (1991), Zocco and Schwartz (1994), Dumont et al. (2011) have analysed the effect of crystallite size and strain in the apatite lattice, which is a way to evaluate the crystallinity index CI (Bartsiokas and Middleton, 1992; Person et al., 1995).

Conversely, Elorza et al. (1999) measured the apatite crystallinity from the width of the (002) peak of dinosaur bones and found it to be significantly higher than for modern bone. They also reported X-ray diffraction (XRD) patterns of bones according to which the replacement of biogenic hydroxylapatite by francolite is related to diagenetic changes.

A multiple-technique approach combining XRD, XRF, FT-IR and Raman analysis proved to be useful to better characterize the mineralogical and chemical composition of fossil bones. This information enables a better understanding of bone fossilization

processes but knowledge of the phase composition is also important in order to choose the appropriate treatment and chemical products for optimal conservation and preservation of the fossils (Suñer et al., 2007).

2. Materials and methods

2.1. Bone samples

Table 1 reports the list of sixty dinosaur bone specimens examined in this work, their geological period and formation, taxa and provenance locations.

All the fossil bone samples are Upper Jurassic/Lower Cretaceous to Upper Cretaceous (~150 to 65 Ma) in age and belong to large dinosaurs of different taxa (Table 1) from three regional deposits, described in the following:

1) The Upper Jurassic and Lower Cretaceous deposits of the southwestern Iberian Basin at Alpuente are formed by deltaic siliciclastic sediments deposited in fluvial, estuarine, beach and shallow-marine environments, controlled by eustatic sea level changes. These sediments belong to "*Villar del Arzobispo*" Formation, consisting of limestone, sandstone and clay minerals, "*Huérguina*" Formation (limestones) and "*Collado*" Formation (sandstones and clays), respectively.
2) The Cretaceous deposits are well distributed from middle to east of the Iberian Peninsula. The "*Cantaperdius*" Formation (composed by fluvial and lacustrine sediments) and the "*Morella*" Formation (Lower Cretaceous, clay stones, formed by deltaic sediments deposited in fluvial, estuarine, beach and shallow-marine environments) crop out in the Maestrat Basin, that is located in the eastern part of the Iberian rift system (Iberian Chain) with Mesozoic sediments up to 5.8 km thickness (Salas et al., 1995, 2001). This important geological structure formed during the Mesozoic rift stage (Caja et al., 2005).
3) The Upper Cretaceous deposits of the northwestern Iberian Peninsula at Tremp Basin are formed by terrestrial sediments with up to 1000 m in thickness. The Tremp Formation has an Upper Campanian to Lower Eocene age and is formed by grey clays with lignite at the base and predominantly red clays with sandstones and fluvial conglomerates or non-marine limestone intercalations (Riera et al., 2009).

The vertebrate material was mechanically separated from the sediment with an engraver drill. Subsequently the bones were washed with distilled water. For all specimens, the bone was sampled in the innermost part of the bone cortex (compacta) of the cortical tissue.

All the sixty fossil dinosaur bone samples were kindly made available from: Colección Museográfica de Cinctorres (Castellón), Museu de la Conca Dellà (Lleida), Universidad de Valencia and Institut Català de Paleontologia, Sabadell (Barcelona).

For comparison to the fossil dinosaur bone samples a modern animal bone as well as synthetic hydroxylapatite was also analyzed using the same techniques. A recent rhesus monkey bone was used for this purpose but any other recent animal or human bone would have been suitable as the phase composition of bone is similar and not taxon-specific.

The modern bone of a rhesus monkey was made available by Teesside University (Middlesbrough, UK); synthetic powder hydroxylapatite was synthesized by Aldrich chemistry®.

3. Methods

3.1. XRD analysis

0.5 g of each dinosaur bone was ball milled in a agate jar for one-minute using a SPEX mixer-mill model 8000. Our sample holder for XRD analysis is a circular cavity of 25 mm in diameter and 3 mm in depth. It contains about 420 mg of powder bone.

The XRD patterns were recorded overnight using Bruker D8, Philips PW-1050 and Siemens D-500 diffractometers in the Bragg-Brentano geometry with CuKα radiation (λ = 1.54178 Å). The X-ray generator worked at a power of 40 kV and 30 mA and the resolution of the instruments (divergent and antiscatter slits of 0.5°) was determined using α-SiO_2 and α-Al_2O_3 standards free from the effect of reduced crystallite size and lattice defects (Enzo et al., 1988).

The goniometer was equipped with a graphite monochromator in the diffracted beam and the patterns were collected with 0.05° of step size which turned out to be adequate for the range of crystallite size in apatite phases here investigated. The powder patterns were collected in the angular range 10°–140° in 2θ, with counting time of 40 s per point. This strategy is suitable also for other phases such as quartz, which has crystallites normally extended in size more than one thousand Å, i.e., above the upper resolution limit of the instrument. Digitized diagrams were analyzed according to the Rietveld method (Rietveld, 1967), using the programme MAUD (Lutterotti et al., 1998). This is an efficient approach that evaluates quantitatively the structure–microstructure parameters and amount of mineralogical phases, taking also into account the instrumental parameters. For inorganic phase mixtures of medium complexity (3–4 phases) the detection limit of the technique is thought to be 1–2 wt.%. One important advantage of the Rietveld method is that no standard is required for quantitative evaluation of phases, thus minimizing the work on sample preparation. Moreover, one merit of the MAUD program is that the numerical evaluation of the whole pattern is accomplished using all recognized phases with a parametric peak shape function convoluting the instrument function with simultaneous broadening due to size and strain effects.

While XRF supplies the element composition of osseous materials, the powder diffraction technique inspects the phase composition. In addition to this, the line broadening analysis of XRD patterns may be applied for a simple evaluation of crystallinity in hydroxylapatite (HA), which is the main biomineral phase of bones. Note that the term crystallinity is instinctively intended as degree of organization of the bone HA phase on an atomic scale.

Rather than referring to the crystallinity of HA, a valid and more correct approach is to evaluate the X-ray peak sharpening of HA bones in terms of the average size of coherently diffracting domains (otherwise referred to as crystallites) and/or average imperfection density, also called lattice disorder or microstrain (Hubert et al., 1996; Michel et al., 1996). These parameters supply a means to define numerically the organization of bones in an atomic scale. In any case, the quantitative evaluation of phases, their lattice parameters and their average coherent diffraction domain size may be obtained by applying the Rietveld method as it was suggested by Michel et al. (1996).

3.2. XRF analysis

XRF measurements have been carried out by using a portable equipment composed of an X-ray tube (molybdenum anode, Oxford Instruments) working at 25 kV and 0.1 mA. We have pressed about 200 mg of powdered bone tissue to form a pellet with diameter of 10 mm and 1 mm thick.

An aluminium collimator 1 cm long and with an internal hole of 1 mm in diameter permits to irradiate an area of about 0.2 cm^2 of the object to be analysed, at a distance tube window-sample of about 2 cm. A Si-PIN detector from AMPTEK was employed with a thickness of about 300 μm and characterized by an energy resolution of about 200 eV at 5.9 keV.

3.3. FT-IR analysis

FT-IR spectra were collected with a Bruker Vertex 70 V spectrometer in terms of absorbance vs. wavenumber ν in the range 400–4500 cm^{-1}.

About 3 mg bone was hand-grinded and mixed with KBr in the weight ratio 1:100 respectively, to make pellets suitable for beam irradiation.

It should be considered that bands of the infrared spectrum of recent and fossil bones are relevant to obtain molecular information concerning the phosphate/carbonate group ratio. Additional bands may also be evaluable due to minerals other than those related to the apatite-like structure.

3.4. Raman analysis

The Raman spectra were collected with by a Bruker Senterra confocal Raman microscope working with a laser excitation wavelength of 785 nm at 100 mW of power and a beam diameter of 1.2 μm. In the confocal mode the 20× objective was selected, an array of 60×78 points was defined to cover a sample area of 90×117 μm with a step of 1.5 μm and each spectrum of the map was obtained by averaging 5 acquisitions of 2 s.

4. Results

In order to describe appropriately the experimental work performed it seems suitable to apply a cross comparison of the techniques employed to evaluate in selected cases how they can help our understanding of processes involved in the fossilization of the dinosaur bones.

4.1. Multi techniques comparison of single phase specimens

Fig. 1, displays the XRD experimental patterns (data points) and the Rietveld fit (full lines) of three fossil specimens compared with a modern bone and with the hydroxylapatite mineral synthesized chemically in the laboratory. The patterns of these specimens, namely *Escapula Ana*, *4ANA75* and *Patiras* are single phase because satisfactorily described using the structure factor of monoclinic apatite, precisely fluorapatite. Following Elliott et al. (1973) we have adopted a monoclinic description of the unit cell (Space Group $P2_1/c$, 4 molecular units) rather than the usual hexagonal cell of S. G. $P6_3/m$ with two molecules of hydroxylapatite because this appears to be more stable from an energetic point of view. As a matter of fact, the lattice parameter of the monoclinic phase a_M ($_M$ refers to monoclinic) coincides with that of the hexagonal phase a_H ($_H$ stands for hexagonal), but b_M is about $2\times a_H$, $c_M = c_H$ and $\beta_M \approx 120°$ (Ikoma et al., 1999).

Thus, the monoclinic unit cell volume V_M is about twice that of V_H.

Fig. 2 shows the XRF spectra of the same specimens reported in Fig. 1.

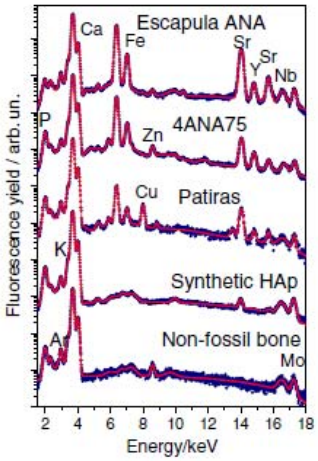

Fig. 2. A comparison of XRF spectra of a modern animal bone (bottom), synthetic apatite, and three dinosaur single-phase (fluorapatite) bones. The synthetic hydroxylapatite shows an element distribution more complex than the non-fossil bone. In addition to calcium, the dinosaur bones show at various levels remarkable presence of iron and strontium as well as other trace elements.

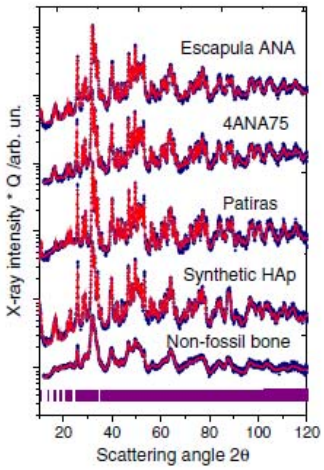

Fig. 1. The XRD patterns (data points) and the Rietveld fit (full lines) for the five specimens. For all specimen just the monoclinic structure factor of natural apatite has been employed. The non-fossil bone at the bottom involves Bragg peaks broader than the four other cases due to the small crystallite size (ca. 170 Å) and high lattice disorder. These effects are partially released in the synthetic hydroxylapatite and fossil specimens on account of growth mechanisms involving larger crystal size and loss of lattice microstrain.

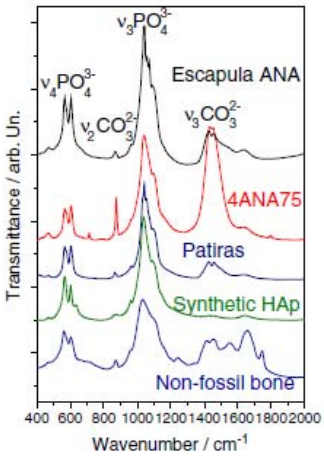

Fig. 3. The FT-IR spectra of the specimens presented in previous figures. Beyond the effects due to the phosphate molecular groups in the range 530–650 cm^{-1} and 900–1200 cm^{-1}, the non-fossil bone shows a complex band envelope in the range 1300–1800 cm^{-1} due to incorporated collagen and water. The latter effects are absent in the synthetic apatite while the fossils show presence of carbonates at various levels in the 1350–1550 cm^{-1} region. The ν_4 band of phosphates at lower frequencies shows both a sharpening and peak intensity ratio change at 570 and 604 cm−1 respectively, from non-fossil to fossil bones.

Table 2
List of the XRD phase analysis of the dinosaur specimens given in Table 1 complemented with average crystallite size, lattice parameters cell volume of monoclinic apatite structure data and major and minor elements detected by XRF.

Sample code	Phase wt.%	Average crystallite size (Å) (±5%)	a/Å (±0.001)	b/Å (±0.002)	c/Å (±0.001)	γ/° (±0.05)	Vc/2/Å^3 (±0.3)	Elements with strong XRF peaks	Elements with medium XRF peaks	Elements with weak XRF peaks
Serrat del Corb	Apatite 55% Calcite 44% Quartz 1%	575	9.342	18.759	6.897	119.90	523.9	Fe,Ca	–	P,Ti,Va,Mn,Pb,Sr,Y
Serrat-R2	Apatite 36% Calcite 59% Quartz 5%	633	9.358	18.711	6.897	120.03	522.8	Ca	Fe,P,Sr	Mn,Ni,Cu,Zn
Molí del Baró	Apatite 48% Calcite 15% Quartz 8% Celestite 25% Kaolinite 4%	740	9.310	18.774	6.902	120.11	521.8	Ca,Fe,Sr	P	S,Ti,Va,Mn,Cu,Zn,As
La Penella	Apatite 96% Calcite 3% Quartz 1%	367	9.337	18.757	6.896	120.00	523.0	Ca,Fe	P,Sr	Ti,Va,Cr,Mn,Zn,As,Nb
Lo Bas	Apatite 68% Calcite 30% Quartz 2%	330	9.345	18.725	6.894	120.05	522.1	Ca,Fe	P,Sr	Ti,Va,Cr,Mn,Cu,Zn,As,Y
La Llau de Bas	Apatite 81% Calcite 12% Goehite 7%	559	9.362	18.705	6.897	119.81	524.0	Ca,Fe	Sr,P	Ti,Mn,Cu,,Pb,Y
Nerets	Apatite 80% Calcite 19% Quartz 1%	581	9.344	18.771	6.900	120.01	524.0	Ca	P,Fe,Sr	Ti,Mn,Y,Rb,Cu,Ni
Pous	Apatite 59% Calcite 37% Quartz 4%	449	9.361	18.674	6.899	119.82	523.2	Ca,Fe	P,Sr	Ti,Va,Cr,Mn,Y,Ni
Basturs Poble	Apatite 55% Calcite 35% Quartz 10%	612	9.333	18.759	6.900	119.99	523.1	Ca,Fe	P,Sr	Ti,Mn,Cu,Pb,Y
Basturs Poble-07	Apatite 76% Calcite 24%	326	9.334	18.703	6.894	120.05	520.9	Ca,Fe	P,Sr	Ti,Va,Cr,Mn,Cu,Zn,Ge,As,Y
Boiga	Apatite 67% Calcite 32% Quartz 1%	326	9.342	18.758	6.897	120.03	523.2	Ca,Fe	P,Sr	Ti,Cr,Mn,Cu,Zn,Y
Peguera 1-Figols	Apatite 74% Calcite 14% Quartz 7% Kaolinite 5%	600	9.344	18.799	6.890	119.99	524.1	Ca,Fe	P,Sr	Ti,Va,Mn,Pb,Y
Psm-Mila	Apatite 82% Calcite 18%	308	9.369	18.769	6.901	120.30	523.8	Ca	P,Fe,Sr	Ti,Mn,Y,Rb,Cu,Ni
Psm-Maite	Apatite 92% Calcite 8% Quartz (traces)	335	9.372	18.798	6.902	120.26	525.1	Ca	P,Fe,Sr	Ti,Mn,Y,Rb,Cu,Ni
Psm-Andres	Apatite 92% Calcite 8%	311	9.368	18.780	6.900	120.24	524.3	Ca	P,Fe,Sr	Ti,Mn,Y,Rb,Cu
Psm-Carles	Apatite 78% Calcite 21% Quartz 1%	361	9.364	18.780	6.904	120.22	524.5	Ca	P,Fe,Sr	Ti,Mn,Y,Rb,Cu,Ni
CerroTadon	Apatite 94% Gypsum 4% Quartz 1% Calcite 1%	333	9.373	18.771	6.898	120.22	524.3	Ca,Fe	P,Mn	Cr,Cu,As,Sr,Y
HTCO4-3	Apatite 61% Gypsum 35% Calcite 4%	306	9.380	18.773	6.900	120.28	524.6	Ca,Fe	P,Mn	Cr,Va,Cu,As,Sr,Y
Rascaña	Apatite 81% Calcite 19%	347	9.371	18.793	6.900	120.23	524.9	Ca,Fe	P,Y,Sr	Va,Cr,Mn,Cu,Pb,Zn
Yac-DaVad	Apatite 88% Dolomite 11% Calcite 1%	300	9.352	18.778	6.902	120.16	523.9	Ca,Fe	P,Sr,Y	Cr,Mn,Pb
Corral de Marín	Apatite 79% Calcite 21%	299	9.355	18.766	6.904	120.11	524.2	Ca	P,Fe,Sr	Ti,Va,Cr,Mn,Cu,Y
229	Apatite 93% Calcite 7%	328	9.370	18.782	6.899	120.19	524.7	Ca,Fe	P,Sr	Ti,Va,Cr,Mn,Y
Losilla	Apatite 40% Calcite 33% Quartz 19% Kaolinite 8%	592	9.347	18.778	6.894	120.15	523.2	Ca,Fe,Cu	P	Ti,Mn,Sr,Y,Pb
Aras de Alpuente	Apatite 58% Calcite 42%	554	9.354	18.711	6.901	119.75	524.3	Ca,Fe	P,Cu,Sr	Mn,Y,Rb,As
La Ventura	Apatite 62% Calcite 29% Quartz 9%	453	9.344	18.766	6.900	120.02	523.8	Ca	P,Fe	Ti,Cr,Mn,Pb,Cu,Sr,Y

(continued on next page)

Table 2 (*continued*)

Sample code	Phase wt.%	Average crystallite size (Å) (±5%)	a/Å (±0.001)	b/Å (±0.002)	c/Å (±0.001)	γ/° (±0.05)	Vc/2/Å^3 (±0.3)	Elements with strong XRF peaks	Elements with medium XRF peaks	Elements with weak XRF peaks
El Collado	Apatite 75% Calcite 25%	522	9.340	18.711	6.905	119.78	523.7	Ca	Fe	Ti,V,Cr,Mn,Cu,Sr,Y,P
El Collado 1	Apatite 92% Calcite 7% Quartz 1%	346	9.364	18.801	6.902	120.18	525.2	Ca,Fe	P,Sr	V,Cr,Mn,Ge,Br,Y
Patiras	Apatite 100%	420	9.3481	18.796	6.897	120.12	524.1	Ca	P,Fe,Sr	Y,Cu,Cr,Mn
SAV-39	Apatite 96% Quartz 4%	399	9.357	18.808	6.896	120.14	524.8	Ca,Fe	P,Y,Sr	V,Cr,Mn,Cu,Pb,Zn
SAV-67	Apatite 85% Quartz 7% Berlinite 1% Kaolinite 7%	457	9.363	18.817	6. 897	120.16	525.3	Ca,Fe	P,Mn,Sr	Ti,Cr,Zn,Pb,Y
Povet	Apatite 67% Kaolinite 25% Quartz 8%	437	9.372	18.735	6.899	120.10	524.0	Ca,Fe	P,Sr,Y	Ti,V,Cr,Mn,Zn,Ge
Camino	Apatite 80% Calcite 20%	2107	9.377	18.748	6.894	120.02	524.7	Ca,Fe	Sr,Mn,P	Y,Ti,As,Zn
EAP 38	Apatite 94% Calcite 1% Goethite 4% Quartz 1%	352	9.344	18.787	6.895	120.06	523.8	Ca,Fe	P,Mn	Ti,Zn,Pb,As,Y
EAP 40-39	Apatite 88% Calcite 12%	382	9.348	18.781	6.895	120.05	523.9	Ca,Fe	Sr,Mn,P	As,Y
EAP 43	Apatite 93% Calcite 3% Quartz 3% Goethite 1%	485	9.345	18.796	6.894	120.00	524.3	Ca,Fe	P,Mn,Sr	V,Cu,Pb,Y
Comptadors A1	Apatite 66% Calcite 24% Quartz 8% Kaolinite 2%	432	9.365	18.822	6.896	120.13	525.7	Fe,Ca	Mn	Ti,P,Sr,Rb
Todolella 1	Apatite 98% Calcite 1% Quartz 1%	436	9.365	18.823	6.894	120.16	525.4	Ca,Fe	P,Mn,Zn,Sr	Ti,Ga
Torre Julian	Apatite 52% Calcite 47% Quartz 1%	411	9.340	18.738	6.901	119.75	524.3	Ca	Fe,P,Sr	Mn,Zn,Ni,Y
A 10	Apatite 68% Quartz 4% Goethite 28%	226	9.355	18.757	6.896	120.25	522.6	Ca,Fe	P,Mn,Sr	S,V,Cr,Zn,Pb,Y
A 13	Apatite 96% Quartz 2% Goethite 2%	255	9.341	18.759	6.895	120.12	522.5	Ca,Fe,Sr	P	Mn,Cu,Zn,As,Br,Y
2ANA12	Apatite 96% Calcite 4%	282	9.349	18.776	6.895	120.11	523.5	Ca,Fe	P,Sr,Mn	Cr,Pb,Y
2ANA61	Apatite 82% Quartz 14% Goethite 4%	310	9.334	18.764	6.902	119.80	524.5	Ca,Fe	P,Sr	Mn,Cu,Zn,As,Br,Y
2ANA77	Apatite 92% Calcite 4% Goethite 3% Quartz 1%	298	9.392	18.735	6.896	120.25	524.1	Ca,Fe	P,Sr	Mn,Cu,Zn,As,Br,Y
3ANA58	Apatite 88% Calcite 5% Goethite 4% Quartz 3%	274	9.357	18.721	6.902	119.92	524.0	Ca,Fe	P,Sr	Mn,Cu,Zn,As,Br,Y
4ANA3	Apatite 68% Quartz 22% Goetite 8%	183	9.340	18.741	6.895	119.85	523.4	Ca,Fe	P,Sr	Mn,Cu,Zn,As,Br,Y
4ANA75	Apatite 100%	312	9.353	18.740	6.893	120.05	522.9	Ca,Fe	P,Sr	V,Cr,Mn,Zn,Y
Escápula-ANA	Apatite 99% Calcite 1%	278	9.376	18.815	6.901	120.30	525.6	Ca,Fe,Sr	P	V,Zn,Y
Mas Roig	Apatite 75% Calcite 3% Kaolinite 22%	347	9.378	18.741	6.904	120.14	524.7	Ca,Fe	P,Sr,Y	Ti,V,Cr,Mn,Zn,Ge
El Maset	Apatite 87% Calcite 13%	312	9.344	18.725	6.898	119.91	523.1	Ca,Fe	P,Sr,Y	Ti,V,Cr,Mn,Cu
Manzanera	Apatite 82% Calcite 18%	391	9.365	18.759	6.898	120.07	524.4	Fe,Ca	Y,Sr	P,Pb,As,Cu,Zn
Mas de Rafael-2	Apatite 91% Calcite 9%	311	9.352	18.739	6.892	119.96	523.2	Ca	P,Mn,Fe,Sr	Ti,Cu,Hf
CL	Apatite 90% Calcite 10%	439	9.366	18.774	6.897	120.22	524.0	Ca,Fe	P,Sr,Y	V,Cr,Mn,Ge,Br
CL 42	Apatite 26%	576	9.362	18.742	6.899	119.94	524.5	Ca,Fe	P	Cr,Mn,Sr,Y

Table 2 (*continued*)

Sample code	Phase wt.%	Average crystallite size (Å) (±5%)	a/Å (±0.001)	b/Å (±0.002)	c/Å (±0.001)	γ/° (±0.05)	Vc/2/Å^3 (±0.3)	Elements with strong XRF peaks	Elements with medium XRF peaks	Elements with weak XRF peaks
	Calcite 72% Quartz 2%									
CL 56	Apatite 89% Calcite 11%	406	9.368	18.732	6.898	120.05	523.9	Ca	Y,P,Fe,Sr	Ti,V,Cr,Mn
La Cuba	Apatite 80% Calcite 19% Quartz 1%	398	9.344	18.750	6.903	119.96	523.9	Ca	P,Fe,Sr	Ti,V,Cr,Mn,Cu,Y
La Fita	Apatite 72% Calcite 28% Quartz 1%	415	9.393	18.763	6.903	120.29	525.3	Ca,Fe	P,Sr	Mn,Pb,Y
La Fita balsa	Apatite 81% Calcite 18% Quartz 1%	399	9.386	18.745	6.897	120.32	523.7	Ca,Fe	P,Sr	Mn,Pb,Cu,Y
Qurolles III	Apatite 84% Dolomite 15%, SiO_2+ $CaCO_3$ (traces)	383	9.366	18.702	6.895	120.20	521.9	Ca,Fe	P,Sr,Y	Cr,Mn,Pb
Qurolles M	Apatite 70% Goethite 24% Calcite 4% Quartz 2%	349	9.330	18.760	6.891	120.08	521.9	Ca,Fe	Y	P,Ti,Cr,Mn,Zn,Pb,Rb,Sr
MC1-5	Apatite 85% Calcite 15% Quartz (traces)	411	9.351	18.772	6.893	120.18	523.0	Ca,Fe	P,Sr	Ti,V,Cr,Mn,Pb,Y

The spectrum of the *Patiras* specimen closely resembles the results reported for a dinosaur bone by PIXE analysis (Goodwin et al., 2007) both in terms of accessed energy range and of relative peak intensities. This similarity suggests that the elemental information from the emissions detected after irradiating the bones with particles rather than electrons is actually very close.

In all spectra of Fig. 2, we easily recognize the Ca doublet and the P peak at lower energies. In addition to these common features there are differences in terms of elemental composition among the modern bone (rhesus monkey), the synthetic hydroxylapatite and the three single-phase fluorapatite fossil bone specimens, on account of the taphonomic and diagenetic processes to which the fossil was subjected.

The multi-technique approach here used may lead to sensible results from the physical point of view using just useful qualitative hints about the composition of elements. In fact, the single-phase character evidenced by the XRD investigation reported in Fig. 1 for the three specimens here considered suggests that Ca atoms found by XRF are divalent cations in the apatite lattice that may be substituted by Sr, Cu and Fe during dissolution-reprecipitation processes like evidenced by Kolodny et al. (1996). Of course also monovalent K cations may be involved in partial replacement of Ca, as well as the other elements that were detected with low concentration like Cr, Mn, Rb and Y.

In Fig. 2 the peaks of *4ANA75* fossil attributed to Fe and Y are stronger than in the *Patiras* specimen. Furthermore, the presence of weak but appreciable emissions due to Zn, As and Pb respectively, have also been inferred from the curve calculated for best-fit.

The case of *Escapula ANA* evidences an even more intense contribution of the Fe and Sr ions that, of course, must replace divalent Ca ions in the structure of fluorapatite at a considerable level since it appeared as a single phase from the diffraction inspection (Fig. 1).

A comparison of FT-IR spectra of these specimens, shown in Fig. 3, supplies further interesting information about the chemistry of the fossils.

The modern bone of the rhesus monkey (bottom spectrum) shows the typical $\nu_4\,PO_4^{3-}$ and $\nu_3\,PO_4^{3-}$ IR vibrations of phosphates belonging to apatite in the range from 530–650 cm^{-1} and 900–1200 cm^{-1} respectively (Lebon et al., 2008, 2010). In addition to the phosphate groups, we can see in the range from 1300 to 1800 cm^{-1} a multitude of bands that may be related to the organic material and water incorporated in the fresh bone (Tadic and Epple, 2004; Stathopoulou et al., 2008).

With respect to the non-fossil bone, the spectrum of synthetic hydroxylapatite (second curve from the bottom of Fig. 3) shows actually an increase of the $\nu_4\,PO_4^{3-}$ splitting factor, which is supplemented by the appearance of a shoulder at 633 cm^{-1}. In addition to this, for synthetic hydroxylapatite no important peak envelope but only weak features indicative of residual carbonate and humidity are observed in the range 1300–1800 cm^{-1} on account of absence of organic matter and water.

Conversely, the spectrum of *Patiras* sample shows the $\nu_4\,PO_4^{3-}$ and $\nu_3\,PO_4^{3-}$ contribution from phosphates groups plus a broad feature inthe range 1350–1550 cm^{-1} that can be attributed to the presence of CO_3^{2-} groups in the fluorapatite structure. In particular, the ratio of the absorbance of the $\nu_3\,CO_3^{2-}$ band at 1415 cm^{-1} to that of the $\nu_4\,PO_4^{3-}$ band at 575 cm^{-1} is reported to be linearly related to the carbonate content of the apatite.

A large amount of carbonate groups may be inferred from the spectrum of specimen *4ANA75* where a very intense $\nu_3\,CO_3^{2-}$ band is observed. The appearance of this band is related to the narrow ν_2 band at 875 cm^{-1} also ascribed to carbonates ($\nu_2\,CO_3^{2-}$). Actually, it is from such comparison that this specimen may be inferred as francolite.

The infrared spectrum of *Escapula ANA* specimen shows a more conventional profile intensity of vibrational activities of the $\nu_2\,CO_3^{2-}$ and $\nu_3\,CO_3^{2-}$ bands, with apparently sharper $\nu_4\,PO_4^{3-}$ and $\nu_3\,PO_4^{3-}$ bands that are difficult to relate to the relatively low average crystallite size extent reported from XRD in Table 2.

It is worth to note that the $\nu_4\,PO_4^{3-}$ cluster of bands in *Patiras*, *4ANA75* and *Escapula ANA* specimens are different with respect to synthetic apatite and modern bone, and this may be related either to fluorination of bones or ionic substitution by Fe and Sr for the Ca sites in the apatite lattice. Fig. 4 is a more detailed view of the $\nu_4\,PO_4^{3-}$ bands of six specimens (modern bone, synthetic hydroxylapatite, *Patiras*, *La Fita*, *La Cuba*, *A10*) in the range 500–700 cm^{-1}.

The experimental data points of the envelope were fitted using symmetric Pearson VII functions and the individual behaviour for each component adjusted at the end of the best fit is reported in correspondence of the maxima and shoulders. One can see that that

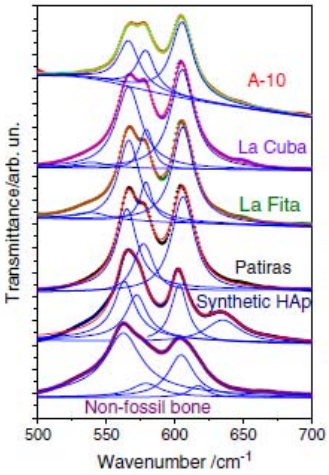

Fig. 4. The ν_4 phosphate band envelope of FT-IR spectra for selected dinosaur bones specimens, in comparison with modern bone and synthetic hydroxyapatite (HA). With respect to the features common to modern bone and synthetic hydroxyapatite, the fit of each band evidence how fossilization involves a band sharpening, a decrease of the two intensity bands around 570 cm^{-1} and the absence of any band at 635 cm^{-1}, probably on account of the OH group disappearance following fluoritization.

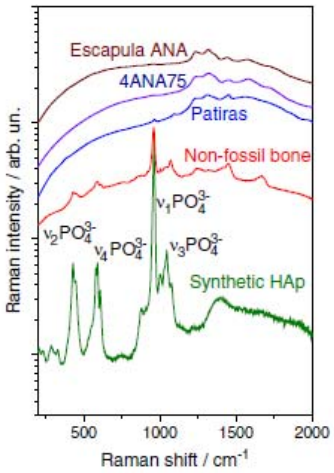

Fig. 5. (See Figs. 1 to 3) The Raman spectra of the specimens studied by XRD, XRF and FT-IR. Synthetic hydroxyapatite shows the best signal-to-background ratio, while the fossils appear completely compromised by a strong fluorescence burying the modes of fluorapatite. Very likely the background of the non-fossil modern bone is due to organic protein and water content.

for non-fossil bone the envelope may be actually described by four partially overlapping bands whose total broadening is related to the crystallinity index throughout the splitting factor SF (Stiner et al., 1995; Surovell and Stiner, 2001; Thompson et al., 2009).

The splitting factor envelope is sharper in the synthetic sample, with emergence of one band shifted at 630 cm^{-1}. However, in the case of fossils we clearly see that the band at 630 cm^{-1} is hidden and that the envelope, though sharp, admit just three bands. Michel et al. (1995) have attributed the phosphate band at 630 cm^{-1} to the P–O–H mode, so we can infer that the fluorination have completely removed the hydroxyl group in our specimens. Conversely, the IR spectra of enamel fossils of Michel et al. (1995) did show four modes of absorption.

In complex substituted apatites it is customary to complement the vibrational activity of the IR spectra with that from Raman (Thomas et al., 2007) since some modes may be both IR and Raman active but others may be only IR or Raman active (Penel et al., 1998). The micro-Raman spectra of the set of specimens previously discussed are reported in Fig. 5 as raw data and turn out to be very different in term of the signal-to-background ratio. It is known that Raman spectroscopy investigations are usually difficult because of fluorescence problems caused from impurities of a contaminated sample or from the matrix surrounding an inclusion. Indeed, the best visibility of the hydroxylapatite bands occur in the synthetic sample, while the modern bone appears to be partially obscured by a background one order of magnitude more intense (Antonakos et al., 2007). Yet, the main bands belonging to biogenic hydroxylapatite are still recognized as well as additional bands that we can attribute to the presence of organic protein and water content, in agreement with the IR observation. These bands are totally lost in a more intense background in the case of the three fossils which have incorporated fluorine, as indicated by the unit cell volume data from XRD. It can be seen that new broad features are emerging in the range 1200–1900 cm^{-1} maintaining a certain degree of similarity. However, they are of difficult assignment in view of the extended ion exchange suffered by the specimens as demonstrated by the XRF spectra of Fig. 2, to the point of making useless any choice of the incident wavelength in order to minimize the background contribution.

4.2. Multi techniques comparison of specific multiphase specimens

Despite the care used in the fossil unearthing procedure, cleaning and sampling the compact part of the bone, the possibility of the incorporation of clay minerals in the internal pore space of buried fossil bones is always very likely, as demonstrated by the results of the *Povet* specimen reported in Fig. 6.

The XRD pattern is described in terms of hydroxylapatite component, accompanied by a large fraction of kaolinite and some quartz. For the sake of completeness we have also reported at the bottom of Fig. 6a the band of residuals, i.e., the difference between experiment and calculation at each data point. Of course both kaolinite and quartz can be ascribed to the most common minerals of embedding sediment and were likely incorporated into the bone pore space.

The fluorescence spectrum in Fig. 6b shows that even this sample contains Fe ions, as well as appreciable quantities of Sr and Y.

In addition to carbonate and phosphate bands of hydroxylapatite, the FT-IR spectrum of *Povet* fossil (see Fig. 6c) shows new bands at low frequencies (470 and 540 cm^{-1}). We note that the principal absorption frequencies of crystalline silica are reported to occur at 1126, 809, and 452 cm^{-1}, respectively. Thus, only the latter band appears to be appreciable since relatively unaffected by nearby peak overlapping. Very likely the shoulder at 540 cm^{-1} can be attributed to frequencies from kaolinite (Balan et al., 2001).

Another interesting case is represented by *Molì del Barò* specimen. Despite the complexity of the data, the pattern was resolved by the Rietveld method in a satisfactory fashion as it can be seen from the best fit of Fig. 7a, which this time reports the bar sequence of peaks for each contributing phase rather than the structure factor optimized after the fit.

Beyond the "apatitic" phase, which is ca. 48 wt.% of the specimen, we have evaluated numerically the presence of celestite phase at a 25 wt.% level, together with calcite, quartz and ca. 4 wt.% of kaolinite.

The presence of calcite, quartz and kaolinite is ascribable to the limestone and clay minerals typical for the sediment of the Tremp basin, while the abundant presence of celestite is unusual compared to other dinosaur bones.

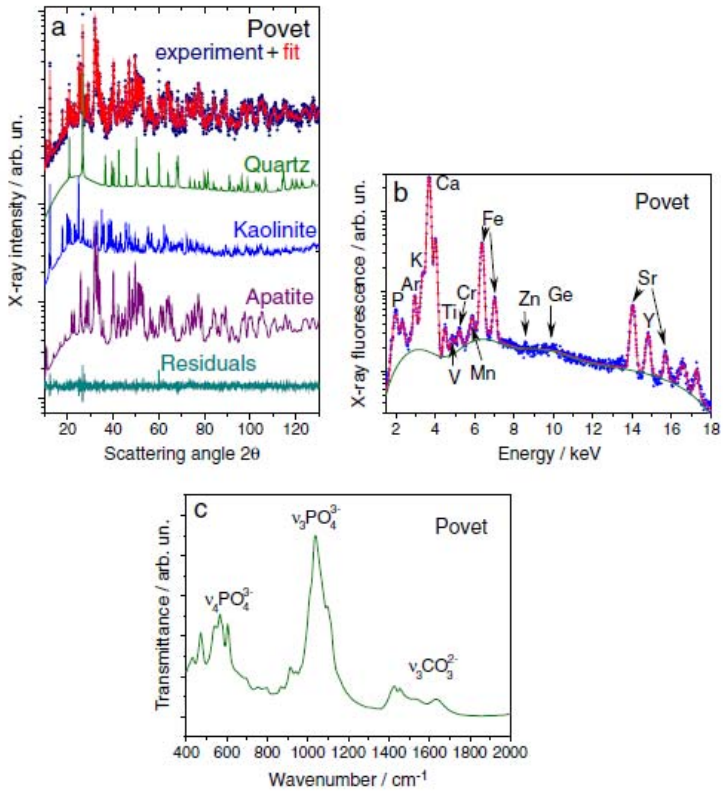

Fig. 6. The XRD, XRF and FT-IR results of the *Povet* specimen. (a) The bone is not anymore single phase apatite as the XRD pattern displays evaluable contributions from kaolinite and quartz infiltrated from the nearby sediment. (b) In addition to calcium and phosphorus from apatite, the correspondent XRF spectrum highlights the presence of iron, strontium and yttrium plus the weak contribution of first series transition elements. (c) With respect to single-phase apatite, the FT-IR spectrum is only slightly affected by the Si–O modes of quartz and kaolinite mainly at frequencies lower than 600 cm^{-1}.

As expected after XRD evaluation, the XRF spectrum of *Molí del Baró* (see Fig. 7b) shows a strong contribution from the Sr Kα and Kβ lines, and a weak signal of sulphur. Both elements are to be related to celestite ($SrSO_4$). The strong contributions due to Fe atoms are not mirrored in the XRD pattern by any oxide–hydroxides Fe-based phases such as goethite and hematite.

In the XRF spectrum of Fig. 7b, we can appreciate and possibly quantify the presence of transitional elements such as Ti, V, Cr, Mn, Cu, Zn, As. These elements are likely hosted in the lattices of the apatite-like and kaolinite-like phases detected by XRD.

Despite the complexity of phase and elemental constitution assessed by XRD and XRF, the FT-IR spectrum of the *Molí del Baró* specimen looks rather "simple" again highlighting phosphate and carbonate bands typical of francolite.

Of course, when using FT-IR investigations, the carbonate band can be also ascribed to calcite because the technique is molecular rather than structure sensitive to the point that there is no sensible numerical way to separate these chemically distinct contributions from the envelope.

On the other hand the principal ranges of observed frequencies for sulphates occur at 1030–1180 cm^{-1} (strong bands) and at 580–670 cm^{-1} (weaker bands) respectively (see Fig. 7c).

It may be deduced that the FT-IR technique is not able to resolve properly also the bands of sulphate groups from those of phosphates.

As it is documented in the XRD pattern of Fig. 8a, gypsum was found in high quantity together with some calcite in the *HTCO4-3* specimen, which was extracted from a basin at least partially affected by shallow-marine environment. The XRF spectrum of this specimen (see Fig. 8b) shows, as customary for this bone fossil collection, the appreciable presence of Fe, accompanied by Mn, Sr, Y and to a lesser extent by V, Cr, Cu, Ge and Rb cations.

Of course the divalent cation of these elements can substitute for Ca in the lattice structures inferred from the Rietveld refinement of XRD patterns.

A further consideration deserves the FT-IR spectrum reported in Fig. 8c. As noted before, the symmetry of sulphate groups makes their vibrational bands to occur close to those of the phosphate, creating overlapping to the ν_4 PO_4^{3-} band at lower frequencies as indicated in the figure.

The combined XRF, XRD and FT-IR inspection of the *Qurolles M* specimen supplies new appealing aspects. The XRD pattern refinement reported in Fig. 9a shows that also in this case the bone specimen is not single-phase. The fluorapatite-like phase (francolite) is the most abundant, but is accompanied by ca. 24 wt.% of goethite and small quantities of calcite and quartz.

The XRF spectrum in Fig. 9b displays a strong contribution from Fe which appears even more intense than Ca. The presence of a high level of Fe inferred from XRF is in good agreement with the considerable fraction of goethite detected by XRD.

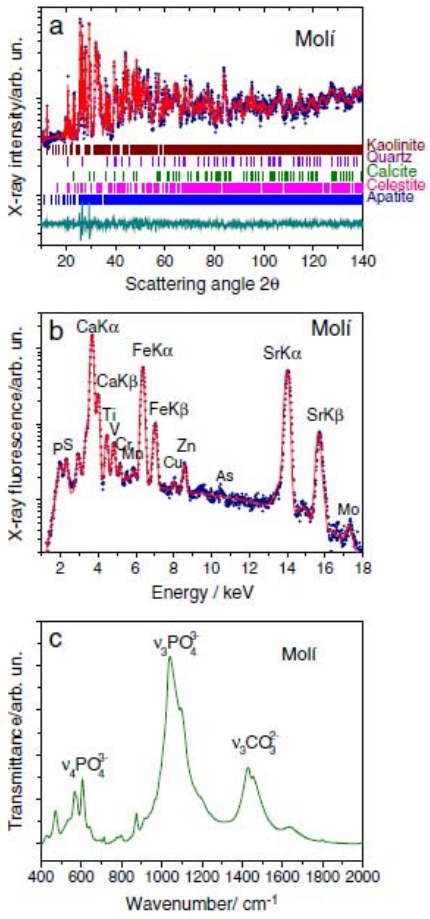

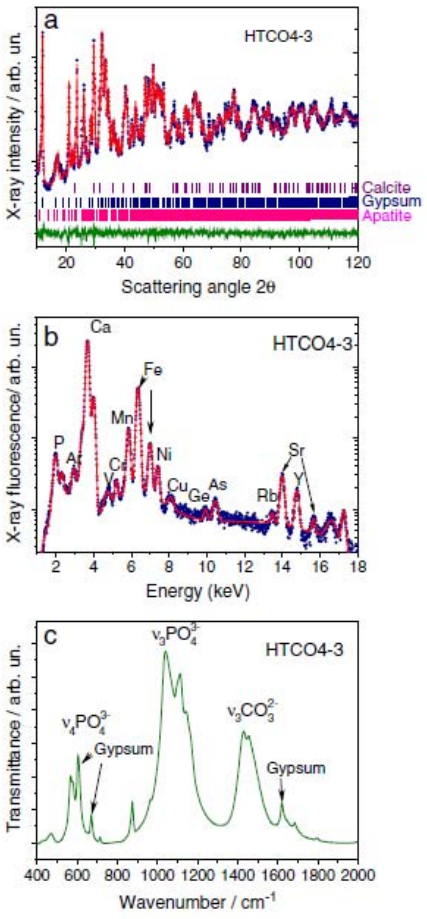

Fig. 7. Multi-technique analysis carried out on a complex dinosaur bone specimen containing several mineral phases. (a) The XRD pattern of *Molí del Barò* was resolved with the contribution of five phases, among those the celestite appears exotic. The corresponding XRF spectrum (b) Shows notable presence of strontium in addition to the usual element distribution expected for bone fossils. (c) The FT-IR spectrum.

Fig. 8. (a) The XRD pattern of *HTCO4-3* specimen showing in addition to francolite a considerable amount of gypsum and some calcite. (b) The XRF pattern shows the presence of iron species together with manganese, strontium and yttrium plus other elements in lower quantity. (c) The FT-IR absorption bands of gypsum are easily recognizable as indicated by arrows and may affect the ν_4 phosphate band.

The FT-IR contribution in the frequency range reported in Fig. 9c is limited to point out the occurrence of relatively weak carbonate bands on account of the 4 wt.% amount of calcite assessed by XRD, while the signals of goethite are not appreciable here.

An important issue concerns the variability of phase and chemical composition of bone specimens from the same geological setting. This comparison is reported in Fig. 10a, which shows the XRD pattern of specimens *Camino* and *EAP 40-39*.

The upper pattern referred to the *Camino* specimen shows line profiles from the fluorapatite sharper than in the *EAP 40-39* specimen at the bottom, reflecting a markedly different average crystallite size. This comparison may be better evaluated across a narrower angular 2θ range (30°–60°) as reported in the plot of Fig. 10b.

The XRF graphs (see Fig. 10c) show a similar elemental distribution, with notable presence of Fe and Sr. The corresponding FT-IR spectra (Fig. 10d) show the presence of carbonate bands in the range 1350–1550 cm^{-1} at different level of concentration that can be correlated with the calcite content from XRD quantitative phase analysis.

Finally, we like to show the micro-Raman spectra obtained by closing the confocal hole and defining a smaller collection volume in order to spatially locate and appropriately distinguish the secondary mineral infilling in fossil bones. In particular, we have surface mapped a portion of the *Torre Julian* sample. The peak of the Raman spectrum in the range 1072–1101 cm^{-1} reported in Fig. 11 (a) was integrated from the visible image of the selected sample area in Fig. 11 (b) thus allowing to define the Raman microscopic image shown in Fig. 11 (c). Indeed, the integration peak originates from carbonate modes belonging to calcite, as it was also confirmed by the Rietveld analysis carried out in the *Torre Julian* specimen.

Raman imaging of the selected area suggests that the calcite phase precipitates just as a surface crust around the haversian canals of the bone.

5. Discussion

5.1. Quantitative evaluation of phases

Table 2 collects the main phases of dinosaur bones found by the XRD investigation with their quantitative estimate according to the Rietveld method, the cell volume of the supposed "apatitic" phase, its

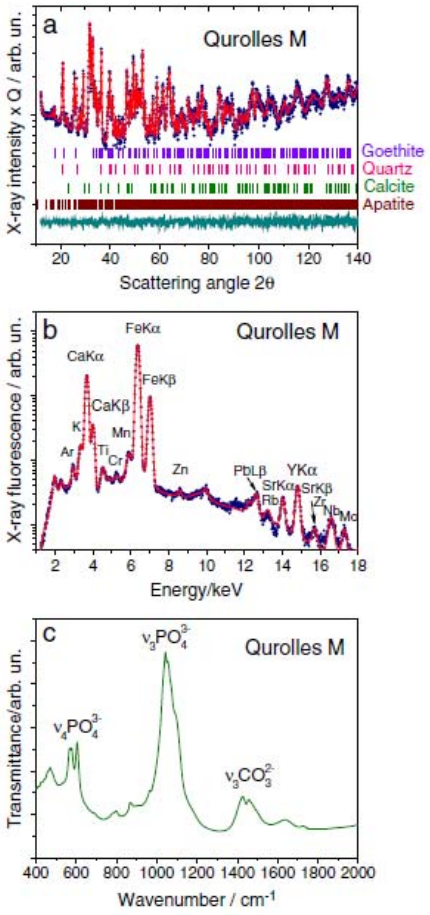

Fig. 9. (a) The XRD pattern of the *Qurolles M* specimen with the contribution of the goethite phase. (b) The XRF spectrum shows a contribution from the iron lines stronger than those of calcium due to the high content of goethite (24%). (c) The FT-IR spectrum displays the higher intensities of molecular carbonate groups of francolite while the contributions of other molecules is difficult to extract.

average crystallite size as well as major and minor elements detected by XRF.

Concerning the phases constituting the fossil bones, a high variability can be pointed out among the various samples. The most frequent phases in the samples studied are mostly fluorapatite, quartz and calcite. The *Molì del Barò* specimen represents the maximum complexity in terms of five minerals detected simultaneously by XRD.

The apatite phase content in the various specimens varies because of the number and amount of the other secondary mineral phases present, ranging from a minimum of 26 wt.% for the sample *CL 42* , up to 100 wt.% in the case of the samples *Escapula Ana*, *4ANA75* and *Patiras*.

These specimens were found in the same sedimentary basin and geological formation made up by clay sediments so it may be suggested that clay minerals constitute an alkaline environment equally suitable as limestone for the best conservation of bone as a single apatite phase, apart from the quick degradation of the organic phase and the well-established fluorine exchange reaction.

However, the presence of clays does not preserve the single-phase property of all fossils necessarily, as it follows from the mineralogical phase constitution for the other specimens of the same basin.

Quartz normally derives from the embedding sediment and rarely is an authigenic mineral. Conversely, the presence of calcite as an authigenic mineral is common in many fossil sites (Hubert et al., 1996; Astibia et al., 2005) and may infill in bone voids or deposit at the surface as a thin and white crust. Our evidence at a micro-scale level from confocal Raman shows that calcite occupies the haversian canals.

In the further specimens here investigated we have also determined several other phases such as kaolinite (25 wt.% $[Al_2Si_2O_5(OH)_4]$, *Povet* specimen), goethite (24 wt.% FeOOH, *Qurolles M* specimen), celestite (25 wt.% $SrSO_4$, *Molì del Barò* specimen), gypsum (35 wt.% $[CaSO_4{\cdot}2(H_2O)]$, *HT-CO4-3* specimen), dolomite (15 wt.%. $[CaMg(CO_3)_2]$, *Qurolles III* specimen) and berlinite (1 wt.% $AlPO_4$*Sav 67* specimen).

It is clear that also the presence of these phases may be ascribed to the mineralogic features of the sediment. Particularly, the *Molì del Baro* site is different from the other sites in terms of deposition environment. The sediment consists of fossiliferous black mudstones, rich in plant remains (including leaves and remains of charred wood) and thin layers of micro-conglomerates. It represents a deposition in an abandoned meander. The presence of the plants, the dark-gray or black color indicates conditions of lack of oxygen in bottom waters, typical of stagnant water bodies. The dinosaur remains, especially hadrosaur bones, are not frequent but they are very well preserved (Gaete and Galobart, 2002).

The molar volume $V_M/2$ of each monoclinic cell of the apatite-like phase is varying from a lower value of 520.9 $Å^3$ (*BP 07* sample) to an upper value of 525.7 $Å^3$ (*Comptadors-A1* specimen). This is consistent with the literature data referred to fluorapatite that supply several unit cell volume values ranging from 522.18 $Å^3$ to 528.41 $Å^3$, respectively (McConnell, 1973; Hughes et al., 1989).

Even the literature values of francolite range from a minimum of 518.73 $Å^3$ to a maximum of 523.81 $Å^3$ (Sudarsanan et al., 1972; Sudarsanan and Young, 1978; Perdikatsis, 1991) and scatter around the values reported for fluorapatite. We have recently estimated that fluorination of bone apatite is taking place in about 4–5 Ma after examining the unit cell volume change of biogenic apatite vs. geological age. (Piga et al., 2009).

5.2. Crystallite size vs. age

The average crystallite size values obtained from the peak sharpening of the apatite-like phase (Chipera and Bish, 1991; Bartsiokas and Middleton, 1992; Person et al., 1995) in the XRD diagrams (see Table 2) were obtained after correction for the instrument function and after separation of the broadening function due to lattice strain. The patterns of the three single-phase fossil bones given in Fig. 1 look similar to the commercial hydroxylapatite synthesized in the laboratory as they appear to have an increased average of the crystallite size (from 280 to 420 Å– see data of Table 2) larger than the average value of ca. 170 ± 10 Å normally found in non-fossil human and animal bones (curve of the rhesus monkey at the bottom of Fig. 1) (Piga et al., 2008). These values are found coherent with the observed change in the Splitting Factor of the ν_4 PO_4^{3-} band of the correspondent FT-IR spectra even though the fluorination of apatite modifies the shape of this band envelope to a certain extent.

However, we have previously observed (Piga et al., 2009) that the recrystallization process brought about by fossilization does not occur homogeneously across the geological times. For example, for the *Camino* and *EAP 40-39* specimens, we have pointed out an evident difference in the peak broadening of the two patterns, on account of average crystallite size of 2107 Å (±100 Å) and 382 Å (±20 Å), respectively. Also, out of the three fossils consisting of single phase apatite examined in Fig. 1, the larger average crystallite size (ca. 410 ± 20 Å) is observed for the sample with the most recent stratigraphic age.

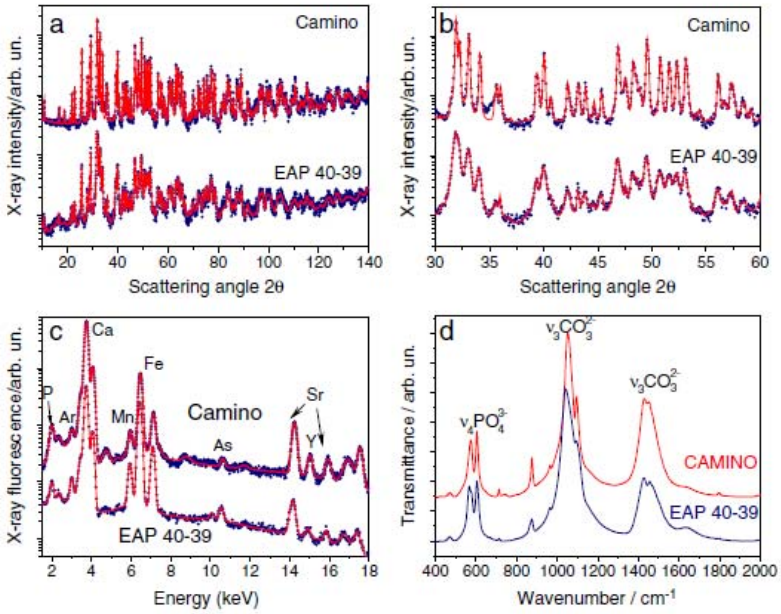

Fig. 10. (a) The XRD patterns of two bones from different dinosaurs sampled from the same geological unit ("*Morella*" Formation). The upper pattern of the *Camino* specimen shows line profiles from the fluorapatite sharper than in the *EAP 40-39* specimen at the bottom, reflecting markedly different average crystallite size of 2107 Å and 382 Å, respectively (Table 2). (b) This comparison may be better evaluated across a narrower angular range as reported in the right hand side plot. (c) The XRF patterns show a similar elemental distribution, with notable presence of iron and strontium in both specimens; (d) The corresponding FT-IR spectra show the presence of carbonate bands in the range 1350–1550 cm^{-1} at different level of concentration that can be correlated with the calcite content from XRD quantitative phase analysis.

In Fig. 12 we report the average crystallite size for apatite of our samples as a function of age in the range 150–65 Ma, ordered according to their geological age, showing the absence of correlation between average crystallite size and age.

The unpredictable change of the average crystallite size values and SFs suggest that correlation between crystallisation indices and bone age has to be regarded with obvious caution, as it was suggested by Person et al. (1995, 1996) and Farlow and Argast (2006).

In our previous study (Piga et al., 2009), we have, however, observed a positive correlation between average bone apatite crystal size and specimen age in another set of fossils ranging in age from the Middle Triassic (around 245 Ma) to present. From the present data it seems that the crystallization induced by just the time is overlapped by other factors depending on the geological Formation that may inhibit (e.g., *4ANA3* sample) or enhance the process.

The *Camino* specimen stands out of any general trend as an outlier since we do not observe an apatite crystallize size that exceeds 740 Å (*Mofi del Barò* specimen) for all other dinosaur bone specimens. Beyond diagenesis the large crystallite size of ca. 2000 Å might be the result of fire exposure to which this dinosaur bone was possibly subjected. In fact, similar high values for the average apatite crystallite size have been reported only for human bones incinerated in a temperature range of 900–1000 °C (Piga et al., 2008, 2010).

5.3. Element distribution and solid solutions

It should be pointed out that, apart from the Ca ions, XRF invariably shows the presence of Fe ions in the fossils, even if this is not always mirrored in the corresponding XRD diagrams by evident Fe-based phases.

For example, the *Escapula ANA* spectrum reported in Fig. 2 (top pattern) shows a large amount of Fe but appears to be single-phase francolite in the corresponding diagram of Fig. 1. This suggests that the mere element distribution from XRF fluorescence analysis alone may not be helpful for a precise account of the fossil diagenesis involved even applying microscale investigations. After this comparison, the strong presence of Fe may be ascribed to a substitution of this element for Ca in the francolite structure. In analogy, for the *Povet* specimen (see Fig. 7), the presence of Fe assessed by XRF and the absence of any Fe-based phase indicated by the XRD investigation can be compatible with substitution either for Ca by Fe ions in the apatite lattice or for Al in the kaolinite phase.

Of course the correlation between Fe found by XRF and goethite phase is immediate in cases like that shown in Fig. 9. Goethite is the only Fe-based phase observed by XRD in our collection of samples (precisely in 8 specimens) and was also reported previously in other dinosaur bones, though not evaluated quantitatively (Elorza et al., 1999). Its presence was attributed to a hydromorphic process because of seasonal variations of the ground water level. It is also possible that the specimens showing high amount of Fe in the XRF spectra but no Fe-based phase in the correspondent XRD pattern may actually contain limonite, i.e., amorphous FeOOH, that cannot be detected by diffraction unless an approximate presence larger than 25 wt.%.

Presence of goethite and calcite together occurs just for *2ANA77*, *3ANA58* and *La Llau de Bas* specimens and is thought to be possible only under oxidising conditions, whereas the precipitation of pyrite and calcite under reducing conditions and the later oxidation of pyrite to hematite is more common (Pfretzschner, 2001; Wings, 2004). In several studies, the presence of hematite and other Fe-oxides in the samples were interpreted as the result of weathering of pyrite (e.g. Wings, 2004). Two further ways of Fe-oxide formation in fossil bones are suggested by Pfretzschner (2001). The first mechanism is likely restricted to early diagenesis and occurs after the oxidation from ferrous to ferric Fe, preserving the histologic structures without replacement of adjacent bone by the Fe oxides. The second possibility occurs via precipitation due to OH change. This is restricted to later

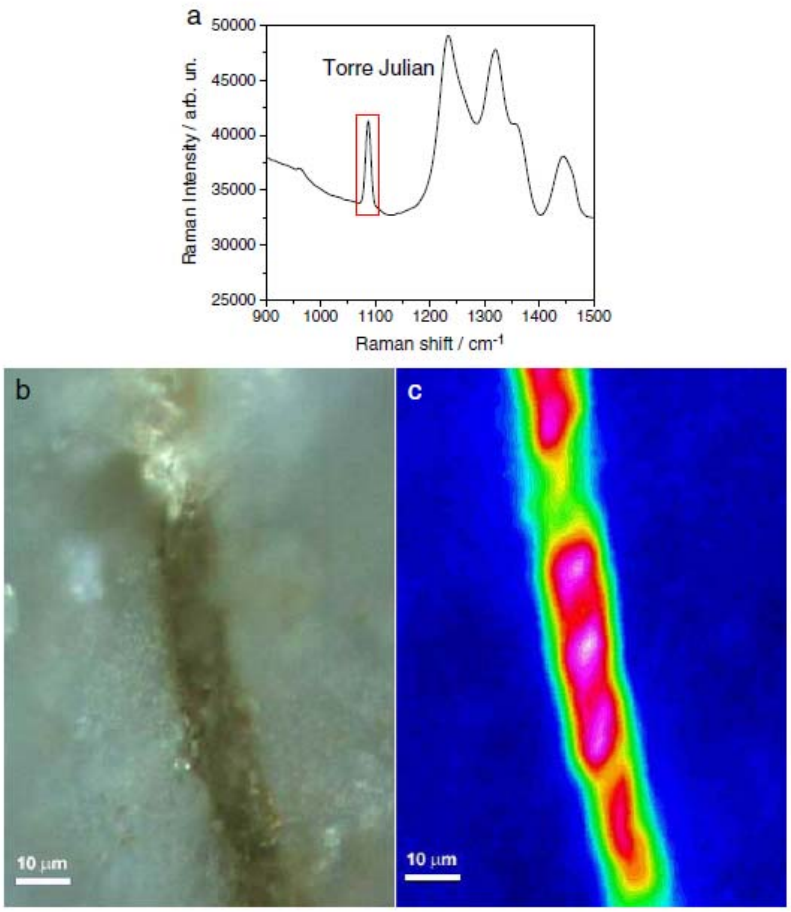

Fig. 11. The Raman confocal investigation for the calcite presumed on the basis of CO_3^{2-} modes of the spectrum in the range 1072–1100 cm^{-1} as in (a). It was carried out considering the area encompassing an haversian canal (b). The Raman image (c) tells us that the supposed calcite forms an inner surface crust around the haversian canal. The violet-white areas of the Raman image, corresponding to the maximum value of the peak integral, indicate the presence of the maximum amount of calcite. Conversely, the blue colour corresponding to the zero value, indicates the total absence of calcite, while all other colours correspond to intermediate amounts of calcite.

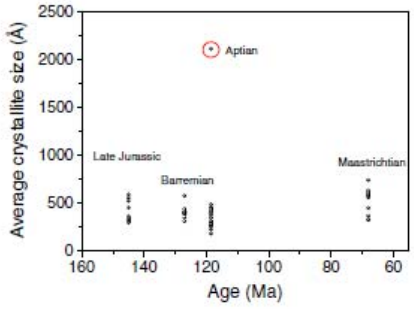

Fig. 12. Plot of average crystallite size for apatite of our dinosaur samples as a function of age in the range 150–65 Ma, ordered according to their geologic age. For the analyzed dinosaur bones the recrystallization of the apatite during fossilization seems not to occur progressively with time. However, the local taphonomic conditions or geological environment can have a significant influence on crystallite size as evidenced by the *Camino* specimen (circled in red). See text for detailed explanation.

diagenesis and a considerable replacement of bone matrix by Fe-oxides and/or hydroxy-oxides is expected as in the case of pyrite oxidation.

6. Conclusions

The precise understanding of diagenetic and taphonomic processes to which dinosaur bones were subjected requires a multidisciplinary approach, taking into account the potentialities and limitations of each analytical technique employed. Particularly, we have used XRD, XRF and FT-IR methods in combination supplemented by confocal microscopic Raman images to investigate a collection of Spanish dinosaur bone specimens being 150 to 65 Ma to characterize the fossilization in terms of chemical and mineralogical composition, crystallite size, precipitation and infiltration, exchange reactions involving atomic and molecular ion species.

From the crystal lattice parameters of the apatite phase determined by powder XRD, it emerged that these fossil bones invariably underwent a *post-mortem* transformation from bioapatite (hydroxylapatite) to authigenic francolite (fluorapatite) structure. The XRF spectra collected

in the energy range from 1.5 to 18 keV supplied analysis profile spectra with the expected presence of Ca and P as major elements. In addition, the presence of carbonate groups substituting for the phosphate group in the hydroxylapatite-like structure was definitely assessed for the single-phase specimens by FT-IR spectroscopy. For a large number of specimens the presence of secondary quartz and calcite phases were frequently observed while dolomite was found in just one specimen. The average crystallite size of the apatite-like phase ranges from 183 Å to 2107 Å and varies unpredictably in the analysed specimens, inhibiting a correlation with fossil age. In all the fossils examined, varying levels of Fe were detected by XRF that may be present in the goethite phase FeOOH. However, no presence of other Fe-bearing phases such as pyrite, hematite or magnetite was observed. For the specimens that displayed considerable amount of Fe but absence of any Fe-bearing phase in the XRD spectra, the analysis suggested that Fe divalent cations may have substituted for divalent Ca cations in the francolite structure even at a considerable concentration level (up to 12%) and without significant changes in the unit cell volume. Frequently the major elements Ca and P were also accompanied by varying amounts of transitional elements such as Ti, V, Mn, Cu, As, Rb, Y, Sr and Nb, to list the most frequently encountered. In particular, the level of Sr was occasionally found in relatively elevated concentrations. Likewise Fe ions, in the absence of specific Sr-based phase it is possible that a considerable amount of Sr substitutes for Ca ions in the structure of francolite. However, in selected cases we have documented remarkable presence of the Sr sulphate (celestite) phase.

Acknowledgements

The authors are particularly grateful to Dr. Thomas Tütken and three anonymous reviewers, for their valuable revision work and for giving us the possibility to present our results in the special issue about bone diagenesis.

The authors also thank: Prof Carlos de Santisteban (Universidad de Valencia), Prof. Salvador Moya Solà (Universitat Autonoma de Barcelona; Institut Català de Paleontologia), Angel Galobart, Jordi Galindo Torres, Laura Celià Gelabert (Institut Català de Paleontologia) and Tim Thompson (University of Teesside) for supplying the osseous materials employed in this study.

This study is partially supported by *PR1-MAB-A2008-443* project from Autonomous Region of Sardinia and CGL2008-06533-C03-03/BTE (Spanish M. of Science and Innovation).

References

Antonakos, A., Liarokapisa, E., Leventouri, T., 2007. Micro-Raman and FTIR studies of synthetic and natural apatites. Biomaterials 28, 3043–3054.

Astibia, H., Payros, A., Suberbiola, X., Berreteaga, A., Elorza, J., Extebarria, N., Tosquella, J., 2005. Sedimentology and taphonomy of sirenian remains from the Middle Eocene of the Pamplona Basin (Navarre, western Pyrenees). Facies 50, 463–475.

Balan, E., Saitta, A.M., Mauri, F., Calas, G., 2001. First-principles modeling of the infrared spectrum of kaolinite. American Mineralogist 86, 1321–1330.

Bartsiokas, A., Middleton, A.P., 1992. Characterisation and dating of recent and fossil bone by X-ray diffraction. Journal of Archaeological Science 19, 63–72.

Bocherens, H., 1997. Chemical composition of dinosaur fossils. In: Padian, K., Currie, P.J. (Eds.), The Dinosaur Encyclopedia. University of California Press, Berkeley, CA, pp. 111–117.

Bradley, D.A., Muthuvelu, P., Ellis, R.E., Green, E.M., Attenburrow, D., Barrett, R., Arkill, K., Colridge, D.B., Winlove, C.P., 2007. Characterisation of mineralisation of bone and cartilage: X-ray diffraction and Ca and Sr Ka X-ray fluorescence microscopy. Nuclear Instruments and Methods in Physics Research B 263, 1–6.

Caja, M.A., Salas, R., Marfil, R., Lago, M., 2005. Heavy mineral composition and geochemistry of the Weald facies from the Maestrat Basin (Spain): Provenance implications for Late Jurassic-Early Cretaceous rifting stage. Geogaceta 38, 11–14.

Chipera, S.J., Bish, D.L., 1991. Applications of X-ray diffraction crystallite size/strain analysis to *Seismosaurus* dinosaur bone. Advances in X-Ray Analysis 34, 473–482.

Denys, C., 2002. Taphonomy and experimentation. Archaeometry 4, 469–484.

Dumont, M., Pyzalla, A., Kostka, A., Borbély, A., 2011. Characterization of sauropod bone structure. In: Klein, N., Remes, K., Gee, C.T., Sander, P.M. (Eds.), Biology of the Sauropod dinosaurs: understanding the life of giants. : Life of the Past. Indiana University Press, Bloomington, pp. 150–170.

Elliott, J.C., Mackie, P.E., Young, R.A., 1973. Monoclinic hydroxyapatite. Science 180, 1055–1057.

Elorza, J., Astibia, H., Murelaga, X., Pereda-Suberbiola, X., 1999. Francolite as a diagenetic mineral in dinosaur and other Upper Cretaceous reptile bones (Laño, Iberian Peninsula): microstructural, petrological and geochemical features. Cretaceous Research 20, 169–187.

Enzo, S., Fagherazzi, G., Benedetti, A., Polizzi, S., 1988. A profile-fitting procedure for analysis of broadened X-ray diffraction peaks. I Methodology. Journal of Applied Crystallography 21, 536–542.

Farlow, J.O., Argast, A., 2006. Preservation of fossil bone from the Pipe Creek Sinkhole (Late Neogene, Grant County, Indiana U.S.A.). Journal of the Paleontological Society of Korea 22, 51–75.

Fricke, H.C., Rogers, R.R., Backlund, R., Dwyer, C.N., Echt, S., 2008. Preservation of primary stable isotope signals in dinosaur remains, and environmental gradients of the Late Cretaceous of Montana and Alberta. Palaeogeography, Palaeoclimatology, Palaeoecology 266, 13–27.

Gaete, R., Galobart, A., 2002. Excavació Paleontològica al jaciment cretaci superior de Molí de Baró. Servei d'Arqueologia i Paleontologia. Biblioteca del Patrimoni Cultural, Barcelona, pp. 1–49.

Goodwin, M.B., Grant, P.G., Bench, G., Holroyd, P.A., 2007. Elemental composition and diagenetic alteration of dinosaur bone: distinguishing micron-scale spatial and compositional heterogeneity using PIXE. Palaeogeography, Palaeoclimatology, Palaeoecology 253, 458–476.

Hedges, R.E.M., 2002. Bone diagenesis: an overview of processes. Archaeometry 44, 319–328.

Heuser, A., Tütken, T., Gussone, N., Galer, S.J.G., 2011. Calcium isotopes of fossil bones and teeth diagenetic versus biogenic origin. Geochimica et Cosmochimica Acta. doi:10.1016/j.gca.2011.03.032.

Hubert, J.F., Panish, P.T., Chure, D.J., Prostak, K.S., 1996. Chemistry, microstructure, petrology, and diagenetic model of Jurassic dinosaur bones, Dinosaur National Monument, Utah. Journal of Sedimentary Research 66, 531–547.

Hughes, J.M., Cameron, M., Crowley, K.D., 1989. Structural variations in natural F, OH, and Cl apatites. American Mineralogist 74, 870–876.

Ikoma, T., Yamazakai, A., Nakamura, S., Akao, M., 1999. Preparation and structure refinement of monoclinic hydroxyapatite. Journal of Solid State Chemistry 144, 272–276.

Jans, M.M.E., Nielsen-Marsh, C.M., Smith, C.I., Collins, M.J., Kars, H., 2004. Characterisation of microbial attack on archaeological bone. Journal of Archaeological Science 31, 87–95.

Kolodny, Y., Luz, B., Sander, M., Clemens, W.A., 1996. Dinosaur bones: fossils or pseudomorphs? The pitfalls of physiology reconstruction from apatitic fossils. Palaeogeography, Palaeoclimatology, Palaeoecology 126, 161–171.

Lebon, M., Reiche, I., Fröhlich, F., Bahain, J.-J., Falguères, C., 2008. Characterization of archaeological burnt bones: contribution of a new analytical protocol based on derivative FTIR spectroscopy and curve fitting of the $\nu_1\nu_3$ PO_4 domain. Analytical Bioanalytical Chemistry 392, 1479–1488.

Lebon, M., Reiche, I., Bahain, J.-J., Chadefaux, C., Moigne, A.M., Fröhlich, F., Sémah, F., Schwarcz, H.P., Falguères, C., 2010. New parameters for the characterization of diagenetic alterations and heat-induced changes of fossil bone mineral using Fourier transform infrared spectrometry. Journal of Archaeological Science 37, 2265–2276.

Lutterotti, L., Ceccato, R., Dal Maschio, R., Pagani, E., 1998. Quantitative analysis of silicate glass in ceramic materials by the Rietveld Method. Materials Science Forum 2, 87–92.

McConnell, D., 1973. Apatite; its crystal chemistry, mineralogy, utilization, and geologic and biologic occurrences. Springer-Verlag, New York.

Michel, V., Ildefonse, Ph., Morin, G., 1995. Chemical and structural changes in *Cervus elaphus* tooth enamel during fossilization (Lazaret cave): a combined IR and XRD Rietveld analysis. Applied Geochemistry 10, 145–159.

Michel, V., Ildefonse, Ph., Morin, G., 1996. Assessment of archaeological bone and dentine preservation from Lazaret Cave (Middle Pleistocene). Palaeogeography, Palaeoclimatology, Palaeoecology 126, 109–119.

Penel, G., Leroy, G., Rey, C., Bres, E., 1998. MicroRaman spectral study of the PO_4 and CO_3 vibrational modes in synthetic and biological apatites. Calcified Tissue International 63, 475–481.

Perdikatsis, B., 1991. X-ray powder diffraction of francolite by the Rietveld method. Materials Science Forum 79–82, 809–814.

Person, A., Bocherens, H., Saliege, J.F., Paris, F., Zeitoun, V., Gerard, M., 1995. Early diagenetic evolution of bone phosphate: an X-ray diffractometry analysis. Journal of Archaeological Science 22, 211–221.

Person, A., Bocherens, H., Mariotti, A., Renard, M., 1996. Diagenetic evolution and experimental heating of bone phosphate. Palaeogeography, Palaeoclimatology, Palaeoecology 126, 135–149.

Pfretzschner, H.-U., 2001. Iron oxides in fossil bone. Neues Jahrbuch für Geologie und Paläontologie Abhandlungen 220, 417–429.

Pfretzschner, H.-U., 2004. Fossilization of Haversian bone in aquatic environments. Comptes Rendus Palevol 3, 605–616.

Pfretzschner, H.-U., Tütken, T., 2011. Rolling bones – taphonomy of Jurassic dinosaur bones inferred from diagenetic microcracks and mineral infillings. Palaeogeography, Palaeoclimatology, Palaeoecology. doi:10.1016/j.palaeo.2011.01.026.

Piga, G., Malgosa, A., Thompson, T.J.U., Enzo, S., 2008. A new calibration of the XRD technique for the study of archaeological burnt remains. Journal of Archaeological Science 35, 2171–2178.

Piga, G., Santos-Cubedo, A., Moya Solà, S., Brunetti, A., Malgosa, A., Enzo, S., 2009. An X-Ray Diffraction (XRD) and X-Ray Fluorescence (XRF) investigation in human and animal fossil bones from Holocene to Middle Triassic. Journal of Archaeological Science 36, 1857–1868.

Piga, G., Hernández-Gasch, J.H., Malgosa, A., Ganadu, M.L., Enzo, S., 2010. Cremation practices coexisting at the *S'Illot des Porros* Necropolis during the Second Iron Age in the Balearic Islands (Spain). Homo 61, 440–452.
Pucéat, E., Reynard, B., Lécuyer, C., 2004. Can crystallinity be used to determine the degree of chemical alteration of biogenic apatites? Chemical Geology 205, 83–89.
Riera, V., Oms, O., Gaete, R., Galobart, A., 2009. The end-Cretaceous dinosaur succession in Europe: The Tremp Basin record (Spain). Palaeogeography, Palaeoclimatology, Palaeoecology 283, 160–171.
Rietveld, H.M., 1967. Line profiles of neutron powder-diffraction peaks for structure refinement. Acta Crystallographica 22, 151–152.
Salas, R., Martín-Closas, C., Querol, X., Guimerà, J., Roca, E., 1995. Evoluciòn tectonosedimentaria de las Cuencas del Maestragzo y Aliaga-Penyagolosa durante el cretacico inferior. Publicacions de la Universitat de Barcelona, Guía de campo de las excursiones científicas realizadas durante el III Coloquio del Cretácico de España, pp. 11–94.
Salas, R., Guimerà, J., Mas, R., Martín-Closas, C., Meléndez, A., Alonso, A., 2001. Evolution of the Mesozoic Central Iberian rift system and its Cainozoic inversion (Iberian chain). 145–185 in: Ziegler, P.A., Cavazza, W., Robertson, A.H.F., Crasquin-Soleau, S. (eds), Peri-Tethys Memoir 6: Peri-Tethyan Rift/Wrench Basins and passive margins. Memoires du Museum National d'Histoire Naturelle 186, 1–762.
Stathopoulou, E.T., Psycharis, V., Chryssikos, G.D., 2008. Bone diagenesis: new data from Infrared spectroscopy and X-Ray Diffraction. Palaeogeography, Palaeoclimatology, Palaeoecology 266, 168–174.
Stiner, M.C., Kuhn, S.L., Weiner, S., Bar-Yosef, O., 1995. Differential burning, recrystallization, and fragmentation of archaeological bone. Journal of Archaeological Science 22, 223–237.
Sudarsanan, K., Young, R.A., 1978. Structural interactions of F, Cl and OH in apatites. Acta Crystallographica B34, 1401–1407.
Sudarsanan, K., Mackie, P.E., Young, R.A., 1972. Comparison of synthetic and mineral fluorapatite, $Ca_5(PO_4)_3F$, in crystallographic detail. Materials Research Bulletin 7, 1331–1338.
Suñer, M., Santisteban, C., Santos-Cubedo, A., Galobart, A., 2007. Dinosaur fossils in marine facies from ANA locality, Arcillas de Morella Formation (Aptian, Lower Cretaceous, Cinctorres, Spain). 55th Symposium of Vertebrate Palaeontology and Comparative Anatomy and the 16th Symposium of Palaeontological preparation and conservation, 43. University of Glasgow Press, Glasgow.
Surovell, T.A., Stiner, M.C., 2001. Standardizing infra-red measures of bone mineral crystallinity: an experimental approach. Journal of Archaeological Science 28, 633–642.
Tadic, D., Epple, M., 2004. A thorough physicochemical characterization of 14 Ca phosphate-based bone substitution materials in comparison to natural bone. Biomaterials 25, 987–994.
Thomas, D.B., Fordyce, R.E., Frew, R.D., Gordon, K.C., 2007. A rapid, non-destructive method of detecting diagenetic alteration in fossil bone using Raman spectroscopy. Journal of Raman Spectrometry 38, 1533–1537.
Thompson, T.J.U., Gauthier, M., Islam, M., 2009. The application of a new method of Fourier Transform Infrared Spectroscopy to the analysis of burned bone. Journal of Archaeological Science 36, 910–914.
Trueman, C.N.G., Martill, D.M., 2002. The long-term preservation of bone: the role of bioerosion. Archaeometry 44, 371–382.
Trueman, C.N.G., Tuross, N., 2002. Trace elements in recent and fossil bone apatite. In: Kohn, M.J., Rakovan, J., Hughes, J.M. (Eds.), Phosphates: Geochemical, Geobiological and Materials Importance: Mineralogical Society of America. Reviews in Mineralogy and Geochemistry, 48, pp. 489–521.
Trueman, C.N.G., Chenery, C., Eberth, D.A., Spiro, B., 2003a. Diagenetic effects on the oxygen isotope composition of bones of dinosaurs and other vertebrates recovered from terrestrial and marine sediments. Journal of the Geological Society 160, 895–901.
Trueman, C.N.G., Benton, M.J., Palmer, M.R., 2003b. Geochemical taphonomy of shallow marine vertebrate assemblages. Palaeogeography, Palaeoclimatology, Palaeoecology 197, 151–169.
Trueman, C.N.G., Behrensmeyer, A.K., Tuross, N., Weiner, S., 2004. Mineralogical and compositional changes in bones exposed on soil surfaces in Amboseli National Park, Kenya: diagenetic mechanisms and the role of sediment pore fluids. Journal of Archaeological Science 31, 721–739.
Tütken, T., 2011. The diet of sauropod dinosaurs – implications from carbon isotope analysis of teeth, bones, and plants. In: Klein, N., Remes, K., Gee, C.T., Sander, P. (Eds.), Biology of the Sauropod Dinosaurs: Understanding the Life of Giants. Indiana University Press, Bloomington, pp. 57–79.
Tütken, T., Pfretzschner, H.-U., Vennemann, T.W., Sun, G., Wang, Y.D., 2004. Paleobiology and skeletochronology of jurassic dinosaurs: implications from the histology and oxygen isotope compositions of bones. Palaeogeography, Palaeoclimatology, Palaeoecology 206, 217–238.
Tütken, T., Vennemann, T.W., Pfretzschner, H.-U., 2008. Early diagenesis of bone and tooth apatite in fluvial and marine settings: constraints from combined oxygen isotope, nitrogen and REE analysis. Palaeogeography, Palaeoclimatology, Palaeoecology 266, 254–268.
Wings, O., 2004. Authigenic minerals in fossil bones from the Mesozoic of England: poor correlation with depositional environments. Palaeogeography, Palaeoclimatology, Palaeoecology 204, 15–32.
Wopenka, B., Pasteris, J.D., 2005. A mineralogical perspective on the apatite in bone. Materials Science and Engineering C25, 131–143.
Zocco, T.G., Schwartz, H.L., 1994. Microstructural analysis of bone of the sauropod dinosaur *Seismosaurus* by transmission electron microscopy. Palaeontology 37, 493–503.

5: DISCUSSION

In the development of the current thesis we have addressed two different although very related topics: analyzing and differentiating the microstructural changes in the bones due to the heat treatment and/or to diagenesis and fossilization processes.

During the study of several human skeletal samples, we have observed that some bones show modifications in colour, texture and morphology that could be interpreted as alterations due to heat exposure. However, colours may also be due to bone interaction with environmental materials. After burial, bone may be altered and may change colour as a result of soil composition, sediment pH, temperature or moisture, and the changes may occur in the bone tissue as ionic substitution.

Thus, we need techniques that permit us to distinguish between diagenesis and thermal treatment and, if possible, that differentiate the various partial thermal exposures. However, as human skeletal materials showing this kind of treatment are unique, these techniques should be as non-destructive as possible.

To address this type of analysis we used different physico-chemical and spectroscopic techniques that have produced important results, which can be applied in various forensic, archaeological and paleontological contexts.

5.1: Burned bones

5.1.1: *evaluating the applications of physico-chemical techniques in Forensic Sciences.*

The ability to distinguish between cremated human remains (cremains) and other materials of similar appearance can be of great importance in a variety of forensic situations. The Tri-State Crematorium incident in Noble, GA, USA (Markiewicz, 2005) is a most leading and meaningful example.

In early 2002, it was discovered that rather than performing the cremations contracted, the owner of Tri-State was dumping bodies unceremoniously around the property. More than 330 bodies were eventually recovered, while the urns many families had received often contained cement dust, silica, rock or other materials. To confuse matters, most bodies received prior to a certain date were actually cremated,

and later on, some bodies may have been sent to other facilities for proper cremation. Hundreds of families were uncertain as to the contents of the urns in their possession.

In particular forensic scenarios non-skeletal inclusions, such as surgical materials, dental restorations and identification tags can survive to cremation and it can be very useful for identification (Murray and Rose, 1993; Schultz et al., 2008). Therefore, other methods are needed for this inspection.

X–ray diffraction (XRD) spectrometry is one of the most powerful analytical tools available for identifying unknown crystalline substances (Jenkins, 1996). since each crystalline structure compound has a unique diffraction pattern, XRD is able to identify the crystalline compounds present in the sample,

By comparing the positions and intensities of the diffraction peaks against a library of known crystalline materials, samples of unknown composition and mixtures of materials can be identified and quantified.

Crystallographically, apatite is easily distinguished from the commonly used filler materials, such as concrete or sand. X–ray diffraction has several advantages to many of the other methods currently employed for cremains identification. It is not destructive, which means that the same sample can be examined several times by various laboratories, if necessary, and little to no sample preparation is required. If the sample is identified as being cremated remains it can be returned to a family in essentially its original condition.

There are cases in which a heat treatment is not particularly clear, which may entail an erroneous line in the investigation of the events. In these circumstances it is particularly useful to analyze the possible structural changes occurring in the bones through of spectroscopic (FT–IR) and physico-chemical techniques (XRD).

Bone structure is altered when exposed to heat. Some physico-chemical methodological approaches have been advanced specifically for burned remains (e.g: Rogers and Daniels, 2002).

A means to estimate the temperature and duration of a forensic burning event, focussing on the microscopic changes in bone and teeth and using powder X−Ray diffraction has been developed (Piga et al., 2008b; 2009b). This technique is particularly appropriate for events within the temperature range 200°C–1000°C for a variety of burning times. This range includes most forensic scenarios, although it should also be

noted that this range would also include most archaeological scenarios too and this methodology, supported by other chemical-physical and spectroscopic techniques, would be applied in those contexts.

The growth process undergone by the hydroxylapatite crystallites in the mineralogical phase of the bone samples follows a logarithmic sigmoid trend with a characteristic temperature around 850°C, as was determined with the four duration of burning times adopted here. This can be used not only to determine whether hard tissues have been burned, but also to suggest the temperature and duration of that burning event. In the thermal treatment of 0 min, the growth rate parameter p seems to be higher than in the results from increased periods of exposure. Thermal treatments for 60 min anticipate about 100°C the growth effects that are otherwise observed after treatments for 0 min.

In the case of teeth, the growth phenomena induced by firing are again described with a logistic type function with a characteristic temperature of 841°C, very close to that of bones, in spite of typical fragmentation induced in the temperature range 700°C-750°C. However, the average crystallite size of hydroxylapatite in untreated teeth (224 Å) is significantly larger than in untreated skeletal bones (ca. 170 Å),. Alternatively, the average size of hydroxylapatite crystallites from burning above 900°C is larger in bones than teeth. This suggests that the two types of natural bioapatite need to be compared to their specific calibration curves when the precise estimation of a fire temperature is desired, and that one curve for all hard tissues is not advised.

Also FT–IR technique can distinguish non-burned from low intensity and high intensity burnings (Thompson, 2009; Piga et al., 2010a). It is clear that the Crystallinity Index or Splitting factor (SF) can make a useful contribution to the study and interpretation of burned bones from archaeological and forensic contexts (Thompson, 2009). The combined use of these techniques provided much more information regarding the changes to the crystal and elemental structure of bone during the process of burning, and it is these changes (dubbed primary-level changes: Thompson, 2004) that have been shown statistically to provide the greatest chance of predicting the specifics of the forensic burning event (such as, temperature of fire, duration of burning, etc.) from the remains themselves (Thompson, 2005).

We are confident that the techniques described here can be honed for use as a more accurate determinant of crystallite change during heating, thus providing an additional means of determining the effects of heat treatment on biogenic hydroxylapatite or tracing burning practices in the forensic and archaeological records.

5.1.2: *evaluating the possibility of a multi-technique approach by XRD, SAXS and FT-IR for the analysis of burned archaeological bones.*

The Fourier transform infrared spectroscopy (FT–IR), small-angle X–ray scattering (SAXS) and X-ray diffraction (XRD) techniques are important tools for the in-depth study of bones whose structure has been modified by heat exposure or diagenesis. They are non-destructive complementary physical techniques that can identify crystalline compounds, provide the morphology of the bone constituents on Ångstrom scale, and determine the morphology as well as the fractal dimension on the nanometre scale.

We have made a combined use of these three techniques on six bones with different intensities of burning, belonging to the necropolis of *S'Illot des Porros* (Majorca, Spain), in order to evaluate the thermal treatment which samples underwent.

Our results show that:

a) The peak broadening and average crystallite size of XRD patterns are indicative of the different thermal treatment to which the bones were subjected. On the basis of a previous calibration (Piga et al., 2008b; 2009b) it was shown that similar apatite crystallinity changes can be related to a fire treatment to which presumably the bodies were subjected and the possible temperature.

b) Infrared spectroscopy is an efficient tool to access the composition and structure of bone mineral matter modifications during heating. The splitting factor (SF) calculated on FT–IR spectra allow the evaluation of hydroxylapatite crystallinity. Our data confirm findings about the thermal treatment samples undergo; the shoulder at ca. 634 cm^{-1} for the less "crystalline" specimens is replaced by a further peak in the specimens which appeared to have been treated at higher temperature. In fact in our previous calibration of FT–IR spectra it was established that the appearance of the

shoulder at ca 634 cm^{-1} indicates fire temperature between ca 700 and 800°C and persists until 1000°C (Piga et al., 2010a). Estimates temperatures obtained with the two techniques, according to our previous calibrations (Piga et al., 2008b; 2009b) are almost concordant, except in a few cases. These differences do not exceed 100°C and are not significant. These differences do not exceed 100°C and are not worthy of further interpretation since they may be thought to coincide within their experimental uncertainty.

c) SAXS provides evidence complementary to that generated by XRD in the characterisation of heated bone. Fine-scale changes in crystallite size and shape that are not measured directly using XRD are readily elucidated using SAXS, however, and therefore changes in the crystal structure that may not be readily apparent otherwise become more clear.

Thus, the combined used of those techniques is a powerful tool to assess whether the bones have subjected to fire and, with fairly good reliability, to which temperature (Piga et al., 2010b).

5.1.3: *applying physical-chemical analysis to different archaeological contexts in order to verify if a bone has been burned or not; finding explanations to some specific funerary rites, getting a reasonably precise temperature range and its duration across the entire body; checking temperature homogeneity throughout the skeleton.*

One of the major goals of this thesis concerns the application of physico–chemical techniques in archaeological and anthropological contexts of particular interest. In this sense the necropolis of *S'Illot des Porros* (Majorca, Spain) represent an emblematic example of how the physico-chemical approach can be useful and appropriate.

All the cremated bones have been found in three different funerary chambers of the necropolis and were attributed at least to 67 individuals (out of a whole of 285). The bones differ in texture and colour, and seem to have been exposed to different thermal degrees.

Our results allowed us to:

a) Describe all the burnt bones structurally using the X–ray diffraction (XRD) partially supported by Fourier Transform Infrared (FT–IR) techniques that differentiated the various degrees of thermal exposure.

b) Give a ritual interpretation of the results obtained; more specifically: the C chamber, the most ancient and with the largest number of inhumated individuals, contains the smallest number of remains that were exposed to fire and just in one case it seems possible to attribute a real high-temperature cremation. Chamber A appears to have lodged high-temperature cremations, while the cremations in chamber B appeared to be carried out at lower temperature.

In these chambers cremations at high and low temperature appear to belong to the lower layers together with some inhumated bodies that matches with a cleaning ritual at low temperature. Thus, the basic distinction between cremations at high and low temperature allows us to suggest very distinct rites, the first one involving a special treatment of the body during the funerary rite, the second likely following a treatment to the chamber rather than to the bodies themselves.

c) Determine for the first time in the Balearic prehistory when the funerary practices involving fire were introduced in relation to specific historical events.

Another extremely interesting case concerns the Phoenician-Punic Necropolis of *Monte Sirai* (Carbonia, Sardinia, Italy). In this necropolis there is a wide archaeological documentation about different and peculiar funeral rites (Piga et al., 2010a; Guirguis et al., 2010, 2011).

The case of grave 252 is particularly important for two reasons: the individual was cremated in a prone position (this is the first case of prone cremation reported in the literature) and the exceptional state of preservation of almost the entire skeleton. This allowed us to apply a combined use of FT–IR/XRD techniques on representative samples of the whole body in order to analyze the distribution of temperature and to determine the possible existence of a central focus.

The results obtained through the techniques of XRD/FT–IR, according to the methodology established by Piga et al. (2008b, 2009b, 2010a) and Thompson et al. (2009, 2010) for both techniques and their application on burnt remains (Piga et al., 2010b; Squires et al., 2011) converge to similar values of temperature. Data obtained

with the two techniques are almost concordant, except in a few cases where the temperatures obtained with the analysis of X-ray diffraction are a little higher.

We conclude that the skeletal remains of *Monte Sirai* have been treated with fire in a temperature range of 1000°C, across the whole of the body, while some specific parts may have been subjected to lower temperature values (e.g. 700°C) because of uncompleted combustion processes related to insufficient oxygen that would have created a reducing, rather than oxidizing atmosphere and/or to a dynamics of the fire influenced by the contact of the body with the wood branches (McKinley, 2000).

5.1.4: *assessing whether the lattice parameters of bioapatite obtained by XRD data are helpful when trying to distinguish human bones from animal bones.*

Our work addresses an important archaeological and forensic question i.e. whether animal and human bones may be distinguished by powder X–ray diffraction following heating. Beckett et al. (2011) reported in a recent paper the possibility of determining the human rather than animal origin of bone from the lattice parameters of the inorganic bioapatite phase subjected to a high temperature heating treatment.

Our large availability of animal and burned human bones supplies an excellent opportunity to exploit this topic thoroughly.

The study addresses a number of important points:

a) Bones typically give broad XRD lines unless heated so it is only possible to compare human and animal bones that have had substantial pre-treatment.

b) The a-axis and c-axis values of bioapatite are not biased by the use of a $P2_1/b$ monoclinic rather than $P6_3/m$ hexagonal unit cell.

c) The chemistry of bone material changes significantly on heating.

d) The apatite unit cell axis can be affected by ion exchange reactions occurring *post-mortem* such fluorination during diagenesis or chlorination during boiling the bones in salted water for cleaning.

All of these factors mean that there are a large number of variables to consider and strongly support our conclusion that it is not easily possible to distinguish animal

and human bones on the basis of powder diffraction patterns, and any such claims to be able to distinguish animal and human bones should be treated with caution.

5.2: Fossil bones:

5.2.1: *applying the physical-chemical analysis to evaluate the diagenesis of fossil bones.*

Over the last 30 years, many research articles have focused on the microstructural study of fossil bones and in particular those of dinosaurs (e.g Elorza et al., 1999).

Using different techniques, a number of studies have dealt with the fossil diagenetic features of bones, especially the diagenetic changes that transformed biogenic bone tissue to francolite (carbonate fluorapatite) crystals while preserving μm-scale organic structures (see Zocco and Schwartz, 1994; Hubert et al., 1996; Kolodny et al., 1996).

The precise understanding of diagenetic and taphonomic processes to which dinosaur bones were subjected requires a multidisciplinary approach, taking into account the potentialities and limitations of each analytical technique employed.

Accordingly we have investigated the microstructural features and the mineralogical diagenetic changes, as well as the chemical fingerprint, of 60 Spanish dinosaur samples from Upper Jurassic/Lower Cretaceous to Upper Cretaceous age.

On the basis of our study we draw the following conclusions:

a) From the crystal lattice parameters of the apatite phase determined by XRD, it emerged that these fossil bones invariably underwent a transformation from bioapatite (hydroxylapatite) to authigenic francolite (fluorapatite) structure.

b) The most frequent phases in the samples studied are mostly fluorapatite, quartz and calcite, but we have also determined several other phases such as kaolinite, goethite, celestite, gypsum, dolomite, and berlinite. It is clear that also the presence of these phases may be ascribed to the mineralogical features of the sediment.

c) The average crystallite size of the apatite-like phase ranges from 183 Å to 2107 Å and varies unpredictably in the analysed specimens, inhibiting a correlation with fossil age.

d) The ν_4 phosphate band envelope of FT–IR spectra for selected dinosaur bones specimens emphasizes how fossilization involves a band sharpening; we note a decrease of the two intensity bands around 570 cm^{-1} and the absence of any band at 635 cm^{-1}, probably on account of the OH group disappearance following fluorination.

e) The XRF spectra show the presence of major elements such as Ca and P, also accompanied by varying amounts of transitional elements such as Ti, V, Mn, Cu, As, Rb, Y, Sr and Nb. In particular, the level of Sr was occasionally found in relatively elevated concentrations. Likewise Fe ions, in the absence of specific Sr-based phase it is possible that a considerable amount of Sr substitutes for Ca ions in the structure of francolite.

f) XRF invariably shows the presence of Fe ions that may be ascribed to a substitution of this element for Ca in the francolite structure when it is not involved in specific iron-based phases.

5.2.2: *evaluating the use of average crystallite size as dating method.*

The apatite crystallinity is used to differentiate the degree of diagenesis in fossil specimens. Compared with "fresh" modern bone, fossil bone shows increased crystallinity (Schoeninger et al., 1989; Sillen, 1989; Hedges and Millard, 1995; Sillen and Parkington, 1996; Elorza et al., 1999; Lee- Thorp, 2002; Reiche et al., 2002; Farlow and Argast, 2006) reflecting changes in apatite crystallite size and strain, as well as incorporation of F into, and loss of CO_3^{2-} from the apatite crystal structure. Crystallinity can increase in bones exposed on the surface of the ground for several years (Tuross et al., 1989), but a time scale of millennia is generally necessary for much crystallinity change in buried bone (Sillen, 1989). We have recently estimated that fluorination of bone apatite is taking place in about 4-5 Ma after examining by XRD the unit cell volume change of biogenic apatite vs. geological age. (Piga et al., 2009a).

Warmer burial temperatures probably result in increased crystallinity, as do other diagenetic modifications of bone (Hedges, 2002). Tooth enamel shows less change in crystallinity between modern and fossil specimens than does bone (Ayliffe et al., 1994; Michel et al.,1996).

Crystallinity is frequently quantified by X–ray diffraction and infrared spectroscopy as these methods are sensitive to structural order (Rogers et al., 2010).

Bartsiokas and Middleton (1992) suggested that numerical indices of bone crystallinity could be used to determine the relative ages of archaeological and paleontological bone samples up to ages of about one million years. Sillen and Parkington (1996) likewise found a relationship between bone crystallinity and age, but only for bones up to about 20,000 years old. Over a time scale of thousands to millions of years, Person et al. (1995, 1996), however, found no relationship between bone crystallinity and age (also see: Hedges and Millard, 1995), and argued that crystallinity changes occur in the earliest phases of inorganic diagenesis.

In our previous study (Piga et al., 2009), we have observed a positive correlation between average bone apatite crystal size and specimen age in a set of fossils ranging in age from the Middle Triassic (around 245 Ma) to present.

The average crystallite size for apatite of this dinosaur samples collection as a function of age in the range 150–65 Ma, ordered according to their geological age, showed the absence of correlation between crystallization process and age. From the present data it seems that the crystallization induced by just the time is overlapped by other factors depending on the geological formation that may inhibit (e.g., *4ANA3* and *Camino* samples) or enhance the process.

The unpredictable change of the average crystallite size values suggests that correlation between crystallisation indices and bone age has to be regarded with obvious caution.

6: CONCLUSIONS

In relation to the analysis of burned bones, we can conclude that:

1. The analysis of different contexts with burned bones permit us to affirm that the physico-chemical techniques described here (XRD, FT–IR) can be used as a more accurate determinant of crystallite change during heating, thus providing an additional means of determining the effects of heat treatment on biogenic hydroxylapatite or tracing burning practices in the forensic and archaeological records.

2. The combined used of XRD, FT–IR and SAXS techniques is a powerful tool to assess whether the bones have subjected to fire and, with fairly good reliability, to which temperature.

3. The application of these techniques to archaeological context is useful to verify if a bone has been burned or not, find explanations to some specific funerary rites, get a reasonably precise temperature range across the entire body, temperature homogeneity throughout the skeleton and its duration.

4. It is not easily possible to distinguish animal and human bones on the basis of powder diffraction patterns. A large number of variables have to be taken into proper account. Therefore, any claims to be able to distinguish animal and human bones should be treated with caution

In relation to the analysis of fossil bones, we can conclude that:

5. The combined investigations and analyses by FT–IR, XRD and XRF techniques supplied detailed and to a certain extent satisfactory accounts of the post-mortem integral changes to which the fossil bones have been subjected during geological times.

6. The crystallization induced by just the time is overlapped by other factors depending on the geological formation that may inhibit or enhance the process. The extreme variability of francolite average crystallite size values suggests that correlation between crystallisation indices and bone age has to be regarded with obvious caution.

7: REFERENCES

Ayliffe, L.K., Chivas, A.R., Leakey, M.G., 1994. The retention of primary oxygen isotope compositions of fossil elephant skeletal phosphate. Geochimica et Cosmochimica Acta 58, 5291–5298.

Barker, M.J., Clarke, J., Martill, D.M., 1996. Mesozoic reptile bones as diagenetic windows. Bulletin de la Société géologique de France 168, 535–545.

Bartsiokas, A., Middleton, A.P. 1992. Characterization and dating of recent and fossil bone by X-ray diffraction. Journal of Archaeological Science 19, 63–72.

Baud., C.A. Durif, S., Morgenthaler, P.W., 1954. Recherches sur la structure cristalline d'os humain fossile. Archives suisses d'Anthropologie générale 9, 37–52.

Beckett, S., Rogers, K.D., Clement, J.D., 2011. Inter-Species Variation in Bone Mineral Behavior upon Heating. Journal of Forensic Sciences 56, 571–579.

Bell, L.S., Skinner, M.F., Jones, S.J., 1996. The speed of post mortem change to the human skeleton and its taphonomic significance. Forensic Science International 82, 129–140.

Bellomo, R. V., 1993. A methodological approach for identifying archaeological evidence of fire resulting from human activities. Journal ofArchaeological Science 20, 525–553.

Bennett, L., 1999. Thermal alteration of buried bone. Journal ofArchaeological Science 26, 1–8.

Bergslien, E.T., Bush, M., Bush, P.J., 2008. Identification of cremains using X-ray diffraction spectroscopy and a comparison to trace element analysis. Forensic Science International 175, 218–226.

Berna, F., Matthews, A., Weiner, S., 2004. Solubilities of bone mineral from archaeological sites: the recrystallization window. Journal of Archaeological Science 31, 867–882.

Bonucci, E., Graziani, G., 1975. Comparative thermogravimetric X-ray diffraction and electron microscope investigations of burnt bones from recent, ancient and prehistoric age. Atti della accademia Nazionale dei Lincei, Rendiconti, classe di scienze fisiche, matematiche e naturali 59, 517–532.

Brain, C.K., Sillen, A., 1988. Evidence from the Swartkrans cave for the earliest use of fire. Nature 336**,** 464–466.

Brock, F., Higham, T., Bronk Ramsey, C., 2010. Pre-screening techniques for identification of samples suitable for radiocarbon dating of poorly preserved bones. Journal of Archaeological Science 37, 855–865.

Carpenter, J.P., Sánchez, M.G., Villalpando, M.E., 2003. Sonora precerámica: del arcaico y del surgimiento de aldeas agrícolas, Arqueología 29, 5–29.

Cattaneo, C., Di Martino, S., Scali, S., Craig, O.E., Grandi, M., Sokol, R.J., 1999. Determining the human origin of fragments of burnt bone: a comparative study of histological, immunological and DNA techniques. Forensic Science International 102, 181–191.

Chakraborty, S., Bag, S., Pal, S., Mukherjee, A.K., 2006. Structural and microstructural characterization of bioapatites and synthetic hydroxyapatite using X-ray powder diffraction and Fourier transform infrared techniques. Journal of Applied Crystallography 39, 385–390.

Chandler, N.P., 1987. Cremated teeth. Archaeology Today, 41–45.

Collins, M.J., Nielsen-Marsh, C.M., Hiller, J., Smith, C.I., Roberts, J.P., Prigodich, R.V., Wess, T.J., Csapó, J., Millard, A.R., Turner-Walker, G., 2002. The survival of organic matter in bone: a review. Archaeometry 44, 383–394.

Costamagno, S., Griggo, C., Mourre, V., 1999. Approche expérimentale d'un problème taphonomique : utilisation de combustible osseux au Paléolithique. Préhistoire européenne 13, 167–194.

Currey, J.D., 2002. Bones: Structures and Mechanics. Princeton University Press, Princeton, NJ.

D'Elia, M., Gianfrate, G., Quarta, G., Giotta, L., Giancane, G., Calcagnile, L., 2007. Evaluation of possible contamination sources in the 14C analysis of bone samples by FTIR spectroscopy. Radiocarbon 49, 201–210.

Dumont, M., Kostka, A., Sander, P.M., Borbély, A., Kaysser-Pyzalla, A., in press. Size and size distribution of apatite crystals in sauropod fossil bones. Palaeogeography, Palaeoclimatology, Palaeoecology 310, 108–116.

Eckert, W.G., James, S, Katchis, S., 1988. Investigation of cremations and severely burned bodies. American Journal of Forensic Medicine and Pathology 9, 188–200.

Elorza, J., Astibia, H., Murelaga, X., Pereda-Suberbiola, X. 1999. Francolite as a diagenetic mineral in dinosaur and other Upper Cretaceous reptiles fossil bones (Laño, Iberian Peninsula): microstructural, petrological and geochemical features. Cretaceous Research 20, 169–187.

Enzo, S., Fagherazzi, G., Benedetti, A., Polizzi, S., 1988. A profile-fitting procedure for analysis of broadened X-ray diffraction peaks. I Methodology. Journal of Applied Crystallography 21, 536–542.

Enzo, S., Bazzoni, M., Mazzarello, V., Piga, G., Bandiera, P., Melis, P., 2007. A study by thermal treatment and X-ray powder diffraction on burnt fragmented bones from Tombs II, IV and IX belonging to the hypogeic necropolis of "Sa Figu" near Ittiri-SS (Sardinia-Italy). Journal of Archaeological Science 34, 1731–1737.

Erickson, G.M., 2005. Assessing dinosaur growth patterns: a microscopic revolution. Trends in Ecology and Evolution 20, 677−684.

Etok, S.E., Valsami-Jones, E., Wess, T.J., Hiller, J.C., Maxwell, C.A., Rogers, K.D., Manning, D.A.C., White, M.L., Lopez-Capel, E., Collins, M.J., Buckley, M., Penkman, K.E.H., Woodgate, S.L., 2007. Structural and chemical changes of thermally treated bone apatite. Journal of Material Science 42, 9807–9816.

Etxeberria, F., 1994. Aspectos macroscópicos del hueso sometido al fuego. Revisión de las cremaciones descritas en el País Vasco desde la Arqueología. Munibe 46, 111–116.

Fairgrieve, S.I., 2008. Forensic cremation: Recovery and Analysis. Boca Raton: CRC Press.

Farlow, J.O., Argast, A. 2006. Preservation of fossil bone from the pipe creek sinkhole (late Miocene, Grant County, Indiana, U.S.A.). Journal of the Paleontological Society of Korea 22, 51–75.

Fernández-Jalvo, Y., Andrews, P., Pesquero, D., Smith, C., Marín-Monfort, D., Sánchez, B., Geigl, E.-M., Alonso, A. 2010. Early bone diagenesis in temperate environments Part I: Surface features and histology. Palaeogeography, Palaeoclimatology, Palaeoecology 288, 62–81.

Fricke H.C., Rogers, R.R., Backlund, R., Dwyer, C.N., Echt, S., 2008. Preservation of primary stable isotope signals in dinosaur remains, and environmental gradients of the Late Cretaceous of Montana and Alberta. Palaeogeography, Palaeoclimatology, Palaeoecology 266, 13–27.

Fröhlich, F., 1989. Deep-sea biogenic silica: new structural and analytical data from infrared analysis e geological implications. Terra Nova 1, 267–273.

Greenlee, D.M., Dunnell, R.C., 1992. Understanding post depositional processes through electron microbeam analysis of archaeological bone from SE Missouri, in: Materials issues in art and archaeology, vol. 3 (eds. P. B. Vandiver et al.), 883–8, Materials Research Society Symposium Proceedings, 267, Materials Research Society, Pittsburgh, PA.

Guirguis, M., 2010. Necropoli fenicia e punica di Monte Sirai. Indagini archeologiche 2005-2007. Studi di Storia Antica e di Archeologia 7. Ortacesus ed., Cagliari.

Guirguis, M., 2011. Gli spazi della morte a Monte Sirai (Carbonia – Sardegna). Rituali e ideologie funerarie nella necropoli fenicia e punica (scavi 2005–2010). Fasti On Line Documents & Research, 230.

Hedges, R.E.M., Millard, A.R., 1995. Bones and groundwater: towards 514 the modelling of diagenetic processes. Journal of Archaeological Science 22, 155–164.

Hedges, R.E.M., Millard, A.R., Pike, A.W.G., 1995. Measurements and relationships of diagenetic alteration of bone from three archaeological sites. Journal of Archaeological Science 22, 201–211.

Hedges, R.E.M., 2002. Bone diagenesis: an overview of processes. Archaeometry 44, 319–328.

Hedges, R.E.M., Stevens, R.E., Koch, P.L., 2006. Isotopes in bones and teeth. In: M. J. Leng (ed.), Isotopes in palaeoenvironmental research. (Berlin, Heidelberg 2006) 116–145.

Herrmann, B., 1977. On histological investigations of cremated human remains. Journal of Human Evolution 6, 101–103.

Herwartz, D., Tütken, T., Münker, C., Jochum, K.-P., Stoll, B., Sander, P.M., 2011. Timescales and mechanisms of REE and Hf uptake in fossil bones. Geochimica et Cosmochimica Acta 75, 82–105.

Heuser, A., Tütken, T., Gussone, N., Galer, S.J.G., 2011. Calcium isotopes of fossil bones and teeth — diagenetic versus biogenic origin. Geochimica et Cosmochimica Acta 75, 3419–3433.

Hiller, J., Thompson, T.J.U., Evison, M.P., Chamberlain, A.T., Wess, T.J., 2003. Bone mineral change during experimental heating: An X-ray scattering investigation. Biomaterials 24, 5091–5097.

Holck, P., 1986. Cremated bones. A medical anthropological Study of an archaeology Material on Cremation Burials, Anthropologiske skifter 1, AnatomiskInstitut, Universitet I, Oslo.

Holden, J.L, Clement, J.G., Phakey, P.P., 1995. Age and temperature related changes to the ultrastructure and composition of human bone material. Journal of Bone and Mineral Research 10(9):1400–1409.

Hubert, J.F., Panish, P.T., Chure, D.J., Prostak, K.S., 1996. Chemistry, microstructure, petrology and diagenetic model of Jurassic dinosaur bones, Dinosaur National Monument, Utah. Journal of Sedimentary Research 66, 531–547.

Jans, M.M.E., 2008. Microbial bioerosion of bone – a review. In: Wisshak, M. and Tapanila, L. (eds.): Current Developments in Bioerosion. Springer, Berlin, Heidelberg, 397–413.

Jans, M.M.E., Nielsen-Marsh, C.M., Smith, C.I., Collins, M.J., Kars, H., 2004. Characterisation of microbial attack on archaeological bone. Journal of Archaeological Science 31, 87–95.

Jenkins, R.L., 1996. Snyder, Introduction to X-ray Powder Diffractometry, John Wiley & Sons, New York.

Kalsbeek, N., Richter, J. 2006. Preservation of burned bones: an investigation of the effects of temperature and pH on hardness. Studies in Conservation 51, 123–138.

Kennedy, K.A.R., 1996. The wrong urn: commingling of cremains in mortuary practices. Journal of Forensic Science 41(4), 689–692.

Koch, P.L., 2007. Isotopic study of the biology of modern and fossil vertebrates. In: R. Minchener/ K. Lajtha (eds.), Stable isotopes in ecology and environmental science2 (Oxford 2007) 99–154.

Kohn, M.J., Cerling, T.E., 2002. Stable isotope compositions of biological apatite. In: Kohn, M.J., Rakovan, J., Hughes, J. (Eds.), Phosphates: Geochemical, Geobiological and Materials Importance. Reviews in Mineralogy, vol. 48. Mineralogical Society of America, Washington, DC, pp. 455–488.

Kohn, M.J., 2008. Models of diffusion-limited uptake of trace elements in fossils and rates of fossilisation. Geochimica et Cosmochimica Acta 72, 3758–3770.

Kolodny, Y., Luz, B., Sander, M., Clemens, W. A., 1996. Dinosaur bones: fossils or pseudomorphs? The pitfalls of physiology reconstruction from apatitic fossils. Palaeogeography, Palaeoclimatology, Palaeoecology 126, 161–171.

Koon, H.E.C., Nicholson, R.A., Collins, M.J., 2003. A practical approach to the identification of low temperature heated bone using TEM. Journal of Archaeological Science 30, 1393–1399.

Koon, H.E.C., 2006. Detecting cooked bone in the archaeological record: a study of the thermal stability and deterioration of bone collagen. Unpublished PhD. thesis, University of York.

Koon, H.E.C., O'Connor, T.P., Collins, M.J., 2010. Sorting the butchered from the boiled. Journal of Archaeological Science 37, 62–69.

Laloy, J., 1981. Recherche d'une méthode pour l'exploitation des témoins de combustion préhistorique. Cahiers du centre de recherches archéologiques, 80–81.

Lebon, M., Reiche, I., Bahain, J.-J., Chadefaux, C., Moigne, A.-M., Fröhlich, F., Sémah, F., Schwarcz, H.P., Falguères, C., 2010. New parameters for the characterization of diagenetic alterations and heat-induced changes of fossil bone

mineral using Fourier transform infrared spectrometry. Journal of Archaeological Science 37, 2265–2276.

Lee-Thorp, J., 2002. Two decades of progress towards understanding fossilization processes and isotopic signals in calcified tissue minerals. Archaeometry 44, 435–446.

Lee-Thorp, J.A., 2008. On isotopes and old bones. Archaeometry 50, 925–950.

López, S., Lagunas, Z., Serrano, C., 1976. Enterramientos humanos de la zona arqueológica de Cholula, Puebla, Instituto Nacional de Antropología e Historia, México.

Lutterotti, L., Bortolotti, M., 2003. Object oriented programming and fast computation techniques in MAUD, a program for powder diffraction analysis written in java. IUCr: Compcomm Newsletter 1, 43–50.

March, R.J. 1996 : R. J. March, L'étude des structures de combustion préhistoriques: une approche interdisciplinaire. In : O. Bar-Josef et al. (éd.), The Lower and middle Palaeolithic Forli, 251–275.

Markiewicz, D.A., 2005. Few takers for fake cremains; GBI seeks ‘closure’ in crematory scandal; families conflicted, The Atlanta Journal-Constitution Metro News, August 10, 2005 1B.

Masciocchi, N., Artioli, G., 1996. Lattice parameters determination from powder diffraction data: Results from a Round Robin project. Powder Diffraction 11, 253–258.

Mayne Correia, P.M., 1997. Fire Modification of Bone: A Review of the Literature. In: Haglund WD, Sorg MH, editors. Forensic Taphonomy: The Post-mortem Fate of Human Remains. USA: CRC Press, Inc, 275–293.

McKinley, J.I., 2000. The Analysis of Cremated Bone. In: Cox M, Mays S. editors, Human Osteology: In Archaeology and Forensic Science. GB: Greenwich Medical Media Ltd, 403–421.

Michel, V., Ildefonse, Ph, Morin, G., 1996. Assessment of archaeological bone and dentine preservation from Lazaret Cave (Middle Pleistocene) in France. Palaeogeography, Palaeoclimatology, Palaeoecology 126, 109–119.

Misner, L.M., Halvorson, A.C., Dreier, J.L., Ubelaker, D.H., Foran, D.R., 2009. The correlation between skeletal weathering and DNA quality and quantity. Journal of Forensic Sciences 54, 822–828.

Mkukuma, L.D., Skakle, J.M.S., Gibson, I.R., Imrie, C.T., Aspden, R.M., Hukins, D.W.L., 2004. Effect of the proportion of organic material in bone on thermal decomposition of bone mineral: An investigation of the variety of bones from different species using Thermogravimetric Analysis couples to Mass Spectrometry, High-Temperature X-ray Diffraction, and Fourier Transfom Infrared Spectroscopy. Calcified Tissue International 75, 321–328.

Munro, L.E., Longstaffe, F.J., White, C.D., 2007. Burning and boiling of modern deer bone: effects on crystallinity and oxygen isotope composition of bioapatite phosphate. Palaeogeography, Palaeoclimatology, Palaeoecology 249, 90–102.

Murray, K.A., Rose, J.C., 1993. The analysis of cremains: a case study involving the inappropriate disposal of mortuary remains, Journal of Forensic Science 38 (1), 98–103.

Nakano, T., Tokumura, A., Umakoshi, Y., 2002. Variation in crystallinity of hydroxyapatite and the related calcium phosphates by mechanical grinding and subsequent heat treatment. Metallugical and Materials Transactions A 33, 521–528.

Nelson, B.K., DeNiro, M.J., Schoeninger, M.J., DePaolo, D.J., Hare, P.E., 1986. Effects of diagenesis on strontium, carbon, nitrogen and oxygen concentration and isotopic composition of bone. Geochimica et Cosmochimica Acta, 50, 1941–1949.

Newesely, H. 1988. Chemical Stability of Hydroxyapatite under Different Conditions. In: G. Grupe and B. Herrmann (eds.) Trace Elements in Environmental History. Berlin: Springer-Verlag, 1–16.

Nicholson, R.A., 1993. A morphological investigation of bumt bone and an evaluation of its utility in archaeology. Journal ofArchaeological Science 22, 411–428.

Nicholson, R.A., 1996. Bone degradation, burial medium and species representation : Debunking the myths. an experiment-based approach. Journal of Archaeological Science 23, 513–534.

Nicholson, R.A., 1998. Bone degradation in a compost heap. Journal of Archaeological Science 25, 393–403.

Olsen, J., Heinemeier, J., Bennike, P., Krause, C., Hornstrup, K.M., Thrane, H., 2008. Characterisation and blind testing of radiocarbon dating of cremated bone. Journal of Archaeological Science 35, 791–800.

Owsley, D.W., 1993. Identification of the fragmentary, burned remains of two US journalists seven years after their disappearance in Guatemala. Journal of Forensic Science 38(6):1372–82.

Parker, S. 1985. An experimental and comparative study of cremation techniques. Unpublished M.Sc. dissertation. Department of Archaeology and Prehistory, University of Sheffield.

Payne, G. 1937. Fossilization of bone. American Journal of Science 34, 148–157.

Perinet, G., 1964. Détermination par diffraction X de la température de cuisson d'un ossement calciné. Application au matériel préhistorique. Comptes Rendus d'Acuadémie des Sciences, Paris (Séries D) 258, 4115–4116.

Person, A., Bocherens, H., Saliège, J.F., Paris, F., Zeitoun, V., Gérard, M., 1995. Early diagenetic evolution of bone phosphate: An X-ray diffractometry analysis. Journal of Archaeological Science 22, 211–221.

Person, A., Bocherens, H., Mariotti, A., Renard, M., 1996. Diagenetic evolution and experimental heating of bone phosphate. Palaeogeography, Palaeoclimatology, Palaeoecology 126, 135–149.

Peterson, V.K., 2005. Lattice parameter measurement using Le Bail versus structural. Rietveld. refinement: A caution for complex, low symmetry systems. Powder Diffraction 20, 14–17.

Pfretzschner, H.-U., 2000. Pyrite formation in Pleistocene long bones – a case of very early mineral formation during diagenesis. Neues Jahrbuch für Geologie und Paläontologie Abhandlungen 217, 143–160.

Pfretzschner, H.-U., 2001a. Pyrite in fossil bone. Neues Jahrbuch für Geologie und Paläontologie–Abhandlungen 220, 1–23.

Pfretzschner, H.-U., 2001b. Iron oxides in fossil bone. Neues Jahrbuch für Geologie und Paläontologie - Abhandlungen 220, 417–429.

Pfretzschner, H.-U., 2004. Fossilization of Haversian bone in aquatic environments. Comptes Rendus Palevol 3, 605–616.

Piga, G., Malgosa, A., Mazzarello, V., Bandiera, P., Melis, P., Enzo, S. 2008a. Anthropological and physico-chemical investigation on the burnt remains of Tomb IX in the "Sa Figu" hypogeal necropolis (Sassari-italy)-Early Bronze Age. International Journal of Osteoarcheology 18, 167–177.

Piga, G., Malgosa, A., Thompson, T.J.U, Enzo, S., 2008b. A new calibration of the XRD technique for the study of archaeological burnt remains. Journal of Archaeological Science 35, 2171–2178.

Piga, G., Santos-Cubedo, A., Moya Solà, S., Brunetti, A., Malgosa, A., Enzo, S., 2009a. An X-Ray Diffraction (XRD) and X-Ray Fluorescence (XRF) investigation in human and animal fossil bones from Holocene to Middle Triassic. Journal of Archaeological Science 36, 1857–1868.

Piga, G., Thompson, T.J.U., Malgosa, A., Enzo, S., 2009b. The potential of X-ray Diffraction (XRD) in the analysis of burned remains from forensic contexts. Forensic Science International 54 (3), 534–539.

Piga, G., Guirguis, M., Bartoloni, P., Malgosa, A., Enzo, S., 2010a. A funerary rite study of the Phoenician-Punic Necropolis of Mount Sirai (Sardinia, Italy). International Journal of Osteoarchaeology 20, 144–157.

Piga, G., Hernández-Gasch J.H., Malgosa, A., Ganadu, M.L., Enzo, S., 2010b. Cremation practices coexisting at the *S'Illot des Porros* Necropolis during the Second Iron Age in the Balearic Islands (Spain). Homo 61, 440–452.

Piga, G., Malgosa, A., Thompson, T.J.U, Guirguis, M., Enzo, S., 2012. A unique case of prone position in the primary cremation Tomb 252 of Monte Sirai necropolis (Carbonia, Sardinia, Italy). International Journal of Osteoarchaeology (DOI: 10.1002/oa.2270).

Pijoan, C., Schultz, M., Mansilla, J., 2004. Estudio histológico de las alteraciones térmicas en el material óseo procedente de Tlatelcomila, Tetepan, D.F., in:

Perspectiva tafonómica: evidencias de alteraciones en restos óseos (eds. C. Pijoan and X. Lizárraga), 109–27. Instituto Nacional de Antropología e Historia. México.

Pucéat, E., Reynard, B., Lécuyer, C., 2004. Can crystallinity be used to determine the degree of chemical alteration of biogenic apatites? Chemical Geology 205, 83–97.

Ravaglioli, A., Krajewski, A., Celotti, G.C., Piancastelli, A., Bacchini, B., Montanari, L., Zama, G., Piombi, L., 1996. Mineral evolution of bone. Biomaterials 17**,** 617–622.

Reiche, I.; Vignaud, C., Menu, M., 2002. The crystallinity of ancient bone and dentine: new insights by transmission electron microscopy. Archaeometry 44, 447–459.

Rho, J.-Y., Kuhn-Spearing, L., Ziuopos, P., 1998. Mechanical properties and the hierarchical structure of bone. Medical Engineering and Physics 20, 92–102.

Rietveld, H.M. 1967. Line profiles of neutron powder-diffraction peaks for structure refinement. Acta Crystallographica 22, 151–152.

Rogers, K., Beckett, S., Kuhn, S., Chamberlain, A., Clement, J., 2010. Contrasting the crystallinity indicators of heated and diagenetically altered bone mineral. Palaeogeography, Palaeoclimatology, Palaeoecology 296, 125–129.

Rogers, K.D., Daniels, P., 2002. An X-ray Diffraction Study of the Effects of Heat Treatment on Bone Mineral Microstructure. Biomaterials 23, 2577–2585.

Schiegl, S., Goldberg, P., Pfretzschne, H.-U., Conard, N.J., 2003. Paleolithic burnt bone horizons from the Swabian Jura: Distinguishing between *in situ* fireplaces and dumping areas. Geoarchaeology 18, 541–565.

Schmidt, C.W., Symes, S.A., editors., 2008. The analysis of burned human remains. New York: Academic Press.

Schoeninger, M.J.; Moore, K.M.; Murray, M.L. & Kingston, J.D., 1989. Detection of bone preservation in archaeological and fossil samples. Applied Geochemistry 4, 281–292.

Schurr, M.R., Hayes, R.G. 2008. Stable Carbon- and Nitrogen-Isotope Ratios and Electron Spin Resonance (ESR) g-Values of Charred Bones: Changes with Heating

and a Critical Evaluation of the Utility of g-Values for Reconstructing Thermal History and Original Isotope Ratios. Journal of Archaeological Science 35:2017–2031.

Schwarz, C., Debruyne, R., Kuch, M., McNally, E., Schwarcz, H., Aubrey, A.D., Bada, J., Poiner, H., 2009. New insights from old bones: DNA preservation and degradation in permafrost preserved mammoth remains. Nucleic Acid Research 37, 3215–3229.

Shahack-Gross, R., Bar-Yosef, O., Weiner, S., 1997. Black-coloured bones in Hayonim Cave, Isreal: differentiating between burning and oxide staining. Journal of Archaeological Science 24, 439–446.

Shemesh, A., 1990. Crystallinity and diagenesis of sedimentary apatites. Geochimica et Cosmochimica Acta 54, 2433–2438.

Shipman, P., Foster, G., Schoeninger, M., 1984. Burnt bones and teeth: an experimental study of color, morphology, crystal structure and shrinkage. Journal of Archaeological Science 11, 307–325.

Schultz, J.J., Warren, M.W., Krigbaum, J.S., 2008. Analysis of human cremains: gross and chemical methods, in: C.W. Schmidt, S.A. Symes (Eds.), The Analysis of Burned Human Remains, Academic Press, London, 75–94.

Sillen, A., Morris, A., 1996. Diagenesis of bone from Border Cave: implications for the age of the Border Cave hominids. Journal of Human Evolution 31, 499–506.

Sillen, A., Parkington, J.E. 1996 Diagenesis of bones from Elands Bay Cave. Journal of Archaeological Science 23, 535–542.

Smith, T.M., 2008. Incremental dental development: Methods and applications in hominoid evolutionary studies. Journal of Human Evolution 54, 205–224.

Sponheimer, M., Lee-Thorp, J.A., 2006. Enamel diagenesis at South African Australopith sites: implications for paleoecological reconstruction with trace elements. Geochimica et Cosmochimica Acta 70, 1644–1654.

Squires, K.E., Thompson, T.J.U., Islam, M., Chamberlain, A., 2011. The application of histomorphometry and Fourier Transform Infrared Spectroscopy to the analysis of early Anglo-Saxon burned bone. Journal of Archaeological Science 38, 2399–2409.

Stiner, M.C., Kuhn, S.L., Surovell, T.A. Goldberg, P., Margaris, A.V., Meignen, L., Weiner, S., Bar-Yosef, O., 2005. Bone, Ash, and Shell Preservation in Hayonim Cave. In; Stiner, M.C. The Faunas of Hayonim Cave, Israel: A 200,000-Year Record of Paleolithic Diet, Demography, and Society. ASPR Bulletin 48, Peabody Museum of Archaeology and Ethnology, Harvard University, 59–79.

Stiner, M.C., Kuhn, S.L., Surovell, T.A., Goldberg, P., Meignen, L., Weiner, S., Bar-Yosef, O., 2001. Bone preservation in Hayonim Cave (Israel): a macroscopic and mineralogical study. Journal of Archaeological Science 28, 643–659.

Surovell, T.A., Stiner, M.C., 2001. Standardizing infra-red measures of bone mineral crystallinity: an experimental approach. Journal of Archaeological Science 28, 633–642.

Susini, A. 1988. Etudes des caractéristiques biophysiques des tissus calcifiés humains (os, émail, dentine) soumis à des traitements thermiques. Applications anthropologiques et médicales. Thèse de l'Université de Genève, Dép. de Morphologie Division I, Dép. d'Anthropologie et d'Écologie,n° 2320.

Taylor, R.E., Hare, P.E., White, T.D., 1995. Geochemical Criteria for thermal Alteration of bone. Journal of Archaeological Science 22, 115–119.

Théry Parissot, I., 1998. Economie du combustible et paléoécologie en contexte glaciaire et periglaciaire. Paléolithique Moyen et Supérieur du sud de la France (Anthracologie, Expérimentation, Taphonomie). Thèse de doctorat de l'Université de Paris 1 Panthéon-Sorbonne.

Thompson, T.J.U., 2002. The assessment of sex in cremated individuals: Some cautionary notes. Canadian Society of Forensic Science Journal 35(2), 49–56.

Thompson, T.J.U., 2004. Recent advances in the study of burned bone and their implications for forensic anthropology. Forensic Science International 146, 203–205.

Thompson, T.J.U., 2005. Heat-induced dimensional changes in bone and their consequences for forensic anthropology. Journal of Forensic Sciences 50, 1008–1015.

Thompson, T.J.U., Gauthier, M., Islam, M., 2009. The application of a new method of Fourier Transform Infrared Spectroscopy to the analysis of burned bone. Journal of Archaeological Science 36, 910–914.

Thompson, T.J.U., Islam, M., Piduru, K., Marcel, A., 2011. An investigation into the internal and external variables acting on crystallinity index using Fourier Transform Infrared Spectroscopy on unaltered and burned bone. Palaeogeography, Palaeoclimatology, Palaeoecology 299, 168–174.

Trueman, C.N., Tuross, N., 2002, Trace elements in recent and fossil bone apatite, in: Kohn, M.J., Rakovan, J.F., Hughes, J.J., eds, Reviews in mineralogy and geochemistry: Phosphates: geochemical, geobiological, and materials: Washington D.C.: The Mineralogical Society of America, 48, 489–531.

Trueman, C.N.G., Martill, D.M., 2002. The long-term preservation of bone: the role of bioerosion. Archaeometry 44, 371–382.

Trueman, C.N.G., Behrensmeyer, A.K., Tuross, N., Weiner, S. 2004. Mineralogical and compositional changes in bones exposed on soil surfaces in Amboseli National Park, Kenya: diagenetic mechanisms and the role of sediment pore fluids. Journal of Archaeological Scence 31: 721–739.

Trueman, C.N., Behrensmeyer, A.K, Potts, R., Tuross, N., 2006. High-resolution records of location and stratigraphic provenance from the rare earth element composition of fossil bones. Geochimica et Cosmochimica Acta 70, 4343–4355.

Trueman, C.N., Privat, K., Field, J., 2008. Why do crystallinity values fail to predict the extent of diagenetic alteration of bone mineral? Palaeogeography, Palaeoclimatology, Palaeoecology 266, 160–167.

Turner-Walker, G., Jans, M.M.E., 2008. Reconstructing taphonomic histories using histological analysis. Palaeogeography, Palaeoclimatology, Palaeoecology 266, 227–235.

Tuross, N., Behrensmeyer, A.K., Eanes, E.D., Fisher, L.W., Hare, P.E., 1989. Molecular preservation and crystallographic alterations in a weathering sequence of wildebeest bones. *Applied* Geochemistry 4: 261–270.

Tütken, T., Vennemann, T.W., Pfretzschner, H.-U., 2008. Early diagenesis of bone and tooth apatite in fluvial and marine settings: Constraints from combined oxygen isotope, nitrogen and REE analysis. Palaeogeography, Palaeoclimatology, Palaeoecology 266, 254–268.

Ubelaker, D.H., 2008. The forensic evaluation of burned skeletal remains: A synthesis. Forensic Science International 183, 1–5.

Wagner, H.D., Weiner, S., 1992. On the relationship between the microstructure of bone and its mechanical stiffness. Journal of Biomechanics 25, 1311–1320.

Wang, X.Y., Zuo, Y., Huang, D., Hou, X.-D., Li, Y.-B, 2010. Comparative study of inorganic composition and crystallographic properties of cortical and cancellous bone. Biomedical and Environmental Sciences 23, 473–480.

Weiner, S., Price, P.A., 1986. Disaggregation of bones into crystals. Calcified Tissue International 39, 365–375.

Weiner, S., Bar-Yosef, O., 1990. States of preservation of bones from prehistoric sites in the Near East: a survey. Journal of Archaeological Science 17, 187–196.

Weiner, S., Traub, W., 1992. Bone structure: from angstroms to microns. The FASEB Journal 6, 879–885.

Weiner, S., Goldberg, P., Bar-Yosef, O., 1993. Bone preservation in Kebara Cave, Israel using on-site Fourier Transform Infrared Spectroscopy. Journal of Archaeological Science 20, 613–627.

Weiner, S., Wagner, H.D., 1998. The material bone: structure–mechanical function relations. Annual Review of Materials Science 28, 271–298.

Wings, O. 2004. Authigenic minerals in fossil bones from the Mesozoic of England: poor correlation with depositional environments. Palaeogeography, Palaeoclimatology, Palaeoecology 204, 15–32.

Wright, L.E., Schwarcz, H.P., 1996. Infrared and isotopic evidence for diagenesis of bone apatite at Dos Pilas, Guatemala: palaeodietary implications. Journal of Archaeological Science 23, 933–944.

Young A.. 1993. The Rietveld Method. IUCr, Oxford Science Publications.

Zapata, J., Pérez-Sirvent, C., Martínez-Sánchez, M.J., Tovar, P., 2006. Diagenesis, not biogenesis: two late Roman skeletal examples. Science of the Total Environment 369, 357–368.

Zocco, T.G., Schwartz, H.L., 1994. Microstructural analysis of bone of the sauropod dinosaur *Seismosaurus* by transmission electron microscopy. Palaeontology 37, 493–503.